





This is to certify that the

# dissertation entitled EXPERIMENTAL STUDY OF LOCAL NATURAL CONVECTION HEAT TRANSFER IN INCLINED AND ROTATING ENCLOSURES

presented by

Fakhri Hamady

has been accepted towards fulfillment of the requirements for

Ph.D. degree in Mechanical Engineering

Date May 15, 1987

7 56.5

MSU is an Affirmative Action/Equal Opportunity Institution

0-12771



RETURNING MATERIALS:
Place in book drop to
remove this checkout from
your record. FINES will
be charged if book is
returned after the date

stamped below.

# EXPERIMENTAL STUDY OF LOCAL NATURAL CONVECTION HEAT TRANSFER IN INCLINED AND ROTATING ENCLOSURES

By

Fakhri Hamady

## A DISSERTATION

Submitted to
Michigan State University
in partial fulfilment of the requirements
for the degree of

DOCTOR OF PHILOSOPHY

Department of Mechanical Engineering

#### ABSTRACT

# EXPERIMENTAL STUDY OF LOCAL NATURAL CONVECTION HEAT TRANSFER IN INCLINED AND ROTATING ENCLOSURES

By

### Fakhri Hamady

The local and mean natural convection heat transfer characteristics have been studied experimentally in an air-filled differentially heated enclosure with cross-sectional aspect ratio one. In the investigation, a Mach-Zehnder interferometer was employed to reveal the entire temperature field which enables the measurement of the local and mean Nusselt numbers at the hot and cold surfaces.

The first part of this investigation was a study of the inclination effect on the flow and heat transfer behaviors. The measurements of local and mean Nusselt numbers are obtained at various inclination angles, ranging between 0 deg. (heated from above) and 180 deg. (Benard convection, heated from below), for Rayleigh numbers between 10 and 10. The measured heat flux at the hot and cold boundaries showed a strong dependence on the angle of inclination and Rayleigh number. In addition, new results and details are made available concerning the local heat transfer distribution as a function of the inclination angle and Rayleigh number.

In the second part, the study is extended to include the effect of combined heating and rotation on the thermal and hydrodynamic boundary layers. The enclosure is rotated about its longitudinal horizontal axis. The experimental results showed how the centrifugal and Coriolis forces arising from rotation have remarkably influenced the local heat transfer behavior when compared with the non-rotating results. Local heat fluxes are obtained as a function of Taylor (Ta <  $10^4$ ) and Rayleigh ( $10^4$  < Ra <  $3 \times 10^5$  ) numbers at different angular positions of the enclosure. Correlations are established for the non-rotating and rotating conditions as a function of Rayleigh and Taylor numbers.

Photographs of the flow pattern and isotherms at different inclination angles and rotational speeds are shown, in order to give a greater understanding of the flow and heat transfer behaviors.

# DEDICATION

To

my belowed parents

and

brothers

Dr. J

advic State

Dr. R

assi

Engin

coope

Natio

Engir

# **ACKNOWLEDGEMENTS**

I would like to record my indebtedness and thank to my advisors, Dr. J. R. Lloyd, and Dr. K. T. Yang for their valuable assistance and advice throughout the completion of my research studies at Michigan State University; to my committee members, Dr. J. Beck, Dr. A. Atreya, Dr. R. Bartholomew, and Dr. D. Yen for their constructive comments, and assistance; to the machinists in the Department of Mechanical Engineering, Mr. L. Eisele, and R. Rose, for their assistance and cooperation in building our Thermo-Optics Heat Transfer laboratory.

I also like to express my gratitude for the support of the National Science Foundation NSF (Grant 713828) and for use of the MSU Engineering Case Center computing facilities.

# TABLE OF CONTENTS

	Page
LIST OF FIGURES	vi
LIST OF TABLES	xii
NOMENCLATURE	xiii
CHAPTER	
1. INTRODUCTION	1
1.1 Problem Statement 1.2 Literature Survey 1.2.1 Thermal Convection in Vertical Enclosures 1.2.2 Thermal Convection in Inclined Enclosures	1 5 5
1.2.3 Thermal Convection in Rotating Fluids	24
2. MATHEMATICAL FORMULATION	35
2.1 Governing Equations	35
Enclosure	37 45
3.1 Mach-Zehnder Interferometer Facilities 3.1.1 Optical Plates	45 48 50 50
3.2 Experimental Apparatus	52
3.2.1 Moving Frame 3.2.2 Rotating Frame 3.2.3 Test Section 3.2.4 Thermocouple Wiring 3.2.5 Temperature Controlled Section 3.2.6 Driving Motor	52 54 57 59 62 66
3.3 Experimental Procedure	68

3.3.1 Test Section Assembly and Leveling 3.3.2 Insulation	68 71 73 73 74 74
4. RESULTS AND DISCUSSION	75
4.1 Natural Convection in an Inclined Rectangular Enclosure	75 76 82
4.2 Natural Convection in a Heated Rotating Enclosure	99
4.2.1 Heat Transfer Results in a Heated Rotating Enclosure at Angular position 90 deg	100 130 136
5. SUMMARY AND CONCLUSIONS	144
APPENDICES	148
1 PHYSICAL PROPERTIES	148
2 INTERFEROGRAM ANALYSIS	149
3 HEAT FLUX MEASUREMENT	154
4 ERROR ANALYSIS	160
5 COMPUTER PROGRAMS AND SAMPLE CALCULATION	162
REFERENCES	197

# LIST OF FIGURES

		•	page
Figure	1	Geometric configurations of the enclosure	36
Figure	2	Rotation referred to a Cartesian frame of reference, O-XYZ	39
Figure	3	Mach-Zehnder Interferomter	46
Figure	4	Interferometer and experimental setup	49
Figure	5	Camera setup	51
Figure	6	Moving and rotating assembly	53
Figure	7	Side view of the test section in the rotating frame	55
Figure	8	Slipring-brush assembly	56
Figure	9	Rotating section	58
Figure	10	Dimensions of the test section and the gage block	60
Figure	11	Schematic diagram of slipring-brush assembly	63
Figure	12	Rotating union assembly	.64
Figure	13	Schematic side view of the rotating union	65
Figure	14	DC motor with variable speed control	67
Figure	15	Top view of the end region	72
Figure	16	Comparison of mean Nusselt numbe results, for $\phi = 90 \text{ deg } \dots$	77
Figure	17	Effect of inclination angle on mean Nusselt number at Ax-1.0	79
Figure	18	Mean Nusselt number at various inclination for air at Ax-1.0	81

Figure	19	Effect of inclination angle on the flow and heat transfer, at $\phi = 0 \text{ deg } \dots$	83
Figure	20	Effect of inclination angle on the flow and heat transfer, at $\phi = 30 \text{ deg } \dots$	85
Figure	21	Effect of inclination angle on the flow and heat transfer, at $\phi = 60 \text{ deg } \dots$	86
Figure	22	Effect of inclination angle on the flow and heat transfer, at $\phi = 90 \text{ deg } \dots$	88
Figure	23	Local Nusselt number distribution along the hot and cold walls, for air at	
		Ax=1.0, Ra= 1.1x10 and \$\phi\$ = 105 deg	89
Figure	24	Effect of inclination angle on the flow and heat transfer, at $\phi = 120 \text{ deg } \dots$	90
Figure	25	Local Nusselt number distribution along the hot and cold walls, for air	
		at Ax=1.0, Ra= 1.1x10 and $\phi$ = 135 deg	91
Figure	26	Effect of inclination angle on the flow and heat transfer, at $\phi = 150 \text{ deg } \dots$	93
Figure	27	Local Nusselt number distribution along the hot and cold walls, for air	
		at Ax-1.0, Ra- 1.1x10 and $\phi$ = 165 deg	94
Figure	28	Effect of inclination angle on the flow and heat transfer, at $\phi = 180 \text{ deg } \dots$	95
Figure	29	Comparison of local Nusselt number distribution for air, at Ax-1.0, and $\phi = 90$ deg	97
Figure	30	Comparison of local Nusselt number	
		distribution for air, at Ax=1.0, and $\phi = 90 \text{ deg } \dots$	98
Figure	31	Local Nusselt number distribution along the hot and cold walls, for air	
		at Ax=1.0, Ra= 1.2x10 rotational rate= + 6.0 rpm (vertical configuration)	102
Figure	32	Local Nusselt number distribution along the hot and cold walls, for air	
		at Ax=1.0, Ra= 1.2x10 rotational rate= + 8.5 rpm, (vertical configuration)	103

Figure 33	Local Nusselt number distribution along the hot and cold walls, for air	
	at Ax=1.0, Ra= 1.2x10 rotational rate= + 10.2 rpm, (vertical configuration)	5
Figure 34	Local Nusselt number distribution along the hot and cold walls, for air at	
	Ax-1.0, Ra- 1.2x10 rotational rate- + 12.5 rpm, (vertical configuration)	6
Figure 35	Local Nusselt number distribution along the hot and cold walls, for air	
	at Ax=1.0, Ra= 1.2x10 rotational rate= + 15.0 rpm, (vertical configuration)	7
Figure 36	Local Nusselt number distribution along the hot and cold walls, for air	
	at Ax=1.0, Ra= 1.2x10° rotational rate= + 17.5 rpm, (vertical configuration)	8
Figure 37	Local Nusselt number distribution along the hot and cold walls, for air	
	at Ax=1.0, Ra= 2.0x10 rotational rate= + 8.5 rpm, (vertical configuration)	0
Figure 38	Local Nusselt number distribution along the hot and cold walls, for air	
	at Ax=1.0, Ra= 2.0x10° rotational rate= + 12.2 rpm, (vertical configuration)	1
Figure 39	Local Nusselt number distribution along the hot and cold walls, for air	
	at Ax=1.0, Ra= 2.0x10 rotational rate= + 15.1 rpm, (vertical configuration)	2
Figure 40	Local Nusselt number distribution along the hot and cold walls, for air	
	at Ax=1.0, Ra= 2.0x10° rotational rate= + 17.5 rpm, (vertical configuration)	3
Figure 41	Local Nusselt number distribution along the hot and cold walls, for air at	
	Ax=1.0, Ra= 3.0x10 rotational rate= + 6.1 rpm, (vertical configuration)	4
	viii	

Figure 42	Local Nusselt number distribution along the hot and cold walls, for air at
	Ax-1.0, Ra- 3.0x10 rotational rate- + 8.5 rpm, (vertical configuration)
Figure 43	Local Nusselt number distribution along the hot and cold walls, for air at Ax=1.0, Ra= 3.0x10
	rotational rate= + 12.2 rpm, (vertical configuration)
Figure 44	Local Nusselt number distribution along the hot and cold walls, for air
	at Ax=1.0, Ra= 3.0x10° rotational rate= + 15.1 rpm, (vertical configuration)
Figure 45	Local Nusselt number distribution along the hot and cold walls, for air
	at Ax=1.0, Ra= 3.0x10 rotational rate= + 17.5 rpm, (vertical configuration)
Figure 46	Local Nusselt number distribution along the hot and cold walls, for air
	at Ax=1.0, Ra= 7.4x10 rotational rate= + 8.5 rpm, (vertical configuration)
Figure 47	Local Nusselt number distribution along the hot and cold walls, for air
	at Ax=1.0, Ra= 7.4x10 rotational rate= + 12.2 rpm, (vertical configuration)
Figure 48	Local Nusselt number distribution along the hot and cold walls, for air
	at Ax=1.0, Ra= 7.4x10 rotational rate= + 15.1 rpm, (vertical configuration)
Figure 49	Local Nusselt number distribution along the hot and cold walls, for air
	at Ax=1.0, Ra= 7.4x10 rotational rate= + 17.5 rpm, (vertical configuration)
Figure 50	Effect of rotation on mean Nusselt number, for air at Ax=1.0, (vertical configuration)
Figure 51	Effect of rotation on mean Nusselt

		(vertical configuration)	126
Figure	52	Mean Nusselt number as a function of Taylor and Rayleigh numbers	127
Figure	53	Local Nusselt number distribution along the hot and cold walls, for air	
		at Ax=1.0, Ra= 1.2x10 rotational rate= - 8.5 rpm, (vertical configuration)	128
Figure	54	Local Nusselt number distribution along the hot and cold walls, for air	
		at Ax=1.0, Ra= 1.2x10 rotational rate= - 17.5 rpm, (vertical configuration)	129
Figure	55	Local Nusselt number distribution along the hot and cold walls, for air	
		at Ax-1.0, Ra= 1.2x10 rotational rate= + 8.5 rpm, (heated from below)	132
Figure	56	Local Nusselt number distribution along the hot and cold walls, for air	
		at Ax=1.0, Ra= 1.2x10° rotational rate= + 12.2 rpm, (heated from below)	133
Figure	57	Local Nusselt number distribution along the hot and cold walls, for air	
		at Ax=1.0, Ra= 3.0x10 rotational rate= + 8.5 rpm, (heated from below)	134
Figure	58	Local Nusselt number distribution along the hot and cold walls, for air	
		at Ax=1.0, Ra= 3.0x10 rotational rate= + 12.2 rpm, (heated from below)	135
Figure	59	Local Nusselt number distribution along the hot and cold walls, for air	
		at Ax=1.0, Ra= 1.2x10° rotational rate= + 8.5 rpm, (heated from above)	137
Figure	60	Local Nusselt number distribution along the hot and cold walls, for air	
		at Ax=1.0, Ra= 1.2x10 rotational rate= + 12.2 rpm, (heated from above)	138
Figure	61	Local Nusselt number distribution along	

	the hot and cold walls, for air at $Ax=1.0$ , $Ra=3.0x10^5$	
	rotational rate + 8.5 rpm, (heated from above)	39
Figure 62	Local Nusselt number distribution along the hot and cold walls, for air	
	at Ax-1.0, Ra- 3.0x10 rotational rate- + 12.2 rpm, (heated from above)	40
Figure 63	Effect of rotation on mean Nusselt number at various angular positions 1	41
Figure 64	Interference fringe patterns, at Ra= 3.0x10	43
Figure 65	Fringe shift evaluation, at Ra = $1.1 \times 10^5$ $\phi$ = 90 deg	51
Figure 66	Estimation of the temperature gradient at the cold wall, for Ra = $1.1 \times 10^{5}$ $cap = 0.134$ , and $\phi = 90$ deg	56
Figure 67	Fringe shift distribution for Ra = $1.1 \times 10^{5}$ $\zeta = 0.134$ , and $\phi = 90$ deg	57
Figure 68	Temperature profile, for Ra = $1.1 \times 10^{5}$ C = $0.134$ . $\phi$ = 90 deg	58

# LIST OF TABLES

Table	1	Sample calculation of the fringe shift	
		and the temperature, at Ra = $1.1 \times 10^{\circ}$ and height, (y/H) = $0.140$	159
Table	2	Sample calculation of the fringe shift and the temperature distribution, from the interference fringe patterns in Figure 65	179
Table	3	Sample calculation of local Nusselt number obtained from the temperature gradients, in Table 2	196

# NOMENCLATURE

Ax	Aspect ratio, (height/width)
Az	Longitudinal aspect ratio, (length/width)
Ср	Specific heat at constant pressure, J/kg.K
D	Enclosure width, m
g	Gravitational acceleration, m/sec 2
G	Gladstone-Dale constant, m /kg
Gr	Grashof number = $g\beta H^3 (T_H - T_C)/\nu^2$
н	Enclosure height (H - D), m
h	Convective heat transfer coefficient, $W/m^2$ .K
k	Thermal conductivity, W/m.K
L	Length of the enclosure, m
Nu	Local Nusselt number $-\frac{k_{H}^{\Delta \theta}}{k_{C}^{\Delta \xi}}$
 Nu	Mean Nusselt number
P	Pressure, N/m (Pa)
P'	Dynamic pressure, Pa
P <sub>1</sub>	Perturbation pressure
Pr	Prandtl number = $\nu/\alpha$
ř	Position vector, m
Ŕ	Non-dimensional position vector $= \overrightarrow{r}/H$
Ru	Universal gas constant, J/kg.K

- Ra Rayleigh number =  $g\beta H^3 (T_H T_C)/\alpha \nu$
- Ra<sub>r</sub> Rotational Rayleigh number =  $\beta \Omega^2 H^4 (T_H T_C)/\alpha \nu$
- Re Rotational Reynolds number =  $\Omega H^2/\nu$
- t Time, sec
- T Temperature, C
- Ta Taylor number =  $4\Omega^2 H^4 / \nu^2$
- x,y,z Coordinates in the x, y, and z-directions
- v Velocity vector, m/sec
- $\vec{V}$  Non-dimensional velocity vector  $-\vec{v}H/\alpha$

#### Greek Letters

- α Thermal diffusivity, m/sec
- β Volumetric thermal expansion coefficient, 1/K
- Non- dimensional distance along the y-direction = y/H
- $\theta$  Non-dimensional temperature  $(T T_C)/(T_H T_C)$
- $\mu$  Dynamic vicosity, kg/m.sec
- ν Kinematic viscosity, m<sup>2</sup>/sec
- $\xi$  Non-dimensional distance along the x-direction = x/H
- ρ Density, kg/m
- $\tau$  Non-dimensional time  $= \alpha t/H^2$
- Inclination angle between the cold surface and the horizontal direction, deg.
- Φ Dissipation function
- Ω Angular speed, rev/sec

# Subscripts

- a Air
- C Cold surface
- H Hot surface
- r Rotation
- s Surface

#### CHAPTER 1

#### INTRODUCTION

### 1.1 Problem Statement

Natural convection in enclosures continues to be the subject of extensive research effort. The convection phenomena studied are usually induced by gravitational body forces. In a fluid where the body force is normal to the direction of the density gradient, flow is produced no matter how small the gradient may be, since no hydrostatic pressure distribution can balance the consequent variation of the buoyancy forces produced. For a fluid with the density gradient parallel and opposite to the gravitational acceleration, the flow can only be observed when the density gradient exceeds a critical value. The critical value depends upon the conditions at the top and bottom surfaces, which may be either free or constrained by rigid conducting surfaces. In enclosures inclined relative to the gravitational field, distinctly three-dimensional flows occur which exhibit patterns closely dependent on the angle of enclosure inclination. A comprehensive review of enclosure heat transfer research up to 1978, has been presented by Ostrach [1] and Catton [2].

If a differentially heated enclosure undergoes rotation, centrifugal and Coriolis force effects on the fluid will interact with the gravitational force in a manner which results in a complex three-dimensional flow and temperature fields. The flow and temperature fields are directly coupled in the momentum equations and this

consequently effects the surface to fluid energy transfer. Cases like that occur in rotating fluid machinery, where the centrifugal acceleration, which is proportional to the square of the angular velocity, may be very large. In geophysical applications involving atmospheric circulation and oceanic rotational motion, the flows are driven primarily by the Coriolis forces and the centrifugal effect can be neglected.

Analysis of flow and heat transfer associated with rotating systems is quite complex due to the simultaneous influence of centrifugal and Coriolis forces. As a consequence, a large amount of analytical and experimental study has been and continues to be devoted for the development of a general treatment of the influence of rotation on the flow and heat transfer in simple geometries. However, studies of natural convection in rotating systems, concerning the effects of centrifugal and Coriolis forces are very few, and experimental data are almost non-existent. In this respect, it is further required that special techniques and experimental methods have to be devised to analyze the process with a view to provide information on the heat transfer rate.

The objective and exclusive purpose of the present research study is to present a systematic study to reveal the motion due to the interaction between gravitational field and the rotationally induced body forces in an air-filled differentially heated rectangular cavity, or slot rotating about its longitudinal horizontal axis. As would be anticipated, the influence of the centrifugal and Coriolis forces arising from the rotation will affect significantly the flow and heat transfer characteristics of natural convection. Emphasis will be centered on the local heat transfer measurements and visualizations to integrate the qualitative visual observations with the quantitative

measurements of heat transfer. This class of rotating flow geometry, may lead to a new area of experimental research, to supplement the available information of natural convection in cavities, in addition to numerous future applications in spacelab, and design development in cooling rotating equipments.

The first part of this investigation will be devoted to the study of thermal convection in a differentially heated, air-filled enclosure driven by the gravitational field only. The effect of inclining the boundaries on the thermal convection for various Rayleigh numbers is to be studied. Visualization of the flow patterns will be employed to give greater insight into the physical phenomena, and to enable greater understanding of the flow and the local heat transfer profiles. This will provide a firm basis of comparison to sort out the effects of rotation.

The second part of the study will focus on the effects of rotation on the flow and heat transfer in enclosures. Local heat transfer measurements with the flow visualization will be performed for various Taylor numbers, to show the significant amount of distortion of the hydrodynamic and thermal boundary layers. The Rayleigh number will be gradually increased to reveal the interaction between centrifugal and gravitational buoyancy on the flow and heat transfer. The data will be correlated based upon the Rayleigh and Taylor numbers.

The Mach-Zehnder interferometer will be used to explore how the local heat flux distribution is influenced by the Rayleigh number and the Taylor number (the square of the ratio of Coriolis force to viscous frictional force), to examine both the effect of the Coriolis force on the thermal convection of fluid at low rotational speeds, and the effect of the buoyant interaction at higher rotational speeds, where the centrifugal buoyancy will become more important relative to the

Co he fo

po

Ďe

Coriolis acceleration. Local values of Nusselt number (dimensionless heat flux) along with the average values will be measured and plotted for different values of Rayleigh and Taylor numbers, and at angular positions of 90 deg. (vertical configuration), 180 deg. (heated from below), and 0 deg. (heated from above).

1.

fe in

to

tri

Sy:

1.3

of end

hea

eit

of sol

ten enc

nua

app nuz

> opt the

dia

## 1.2 Literature Survey

The general purpose of this review is to present the main features of natural convection in enclosures or cavities, as presented in the technical literature. The main concern will be devoted entirely to aspects of theoretical and experimental investigations of heat transfer and flow pattern in vertical, inclined, and rotating fluid systems.

#### 1.2.1 Thermal Convection in Vertical Enclosures

The first part of this review is therefore to draw together some of the recent information about the physical processes in vertical enclosures, which are composed of two vertical plates differentially heated in the horizontal direction, where all the other surfaces are either perfectly conducting or insulated.

G.K. Batchelor [3], in 1954 initiated the first analytical study of free convection in enclosed gas layers, and through an approximate solution he concluded that the heat transfer is a function of the temperature difference between the walls, the Prandtl number of the enclosed fluid, and the aspect ratio of the enclosure. Poots [4] numerically solved the equations for a very limited range of Grashof number and substantiated Batchelor's prediction. His solution is applicable only for Gr <2000 and only for air.

In 1956, Carlson [5] conducted an experimental study using optical techniques. His results showed that the mean temperature of the cell is a function of the height increasing with the vertical dimension. The precise variation is not known, and it is expedient to

the h
Machcondi
heat
gradi
flow
enclo
certa
core
On th

into Tevie

recer

canno:

the bo

and t

analy

aspect geome

artic

theore

on the

energy

consider the mean temperature as a constant, given by the average of the hot and cold wall temperatures. Eckert and Carlson [6], used the Mach-Zehnder interferometer to investigate the temperature and flow conditions in an air layer enclosed between two vertical plates. Local heat transfer coefficient were derived from the local temperature gradients normal to the plate surfaces. They concluded that various flow regimes exist depending on the value of Rayleigh number and the enclosure geometry. That is, below a certain Grashof number and above a certain aspect ratio heat is transferred primarily by conduction in the core of the layer. Convection contributes only in the corner regions. On the other hand, for large Grashof number, and below a certain aspect ratio, boundary layers exist along the surfaces of the enclosure.

Excellent review papers on internal flows have appeared recently, including enough information to allow one to gain insight into the natural convection phenomena. Ostrach [1,7] emphazised in his review works that, after all the research activities, the flow pattern cannot be predicted in advance from the given geometry and boundary conditions. Because in confined natural convection the core region and the boundary layer near the walls are closely coupled, neither one can be determined from the boundary conditions. Hence, the boundary layer and the core region coupling makes it very difficult to obtain an analytical solution to internal problems.

Catton [2] considered in his review enclosures of different aspect ratios and at various inclination angles, besides the honeycomb geometries that can be used efficiently in solar collectors. His article contributed greatly to the physical understanding of the theoretical and experimental work in this field by providing insights on the coupling between the conservation equations for momentum and energy, and by obtaining engineering correlations for heat transfer.

recer inves [8] recta probl his s level throu . [9,10 inter therm regio relat tempe appea resemi

subje

vertion 5.5xl

secor

turbu

of th

chara intern

coeff;

numbe Nu-Nu

The intensifying desire to present all the aspects of this subject contributed in an expansion of knowledge in fields considered recently, and still attracts the attention and interest of many investigators from many conventional fields of fluid mechanics. Gill [8] in his work on the boundary layer region for convection in a rectangular cavity, attempted to find an analytical solution to the problem mentioned earlier by Batchelor. In this regard, comparison of his solution with Elder's experimental results showed a satisfying level of agreement, except near the horizontal boundaries. Elder through his experimental works on natural convection in a vertical slot [9,10], explained the features of the boundary layer flows and the flow interaction between the thermal boundary layers. The influence of the thermal conductivity will accordingly become important in the near-wall regions. In other words a boundary layer flow might be expected in a relatively thin region close to the walls which results in a vertical temperature gradient. He also claimed that the secondary flow appearance in the interior region at Rayleigh numbers greater than 10° resembles a "cats-eye" pattern. In addition to this, he studied in a second report the transition process from laminar to unsteady to turbulent flow.

Mynett and Duxbury [11] investigated natural convection in a vertical enclosure for Rayleigh numbers within the range,  $10^3$  <Ra <  $6.5 \times 10^5$ , and aspect ratio range 1.25 < Ax < 20. Within these limitations of the variable parameters Ra and Ax, they found distinct regimes of characteristic temperature distribution by using a Mach-Zehnder interferometer. From the temperature profiles the local heat transfer coefficient were determined on the vertical walls. The overall Nusselt numbers have been correlated by a relationship of the form Nu-Nu(Ra,Ax), which is influenced by various regimes described by the

ter into

dis

flo

pred lay

tem; Com

dis

gene

col

[13

and

to 1

Pro Whi

.00*1* 

con the

on

Prec

שני

terms conduction, transition, and boundary layers. Their interferometric studies and the smoke tests showed that the temperature distribution and flow within the cavity were time independent, and the flow nature became complex beyond the maximum value of their Rayleigh number.

Raithby, Hollands, and Unny [12] presented an analysis to predict the heat transfer in both the laminar and turbulent boundary layer regimes, and established an equation to estimate the midslot temperature distributions for aspect ratios of about five or larger. Comparison of the average Nusselt number, and the temperature distribution with experimental data showed good agreement. Also, they generalized the heat transfer equation to include inclined layers up to 20 deg. from the vertical, which can be used in the design of solar collectors.

An experimental investigation has been conducted by Yin, et al. [13] for various aspect ratios ranging from 4.9 to 78.7 and Grashof numbers ranging from 1.5x10<sup>3</sup> to 7.0x10<sup>6</sup>. Both temperature distributions and heat transfer rates were reported. Temperature profiles were found to be independent of the temperature difference for each ratio, and provided further insight into the temperature inversion phenomena, which was believed to be the result of the high rate of tangential convection of heat relative to the horizontal transport.

Bejan [14], recently reviewed the analytical work on free convection in rectangular enclosures. The review described in detail the most important features to predict the effect of the aspect ratio on the net heat transfer rate over the entire geometry spectrum. He concluded that, sufficient analytical means are available for predicting the influence of the aspect ratio on the heat transfer rate, but further studies are required to explain the transition process from

the theo

Neve

conv

and

cavi The

aspe

cav

ess

and

rat:

con

hor

the bet

dif

dri

5.4

res nun

tem

Ver

Ъу

the conduction to the convection boundary layer regime, and more theoretical analysis should be developed in a square cavity. Nevertheless, despite the large number of works on confined natural convection, the majority have dealt with aspect ratios greater than one and Rayleigh numbers in the range from  $10^4$  to  $10^7$ .

Meanwhile, a second class of experiments focussed on small aspect ratios were motivated by its diverse applications in gas filled cavities surrounding a nuclear reactor core and in double-pane windows. The earliest investigation on natural convection of low aspect ratio in cavities has been made by Boyak and Kearney [15] who studied the essential properties required to understand the convection in crystal growth and in cooling equipment. Sernas, et al. [16-18] experimentally and numerically studied the problem of natural convection in the aspect ratio range of 0.1 to 1.0 and 2.64x10 cm ( Gr < 5.54x10 cm). The significant effect of the boundary conditions on the horizontal surfaces was considered by comparing the results of two tests. One with isothermal horizontal boundaries and the other with adiabatic ones. Based on their experimental observations, significant difference was found between the heat transfer characteristics and the flow pattern. This difference was also verified through their numerical study [17].

Experimental results and numerical calculations of buoyancy-driven convection in room geometries in the range  $1.6 \times 10^9$  <Ra <  $5.4 \times 10^{10}$  was presented by Bauman, et al. [19]. The numerical simulation results showed excellent agreement with existing experimental and numerical results for  $10^4$  < Ra <  $10^9$ . The Nusselt numbers and temperature profiles predicted by their numerical techniques matched very well their experimental results.

An excellent survey in low aspect ratio enclosures is presented by Ostrach [7]. In this event, several numerical methods have been

partia flow i than t preinf the bo diffic conve rectan Grasho agreem Landi and Ch Filke stabil that soluti Berko to stu solut vith t differ high G the Ra Ra. W  $^{can}$  p

Theref

boundar

in then

develo

•

developed to obtain numerical solutions to the coupled nonlinear partial differental equations, which describe the natural convection flow in enclosures. Numerical methods are presumably more effective than the analytical boundary layer approach, because they require no preinformation of the core region, whereas the strong coupling between the boundary layer and core makes the boundary layer analysis very difficult. Wilkes and Churchill [20] numerically solved the natural convection problems of a fluid contained in a long horizontal rectangular enclosure with vertical walls differentially heated. For Grashof numbers less than 2x10°, their results were stable and in good agreement with analytial solutions. De Vahl Davis [21], Rubel and Landis [22,23], Quon [24], Thomas and de Vahl Davis [25] and Spradley and Churchill [26] developed numerical techniques similar to that of Wilkes and Churchill [20], but with more discussion concerning stability, physical acceptance of parameters and boundary conditions that may be used in the solution. The limitations imposed on the solutions, make the subject of further concern to many investigators. Berkovsky and Polevikov [27] developed and applied a numerical scheme to study the natural convection in closed cavities. Steady state solutions for a large range of characteristic parameters were found, with the emphasis on the mesh size, and approximation order of the difference technique to obtain accurate and satisfactory results at high Grashof numbers. Their calulations have shown that an increase in the Rayleigh number disturbs the structure of solutions typical for low Ra. Whereas, the formation of the boundary layers in the wall region can proceed in a wide range of Rayleigh numbers from  $10^4$  to  $10^7$ . Therefore, an increase in Grashof number yields a decrease in the boundary layer thickness, while the growth of the temperature gradients in them is less intensive with Prandtl number increase. Moreover,

their (

implic

[28] c

develor from t

these :

case o

the pro

other (

points

fluid o

conditi

method

reducti

Merker

determi Based (

other n

Davis a

results

Rubel

density

Their .

modifyir.

unaffec

their empirical formulae, for heat transfer described the dependence of Nu on Rayleigh number and have a number of functional and practical implications, according to the excellent comparison with Catton, et al. [28] calculations and other existing works.

Hutchinson and Schiesser [29] and Churchill, Chao, and Ozoe [30] developed extrapolation formulae to the limiting case of zero grid size from the finite grid analysis. However, they did not confirm that these formulae can be applied in other conditions, especially in the case of nonlinear partial differential equations. Quon [31,32] solved the problem numerically using variable mesh size, for Rayleigh numbers 10 and 10, and Prandtl number 0.71. The results were compared with other computations of various mesh sizes and different number of grid points in an attempt to set up bench marks for numerical algorithms in fluid dynamics, and heat transfer. The effect of horizontal boundary condition and Rayleigh number on the flow was also presented.

Adaption of the A.D.I. method (alternating direction implicit method) for the vorticity and energy equation and the method of cyclic reduction for the Poisson equation appeared in the work of Kublbeck, Merker, and Straub [33]. A transformation relation is formulated to determine accurately the boundary layer characteristics near the walls. Based on their observations 'exact' solution can be predicted from other numerical solutions with three different mesh sizes. De Vahl Davis and Jones [34] presented a summarizing paper including the main results of the various numerical methods in varying degrees of details. Rubel and Landis [23] analysed the effects of both transport and density variations in gases, viscosity and conductivity in liquids. Their results showed the influence of the density variations in modifying the flow field, while the thermal field remains relatively unaffected by the temperature difference increase. In liquids,

vi fi [35 **S** 0 cor th Ray of sta rat der. Ira COD V0] tra det beha Zho soly Som tez var: Proj corr  $\mathtt{has}$ and Yang

impo

viscosity and conductivity variations both influence the temperature field, while the flow field is mostly effected by viscosity. Graham [35] illustrated the feasibility of using finite difference methods in solving the equations for compressible convection with variable conductivity and viscosity. The difference scheme has been extended to three-dimensions and solutions up to 100 Ra (Ra is the critical Rayleigh number for the onset of convection) and for pressure variation of a factor of 300 within the fluid have been obtained with remarkable stability. Also flow patterns have been observed for large aspect ratio. A study by Leonardi and Reizes [36] considered the effects of density variations with temperature. Fourier analysis-Fast Fourier Transform (FA-FFT) was used to solve the system of equations for compressible fluids in cavities, but in their investigations a constant volume cavity is assumed which yields a pressure increase due to the transient heat transfer from the hot wall. An excellent study to determine the variable property effects on the thermal and hydrodynamic behaviors of natural convection in square enclosure was presented by Zhong, Yang, and Lloyd [37,38]. Specific consideration was given to solve the full variable property, governing differential equations. Some of the more interesting results were, the estimation of the temperature range for the validity of Boussinesq approximations, the variable property effects on vertical velocity and heat transfer, the proper use of a reference temperture, and the variable property correlation of the heat transfer rate.

Natural convection in square enclosures with internal partitions has also been investigated experimentally and numerically by Bajorek and Lloyd [39,40], Chang, Lloyd, and Yang [41], and Bilski, Lloyd, and Yang [42]. Their studies included an extensive discussion of the most important aspects of the subject and a vast amount of information on

radi simi

both

52].

were sign

conv

inte

the [50,

state

natu gene:

the (

Ozoe

Yang

using smal

numbe

1.2.2

incli to co

forc

incli modif radiation-convection interactions in complex enclosures. A somewhat similar numerical technique to solve the differential equations using both finite element and finite defference was described in [43,44,45-52]. The essential features of the methods in several important areas were introduced in terms of their practical applications and physical significance.

More recently, the solutions to three-dimensional natural convection in an enclosure have received considerable amount of interest and numerical techniques have provided a beginning solution of the physical mechanisms involved. Mallinson and de Vahl Davis [50,53,54] presented a method for the numerical solution of the steady state Navier stokes equations in three-dimensions for the problems of natural convection in a rectangular cavity. The main results generating the three-dimensionality have been developed together with the essential concepts of the numerical scheme. Aziz and Hellums [55], Ozoe, et al. [56], Lipps [57], Pepper, Harris, and Reddy [58], Yang, Yang, and Lloyd [89] have approached the three-dimensional problem, using various numerical techniques. Most of the results indicated that small longitudinal aspect ratios, low Rayleigh number, and low Prandtl number increase the three-dimensionality in the flow.

### 1.2.2 Thermal Convection in Inclined Enclosures

In a wide variety of practical applications, the enclosure is inclined to the local direction of gravity, which results in the need to consider both the tangential and normal components of the buoyancy force relative to the differentially heated walls. At large inclination the normal component of buoyancy becomes very important, in modifying both the flow structure and heat transport. Such processes

have expe

physi

surv

which incl

the

resu.

subj

tra:

rat

set

flo

co1:

inv

ne;

e ci

an Pr

Nu

7a

de

Но

have received interest and a considerable amount of detailed experimental and analytical study that provided an understanding and physical insight into the flow mechanisms. Accordingly, this part will survey pertinent works of natural convection in inclined enclosures, which is influenced by the boundary conditions, the angle of inclination, the aspect ratio, and the temperature difference across the fluid layer.

The apparent importance of the inclined convection problem resulted in a sequence of review papers given by Ostrach [1] and Catton [2]. The exprimental work of De Graaf and Van der Held [61] on this subject, is considered one of the earliest study. The average heat transfer rates were measured for different Rayleigh numbers and aspect ratios. However, their results showed no dependence on the aspect ratio and overall angles of inclination. Their visualizations of the flow pattern of an inclined air layer heated from below at different setting of inclination angles showed the existence of longitudinal convection rolls.

Dropkin and Somerscales [62] carried out an experimental investigation in inclined enclosures of different aspect ratios to measure the heat transfer in silicone oils, and mercury at various angles. The results of their experiments are a set of correlation equations which indicate no effect of the aspect ratio. Using these correlations the average heat transfer rates were determined at various angles and for Rayleigh numbers ranging from  $5 \times 10^4$  to  $7.17 \times 10^8$ , and Prandtl numbers between 0.02 and 11560. Their computed values of Nusselt numbers, exhibited a reasonable agreement with the De Graaf, Van der Held-study [61] for the vertical configuration, and indicated a decrease with reducing the angle of inclination from the horizontal. However, their prediction of the turbulent flow at Rayleigh number

disc plat inst Gras expe

abov

the ach

**s**ys

an an

di

fea vi

di in

co

ar Ra

f

r

đ

V

above  $5 \times 10^4$  was double that given by Landis [63]. Kurzweg [64] discussed the stability of natural convection between infinite inclined plates, and related the longitudinal roll appearance to the convective instability. Then, a secular relation was derived for the critical Grashof number at the onset of roll instability and compared with the experimental points.

Until about 1970 there had been little consideration given to systematic study of the effect of inclined boundaries on thermal convection, and of the inclusion of simultaneous important factors like the aspect ratio and various angles of inclination that permit one to achieve a rather broad understanding of the flow pattern, and how the heat transfer rate is influenced. Most of the works performed on different aspects of the subject, were very limited. During that time an extensive work has been conducted by Hart [65], who used both the analytical and experimental procedures to reveal the significant features of the effects of enclosure inclination. In a series of flow visualization studies the effect of inclined boundaries in a differentially heated shallow box was revealed for a variety of inclination angles ranging between the two limiting cases, Benard convection and convection in a vertical slot. The development of the flow from the primary state to the secondary motions, the unsteadiness, and ultimately turbulence, was analysed with the gradual increase of Rayleigh number. In the first experiment, the horizontal state (heated from below) was considered, and from the visual study detailed insight into the flow process was established. Evidently the primary state represents no motion, followed by the secondary motion in a roll-like mode influenced by the lateral boundaries, and characterized by the appearance of striation structure at a certain Rayleigh number, above which the unsteadiness stage may be reached. Through a number of

experiments and a study of the flow regime that describes the phenomena, Hart gave an inclusive discussion of the successive configurations. For 180 deg.>  $\phi$  > 100 deg. (heated from below), the instability growth appeared as longitudinal rolls with axes oriented along the upslope. The circulation modes generated indicate a relative dependence on the Rayleigh numbers. For 100 deg.  $> \phi > 80$  deg. instabilities are characterized by transverse waves oriented across the slope. However, for 80 deg.>  $\phi$  >5 deg. and large Rayleigh number, longitudinal instabilities are the overwhelming modes where one expected to examine stable convection for cavities heated from above. Based on experimental observations instability occurred when a critical value of Rayleigh number is exceeded, and more apparent by increasing Rayleigh number. It is, also important to note that, besides the qualitative study, Hart provided quantitative analysis for some of the experimental results. But in spite the influence of the type of flow regime on heat transfer, no measurements have been made.

Hollands and Konicek [66,67] attempted to study the various flow regimes in terms of the range of values of the critical Rayleigh numbers closely related to the stability of the horizontal, vertical, and inclined air layers. Their results for the measured critical Rayleigh numbers are in close agreement with the work reported by Unny [68], and through their experimental analysis the principal modes of flow were discussed. For the horizontal mode (Benard problem), the instability is associated with what may be called a "top-heavy" situation. Heat is transferred by conduction across the fluid layer, where the Rayleigh number is less than the critical (Ra<sub>C</sub>< 1708) value, while for the inclined layer two types of instabilities should be considered, the static top-heavy, and the gravitational buoyancy associated with the vertical slot. The relative magnitude of influence

of ea

which a tra

an ir

large

on t

conc

thei

flu

incl

COR

ana)

num

the bou

the ade

int

Ayy so:

di

de

nu

٦a

of each depends on the angle of inclination, and at a critical angle, which was determined by Hart to be 162 deg. and by Unny to be 168 deg., a transition from one mode into another can be seen. The instability in an inclined layer manifests itself in longitudinal rolls [61,65] for large Prandtl number.

Clever [69] considered the effects of the angles of inclination on the transition process, and pointed out that, a visual study of the hydrodynamic instabilities near the vertical can yield a definite conclusion on the preferred mode for larger Prandtl numbers, since their experiments were performed only on air and water as the contained fluid. On this basis of analysis, Nusselt number results were expressed as a function of Rayleigh number, and the angle of inclination where the flow is still in longitudinal rolls.

Recent developments, however, pointed to the need of more comprehensive treatment of the subject. Ayyaswamy and Catton [70] analytically considered fluid flow in a differentially heated, inclined rectangular cavity, and developed a correlation for the average Nusselt number in terms of the average Nusselt number for the vertical case and the angle of inclination. The result for a given aspect ratio and boundary layer regime predicted a satisfying level of agreement with their numerical solutions. In addition, their correlation is an adequate guide for the applied engineer to establish the first insight into the measurements of the heat transfer rates in many cases. Catton, Ayyaswamy and Clever [28] have applied the Galerkin method for the solution of natural convection flow of a large Prandtl number in a differentially heated inclined rectangular slot. The method has been demonstrated, in the case of Boussinesq approximations, for Rayleigh numbers up to 2x10 and aspect ratio range between 0.1 and 20. For various angles of inclination both temperature and velocity profiles

were obtained to reveal the heat transport and flow structure dependence on the aspect ratio, angle of inclination and Rayleigh numbers effects. In this respect, they suggested that, the mean Nusselt number should be expressed in terms of these parameters and the aspect ratio effect can not be ignored as illustrated in Dropkin and Somerscales [62] correlations. Comparisons of their results with De Vahl Davis [21,60] numerical analysis showed good agreement for an aspect ratio of 5 but did not agree for the square cavity. In their discussion the essential role of inclined boundaries has been considered together with the effect of increasing Rayleigh numbers on the heat transport and the flow configuration. In addition, they analysed the case for inclination angles when the hot plate is on top, and predicted that a large amount of heat is associated with the convective mechanisms. Further, decreasing the aspect ratio induces a transverse fluid motion which enhances the convective heat transport, and the presence of the end walls inhibits the longitudinal mode.

In a series of papers Ozoe, et al. [71-74] carried out a number of experimental and numerical studies to determine the nature of the fluid flow, temperature distributions and the corresponding heat transfer rates under vertical, horizontal, and inclined conditions with various thermal boundary conditions, and aspect ratios of the enclosures. Their studies were thoroughly conducted and provided valuable information concerning flow patterns, velocities, and temperature distribution. The flow patterns which the authors observed were of the following nature. In a vertical square channel (angle of 90 deg.) the preferred mode was a single longitudinal two-dimensional roll-cell dominating the flow. This pattern remained until the angle of inclination increased up to about 170 deg. where the flow modification was observed. For large angles between 170 deg. and 180

deg. (horizontal), a complex flow pattern was found. Near 179 deg. of inclination or more a gradual rearrangement of the convective flow pattern was seen and a series of two-dimensional roll cells aligned with their axes horizontal and perpendicular to the long dimension of the channel appeared.

The heat transfer measurements follow quite well what would be anticipated based on the observed flow patterns. From both the numerical and experimental results, which compared well with [70], the heat transfer rate was found to reach a maximum at about 130 deg. of inclination where the longitudinal mode prevailed and a minimum at about 170 deg. from the horizontal where the transition from the longitudinal roll cell to a series of two dimensional roll-cells has occurred. Additional studies were conducted for aspect ratios of 1,2,3,4.2,8.4 and 15.5 and Rayleigh number from  $3 \times 10^3$  to  $10^5$  to reveal what effect they may have on the heat transfer rates and flow patterns. A consequence of this study is that the critical angle of inclination related to the transition in the mode of circulation appeared to be strongly dependent on the aspect ratio and weakly dependent on the Rayleigh number. For aspect ratios of 3 and 4 the transition from a longitudinal roll-cell to a series of oblique roll-cells with their axes directed upslope occurred at small angles of inclination. Furthermore, the heat transfer rate decreased with a slight decrease in the angle of inclination from the horizontal which is caused by the greater drag of the oblique cells and by the significant reduction of circulation. When the angle was further decreased a minimum value was reached, followed by a maximum value at an inclination of about 130 deg. from the horizontal. In further papers Ozoe, et al. [75-78] have generalized the work to include various heat transfer problems. For instance, in [75,76] along with three-dimensional numerical results, a

visual atudy presented the flow pattern in three orthogonal planes which agreed reasonably with numerical results for various inclination angles. Also, the average Nusselt number measurements showed significant dependence on the flow patterns, and results from both numerical and experimental works compared very well despite the differences in Rayleigh, Prandtl number and the finite length of the box.

In view of the very wide applications, natural convection was considered in doubly inclined rectangular boxes, and inclined rectangular boxes with the lower surface half heated and half insulated. The same authors showed in [77] that, the heat transfer rate is influenced by both the angles of inclination and rotation in case of two different aspect ratios and hence, the flow mechanism will be composed of one or two roll-cells each in the form of closed helix pairs. However, there was some uncertainty in the numerical results due to the extrapolation from finite grid size, and in the experimental values because of the heat losses involved in the long duration of the experiments. In [78] the roll-cells remarkably appeared on the heated segment rather than on the whole surface and apparently the result is, a decrease in the absolute heat transfer compared to that of a uniform temperature on the lower surface.

Arnold, Catton, and Edwards [79] conducted an extensive experimental study to examine the influence of the angle of inclination and the aspect ratio on the heat transfer rate. At a given Rayleigh number their results showed an increase in Nusselt number as the angle of inclination increased from 0 deg. (heated from above), until a local maximum was attained at an angle of 90 deg. (vertical). However, a local minimum is always appeared for angles between 90 and 180 deg., and smaller than the value at either 90 or 180 deg. for all the aspect

ratios. Further, it was noted that for smaller aspect ratio the local minimum becomes more pronounced and closer to the 180 deg. (horizontal). This occurrence of a local minimum predicts that the unicell and the Benard convection do not superpose. Although, their results agreed reasonably with those of Ozoe, et al., the location of their minimum seems to be closer to the vertical. Values from their scaling law are valid only for inclination angles from 180 to 90 deg.

Buchberg, et al. [80] presented a review of the subject, in which a set of empirical correlations were obtained. These correlations have been used to calculate the Nusselt number which is of great importance in the application of solar collectors, where the free convection constitutes the main mode of the heat loss. Another interesting experimental analysis across inclined air layers was developed by Hollands, et al. [81]. The Rayleigh number considered is from subcritical to  $10^5$  and angle of inclination from 180 deg. up to 110 deg.. Subsequent results, showed considerable deviation from the Nusselt values obtained from the horizontal layer when Ra is replaced by Ra·cos $\phi$ , especially in the range 1708
Ra·cos $\phi$  < 120 deg. However, under these conditions their correlation predicted excellent agreement with the experimental data points, and fits closely all data as reported.

Quite recently, local heat transfer measurements in inclined air-filled enclosures have been made by Linthorst, Shinkel, and Hoogendoorn [82-84] to further elaborate on essential features of the physical phenomena, at the side wall region. For the determination of the local heat transfer rates a holographic interferometer was employed. Results of the local Nusselt number measurements obtained on the basis of the local wall temperature gradients, provided valuable information on the physics of the heat transfer near the walls. At

þ as be ef ро Nu 0f au th ещ as ra ino angle of inclination of 160 deg., local heat transfer rate measurements showed several maximum and minimum along the hot plate, while for 100 deg. the local heat transfer rate was maximum at the lower region and In general, their predictions of the minimum at the upper region. flow regime were consistent with other investigators works [65,71,72]. Interferograms for angles of inclination ranging from 180 up to 150 deg. and from 150 to 90 deg. were similar to those of the horizontal and vertical orientation respectively. However, for the range between 150 and 130 deg. transition from one mode into another has occurred. More importantly, average heat transfer rate values were maximum at the horizontal when plotted for various orientations, and in good agreement with those of De Graaf and Van der Held for Ra-1.4x10 . However, for Ra > 10° results compared favorably with those of Jannet and Mozeas [85]. A similar experimental study using interferometric techniques was reported by Randal, Mitchell and El-Wakil [86], along with the local heat transfer measurements. Grashof number, inclination angle and aspect ratio effects on both the local and average Nusselt number have been considered. As a result it was shown that is no substantial effect of the aspect ratio on the average heat transfer in the laminar boundary layer regime. Correlations for both the local and average Nusselt numbers are expressed in terms of Grashof number and the angle of inclination, and indicated fair agreement with the results of other authors [80,81]. In further study [87], the same authors extented their work to include enclosures of moderate aspect ratio, in which emphasis is made on the convection heat transfer dependence on the aspect ratios less than 4. It has also shown that, for the same aspect ratio adding spacers directed upward between the plates yield an increase in heat transfer rate and a decrease when oriented downward.

Some of the very recent contribution to the basic aspects of natural convection in inclined enclosures, was the introduction of, variable properties in the numerical methods and the establishment of the limits of validity of Boussinesq approximations. Zhong, Lloyd and Yang [88], and Yang, Yang, and Lloyd [89] have applied in their numerical analysis to a study of the effects of variable thermal properties, a very general law of dependence of thermal conductivity, viscosity and heat capacity on temperature. Throughout their study the various types of flow patterns and heat transfer were analyzed for a complete set of inclination angles. Conductive heat transfer was found to dominate the flow motion for inclination angles ranging from 0 deg. (heated from above) up to 45 deg. For larger angles of inclination convection was remarkably the prevailing heat transfer mode because of the apparent increase of gravitational effects along the differentially heated walls. Transition from unicell to three-dimensional oblique rolls have been seen at critical angle between 150 deg. and 180 deg. (horizontal), with a local minimum in heat transfer rate. Moreover, their correlation for the Nusselt number based on the full variable properties compared favorably with the results of [28,79].

Although papers in this field are still appearing [90-97] it would seem that, much is yet to be learned about the effects of inclined boundaries and their important functions in heat transfer. It is apparent from the preceeding sections that a substantial amount of theoretical and experimental work has been conducted to develop the important aspects of heat transfer in enclosures. However, local Nusselt number distribution has not received such detailed attention, especially for the heated from below configuration (Benard convection), which is not reported to the best of my knowledge in the literature.

# 1.2.3 Thermal Convection in Rotating Fluids

Studies of the effect of the various physical factors on the motions produced in a rotating fluid have been conducted with great concern over the last two decades. Most of the theoretical and experimental works dealt mainly with slow rotational speed, and it was assumed that the fluid was in a solid body rotation. A monograph of the theory of rotating fluids by Greenspan [98] contains most of what is necessary for a basic understanding of the theory to treat both large-scale atmospheric convection and small-scale flows commonly produced in laboratory experiments. Further, the general theory of contained rotating fluid motions has been presented at length in [99,100] for viscous imcompressible fluids with the development of new theorems and results. A second, somewhat similar monograph on heat transfer and fluid flow in rotating coolant channels was prepared by Morris [101]. Interest was centered on design requirement for cooling rotating components, beside an inclusive review of current research in cylindrical and rectangular ducts which are constrained to rotate about an axis parallel to the duct (parallel-mode rotation), or perpendicular to the duct (orthogonal-mode) which is important in cooling turbine rotor blades.

The first treatment of heat transfer in a tube rotating about a perpendicular axis to cool turbine blades, was studied by Schmidt [102]. He suggested flowing cooling fluid through narrow radial passes in a blade opened to a reservoir of circulating cool fluid in the hub. The density gradients caused by the hot wall will interact with the centrifugal acceleration to force the cold denser fluid in the hub to

flow radially outward, whereas the hot and less dense fluid near the walls flows inward toward the axis of rotation.

Mori and Nakayama [103], analyzed theoretically the fully developed laminar flow, and temperature field in a pipe rapidly rotating around a perpendicular axis using an integral method. Assuming the validity of a velocity and a thermal boundary layers analysis, it was shown that the resistance coefficient and the Nusselt number increase remarkably due to a secondary flow driven by the Coriolis force. In this event, the authors reported that the effect of the secondary flow predominates over almost the whole cross section of the pipe (core region), except near the pipe wall, where the viscosity and heat conduction effects are confined (boundary layer).

The Coriolis force, due to the velocity component in the direction of pipe axis is normal to the main flow, while the Coriolis force due to the secondary flow and angular velocity is in the direction of the pipe axis. This secondary Coriolis force yields a characteristic influence on the flow, and distorts both the velocity and temperature fields from their patterns under stationary conditions.

In a second report, Mori, et al. [104] extended their work to include both an experimental and a theoretical analysis of the turbulent regime with fully developed velocity and temperature fields. Applying a boundary layer technique, it was found that the increase in Nusselt number and flow resistance for turbulent flow, when compared to those without a secondary flow, are less than the corresponding increase for laminar region. Thus, the influence of a secondary flow produced by the Coriolis force is not as significant in turbulent flow as in laminar flow. The increase in mean Nusselt number is more than 10 percent, and a little variation of the local Nusselt number in the circumferential direction was shown to exist. Moreover, experimental

results of heat and mass transfer obtained by using the naphthalenesublimation technique in laminar, and turbulent regions are in good agreement with the theoretical solution.

Cannon and Kays [105] examined heat transfer to a fluid flowing through a pipe rotating about its horizontally aligned axis. That can be applied to cooling power transmission rotating shafts. Their experimental results revealed that rotation stablized laminar flow and delayed transition to turbulence to higher Reynolds numbers. However, in other cases transition was characterized by periodic bursts of turbulence due to local collapse of the rotating laminar structure, and hence heat transfer was found to be a mixture of laminar conduction and turbulent mixing of the bursts.

Flow and heat transfer in a circular tube rotating about an axis parallel to its axis, have been considered recently in many theoretical and experimental works. Also the effect of rotation on the hydrodynamic and thermal characteristics was treated in detail according to its significant practical importance in the design of cooling systems for electrical machines. Morris [106], and Davis and Morris [107] studied such a model to examine the influence of rotation on laminar convection when the fluid flows through a vertical tube rotating about a parallel axis subjected to a uniform heat flux. Solutions obtained for the velocity and temperature distributions by using a series expansion are valid only for low rates of heating. Their results indicated clearly that rotation induces a secondary free convection flow in a plane perpendicular to the axis, and caused a distortion in both the velocity and temperature profiles which modify the resistance to the flow and heat transfer rate.

Secondary flows augment the flow resistance and heat transfer coefficient. Mori and Nakayama [108] employed an analytical procedure

to analyze the effect of the secondary flow on convective heat transfer to laminar flow in a straight pipe rotating about a parallel axis. Their analysis of fully developed flow under uniform heat flux showed that, the secondary flow is driven by centrifugal buoyancy in almost the whole region of the cross section, and distorts the axial flow and the temperature distributions. Apparently, this is similar to the gravity distortion in a horizontal heated pipe. However, the results indicated that the effect of Coriolis force is to rotate the plane of symmetry to a plane passing through the pipe axis and the axis of rotation. Consequently, this will reduce the secondary flow which reduces both the pressure drop and the heat transfer rate. Further, this phenomenon becomes more evident in a pipe with a small radius of rotation and constant circumferential velocity, due to the increase of the Coriolis effect.

Humphreys, Morris, and Barrow [109] experimentally studied the characteristics of the local and mean heat transfer for air in turbulent flow through the entrance region of a tube rotating about a parallel axis. The authors pointed out that the development of the secondary flow components in a plane perpendicular to the main flow direction caused under the influence of a body force, an asymmetry in the thermal boundary condition, or an inherent characteristic of the flow. In any real situation, these components may occur simultaneously. However, in an attempt to obtain a clear understanding of these individual secondary flow effects, their treatment of this problem illustrated which one of the effects in dominant. Also their results showed a significant change in heat transfer over the range of Reynolds numbers and rotational rates studied. For higher rotational speeds, it was observed that the combined effect of entry swirl and

centrifugal buoyancy dominated the heat transfer, not the Reynolds number.

Measurement of heat and mass transfer coeffecients were considered by Sakamoto and Fukui [110] for air and oil flowing through a rotating tube about a parallel axis. Results showed that the significant increase in heat and mass transfer over the range of rotational speed, 420-2700 rpm, are closely related to the increase of rotational number and Graetz number.

Studies of flow and heat transfer in square-sectioned tubes rotating about a parallel axis with laminar or turbulent flow are few and very limited. Recently Morris [101], analyzed theoretically this case for laminar and turbulent heated flow. However, limited data are available to determine the flow resistance and heat transfer.

Neti, et al. [111,112] presented a finite difference solution of laminar heat transfer for air in a rotating rectangular duct of aspect ratio two. Their results showed the effect of the secondary flow caused by the Coriolis force and density gradient on heat transfer and pressure drop characteristics. Moreover, solutions for Nusselt number and friction factor were obtained in both the inlet and fully developed regions for different Grashof and Reynolds numbers.

Study of flow and heat transfer due to rotating disks has been considered with great concern, in view of its relevant importance in cooling design and performance. Recently, Luk, Millsaps, and Pohlhausen [113] developed an exact solution for the combined free and forced convection in flows adjacent to a uniformly heated rotating disk. Solutions of velocity and temperature fields were obtained by numerically solving the system of governing equations.

Riley [114] considered situations in which rotating fluid is bounded by plane surfaces having the same angular velocity. Initially both fluid and plane are in a solid body rotation. However, changes in the boundary temperature disturbed the rotation of the fluid, since changes in temperature yields density changes which will modify the effect of pressure gradient, and thus a radial flow will be developed. Analysis was confined to fluids of small viscosity such that the resulting radial flow disturbances are effectively considered to be in a thin Ekman layer near the surface.

By using a boundary layer approach, Edwards [115] obtained a solution for the problem of heat transfer at the boundary of a finite disk rotating with the same angular velocity as the fluid.

Furthermore, Kreith, Dougham and Kozlowski [116], conducted an experimental study of mass and heat transfer from an enclosed rotating disk. Correlations for heat and mass transfer were developed for turbulent flow, as well as the visual study of the flow pattern.

Axisymmetric convection in a fluid contained between two finite infinite horizontal disks rotating about a vertical axis with the same angular velocity was presented by Duncan [117]. In his investigation inertial accelerations were neglected in comparison with Coriolis accelerations and viscous effects are confined to Ekman layers at the disks. Conditions required for either conduction or convection to predominate. The corresponding structures of the velocity and temperature fields were also discussed.

Centrifugally driven thermal convection in a vertical rotating cylinder heated from above, have recently been considered by Homsy and Hudson [118]. By applying boundary layer methods, solutions for both conducting and insulated side walls boundary conditions, were obtained on top, bottom, and in the inviscid core of the cylinder, where the axial flow was strongly influenced by the horizontal Ekman layers. Critical parameters governing the solutions in all boundary conditions

were found to be the aspect ratio, the Prandtl number, the Ekman number and the thermal Rossby number for the flow. Moreover, gravity is seen to have at most only a local effect on the flow near the side walls, whereas the heat transfer was considerably increased by rotation. In a further study [119], the same authors extended their analysis to reveal the effect of the side wall and heat losses on the Nusselt numbers which was determined for the top and bottom surfaces of the cylinder, where constant heat flux boundary conditions have been applied instead of the isothermal conditions considered in [118].

Abell and Hudson [120] examined this problem experimentally in an effort to provide more physical insight into the mathematical analysis and the experimental data. Distinction between rotating and non-rotating convection due to the various important forces involved was presented in terms of the centrifugal acceleration, which is a strong function of the radial position, and the Coriolis acceleration that may play a significant role in transfering heat as a consequence of the induced secondary flow. Nusselt number correlations were derived for low and high visosity oil in terms of thermal Rossby and Ekman numbers which reflect the influence of temperature difference and rotational rate in increasing the heat transfer rate.

The stability of a horizontal layer of fluid heated from below subject to the gravity field and the Coriolis force resulting from a rotation about a vertical axis normal to the surface was examined by Chandrasekhar [121]. It was shown that the effect of the Coriolis force is to inhibit the onset of convection; and that the extent of the inhibition depends on the value of Taylor number. Critical Rayleigh number for the onset of convection as a function of Taylor number was determined for three types of boundary conditions: (a) both boundary

surfaces free, (b) both boundary surfaces rigid, and (c) one boundary surface free and the other rigid.

Veronis [122,123] has conducted a numerical study of Benard convection in a rotating fluid confined between free boundaries over a certain range of Taylor, and Rayleigh numbers. In his analysis it was indicated that for Prandtl number greater than /2 the velocity and temperature fields were dominated by the rotational constraint even for moderate values (10<sup>3</sup>) of Taylor number. That is, the horizontal temperature gradients is largely balanced by the vertical shear of the velocity component normal to the temperature gradient. On the other hand, for Prandtl number less than /2, the possibility of a finite-amplitude instability at subcritical Rayleigh number exhibited a different structure of steady velocity and temperature fields from that of a fluid with large Prandtl number. Nonetheless the heat flux, once convection is established, was closely dependent on both the Rayleigh and Taylor numbers.

Recently, an extensive study of Benard convection with and without rotation was presented by Rossby [124]. Stability of fluids was considered in detail relative to parameters describing its state such as Rayleigh, Taylor, and Prandtl numbers. Measurements performed on two Prandtl numbers corresponding to water and mercury exhibited markedly different behaviors. The results for water showed excellent agreement with the predictions of the linear stability theory. At Taylor number greater than  $5\times10^4$ , the presence of a subcritical instability appeared at larger Taylor numbers. Thus, the difference between the measured critical Rayleigh number and that predicted by Chandrasekhar's linear stability theory [121] is as much as 30 percent. Further, water exhibited a maximum heat flux at large Taylor which is an increasing function of Rayleigh number, and that was attributed to 'Ekman-layer

like' modification of the viscous boundary layer. In contrast, mercury responded quite differently from water, and consequently the heat flux was found to be a decreasing function of Taylor number. This was evident, because oscillatory convection was the preferred mode which is inefficient at transporting heat, and no steady flow was observed. Nusselt number results were also plotted as a function of Rayleigh number for three values of Taylor number.

Catton [125] has employed the Landau method to analyze the effect of rotation on natural convection in horizontal liquid layers. Convective heat transfer was measured over a wide range of Rayleigh and Taylor numbers. Results compared quite well with Rossby's experimental results up to a Taylor number  $10^{5}$ . However, the theoretical predictions were found to deviate at large Rayleigh numbers and this deviation was believed to be due to centrifugal effects in thinning the boundary layers.

Effects of centrifugal convection on the onset of gravitational instabilities of a bounded rotating fluid heated from below was treated by Homsy and Hudson [126]. In their treatment, dependence of the dimensionless temperature, velocity field, and thus the Nusselt number on Prandtl number, Ekman number, aspect ratio, inverse Froude number, and thermal Rossby number was emphazised. Furthermore the authors pointed out that the centrifugal effects can account for the distortion of the vertical temperature gradient, and therefore, for the initial increase of the Nusselt number which was observed in Rossby's experiment. In addition, the effect of the centrifugal circulation away from the cylinder wall was found to increase the critical Rayleigh number at which gravitational instability may exist.

For large Rayleigh numbers in excess of 10 , Hunter and Riahi [127] conducted a theoretical study of nonlinear convection in a

horizontal layer of fluid rotating about a vertical axis. From their solutions, obtained by using the boundary layer method, it was noted that the influence of rotation should not always be to delay the onset of convection, because the heat transfer was increased in the intermediate range of rotational parameter. In addition, maximum heat transfer was attained when the thermal and Ekman boundary layers coincide.

Using the Galerkin method, Clever and Busse [128] showed the existence of a steady subcritical finite amplitude two-dimensional solutions in a horizontal fluid layer heated from below for Prandtl numbers less than one. This was established by superimposing arbitrary three-dimensional cellular convection. Transition from two dimensional roll-like convection to three-dimensional cellular convection was also considered in detail in their analysis. In this event, results indicated that beyond a certain Rayleigh number for a large range of rotational rates, Coriolis forces enhance the Nusselt number, but there is no evidence that heat transport in a rotating layer will exceed the heat transport in a non-rotating layer at a given value of the Rayleigh in the case of large Prandtl number.

A recent theoretical and experimental study of thermal cellular convection in rotating rectangular boxes by Buhler and Oertel [129], was centered on the effects of variable Prandtl numbers. Linear stability theory with Boussinesq approximations was employed in the analysis and a differential interferometer was used to study the stability behavior and the configuration of the three-dimensional convection flow. The computations showed that the roll-cells change their orientation with increasing Taylor number, and concluded that the centrifugal forces dominate in high Prandtl fluids, while the Coriolis force dominates in low Prandtl number fluids.

In closing this review, it is fitting to mention the vital role played by the analytical, numerical, and experimental studies in describing the fundamental aspects and demonstrating the influence of rotation on the convective heat transfer in ducts of arbitrary crosssection which are constrained to rotate in either a parallel or orthogonal modes. In addition, natural convection was only considered in enclosures differentially heated in the vertical direction (Benard convection, or heated from above), and rotated about a vertical axis passing through the center point of the enclosure. Unfortunately, all theoretical and experimental investigations to date have not included the influence of Coriolis acceleration and buoyant interaction between centrifugal and gravitational buoyancy on the flow and heat transfer in a differentially heated enclosure rotating about its longitudinal horizontal axis. Therefore the purpose of this experimental study is to investigate the effect of the additional controlling parameters, like the Coriolis acceleration and centrifugal buoyancy on the flow and heat transfer mechanisms relative to the non-rotating situation. The way in which rotation affects the variations of local and mean Nusselt number will be presented when the enclosure is at angular positions of 90 deg. (vertical configuration), 180 deg. (heated from below), and 0 deg. (heated from above).

On the whole, the articles presented in this review are by no means the only important ones; but the intent was to emphazise on the essential part of the basic source materials related to the subject treated in this investigation.

2.1

consi

enclo

under

surfa angle

basis

abov

incli

enclo

horiz

conve

inclu

Conti

#### CHAPTER 2

#### MATHEMATICAL FORMULATION

## 2.1 Governing Equations

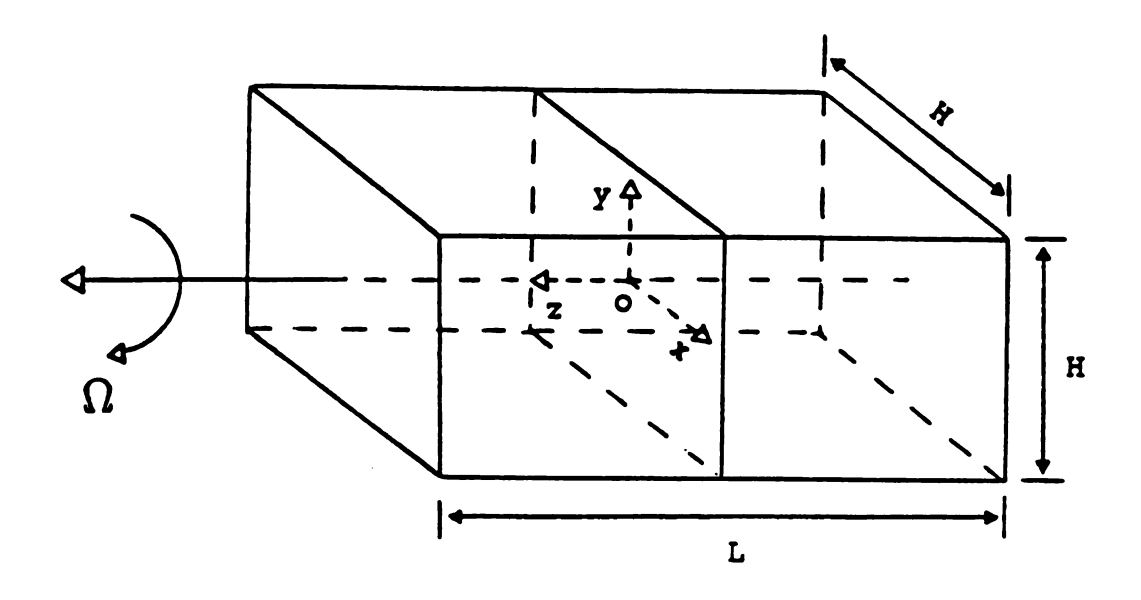
In the present work, the problem of natural convection is considered in a square cross-section rectangular air-filled enclosure of side H and horizontal length L, as is shown in figure 1. The enclosure is differentially heated from the sides, which are maintained under an isothermal temperature conditions, whereas all the other surfaces are insulated. The inclination angle,  $\phi$ , is defined as the angle between the horizontal plane and the cold surface. On this basis, inclination angles less than 90 deg. represent heated from above, and greater than 90 deg. heated from below. In addition, inclinations of 90 deg. and 180 deg. describe respectively a vertical enclosure (differentially heated in the horizontal direction), and a horizontal enclosure (heated from below).

The governing conservation equations for laminar natural convection of Newtonian fluids with the gravitational body force included in the momentum equations are written as follows:

Continuity Equation

$$\frac{\partial \rho}{\partial t} + \nabla \cdot (\rho \vec{v}) = 0 \tag{2.1}$$

a) Three-dimensional enclosure, rotating about the z-axis



b) Section through xy plane

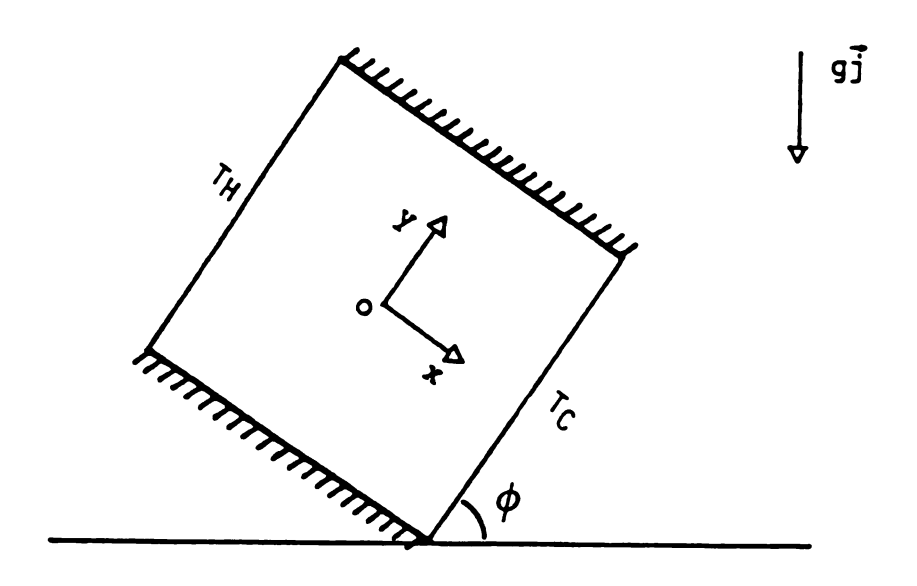


Figure 1 Geometric configurations of the enclosure.

Momentum Equations

$$\rho \stackrel{\overrightarrow{Dv}}{Dt} = - \nabla p + \rho \nu \nabla^2 \overrightarrow{v} + \frac{1}{3} \rho \nu \nabla (\nabla \cdot \overrightarrow{v}) + \rho \overrightarrow{g}$$
 (2.2)

**Energy Equation** 

$$\rho C_{\mathbf{p}} \frac{\mathbf{DT}}{\mathbf{Dt}} - \nabla \cdot \mathbf{k} \nabla \mathbf{T} + \mu \Phi \tag{2.3}$$

The boundary conditions, assuming insulated means adiabatic, can be stated as,

$$x = -\frac{H}{2}$$
,  $u = 0$ ,  $v = 0$ ,  $w = 0$  and  $T = T_H$  (2.4)

$$x = +\frac{H}{2}$$
,  $u = 0$ ,  $v = 0$ ,  $w = 0$  and  $T = T_C$  (2.5)

$$y = -\frac{H}{2}$$
,  $u = 0$ ,  $v = 0$ ,  $w = 0$  and  $\frac{\partial T}{\partial y} = 0$  (2.6)

$$y = +\frac{H}{2}$$
,  $u = 0$ ,  $v = 0$ ,  $w = 0$  and  $\frac{\partial T}{\partial y} = 0$  (2.7)

$$z - + \frac{L}{2}$$
,  $u - 0$ ,  $v - 0$ ,  $w - 0$  and  $\frac{\partial T}{\partial z} - 0$  (2.8)

$$z = -\frac{L}{2}$$
,  $u = 0$ ,  $v = 0$ ,  $w = 0$  and  $\frac{\partial T}{\partial z} = 0$  (2.9)

# 2.2 Governing Equations of a Fluid in an Enclosure which Rotates About its Longitudinal Axis in the Horizontal Direction

In this section the enclosure is constrained to rotate with uniform angular velocity,  $\Omega$ , about its longitudinal axis. Figure 2 illustrates the rotational flow configuration. Let the motion of a

typical particle A be referred to the cartesian frame 0-XYZ, rotating with the enclosure, and origin located on the axis of rotation (z-axis).

The position vector,  $\overrightarrow{r}$ , of A relative to the origin 0 of the inertial frame is,

$$\vec{r} = x\vec{i} + y\vec{j} + z\vec{k} \tag{2.10}$$

where i, j and k are the unit vectors in the ox, oy, oz directions and x, y and z are the coordinates in the inertial frame oxyz. The angular velocity vector is,

$$\vec{\omega} = \Omega \vec{k} \tag{2.11}$$

Now, the velocity and acceleration vectors with respect to the inertial frame at 0, can be written as,

$$\vec{v} = \frac{d\vec{r}}{dt} = \frac{\partial \vec{r}}{\partial t} + (\vec{\omega} \times \vec{r}) ; \quad \frac{\partial \vec{r}}{\partial t} = \vec{v}_r$$

or

$$\vec{\mathbf{v}} - \vec{\mathbf{v}}_{\mathbf{r}} + (\vec{\omega} \times \vec{\mathbf{r}}) \tag{2.12}$$

$$\left(\frac{\overrightarrow{Dv}}{Dt}\right)_{\text{inertial}} = \left(\frac{\overrightarrow{Dv}}{Dt}\right)_{\text{rotational}} + \overrightarrow{\omega} \times \overrightarrow{v} \qquad (2.13)$$

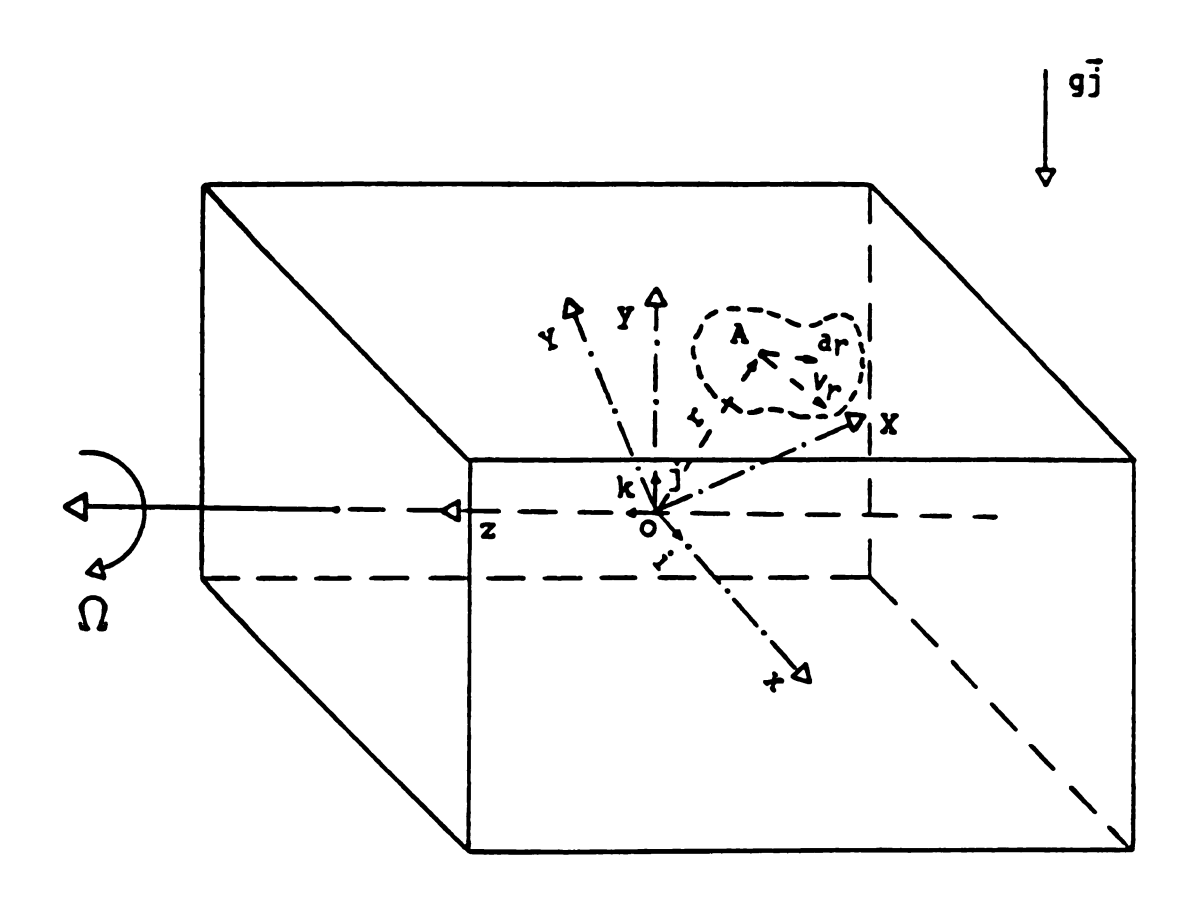


Figure 2 Rotation referred to a Cartesian frame of reference, O-XYZ.

Su

No

V

Th

in

an

equ

o Dt

Substitution of equation (2.12) into equation (2.13) gives,

$$\left(\frac{\overrightarrow{Dv}}{Dt}\right)_{\text{inertial}} - \left(\frac{\overrightarrow{Dv}_r}{Dt}\right)_{\text{rotational}} + 2\overrightarrow{\omega} \times \overrightarrow{v}_r + \overrightarrow{\omega}(\overrightarrow{\omega} \times \overrightarrow{r}) \qquad (2.14)$$

Note that the two terms from equation (2.14) involving the angular velocity of the rotating frame are used to determine the acceleration with respect to the inertial frame oxyz.

The term  $\vec{\omega} \times (\vec{\omega} \times \vec{r})$  represents the centrifugal acceleration, whereas  $2\vec{\omega} \times \vec{v}_r$  represents the Coriolis acceleration. It is also desirable to indicate that,

$$\vec{\omega} \times (\vec{\omega} \times \vec{r}) = -\Omega^2 \vec{r}_1 \quad , \quad \vec{r}_1 = x\vec{1} + y\vec{j}$$
 (2.15)

and

$$\nabla^{2}(\vec{\mathbf{v}}_{\mathbf{r}} + \vec{\omega} \times \vec{\mathbf{r}}) = \nabla^{2}.\vec{\mathbf{v}}_{\mathbf{r}}$$

$$\nabla.(\vec{\mathbf{v}}_{\mathbf{r}} + \vec{\omega} \times \vec{\mathbf{r}}) = \nabla.\vec{\mathbf{v}}_{\mathbf{r}}$$
(2.16)

Under these conditions the momentum equations (2.2) yield, using equations (2.14), (2.15) and (2.16),

$$\rho \frac{\overrightarrow{\text{Dv}_r}}{\text{Dt}} + 2\rho \vec{\omega} \times \vec{v}_r - \rho \Omega^2 \vec{r}_1 = -\nabla p + \rho \nu \nabla^2 \vec{v}_r + \frac{1}{3} \rho \nu \nabla (\nabla \cdot \vec{v}_r) + \rho \vec{g} \qquad (2.17)$$

a į Applying the generalized Boussinesq approximations [118,130] in the equations of motion, which are based on the assumption of constant physical properties, except the density when multiplied by the centrifugal force or gravity, and negligible viscous dissipation. The equation of state of the fluid is,

$$\rho = \rho_{\rm c} [1 - \beta(\text{T-T}_{\rm C})] \tag{2.18}$$

and the continuity equation is

$$\nabla . \vec{v}_r = 0 \tag{2.19}$$

these can be substituted in equation (2.17) to give,

$$\frac{\overrightarrow{Dv_r}}{\overrightarrow{Dt}} - \nu \overrightarrow{\nabla^2 v_r} - \frac{\overrightarrow{\nabla p_1}}{\rho_c} - 2\overrightarrow{\omega} \times \overrightarrow{v_r} - \beta (T - T_C) \Omega^2 \overrightarrow{r_1} - \beta (T - T_C) \overrightarrow{g} \qquad (2.20)$$

where,

$$p_1 = p + \rho_c gy - \rho_c \left[ \frac{1}{2} (\Omega^2 r_1^2) \right]$$
 (2.21)

and  $\boldsymbol{p}_1$  is defined as the perturbation pressure.

In this respect, equations (2.3), (2.19), (2.20) can be written in nondimensional forms. As follows

$$\vec{R} - \frac{\vec{r}_1}{H}$$

3

P: Fo

۷.۶

ÿ.

$$\vec{v}_r - H \frac{\vec{v}_r}{\alpha}$$

$$r - \frac{\alpha t}{H^2}$$

$$p_2 - \frac{H^2}{\alpha \nu \rho_2} p_1$$
(2.22)

$$\theta = \frac{\mathbf{T} - \mathbf{T}_{\mathbf{C}}}{\mathbf{T}_{\mathbf{H}} - \mathbf{T}_{\mathbf{C}}}$$

Continuity Equation

$$\nabla . \vec{\nabla}_r = 0 \tag{2.23}$$

Energy Equation

$$\frac{\mathrm{D}\theta}{\mathrm{D}\tau} = \nabla^2\theta \tag{2.24}$$

Momentum Equations

$$\frac{1}{Pr} \frac{D\vec{V}_r}{D\tau} - \nabla^2 \vec{V}_r - \nabla P_2 - (Ta)^{1/2} (\vec{k} \times \vec{V}_r) - Ra_r \theta \vec{R} + Ra \theta \vec{J} \qquad (2.25)$$

For the onset of steady convection the following set of equations can be deduced from (2.23), (2.24), and (2.25)

$$\nabla.\vec{\nabla}_r = 0 \tag{2.26}$$

$$\vec{\nabla}_r \cdot \nabla \theta = \nabla^2 \theta \tag{2.27}$$

a

f

re

iı

ef

the con

$$\frac{1}{Pr} (\vec{v}_r \cdot \nabla - \nabla^2) \vec{v}_r = - \nabla p_2 - (Ta)^{1/2} (\vec{k} \times \vec{v}_r) - Ra_r \theta \vec{R} + Ra \theta \vec{j}$$

(2.28)

The important dimensionless parameters entering the equations of motion are

$$Ra = \frac{g\beta H^{3}(T_{H} - T_{C})}{\alpha\nu}$$
 (Rayleigh number)
$$Ra_{r} = \frac{\beta(T_{H} - T_{C})\Omega^{2}H^{4}}{\nu\alpha}$$
 (Rotational Rayleigh number)
$$Ta = \frac{4\Omega^{2}H^{4}}{\nu^{2}} - (2Re)^{2}$$
 (Rotational Reynolds number)
$$Re = \frac{\Omega H^{2}}{\nu^{2}}$$
 (Rotational Reynolds number)

Equations (2.28) give the correction terms required to specify the acceleration vector of the inertial frame with respect to the rotating frame. For instance the second term on the right characterizes the influence of Coriolis forces, the third and last terms represent respectively the centrifugal and the gravitational buoyancy forces effect.

(Rotational Reynolds number)

Evaluation of equations (2.28) in a non-rotating enclosure give the appropriate equations of motion, that describe steady natural convection in vertical or inclined enclosures. Accordingly, all the

terms involved with the angular velocity will become zero, and other terms will be referred to the inertial frame. Thus equations (2.26), (2.27) and (2.28) may be written in a non-rotating frame as,

$$\nabla . \vec{\nabla} = 0 \tag{2.29}$$

$$\vec{\nabla} \cdot \nabla \theta - \nabla^2 \theta \tag{2.30}$$

$$\frac{1}{Pr} (\vec{\nabla} \cdot \nabla - \nabla^2) \vec{\nabla} = - \nabla p^1 + Ra \theta \vec{j}$$
 (2.31)

It must be remembered, however, that the components of equations (2.31) along the x, y and z directions will give the equations of motion for the inclined enclosure.

#### CHAPTER 3

## EXPERIMENTAL FACILITIES AND TECHNIQUES

#### 3.1 Mach-Zehnder Interferometer Facilities

The importance of interferometry for heat transfer studies is due to the fact that interferometr provides a non-intrusive, instantaneous and complete quantitative measurement of the refractive index, and subsequently the temperature field. The refractive index changes through the medium imply changes in the density which in turn reveal the temperature distribution.

The basic geometrical arrangement of the Mach-Zehnder interferometer is illustrated in Figure 3. It contains two beamsplitters S1,S2 and two mirrors M1,M2 which occupy the corners of a rectangular frame.

Light from a high pressure mercury lamp LS passes a dual filter F, to a condenser system L1,L2 which in turn focusses the light beam on a small mirror m1, which acts as a point light source for the system. This is properly adjusted to be at the focal point of the parabolic mirror C1. Light collimated into a parallel beam by C1, enters the interferometer through the beamsplitter S1. At S1, approximately half of the light is reflected and half is transmitted. The two parts of the original beam will be called, beam I (measuring beam), and beam II (reference beam) respectively. In Figure 3, the partially-reflecting surfaces are marked by heavy lines.

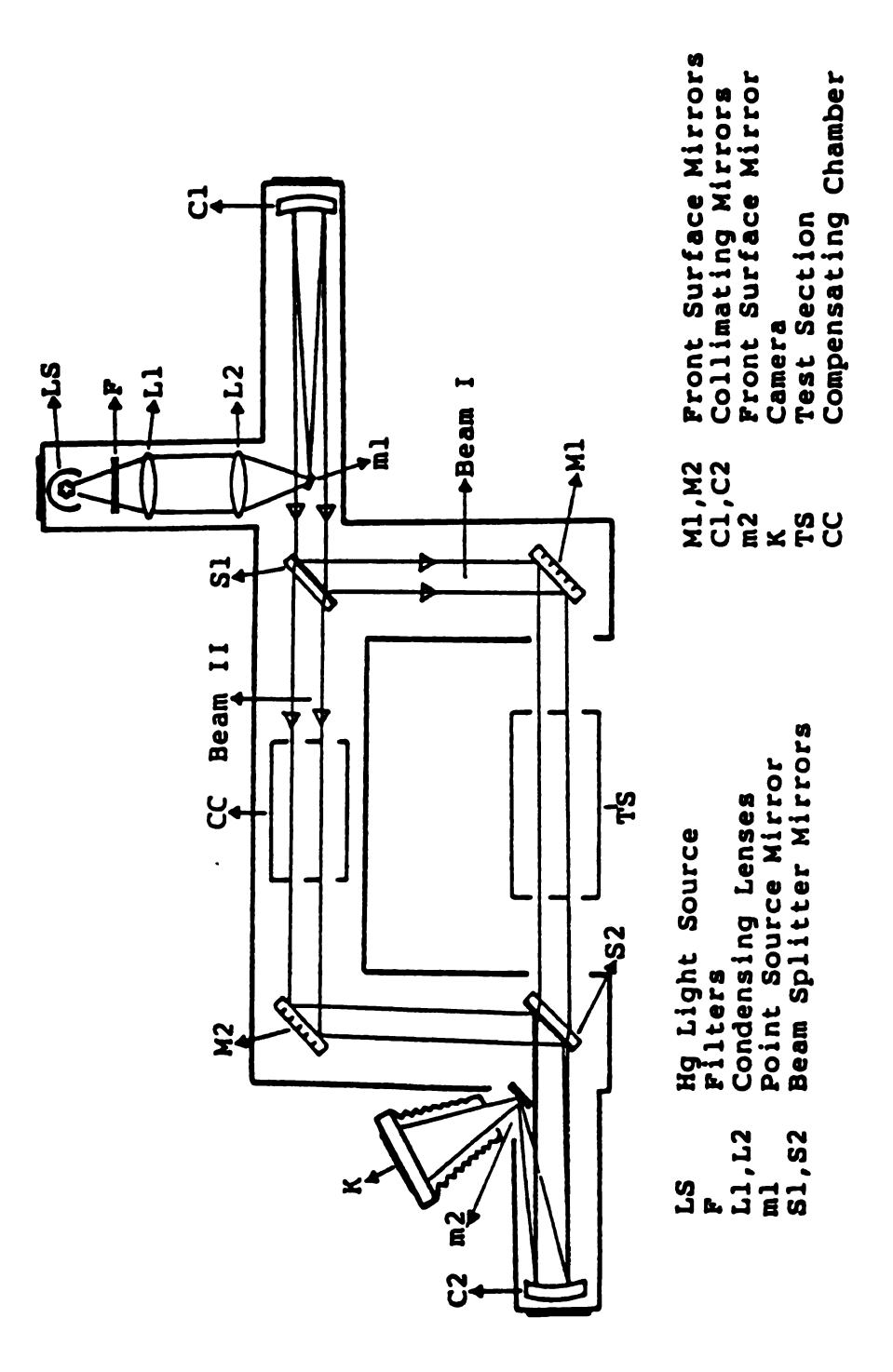


Figure 3 Mach-Zehnder Interferomter

Beam I, the reflected portion of the light beam is totally reflected from plate M1 to plate S2. At S2, half of beam I is transmitted through the reflecting coating toward the screen, and the other half is the unused part. In this event, it is appropriate to mention that the small amount of reflection within the splitter plates S1,S2 has no adverse effects on the interference patterns.

In contrast, beam II, the transmitted part of the light beam, is totally reflected on plate M2, and travels toward the semi-reflecting plate S2, where it is divided into reflected and transmitted parts. In this case, the transmitted beam is the unused portion. Finally, the transmitted part of beam I is then recombined with the reflected part of beam II at plate S2 which in turn can lead to interference patterns. When the light paths of the two coherent beams I and II are exactly equal, an infinite fringe field will appear. On the other hand, interference fringes can be seen by rotating either plate M2, or S2 through a few angular minutes. A further rotation of any plate will then change the location as well as the structure of the fringes. This is desirable because fringes can be focussed at the test plane, so that an interfence-photograph may be taken for analysis.

Interference fringes, are then reflected by the spherical mirror C2, toward a small mirror m2, which serves to focus the test plane and the interference fringes on a photographic film or a ground glass screen K. In Figure 3, TS represents the test section and CC the compensating chamber with identical windows, the later is being used to produce equal optical paths through the test section glass. Figure 4 shows a picture of the interferometer with the experimental setup. Comprehensive studies and adjustements of the Mach-Zehnder Interferometer are available in [131-146].

3.1

10

wh tr

su li

li vi

> no re

a c

s

d:

f

C

### 3.1.1 Optical Plates

The interferometer consists typically of two beamsplitters, 10.16 cm in diameter, coated with a non-metallic evaporated coating which absorbs a few percent, while it gives nearly 50 percent transmission and reflection.

The full mirrors M1,M2 are 10.16 cm in diameter, are front surface coated with aluminum, and reflect more than 90 percent of the light. All surfaces are flat to better than 1/4 wavelength of green light (5461Å). This would give exactly parallel fringes of constant width.

The interferometer adjustment requires that, all the plates are mounted by gimbal mirror/beamsplitter mounts, which provide high-resolution angular orientation with coplanar, orthogonal gimbal adjustments. Further, plate M1, is mounted on a sliding guide for pure translation in order to vary the path difference.

The illuminating mirror ml is a small front surface mirror, 2 mm square suspended on a very thin wire at the center of a metal ring which can be adjusted in both the vertical and the horizontal directions in front of the parabolic mirror Cl. However, the diverting mirror m2 is a little larger, and it reflects the interference fringes from the spherical mirror C2 into a camera.

Finally, the glass windows of the test section and the compensating chamber are made of a high quality glass, accurate to 1/10 of a wavelength, and of 2.54 cm thick.



Figure 4 Interferometer and experimental setup

. 3 . • •

var e :

5<sup>99</sup> ,

## 3.1.2 Light Source

The light source LS is a 100-Watt General Electric high pressure mercury vapor lamp mounted on a support post, inside a lamp housing which allows horizontal and vertical adjustments, besides the angular orientation. Mercury light emits three wavelengths of 4410, 5460, and 5790Å, however, the dual filter placed in front the light source permits only one wavelength to pass, in order to obtain a contrast interference patterns.

# 3.1.3 Photographic Equipment

The camera used is a 4 X 5 inch Super Speed Graphic type, as shown in Figure 5. The lens has been removed from the shutter, which can be adjusted to allow the light beam to travel through the opening to either a groung glass screen or a film. For the stationary part of the experiment the shutter was operated by a cable release. However, for the rotating part the shutter was operated by an electric cable control release, equipped with two switches and an electromagnetic rotary solenoid. The switches are used to control both the timing of the cable release, and the angular location of the test section. The film used is a Polaroid 4X5 land film type 57/high speed, and medium contrast.



Figure 5 Camera setup

5 500 4

.1 3

s- 4.

Constitute to:

÷ ខណៈ ២០ ២៩៦ និ

1. L.D.

.

# .3.2 Experimental Apparatus

## 3.2.1 Moving Frame

The moving frame consists mainly of a heavy duty table, made by Economy Engineering Co. that provides, smooth height adjustment and high load capacity. The left or right height adjustment hand lever controls a gear set connected to chain-coupled drive screws which vary the jack height. The table support system is carried by V-grooved pulleys moving on two rails, which are positioned on rubber pads placed on the floor underneath the interferometer frame. The rubber pads are used to isolate the optical system from vibrations that may occur during the rotation of the test section. On the table an 88 cm long, 61 cm wide, and 2 cm thick aluminum base plate is placed, and securely fastened to the table by a bolt passing through a hole in its center. In addition, four adjusting bolts are threaded into the base plate, to provide a flexible three-dimensional adjustment of the apparatus.

Two steel shafts, 2 cm in diameter are used to carry 2.54 cm thick flanged wheels of 15.24 cm in diameter. These are mounted firmly near each end of the shaft by a screw-pin lock set, as is shown in Figure 6. At the end of each shaft a bearing is fitted, which is contained inside a bearing frame support by an aluminum block. The blocks are themselves bolted to the base plate near the corners to provide steady rotation.

Close to one end of the shafts, a gear box of reduction rate 1/40, was fixed by four bolts to the base plate, which connects one shaft through a connecting rod, and universal joints to a D.C. motor equipped with a variable speed control. Moreover, rubber 0-rings, 0.7 cm in cross-sectional diameter are fitted snugly into grooves milled in

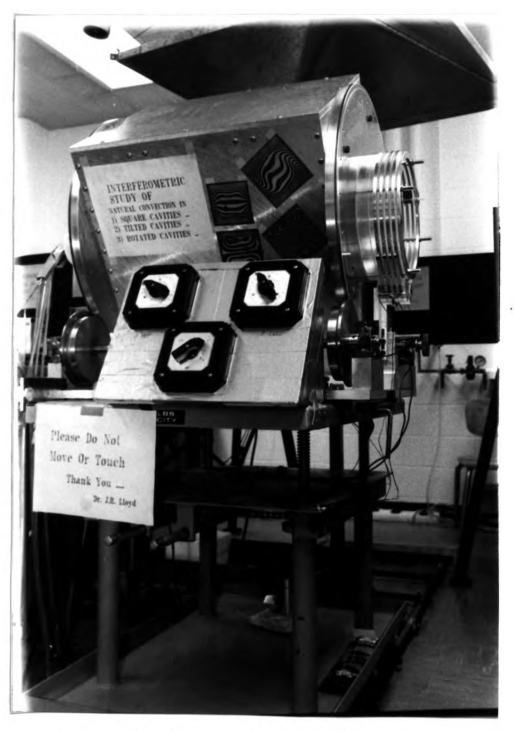


Figure 6 Moving and rotating assembly

the two wheels of the driving shaft, to avoid slipping, and add smoothness to the rotation. In general, the base plate, the shafts, and the four flanged wheels form the base for the rotating section. Figure 6 shows the picture of the moving system.

#### 3.2.2 Rotating Frame

The rotating section contains a rectangular box of, 51.435 cm long, 40.64 cm wide, and 51.435 cm high. All the side plates are made of aluminum tooling plate 1.27 cm thick, and they are bolted together with equispaced Allen bottom screws, 5 cm apart to maintain enough rigidity. The front and back side plates are made of hard aluminum (6061), 2.54 cm thick. The box itself is bounded by two hard aluminum wheels, 60.96 cm in diameter, and 2.54 cm thick, each bolted at the front and back sides by four shoulder bolts. The wheels of the rotating section are then carried securely by the four flanged wheels of the moving frame.

Inside the box four metal horizontal slotted support brackets are held by Allen screws near the corners of the top, and bottom sides, to form an adjustable support frame for the test section hot and cold plates, as shown in Figure 7. In contrast, four aluminum vertical slotted brackets are fastened by Allen screws on the front and back sides inside the box, which are used to form an adjustable support frame for the horizontal plexiglas plates of the test section. Air tight plexiglas window frames holding the optical flats are fitted by Allen screws in their position at the front and back sides of the rotating assembly to give access for the light of the measuring beam.

Thermocouple leads from the hot and cold plates can leave the rotating section through a slipring-brush assembly as displayed in,

11 12 2

res .

. . . . . . . . .

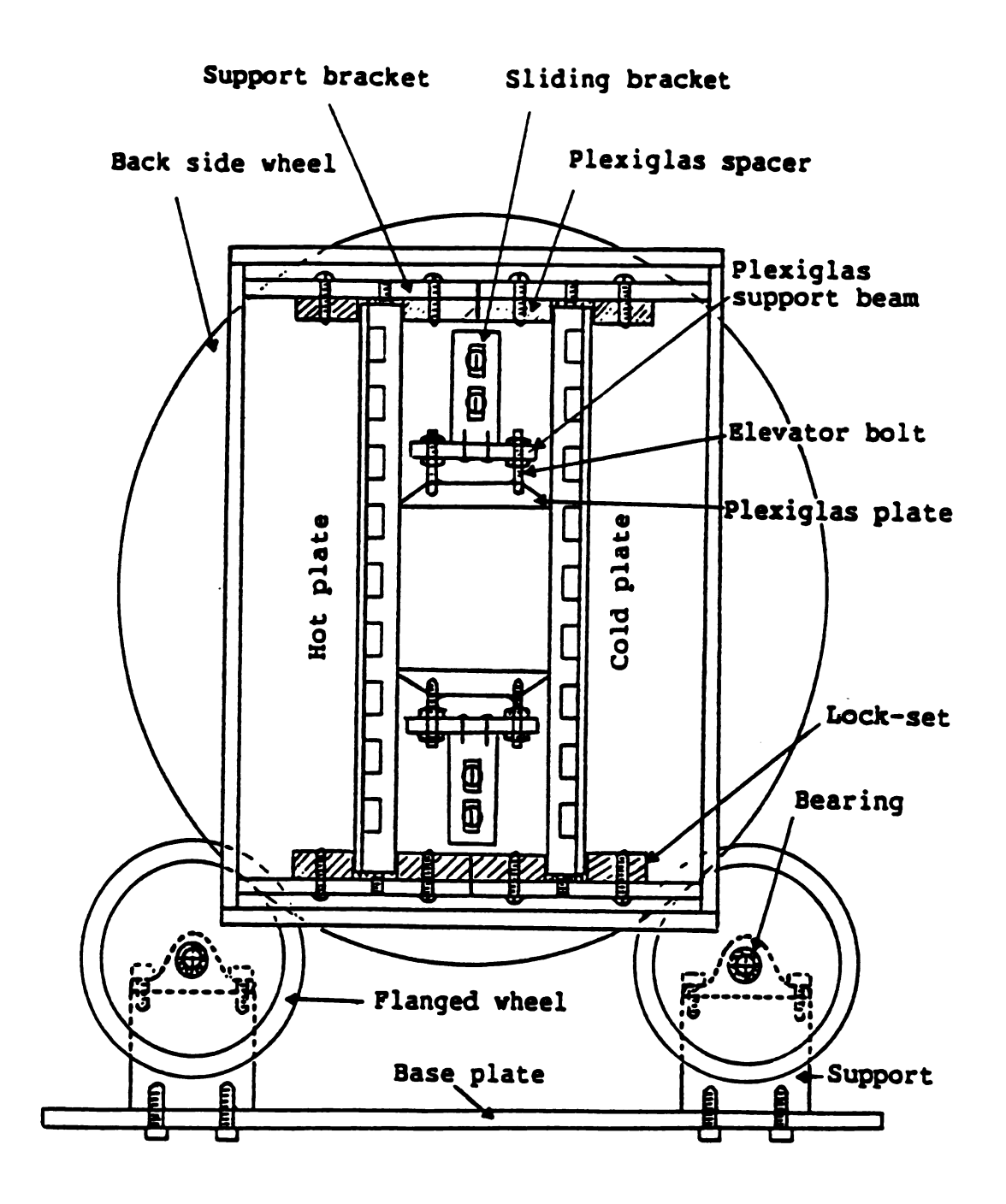


Figure 7 Side view of the test section in the rotating frame

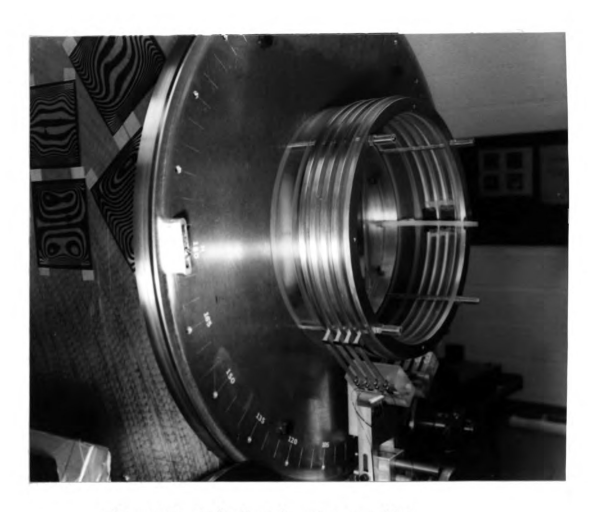


Figure 8 Slipring-brush assembly

fou flo sec

Fig

tri pic

. .

1.00 m

. . .

á ha

3 mg.

. 28

1500

70

3.:

sy

th de

tł

an

ā

Figure 8. On the other hand, the water circulation from the constant temperature baths to the hot and cold plates is established through a four channels rotary union. Both the thermocouple wiring, and the water flow will be described in later sections.

The front wheel is calibrated in, 5 deg. steps, so that the test section can be set at any angular position. In addition it carries a triggring switch for the electrical cable release. Figure 9 shows the picture of the rotating section.

#### 3.2.3 Test Section

The test section consists of two vertical aluminum plates and two horizontal plexiglas plates which are contained inside the rotating system.

The two vertical plates used in the present investigation are the same hot and cold plates employed in Bajorek's work [40], where a detailed description is given. However, it is of interest to mention that, both plates are 50.80 cm square and 2.54 cm thick, made of aluminum tooling plate. The channels for water circulation from the hot and cold constant temerature baths are, 1.27 cm wide and 1.27 cm deep milled into the back sides of the aluminum plates. The use of thick aluminum plates of high thermal conductivity, and the channel design to act as a counter flow heat exchanger are intended to balance out possible temperature gradients and to maintain isothermal working surfaces. The plates were polished to a smooth finish of 25  $\mu$ m flatness.

Copper constantan thermocouples are installed to both the hot and cold plates. The cold plate is instrumented with nineteen thermocouples. Their test junction are cememted in small holes drilled



Figure 9 Rotating section

into the back side of the plate, approximately 2.4 mm from the front surface. Eighteen thermocouples are installed to the hot plate with test junction located nearly at 4.0 mm from the front surface. Details of the thermocouple locations are reported in [40]. All thermocouple wires were fitted into grooves milled in the water channel, and left the plates through 0.318 cm holes sealed with epoxy.

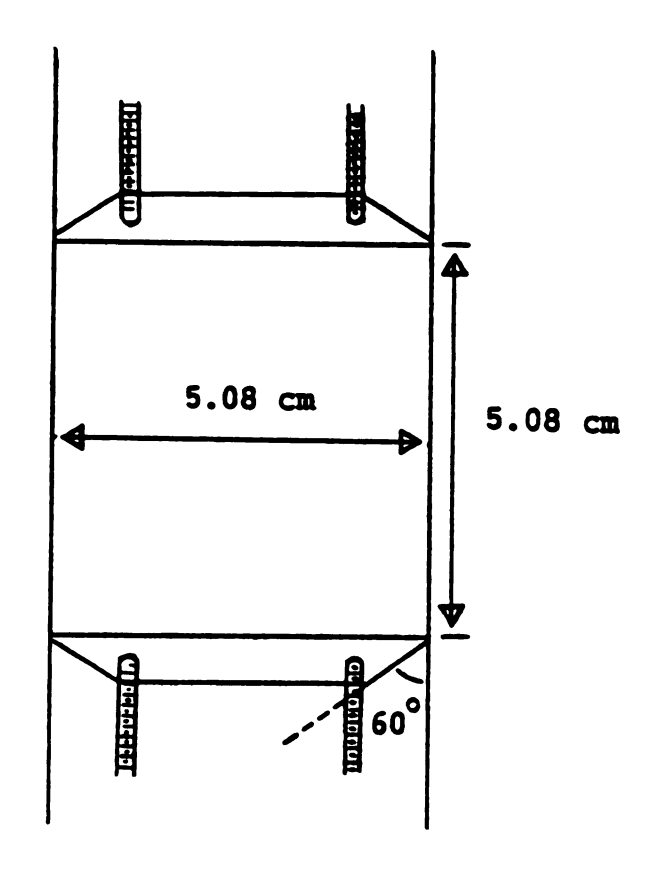
The horizontal surfaces, 5.08 cm wide, 50.80 cm long, and 1.27 cm thick, were made from clear plexiglas, in order to conduct a very small portion of heat across the horizontal plates. Moreover, the edges are milled at 60 deg. as shown in Figure 10 to keep a very small contact area with the isothermal plates, thereby reducing conduction. The test section is carefully covered with layers of fiberglass wool insulation, 7.0 cm thick to minimize the heat loss.

## 3.2.4 Thermocouple Wiring

The thermocouple wiring is accomplished in two different setups, to cover both the stationary and the rotating phases of this study.

In the stationary phase, sixteen thermocouples are carried out from each plate through a hole drilled in the back wheel of the rotating section. Thermocouple extension wires from the hot and the cold plates are connected to two rotary switches. A third rotary switch common to both switches is connected by thermocouple wires to an Omega model (MCJ) electronic ice junction, and then by copper leads to a Hewlett Packard model 3465A digital multimeter with a resolution of 0.001 mV. The common switch is used to connect either set of thermocouples to the reference junction-multimeter circuit.

For the rotating phase, a slipring-brush assembly as displayed in Figure 8 is used to transfer the thermocouple signals out of the



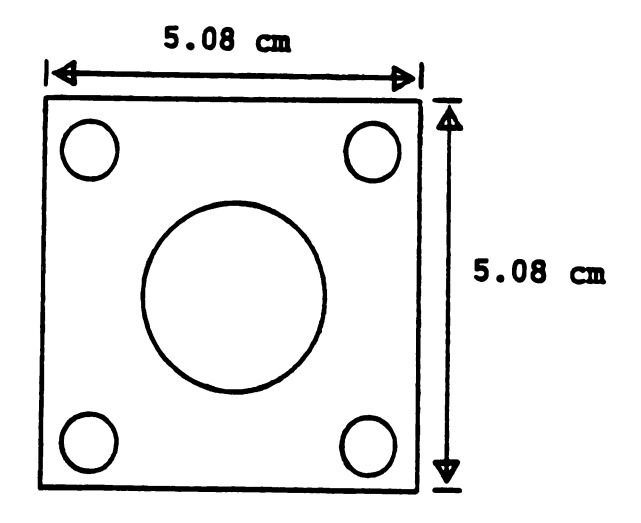


Figure 10 Dimensions of the test section and the gage block.

rotating system. The slipring assembly is composed of four silver plated copper rings, 28.575 cm in diameter, 0.635 cm wide, and 0.635 cm thick. The sliprings are supported rigidly by flanged plexiglas rings, 0.7 cm apart. The flanged rings are held together firmly by four long screws passing through holes in the plexiglas, and then bolted into threaded holes in the front wheel. Thermocouple connections to the sliprings are established by passing the extension wires through a hole drilled in the front wheel to the slipring assembly. Then the copper constantan wires are inserted snugly into small holes drilled in the plexiglas beneath the silver plated rings for a secure contact.

The brushes were made from the Graphite Metallizing Corporation type TS-109096-6 grade " silver graphalloy," an alloy of silver and graphite. According to the manufacturer's specifications it contains 50 percent silver by weight. Each brush has a front curved surface of 1.3 cm by 0.3 cm. The brush holders consist of silver plated brass spring sheets to provide the required pressure and good connection between the brushes and the external circuit. Two plexiglas blocks carried by two bolts fastened to an adjustable aluminum holder, as shown in Figure 11, are used to hold the brush holders, four on each one. An adjustable spring fitted into the two blocks is used to monitor the pressure between the brushes and the sliprings. The holder is in turn fastened to the base plate of the moving frame. Each slipring has two brushes pressing against it to insure a continuous electrical connection. The two brushes are reconnected into one wire which goes to the rotary switches of the external circuit.

Thermocouple readings are taken with and without rotation, to examine the frictional heat effect between the sliprings and the brushes. However, in all the cases the thermocouple readings varied by less than 0.05°C.

s in the second second

# 3.2.5 Temperature Controlled Section

The two vertical plates of the test section are maintained at isothermal temperature distributions by circulating hot and cold water inside the plates.

Water enters the rotating system through a four channel rotary union mounted on the back side wheel using four aluminum pipes, 0.8 cm in diameter, which are threaded into the plexiglas. Figure 12 shows the picture of the rotating union. The rotary union is designed particularly for this experiment. It consists mainly of two plexiglas disks, 10.16 cm in diameter and 2.5 cm thick. Four square grooves, 0.635 cm wide, and 1.587 cm deep are milled in each one, so that four channels, 0.635 cm square in cross-section, are formed when the two parts are fitted together. Further, small grooves, 1.5 mm wide and 0.5 cm deep, are milled inside the channels to mount teflon 0-rings, lubricated with water resistant grease to avoid any leakage, as well to prevent hot and cold water mixing.

The two parts of the union are held together by a flanged plastic ring threaded on the inner part, and pressed on teflon studs are fitted into the outer part to reduce friction. Figure 13 shows the details of this section. The outer part of the union is kept stationary relative to the one mounted at the rotating frame wheel, by using an adjustable clamp mounted on the pipes which is threaded into the outer part and then connected to a string wrapped around a spring-loaded pulley bolted to the base plate.

The cold and hot water which leave the rotating system through the rotary union are piped through a set of tygon pipes into a heat bath type D3 made by Haake Co., and a refrigerated bath model 90, made by Fisher Scientific Co. The water is then brought to the desired

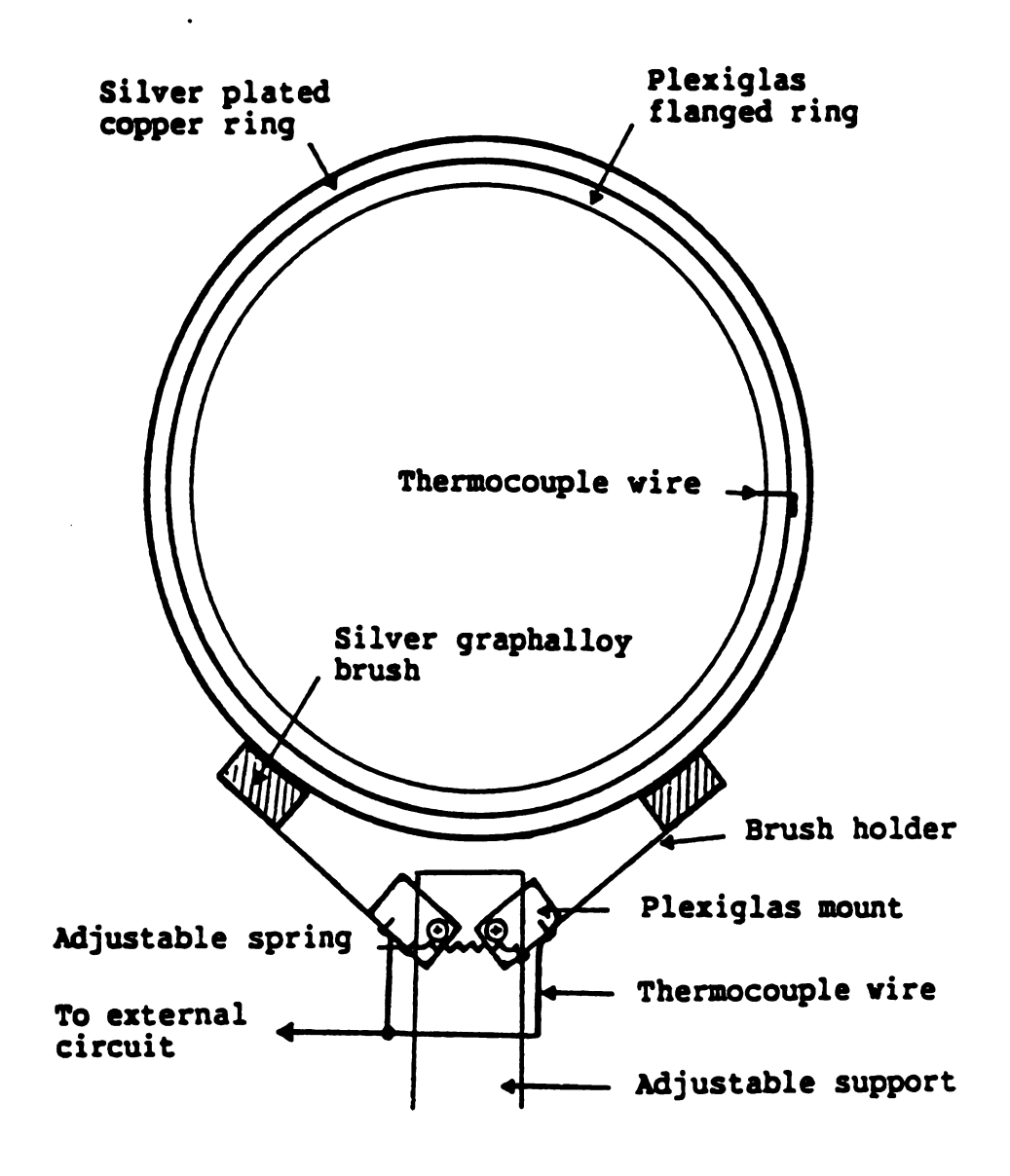


Figure 11 Schematic diagram of slipring-brush assembly.



Figure 12 Rotating union assembly

	- na Bhairte.	

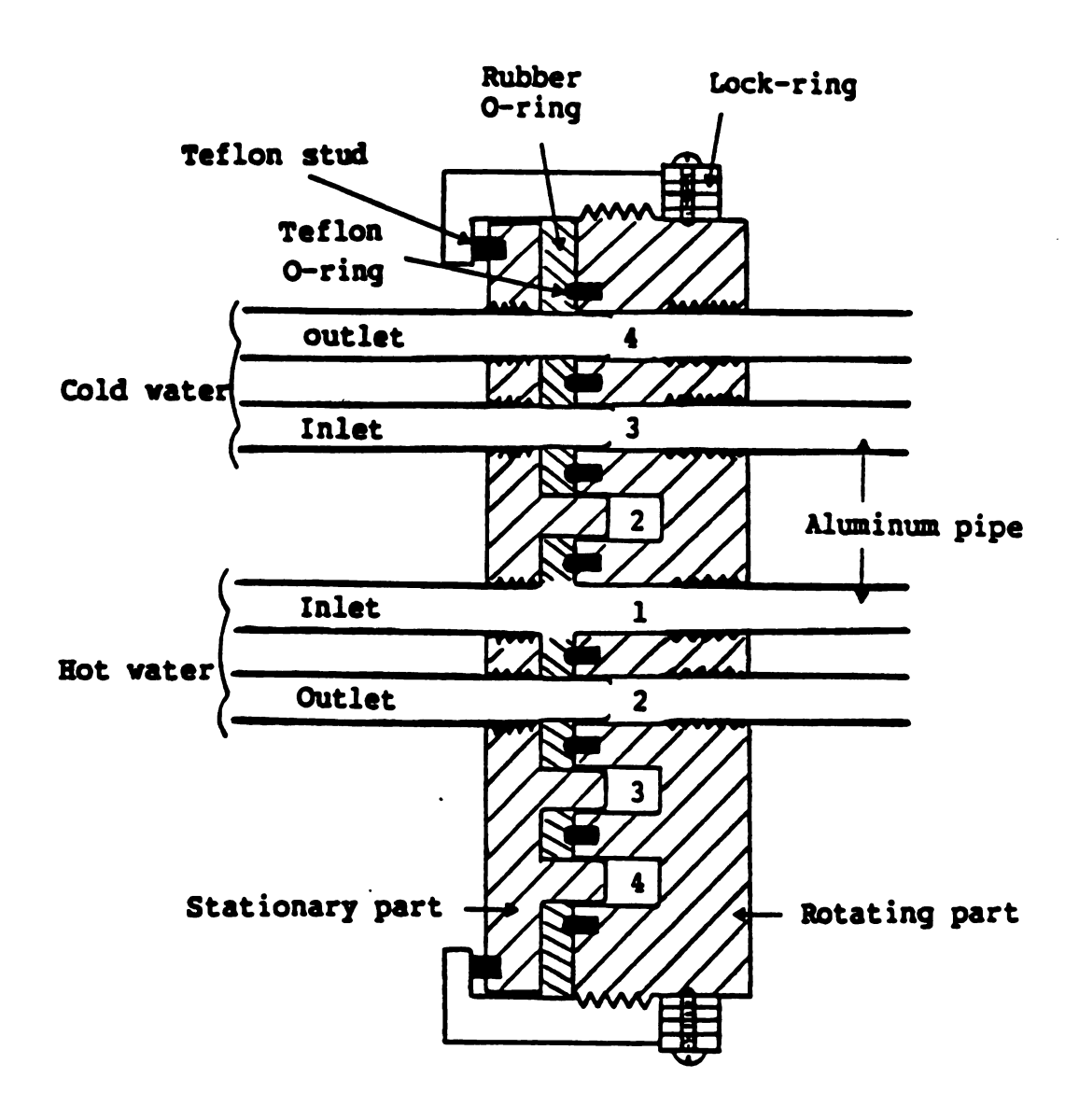


Figure 13 Schematic side view of the rotating union.

a golvino

ALC:

th ci

th

te

3.

sp va

is

of wh

ch dr

٥f

pi

Но

temperature in both baths which control the temperatures according to the manufacturer's specification to within 0.01°C of the set temperature. The water is then pumped out through tygon pipes to enter the rotating system through the inlets of the union, for a complete circulation.

# 3.2.6 Driving Motor

The rotating apparatus is driven by motor, 1/4 hp, constant speed (1750 rpm) D.C., made by Century Electric Co. It is equipped with variable speed control, manufactured by Minarik Electric Co. The power is transmitted from the motor shaft to the drive shaft, by an assembly of universal joints, steel rod, and a gear box of reduction rate 1/40, which is bolted to base plate. The output shaft of the gear box, to change direction and power, is then joined to the driving shaft. The drive motor and the variable speed control are both mounted on the top of a movable table, for adjustment requirements. Figure 14 shows the picture of the driving motor.

The speed of the rotating system can vary between 0-17.5 rpm. However, another range can be obtained by replacing the gear box.



Figure 14 DC motor with variable speed control

·

ាក្នុង ប្រសាស ។

of the state of the

· 3 . 2 ·

## 3.3 Experimental Procedure

In an experimental investigation, it is important to develop and use reliable methods for proper adjustment of the apparatus, in order to satisfy the requirements of the experiment. The subsequent sections will present the basic arrangements of test section assembly and leveling, insulation, thermocouples, inclination angle and rotational speed, temperature measurement, and photography.

# 3.3.1 Test Section Assembly and Leveling

The condition that the measuring and reference beams of the interfermoter are in the same horizontal plane is fulfilled during the assembly of the instrument. The support frame was leveled horizontally by a 30 cm air bubble level positioned on a machinist's precision edge. By repeating the leveling, the four corners of the frame are adjusted horizontally within a satisfactory level. Further, the measuring beam is aligned horizontally, by using an open U-tube manometer composed of two glass tubes fitted into the ends of a long tygon pipe. The two glass tubes are adjusted to intercept the measuring beam close to the optical plates M1, and S2 respectively. The shadows of the water levels observed on a piece of paper placed right after the second tube, are used as an alignment aid to set the meauring beam horizontal. This condition can only be satisfied when the shadows of the water levels in the U-tube coincide.

The wheels of the rotating section are first placed securely on the four flanged wheels of the moving frame. They are then aligned with respect to the base plate and set parallel to each other by using a machinist's precision square. Next, the moving frame is leveled using

ika Milake di Malaka baratan k

3.7

the four bolts in the base plate. Alignment is examined continuously with a 30 cm air bubble level, until the frame is horizontal.

For the sake of a more refined adjustment particular care was taken in the fabrication of the components. It was therefore, possible to handle throughtout the assembly almost all the primary adjustments.

In the following description and adjustment of the test section will be illustrated toward the completion of the experimental procedure. First, the hot and cold plates are placed inside the rotating box. The horizontal slotted brackets are then bolted in the their positions, to form a supporting frame for the two plates. Plexiglas spacers of, 5.08 cm fixed at the center of each bracket are used to set the plates parallel to each other. Next, the face of the hot plate near the edges, is brought in contact with the spacers. At this point, the frame is rotated by 90 deg., to bring the hot plate in a horizontal plane, pressed by its weight against the spacers. Here, it is necessary to center the plate inside the box, and hold it securely from the back side using a lock set formed from a washer-Allen screw that passes through a slot in the supporting bracket into a threaded hole in a flanged T-slot nut sliding in the slot. Each bracket was provided with the same setup. In addition a small socket-head screw is fastened in the bracket near the end of the spacers to press on a teflon piece inserted between the bracket and the edge of each plate, which are used to prevent any movement during the rotation. For more convenience, the frame is rotated once again to set the hot plate horizontally, with its surface in the upward direction.

The two plexiglas plates which represent the insulated sides of the test section are then placed with their supporting beams between the hot and cold surfaces, the cold plate is not yet fixed in its position. The supporting beams are carried by steel elevator bolts threaded in the plexiglas plates near each of their corners, and aligned parallel to each other. Following the preceeding arrangement, a vertical sliding bracket is then fixed to the end of each supporting beam by two Allen screws. The sliding brackets are attached to the front and back sides of of the box, with Allen screws through slots that allow single-axis positioning over 5 cm range and a rigid lockdown for close adjustment. Figure 7 illustrates a side view of the test section configuration. In conjunction with this adjustment, two gage plexiglas blocks are precisely machined 5.08 cm square, as is shown previously in Figure 8, to provide a convenient and effective way to mount the test sides at the desired locations. Along the side the gage block are positioned on the hot plate near each end. Then the plexiglas plates are compressed lightly around the gage blocks. In addition, the plates are centered relative to the window openings using a machinist scale before locking the sliding brackets. Finally, the cold plate is positioned securely against the horizontal plates and the spacers in a similar way to the hot plate. Before mounting the top and the bottom covers, insulation is packed as will be described later.

Besides all the preceeding basic elements of adjustment and centering the test sides in the rotating frame, it is still required to perform the alignment relative to the measuring beam. In this case, the hot and cold surfaces are brought back to a vertical position by holding the front wheel at a 90 deg. setting and by using the angle indicator which is fastened to the base plate. The apparatus is then moved on the two rails until the holes in the gage blocks intercept the measuring beam light, which can be seen on the ground glass screen of the camera. First, the holes appeared as circular arcs, but after aligning the test section with the measuring beam and using the leveling bolts in the base plate, the circular holes are observed on



the screen. This indicates that the test section is parallel to the measuring beam.

The window frames carrying the optical flats are mounted firmly in their positions using Allen screws after removing the gage blocks. Similarly the optical flats of the compensating chamber are also placed in their mounts to intercept the reference beam, as is shown in Figure 15. All optical flats are aligned parallel to one another by bringing together the images of the light source produced by each optical flat due to a slight reflection on the surface. Under these conditions, it was essential to check the alignment of the test section using both reflection and diffraction of light on the test sides. This method is frequently used during the experiment. After the hot and cold plates are aligned in the vertical direction, using a plumb axis placed after the second beamsplitter S2, the test section is in a satisfactory condition for heat transfer measurements. Note that all these adjustments were performed at least one day before operating the experiment.

## 3.3.2 Insulation

The sides of the test section are covered with two layers of fiberglass wool insulation, of about 7.0 cm thick. Layers of fiberglass are also carved to fit closely between the horizontal plexiglas plates and their supporting beams, as well as between the hot and cold plates to avoid any air circulation outside the test section. The optical flats are compressed slightly against a styrofoam rubber frame mounted at each end of the test section, to avoid thermal and mechanical stresses. Moreover, small aluminum pipes of 1 mm I.D are fitted in the

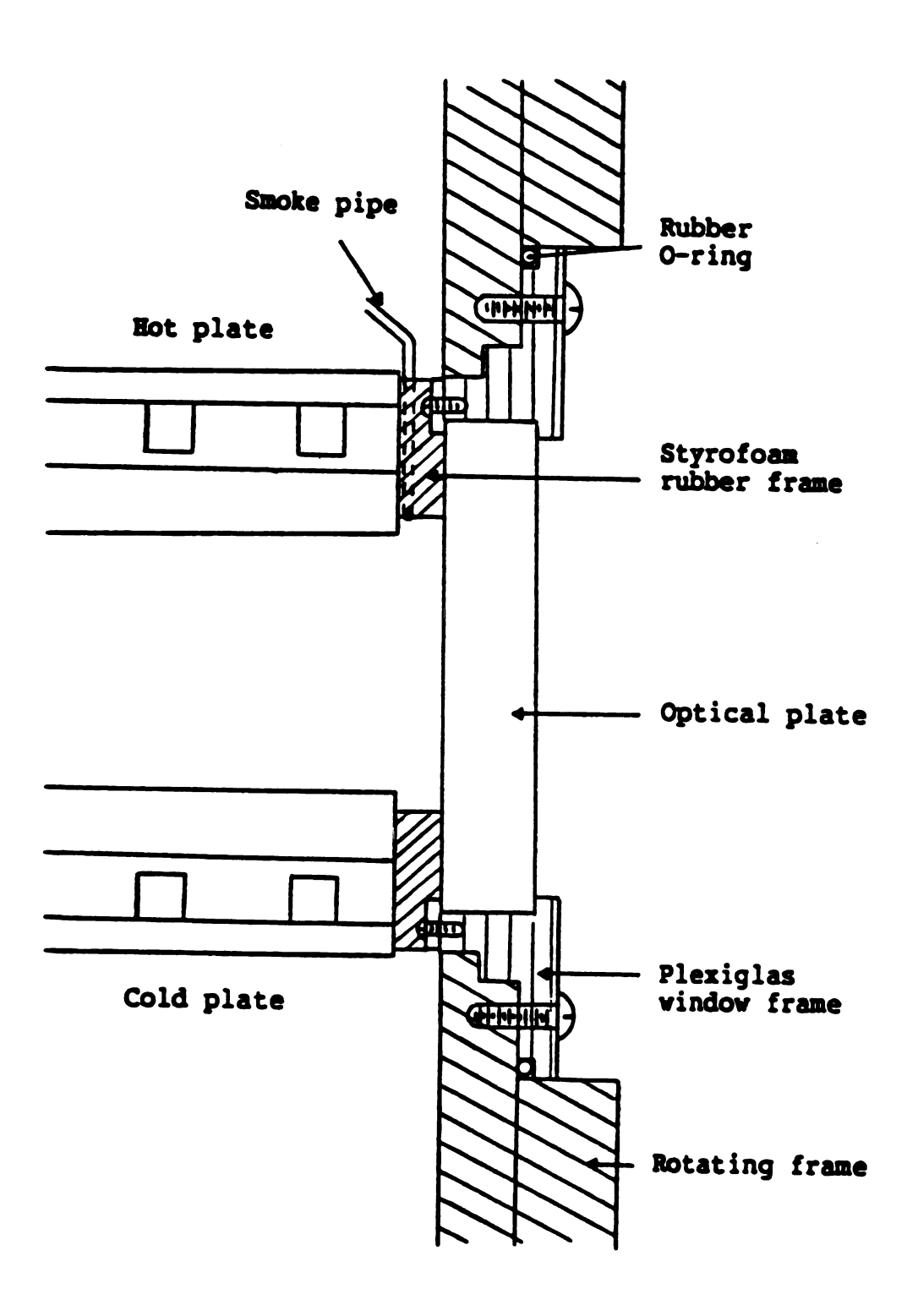


Figure 15 Top view of the end region

styrofoam at the two ends to allow smoke injection for the visual study. The insulation of the test section is secured by pieces of styrofoam to keep the same arrangement during rotation.

# 3.3.3 Thermocouples

Thermocouple connections are presented in two different types of setup. For the stationary phase sixteen thermocouples from each plate are connected directly to the external circuit. For the rotation studies, thermocouple leads were connected through a slipring-brush assembly to the external circuit as previously described. In the two setups, thermocouples connections are read using the electronic ice point, and the digital multimeter. The behavior of thermocouples are checked also for continuity in the rotating part.

# 3.3.4 Inclination Angle and Rotational Speed

The front wheel of the rotating section is calibrated into steps of 5 deg. in order to provide a continuous means to determine the angle of inclination of the test section. Therefore, after aligning the test section in the vertical direction, which corresponds to 90 deg. on the front wheel, it was possible to determine any other angular orientation with an accuracy of 0.1 deg.

On the other hand, the rotational speed is set by monitoring the variable speed control. The rotational speed is determined by a tachometer. For the range of speed used in this work, the error is no more than  $\pm$  0.1 rpm. Moreover, the weight of the rotating section acts like a flywheel to stabilize the rotational speed.

3.3.

temp the

appr heat

prac

temp

cond

mult

them

0.05

3.3.

focu

micr

reso]

# 3.3.5 Temperature Measurement

Several basic conditions are considered before taking the temperature measurements of the hot and cold surfaces. For instance, the average temperature of the hot and cold surfaces, is adjusted to be approximately equal to the ambient temperature, in order to reduce the heat loss, and radiation through optical flats to a minimum. In practice, this can be eventually achieved by adjusting of either the constant temperature baths, or in a few cases, the laboratory temperature.

The requirements which are applied to obtain steady state condition are as follows. First, the experiment is operated for at least 4 hrs. while the thermocouple readings are observed on a digital multimeter. Secondly, it is very essential to satisfy that; (a) each thermocouple variations are no more than 0.1°C for a period of at least 15 minutes, (b) the temperature difference variations are not to exceed 0.05°C over a span of 15 minutes.

# 3.3.6 Photography

After the steady state condition was reached, an interferogram focussed at the test section was taken followed by recording the corrected barometric pressure and the ambient temperature. A traveling microscope made by Gaertner Scientific Corporation of 0.0001 inch x-y resolution was used to analyse the interferograms.

#### CHAPTER 4

#### RESULTS AND DISCUSSION

All the experimental results of local and mean heat transfer coefficients along the hot and cold surfaces of the non-rotating and rotating enclosures are derived from the local temperature gradients as illustrated in Appendix 3. The temperature gradients are determined from Mach-Zehnder interferograms that allow a subsequent calculation of the entire temperature field at one time without introducing any disturbance into the natural convection phenomena.

In this investigation the average temperature of the differentially heated walls is maintained approximately equal to the ambient temperature. Physical properties of air are evaluated at the cold wall temperature which is kept close to 19°C, while the temperature difference between the hot and cold walls is varied between 7°C and 28°C.

Errors associated with the interferometric measurement of convective heat transfer coefficients are discussed in Appendix 4.

# 4.1 Natural Convection in an Inclined Rectangular Enclosure

The first part of this study will concentrate on the influence of inclination angle on the mean and local heat transfer rates by natural convection in a rectangular enclosure of cross-sectional aspect ratio Ax=1.0 and longitudinal aspect ratio Az=10.0 for Rayleigh numbers between 10 and 10 and inclination angles between 0 deg. (heated from

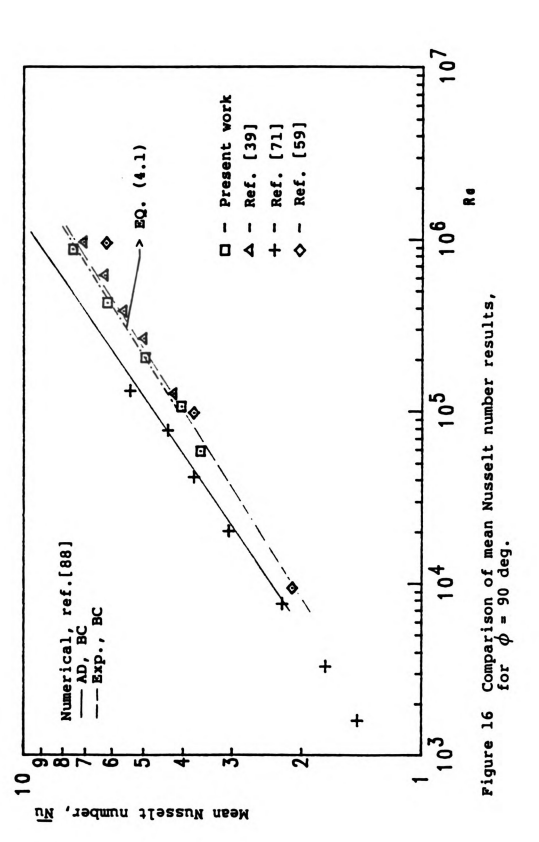
above) and 180 deg. (heated from below). The enclosure is inclined about its longitudinal axis (z-axis).

### 4.1.1 Mean Nusselt Number Results

A large number of experimental and theoretical results of mean Nusselt number are now available in the literature. It is for this reason mainly that Nusselt number results are presented first to make a comparison and verify the extent of validity of the experimental technique. In this regard, Figure 16, illustrates a comparison of the present mean Nusselt number as a function of the Rayleigh number with previous experimental and numerical calculations for a vertical enclosure (90 deg.). The first point to observe in Figure 16, is the difference between adiabatic and experimental insulated boundary conditions. For instance, Zhong, Yang, and Lloyd's numerical calculations [88] fitted within 3 percent with the present results when similar experimental insulated boundary conditions are incorporated in their numerical scheme. On the other hand, for adiabatic boundary conditions the Nusselt number is overestimated, as would be anticipated, due to the suppression of conduction effect near the end walls.

Natural convection in a vertical enclosure is considered to be a well defined problem for comparison and for devising various numerical and experimental methods. However, the data scatter in the reported results is attributed mainly to some pertinent physical parameters encountered in the problem such as the longitudinal aspect ratio and boundary conditions which in turn effect the flow field and hence the heat transfer behavior in the enclosure. The Bajorek and Lloyd results





[39], obtained by using the same experimental technique and for similar boundary conditions, exhibited excellent agreement, within 1-2 percent, with the present data. Examination of the experimental data permitted the following equation to be constructed for correlation of mean Nusselt number.

$$\overline{Nu} = 0.175 \text{ Ra}^{0.275}$$
 (4.1)

This equation correlated the data with a maximum deviation of  $\pm 3$  % and was derived for data over a Rayleigh number range of  $10^4$  -  $10^6$ .

The influence of inclination on natural convection in the enclosure has a significant effect on the flow phenomena and heat transfer characteristics. Results of different numerical and experimental investigations with various boundary conditions are displayed in Figure 17 together with the present experimental calculations. The mean Nusselt numbers are plotted as a function of the angle of inclination over a range of 0-180 deg., with Rayleigh number as a parameter. In the following, attention will be focussed on the inclination effects on the general trend of heat transfer. A detailed analysis will be presented in the next sub-section of the flow patterns (longitudinal roll-cell and cellular motions), and the local heat transfer results. It is quite clear from the plotted data that an increase of the angle of inclination above 0 deg. (heated from above) causes an increase in the driving potential of natural convection. This fact stems from the increased influence of gravitational buoyancy on the flow and temperature fields at 90 deg. (vertical enclosure) along the thermal boundary layers, where buoyancy-driven flow is the dominant mode. A further increase of the inclination angle will reduce the gravity component along the isothermal walls, although the heat transfer rate continues to increase until a local maximum value is

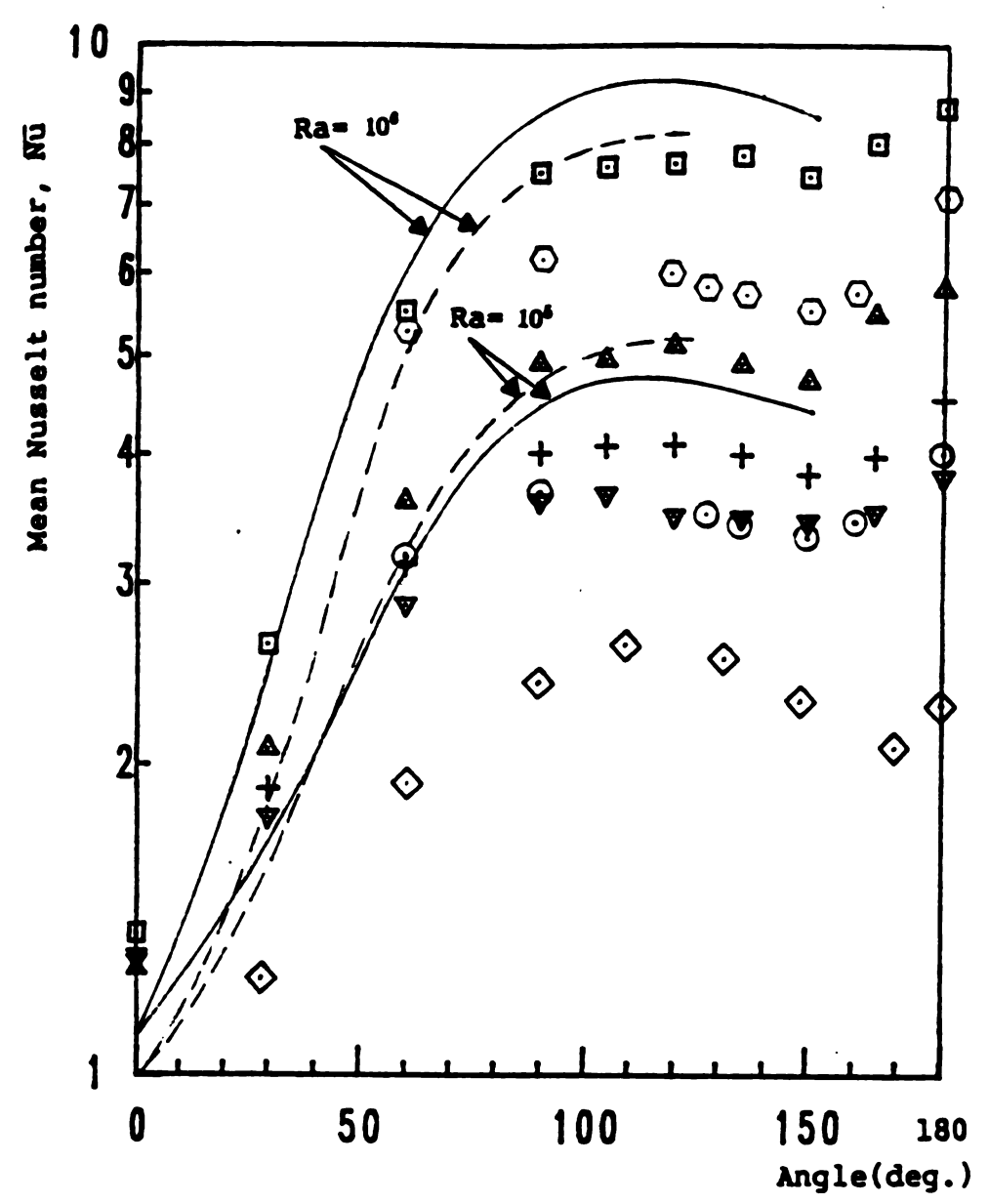


Figure 17 Effect of inclination angle on mean Nusselt number at Ax=1.0.

Numerical	Present work
Ref. [28], AD	$\nabla$ Ra= 5.8× 10 <sup>4</sup>
Ref. [88], AD	$+$ Ra= $1.1 \times 10^{5}$
Experimental, Ref. [71]	$\triangle Ra = 2.1 \times 10^{5}$
$\bigcirc$ Ra= 1.5×10 <sup>4</sup>	
Experimental, Ref. [79]	
⊙Ra= 10 <sup>6</sup>	
O Pas 10 <sup>4</sup>	

reached at an angle between 110-120 deg. Beyond this point, it is found that increasing the angle will result in a gradual decrease of the heat transfer until a local minimum is obtained somewhat between 150-160 deg. before a maximum value at 180 deg. (heated from below) is reached which is slightly greater than the local maximum. This local minimum accounts for the transition from a longitudinal roll cell to a threedimensional flow, which tends to dissipate some of the thermal driving potential before the cellular motions take place. On the whole, the present experimental results showed excellent agreement with the Arnold, Catton, and Edwards experimental results [79]. Their prediction of the local minimum lies at 155 deg. for an aspect ratio one, and Rayleigh number between 5x10 and 10 rather than at 175 deg. as depicted by Ozoe, Sayama, and Churchil experimental measurements [71] for Rayleigh numbers of 3800, 4950, and 15000 and aspect ratio one. This shift of the local minimum toward the horizontal (180 deg) is presumably a result of the low Rayleigh numbers. Also shown are the numerical results of Zhong, Yang, and Lloyd [88], and Catton, Ayyswamy, and Clever [28] for inclination angles up to 150 deg., neither of which predicted the minimum and the subsequent rise in Nusselt number as the heated from below convection is approached since their numerical schemes became unstable at an inclination angle greater than 150 deg.

Figure 18 presents the Nusselt number as a function of the Rayleigh number with the angle of inclination as a parameter. It also, provides a comparison between the present experimental data and the theoretical predictions of Catton, Ayyaswamy, and Clever [28]. The apparent deviation at 120 deg. is thought to be due to the differences caused by the adiabatic boundary condition which is used in the calculation, instead of the experimental insulated boundary condition.

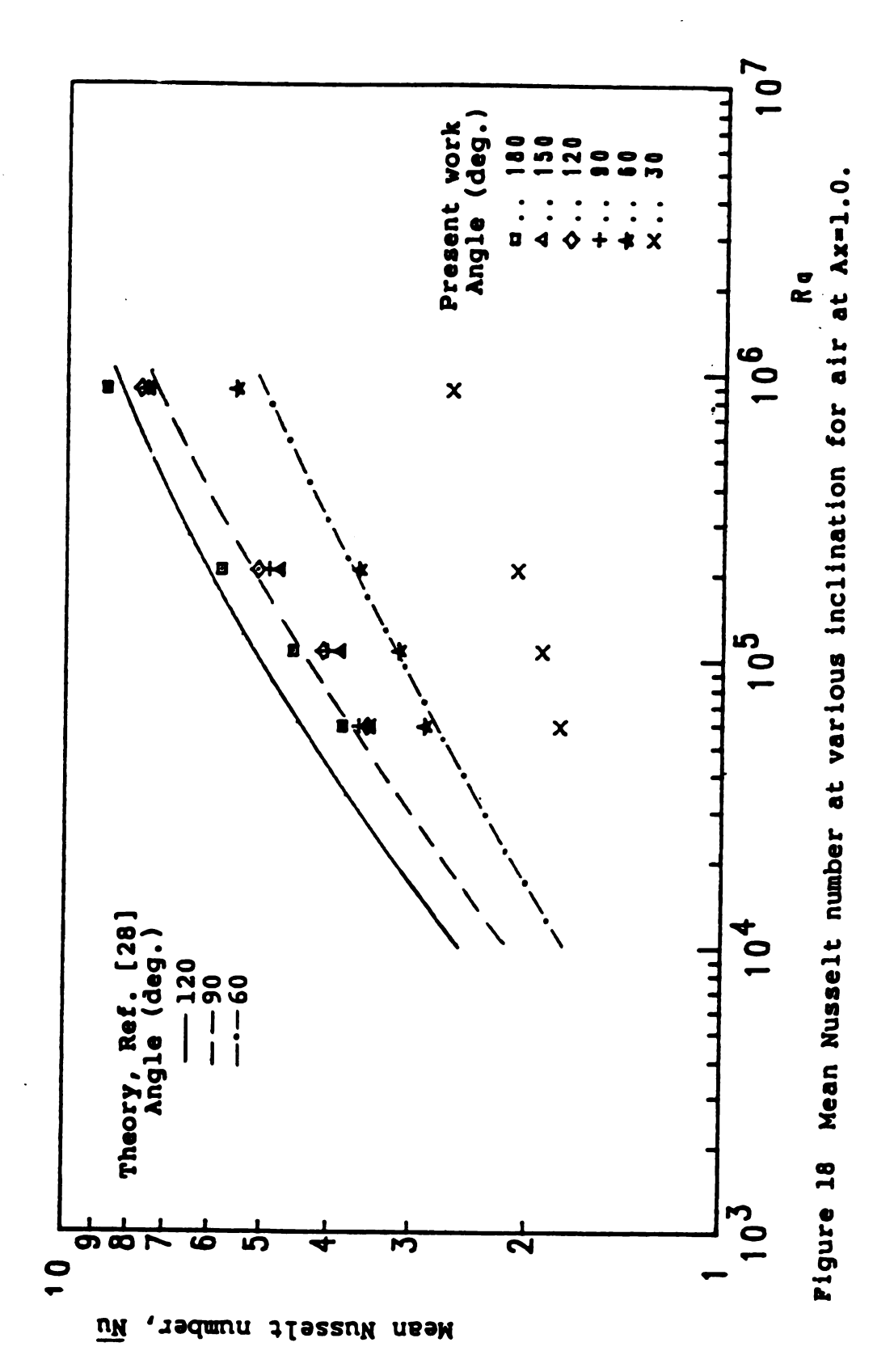


Figure 18 illustrates the general trend in which the inclination angle affects the mean Nusselt number when plotted against the Rayleigh number. Moreover, it suggests a significant improvement in heat transfer with increasing the angle of inclination.

### 4.1.2 Local Nusselt Number Results

In this sub-section the analysis of the experimental data will be centered on the influence of the inclination angle on local heat transfer rate and flow behaviors. In addition, a series of interferograms will be presented in this connection along with a smoke flow visualization to facilitate understanding of the fundamental aspects of the convective structure. Local Nusselt numbers will be presented along the hot and cold surfaces as a function of the non-dimensional enclosure height with the angle of inclination as a parameter varying between 0 and 180 deg.

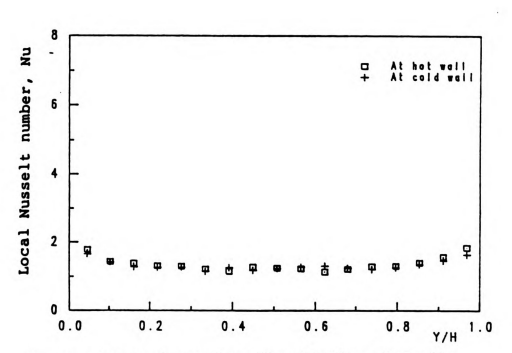
Figure 19c shows the profiles of Nusselt numbers in terms of the non-dimensional height at 0 deg. (heated from above). It is clearly noted that the local values of the heat transfer rate are almost equal to one as a consequence of pure conduction along the differentially heated walls except near the ends, which is an evidence of a convective flow existence. The flow pattern picture, Figure 19a, indicates this convective nature near the corners, however the flow is extremely slow because of the gravitational stable condition. It is for this reason mainly that the results of mean Nusselt number are different from unity, as reported in previous numerical and theoretical calculations which utilize Boussinesq approximation (linear variation of the density) and adiabatic boundary condition. The later is a basic element required to eliminate the end walls effect. Moreover, the interference



a) Flow pattern in xy-plane at Ra=  $3.0 \times 10^5$ 



b) Interference fringe pattern, at Ra=  $1.1 \times 10^5$ 

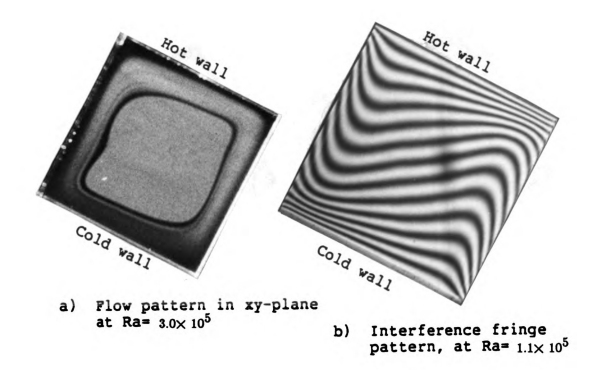


c) Local Nusselt Number distribution along the hot and cold walls, at Ax=1.0 and Ra=  $1.1\times10^5$ 

Figure 19 Effect of inclination angle on the flow and heat transfer, at  $\phi$  = 0 deg.

fringe pattern of the isotherms, Figure 19b, depicts a stable stratified condition, but the isotherms bending near the end walls indicates the existence of some convective motion. Another aspect to consider from the isotherms picture is the fact that they represent the thermal boundary layer configuration in the immediate vicinity of the differentially heated surfaces. Thus a qualitative understanding of the local heat transfer distribution may be obtained which in turn is related to the inverse of the thermal boundary layer thickness.

For inclination angles of 30 and 60 deg., the existence of the convective flow near the heated walls is noticeable as is shown in Figures 20a and 21a. At 30 deg., Figure 20a shows that the core region is almost quiescent and the flow is confined to the boundary layer region. At 60 deg., as shown in Figure 21a, the driving potential of the convective flow is extended to include not only the boundary layer, but also the core region. This fact is clear from the appearance of two symmetrical vortical tubes that reside near the centers of the differentially heated walls. Actually no matter how slow the flow is inside these vortical tubes, thermal energy is still be transported via convection in the core region. Accordingly the interference patterns of the isotherms, Figures 20b and 21b, will make the above analysis more understandable due to the observed development of the thermal boundary layer regions near the differentially heated walls. Also, the thinning of the thermal boundary layers seems to be strongly dependent on the angle of inclination, which in turn yields a consequent increase of the convective flow . In accordance with this qualitative agreement between the flow and temperature fields, the experimental data of the local Nusselt numbers, Figures 19c, 20c, and 21c, demonstrate quantitatively the effect of inclination angle on the heat transfer and the transition process from the conduction dominated gravitationally stable condition



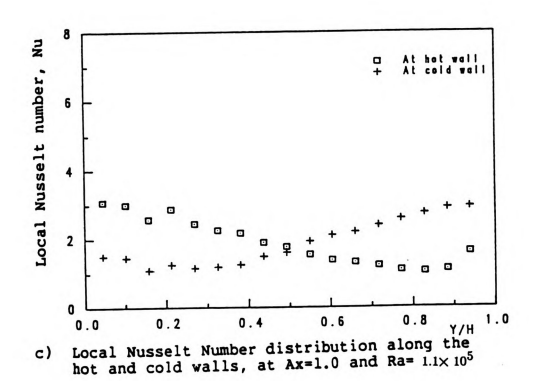
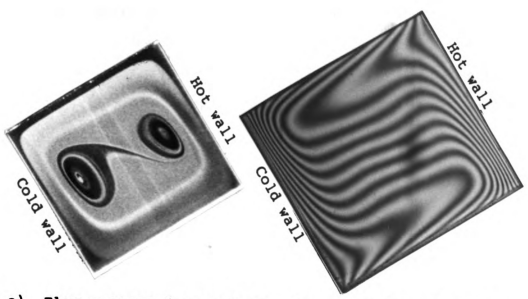
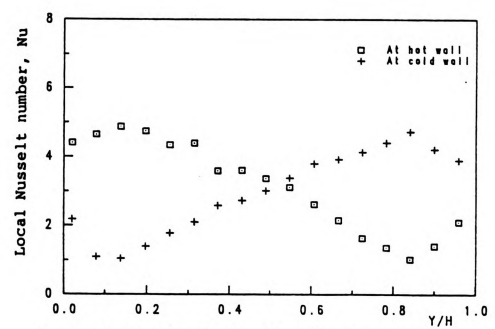


Figure 20 Effect of inclination angle on the flow and heat transfer, at  $\phi$  = 30 deg.



a) Flow pattern in xy-plane at Ra=  $3.0 \times 10^5$ 

b) Interference fringe pattern, at Ra=  $1.1 \times 10^5$ 



c) Local Nusselt Number distribution along the hot and cold walls, at Ax=1.0 and Ra=  $_{1.1\times}\,10^5$ 

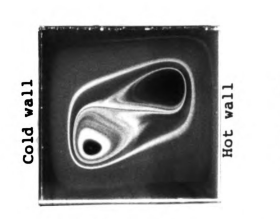
Figure 21 Effect of inclination angle on the flow and heat transfer, at  $\phi$  = 60 deg.

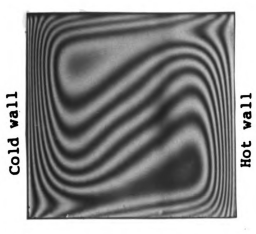


at 0 deg. (heated from above) to a convective thermally stratified condition at 60 deg.

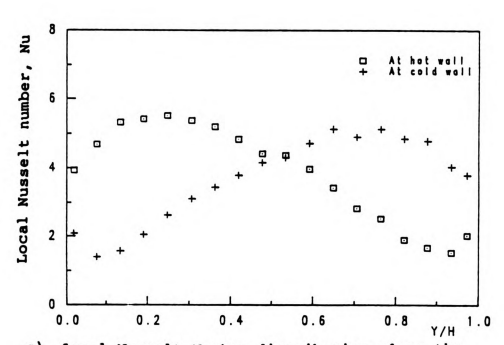
When the enclosure is in a vertical configuration, gravitational buoyancy becomes very apparent in a thin layer of fluid near the wall region, and buoyancy-driven convective flow will be the preferred mode for transporting energy. The effect of gravity on the flow can be noted in Figure 22a. The first development in this event is the repositioning of the vortical tubes, near the upper and opposite lower edge of the hot and cold walls. This consequent skewness in the vortical structure is responsible for the change in direction of the velocity field in the core region. It also tends to minimize the heat transfer from the heated wall by thickening the thermal boundary layer as seen in Figure 22b. Based on these factors, the experimental determination of the heat transfer rate, Figure 22c, showed maxima near the lower and opposite upper corners of the hot and cold walls respectively and minima on the other facing edges. These findings are in good agreement with both the flow and thermal boundary layer configurations.

A further increase of the inclination angle beyond the vertical, will permit the heated from below configuration to commence its influence on the flow pattern and energy transport process. Figure 24a at 120 deg. shows the flow structure as a single roll-cell oriented with the enclosure longitudinal axis (z-axis). A growing secondary flow near the upper and opposite lower corners of the enclosure also appears. Under these circumstances the corresponding developments in the thermal boundary layers are illustrated in Figure 24b. This in turn will provide the necessary information for the local heat transfer distribution, and demonstrates clearly the shifting of the maximum value of local heat transfer toward the center of the differentially heated walls. This is related to the flow development in the



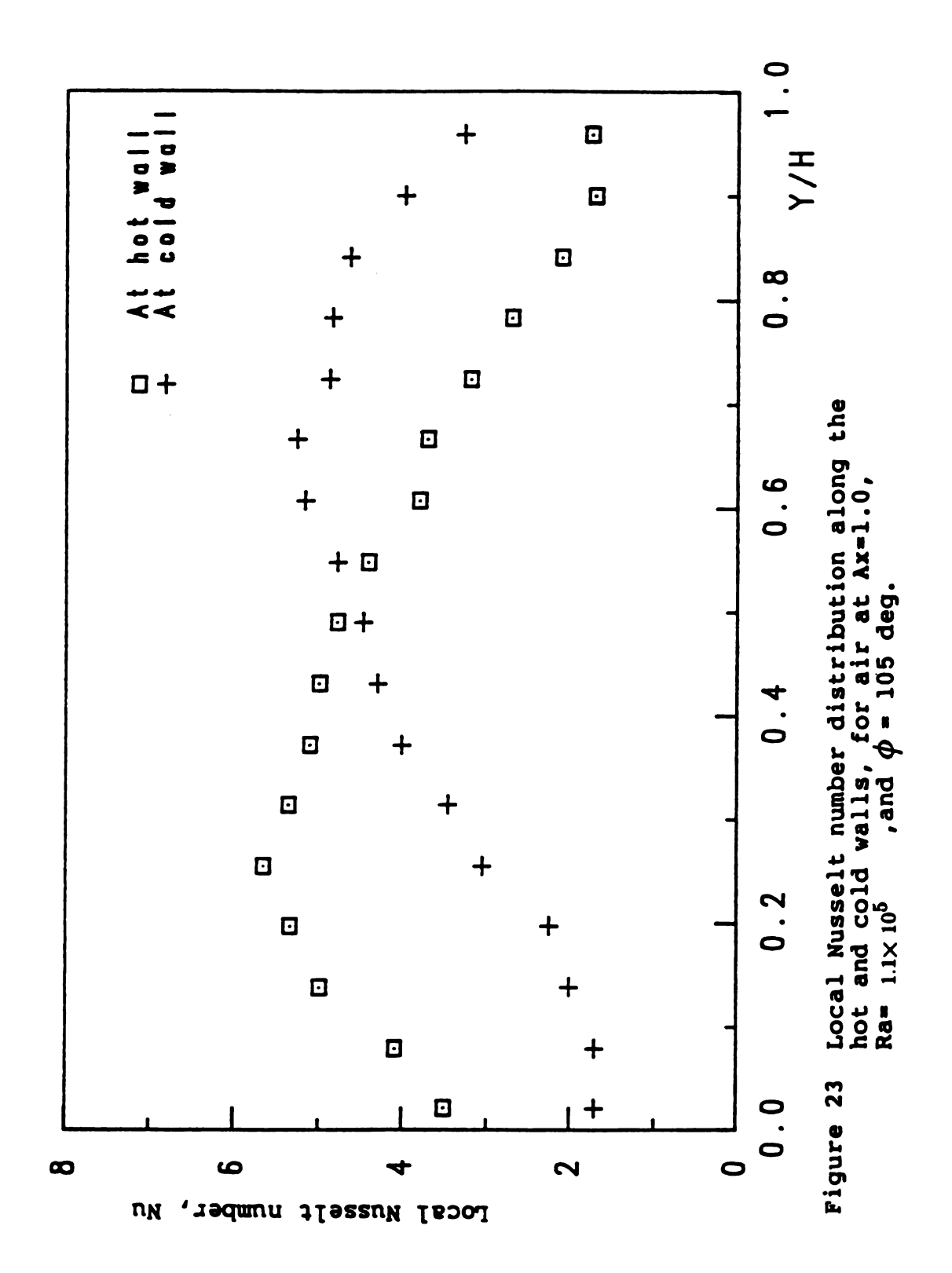


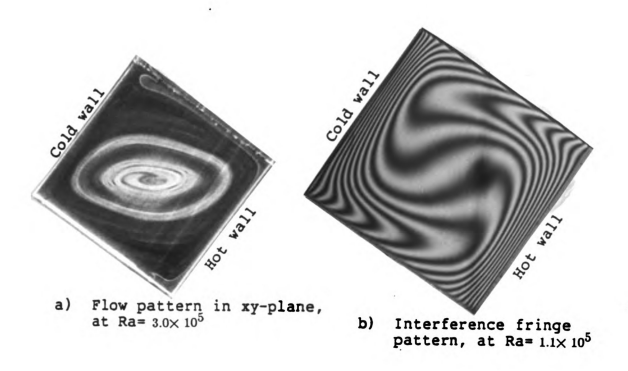
- a) Flow pattern in xy-plane at Ra= 3.0×10<sup>5</sup>
- b) Interference fringe pattern, at Ra=  $1.1 \times 10^5$



c) Local Nusselt Number distribution along the hot and cold walls, at Ax=1.0 and Ra=  $1.1\times10^5$ 

Figure 22 Effect of inclination angle on the flow and heat transfer, at  $\phi$  = 90 deg.





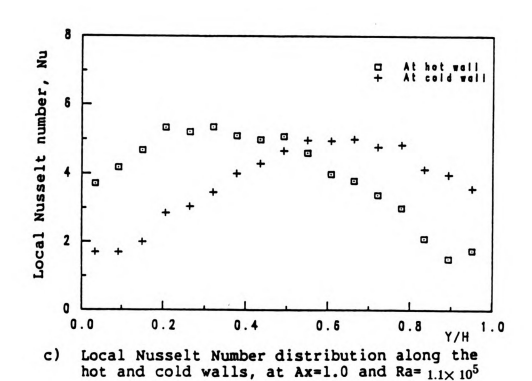
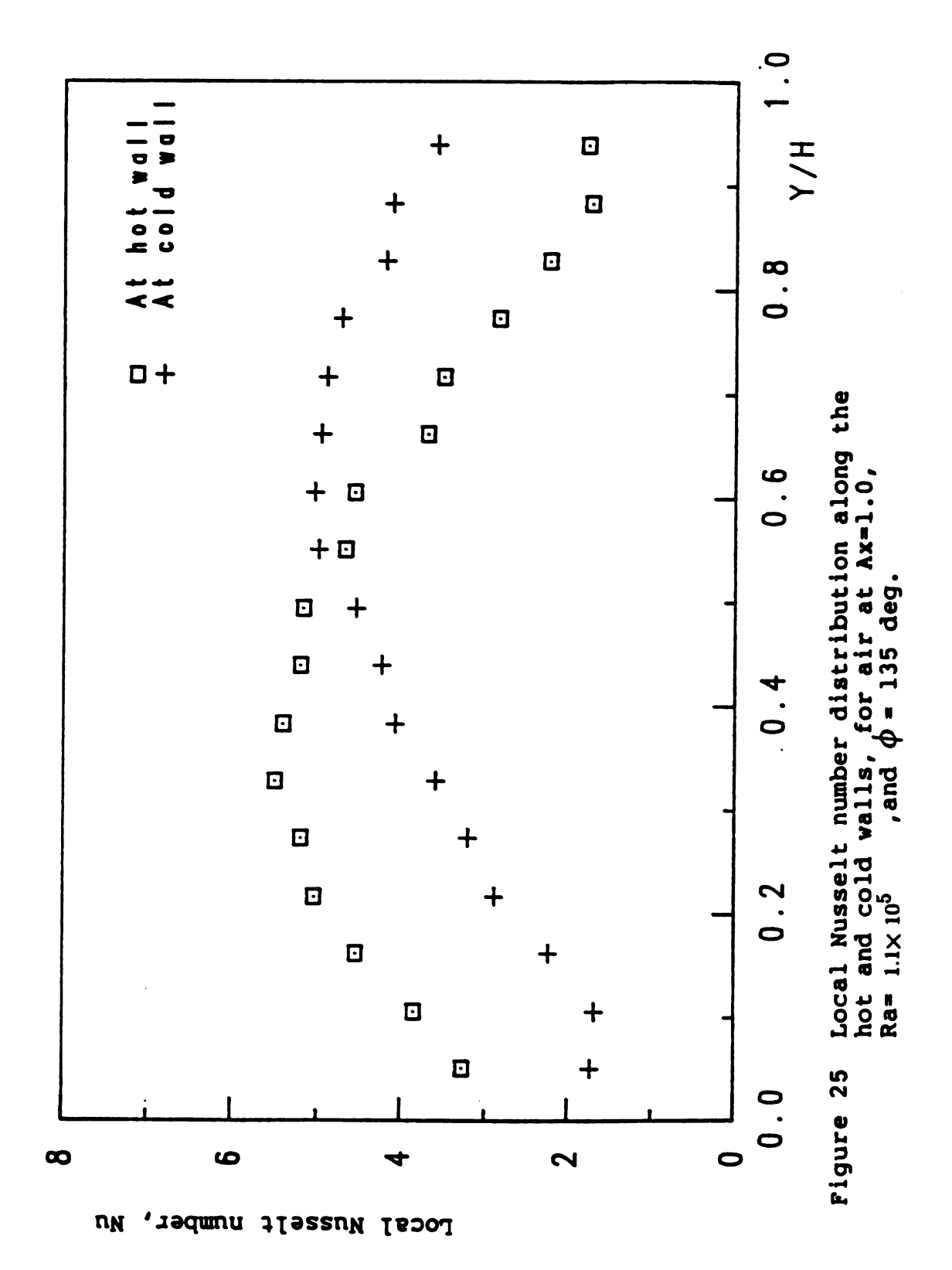


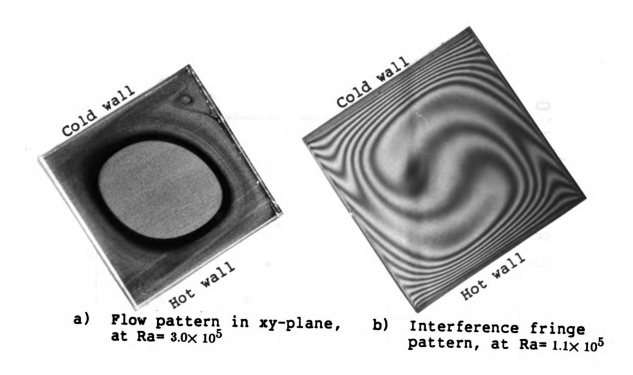
Figure 24 Effect of inclination angle on the flow and heat transfer, at  $\phi$  = 120 deg.



hydrodynamic boundary layer near the wall region. Figures 23, 24c, and 25 at 105, 120, and 135 deg. of the local heat transfer experimental data can be used to notice the shifting in the location of the maximum value of local Nusselt number distribution along the walls.

At inclination angle of 150 deg., Figure 26a, the longitudinal roll-cell is well defined and nearly in a circular form. In addition, the secondary flow which is developed at the upper and opposite lower corners of the enclosure is almost stagnant, which in turn may lead to a reduction in the convective heat transfer. The interferogram for this case, Figure 26b, shows the corresponding effect of the circulating flow on the temperature field. The thermal boundary layer clearly demonstrates the shifting of the location of the maximum value of local Nusselt number from the near ends toward the center of the heated walls, which is proportional to the inverse of the boundary layer thickness. For further insight to this process, the experimental data of local heat transfer plotted in Figures 26c and 27 at inclination angles of 150 and 165 deg. reflect these important features of the thermal boundary layer and the flow pattern. Accordingly, it is worth pointing out that the location of the local maximum value can not exceed the midheight of the isothermal walls. This is due to the buoyancy-induced secondary flow in the outer region near the upper and lower corners of the enclosure.

The onset of cellular convection at 180 deg. (Benard convection) is shown in Figure 28a, which presents a picture of the flow pattern in the yz-plane, where the flow is aligned in a series of roll cells with their axes normal to the isothermal walls. Furthermore, the subsequent unstable temperature stratification in the vertical direction is illustrated by the interference fringe pattern Figure 28b. It is apparent, from the isotherm structure that the temperature



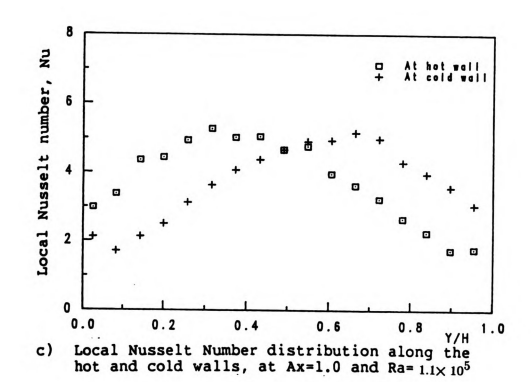
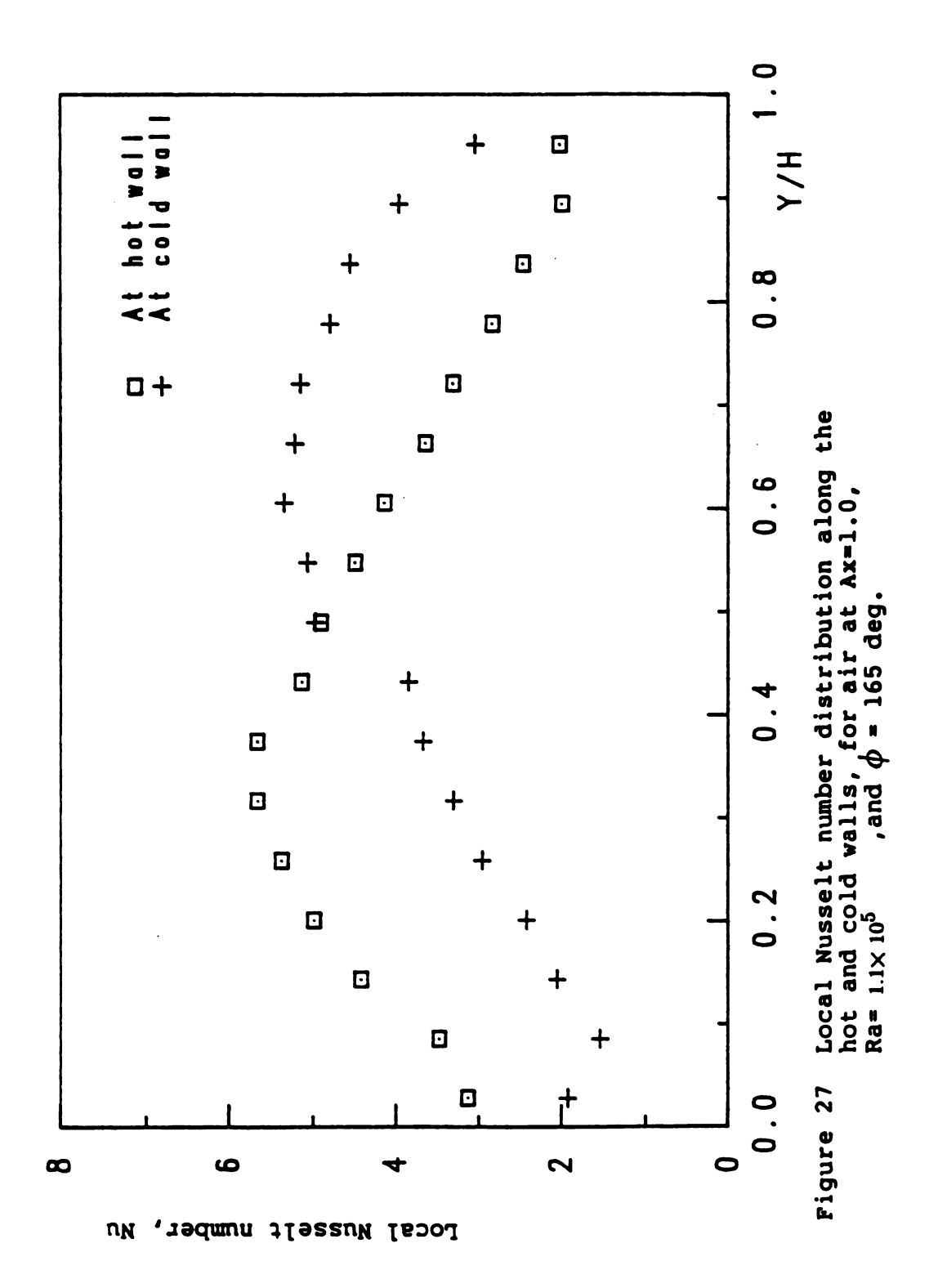


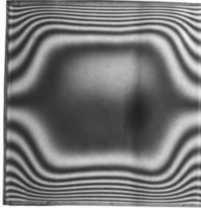
Figure 26 Effect of inclination angle on the flow and heat transfer, at  $\phi$  = 150 deg.



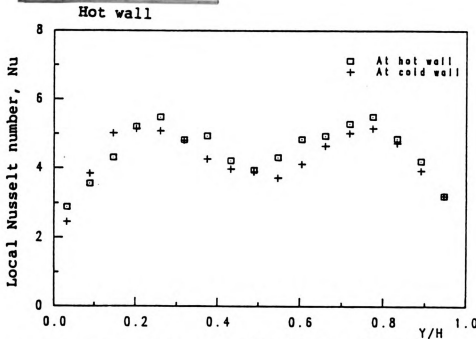
Cold wall



 a) Flow pattern in yz-plane, at Ra= 3.0× 10<sup>5</sup>
 Cold wall



b) Interference fringe pattern, at Ra=  $1.1 \times 10^5$ 



c) Local Nusselt Number distribution along the hot and cold walls, at Ax=1.0 and Ra=  $1.1\times10^5$ 

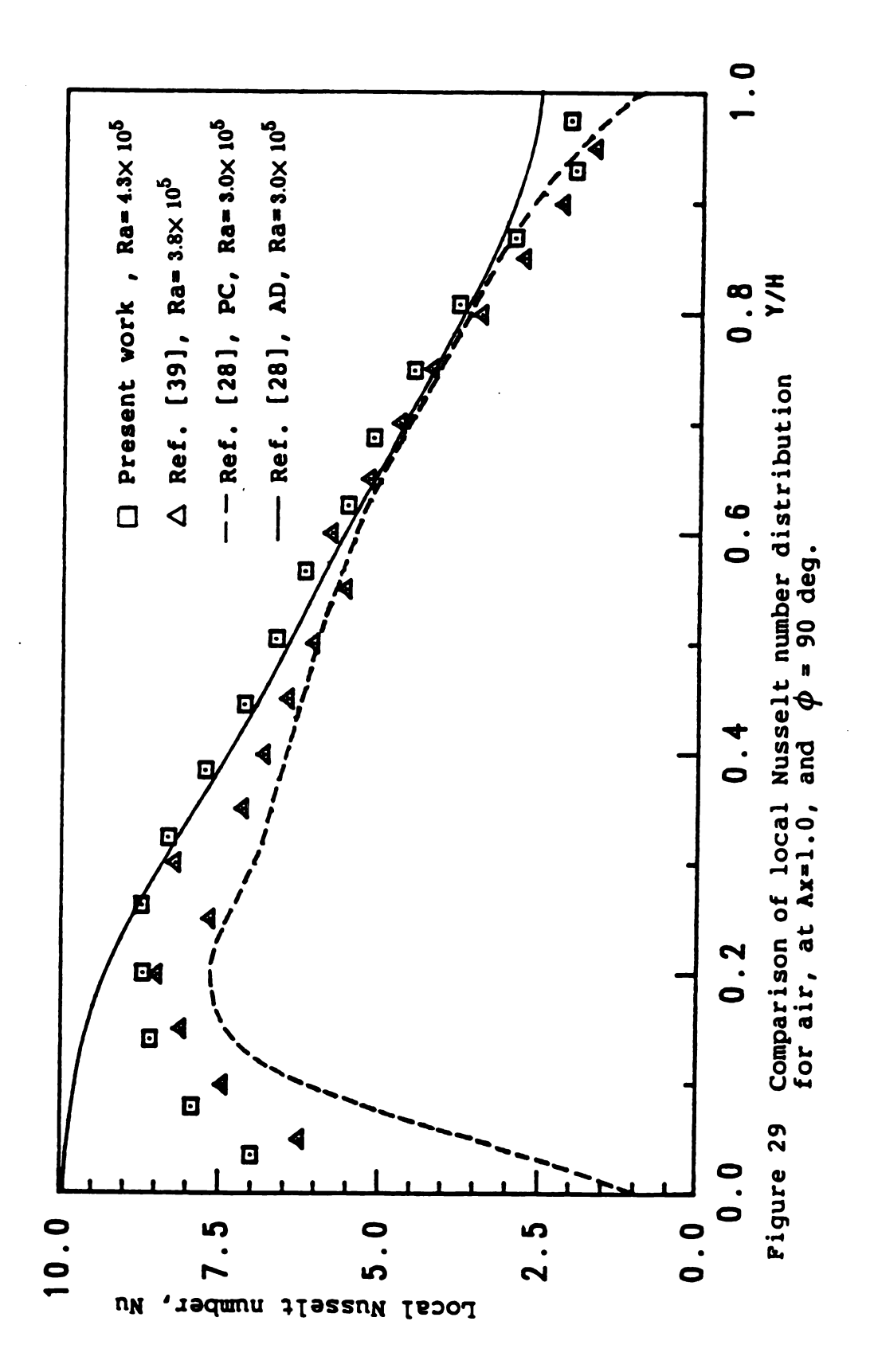
Figure 28 Effect of inclination angle on the flow and heat transfer, at  $\phi$  = 180 deg.

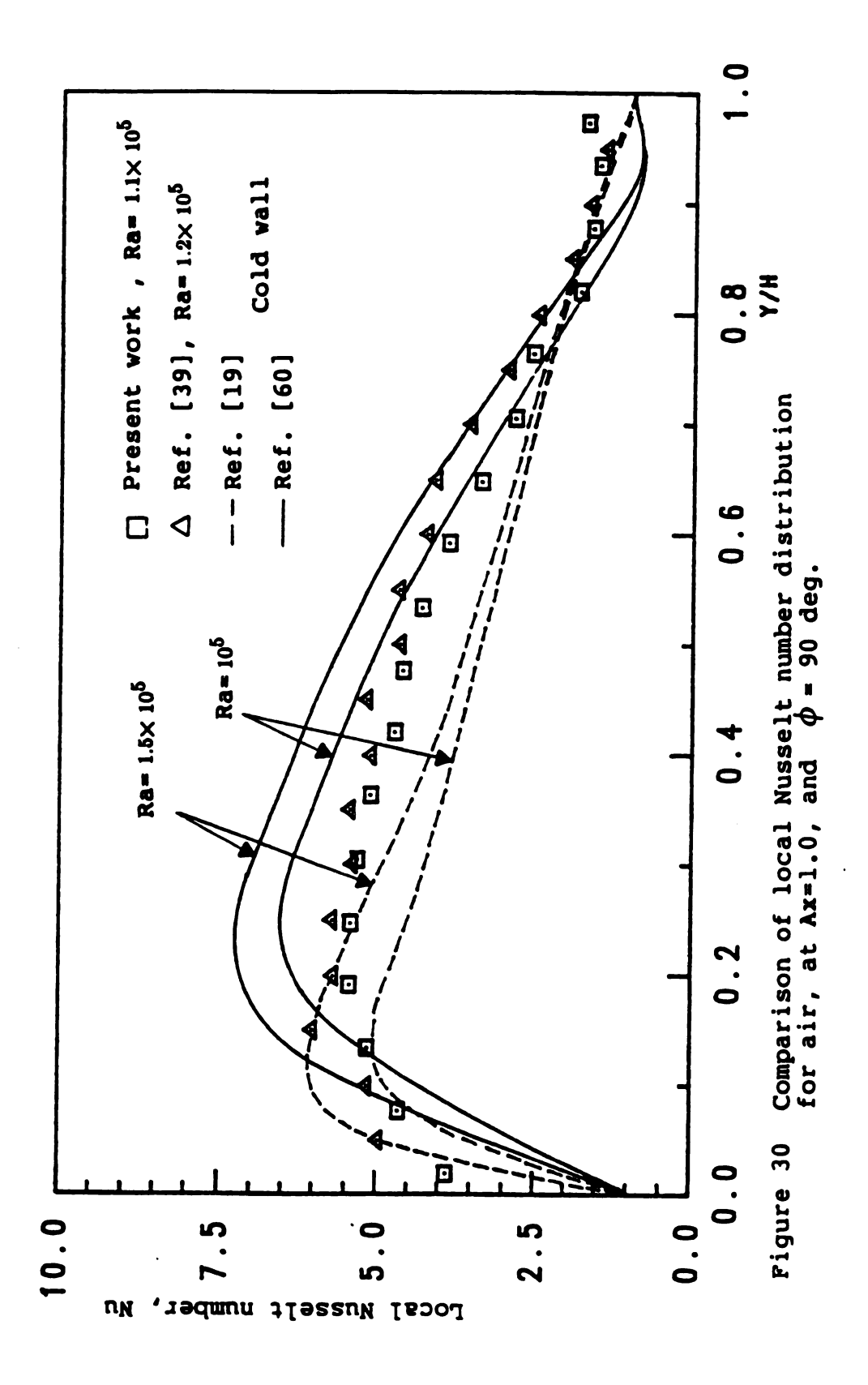
distributions along the insulated walls are almost linear, while the core region remains nearly at a uniform temperature. Close to the isothermal walls, as is shown in Figure 28b, the thermal boundary layers indicate the existence of two maxima of local Nusselt number which are symmetric about a vertical plane passing through the center of the enclosure. The measurements of local Nusselt numbers displayed in Figure 28c, are in good qualitative agreement with the picture which emerged from the thermal boundary layer structure.

So far in this sub-section the investigations have been entirely focussed on the influence of inclination angle on some hydrodynamic and thermal aspects of the flow, besides the measurement of local Nusselt number. Let us now consider the experimental data from these analyses in relation to the available experimental and numerical data, in order to outline some levels of agreement.

A comparison of the present experimental data for vertical enclosure with the experimental data of Bajorek, and Lloyd [39] and numerical predictions of Catton, Ayyaswamy, and Clever [28] is given in Figure 29. Agreement with the results of Bajorek, and Lloyd [39] is very good. Their experiments are performed under similar boundary conditions. Although the trend of the numerical predictions of [28] are similar to the experimental data, the quantitative difference is large near the ends of the walls. The calculations in [28] are presented for adiabatic and perfectly conducting boundary conditions. Thus, it is interesting to note from these results near the ends of the walls, the difference in the meaning between insulated and adiabatic boundary conditions.

Figure 30 presents another comparison of local Nusselt number variations from various experimental and numerical results. In general terms the experimental data of [39] are in excellent agreement with the





present results. However, the numerical predictions of [19,60], after assuming similar local Nusselt number variations along the hot wall, are in a quantitative disagreement with the experimental data and even with each other, this could partially accounted for the different grid-sizes and the calculations schemes used in their numerical analysis.

## 4.2 Natural Convection in a Heated Rotating Enclosure

In this section the simultaneous influence of the Coriolis, centrifugal and gravitational forces on the natural convection heat transfer will be presented for the case where the air-filled differentially heated rectangular enclosure is constrained to rotate about its longitudinal horizontal axis (z-axis).

The influence of rotation on the behavioural pattern of natural convection, can best be described by referring to equation (2.25) in Chapter 2 which introduces the Taylor and rotational Rayleigh numbers which emerge from the Coriolis and centrifugal terms respectively in the momentum equations. In this instance, the rotational Rayleigh number Ra is similar to the Rayleigh number Ra encountered in the gravitational buoyancy but, the gravitational acceleration is replaced by the centrifugal acceleration. In a rotating flow the Taylor number Ta describes the importance of Coriolis effect.

Measurements of local and mean Nusselt numbers are presented as a function of Tayor (Ta <  $10^4$ ), and Rayleigh number ( $10^4$  < Ra <  $3 \times 10^5$ ) at angular positions of 90 deg. (vertical enclosure), 180 deg. (heated from below), and 0 deg. (heated from above) for the rotating enclosure.

## 4.2.1 Heat Transfer Results in a Heated Rotating Enclosure at Angular Position of 90 Deg. (Vertical Configuration)

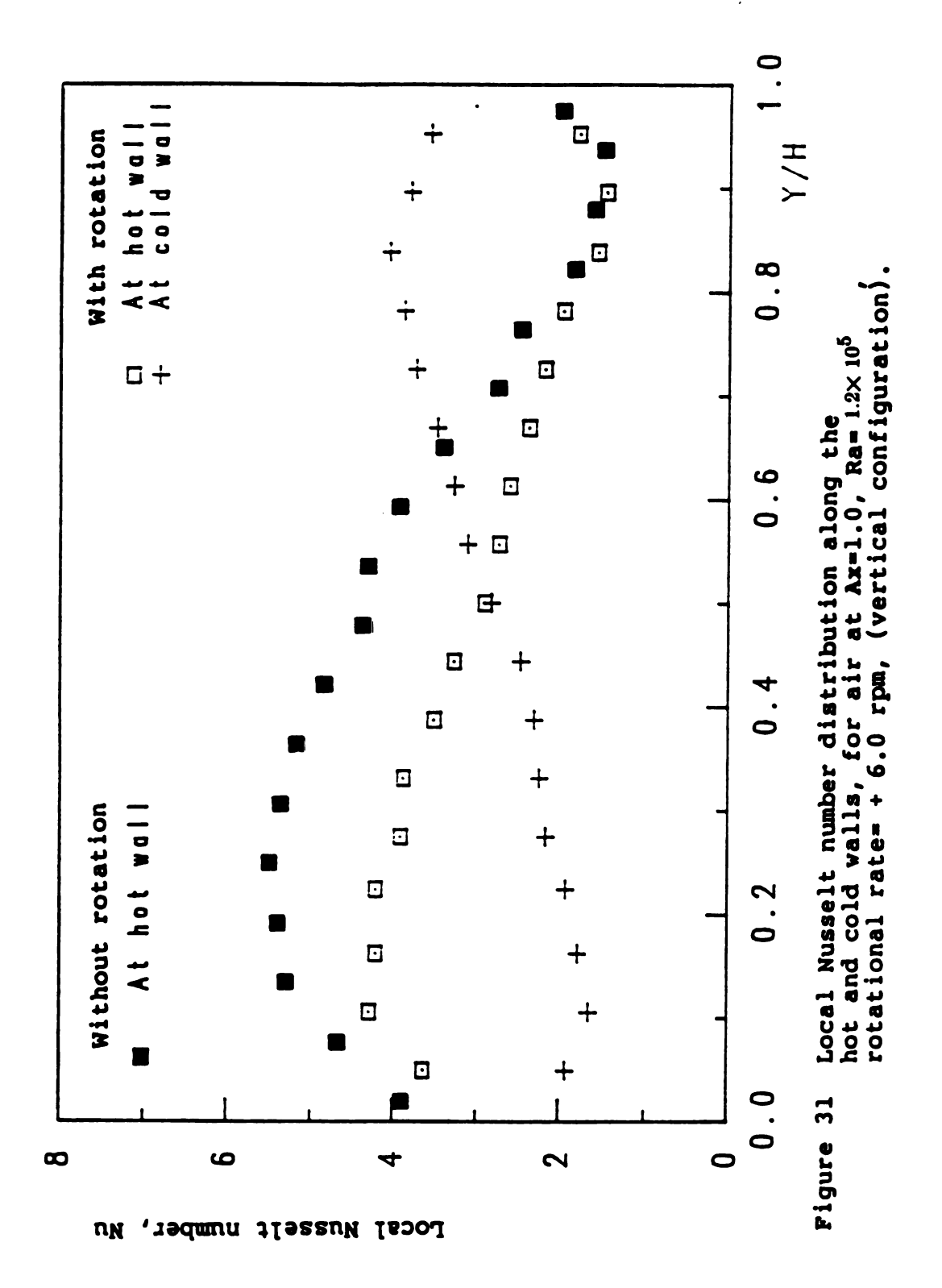
In view of the comments made earlier, the influence of rotation on the heat transfer will be discussed based on the local and mean Nusselt number results. In this event, the effect of the Coriolisinduced flows will be characterized by the Taylor number, Ta, and the centrifugal buoyancy induced flows by the rotational Rayleigh number,  $Ra_{r}$ , which tends to reduce the Coriolis acceleration effect at high rotational rate.

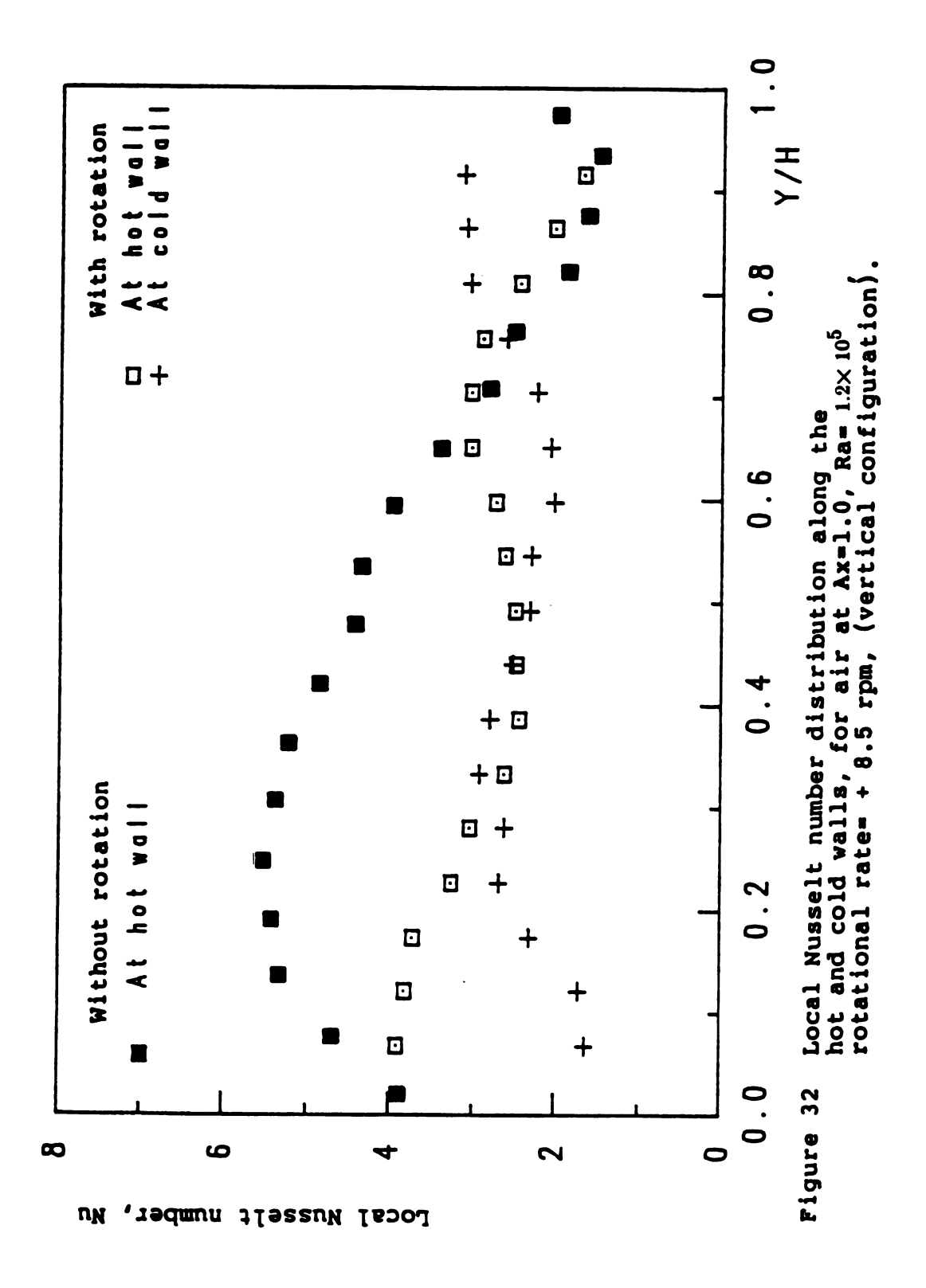
At low rotation rate the Coriolis effect will be very important due to the induced cross-secondary flow near the differentially heated walls which causes the fluid to recirculate toward the core region. At this point, the centrifugal buoyancy effect is less significant than the Coriolis effect and results in a slight distortion of the temperature distributions. Figure 31 compares the variations of the local Nusselt number along the hot and cold surfaces under rotating and non-rotating conditions. The reduction in local heat transfer at a Taylor number of 1.12x10 (-6.1 rev/min), is very significant compared to the non-rotating results as shown in the figure, although the same qualitative local heat transfer distribution is maintained at this level of rotation. The decrease in the heat transfer is related to the increase of the thermal boundary layer thickness near the wall region. This is largely generated by the effect of the influence of the Coriolis force relative to the centrifugal buoyancy. This effect promotes the mixing and thereby reduces the temperature difference between the heated walls.

The complex interaction of the Coriolis and centrifugal effects on the flow and heat transfer behaviors starts to develop at a Taylor number of 2.27x10 (-8.5 rev/min). Figure 32 shows the importance of the Coriolis and the centrifugal forces. It is apparent from the local heat transfer variations the amount of distortion caused by the interaction between the centrifugal buoyancy flow which tends to improve the heat transfer and the Coriolis effect which is still influencing the temperature and the flow fields.

At Taylor numbers of 3.28x10<sup>3</sup> (=10.2 rev/min), and 4.69x10<sup>3</sup> (=12.5 rev/min), Figures 33 and 34 reveal the effect of centrifugal buoyancy through observation of the enhancement of the local heat transfer with increases in the rotational rate. It is interesting to note in Figure 34 the movement of the local maximum of Nusselt number to the upper end of the hot wall from the lower end for the non-rotating condition. This in turn could be a result of an interaction between the centrifugal buoyancy, which has the tendency to force the cold denser fluid to move towards the outer region of the enclosure, and the gravitational buoyancy, which in turn maintains the boundary layer flow in a relatively thin region near the heated walls. Hence the hydrodynamic and thermal boundary layers near the walls will grow and the movement of local Nusselt number maximum was observed along the hot and cold surfaces.

Figures 35 and 36 show how the local Nusselt at Ra=1.2x10 number responded to increases in rotational speeds as characterized by Taylor numbers of  $7.10x10^3$  (=15.1 rev/min), and 9.66x10 (=17.5 rev/min), respectively. The important feature to observe is the increase in local heat transfer as a result of increasing the rotational speed. However,

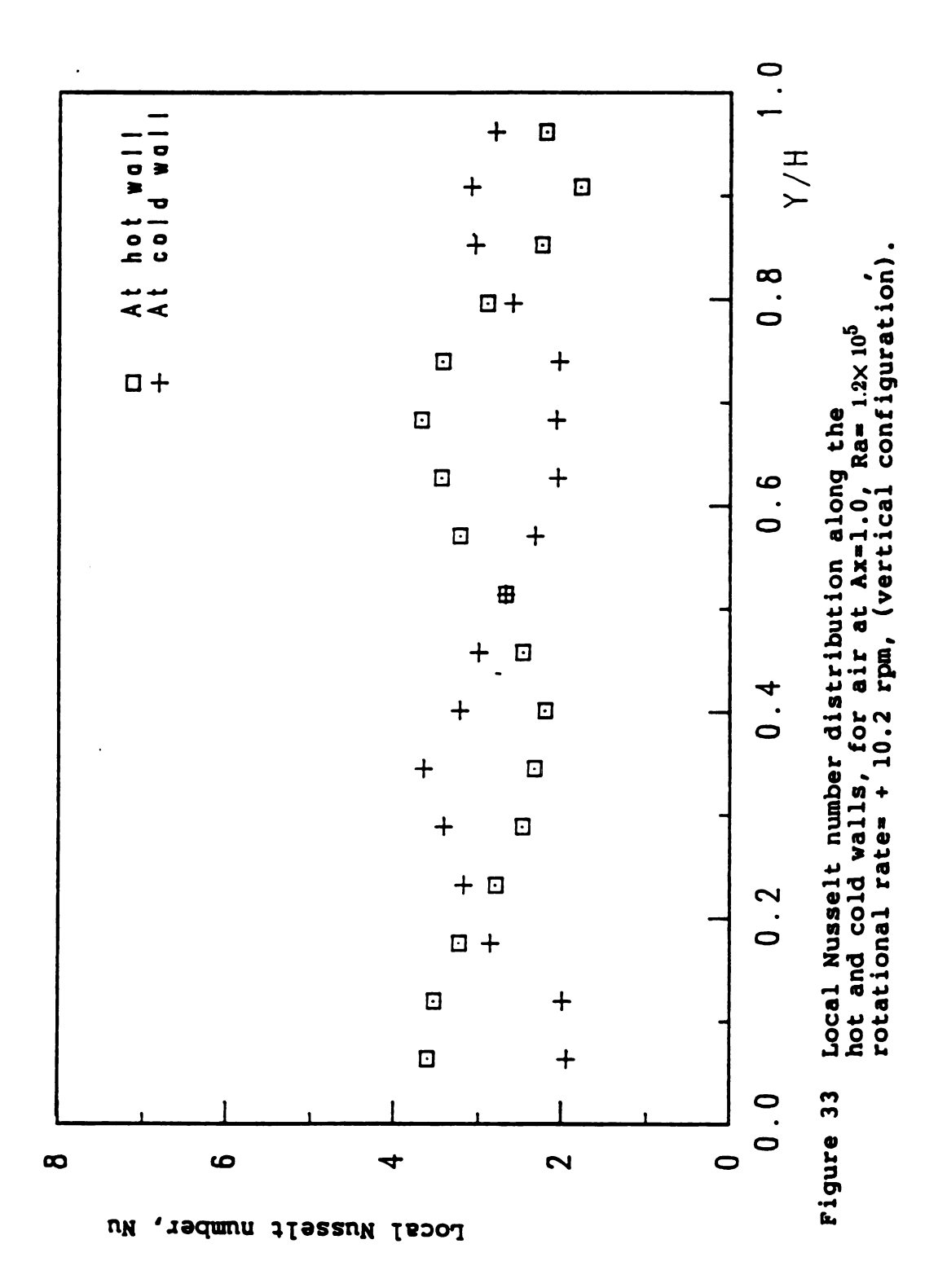


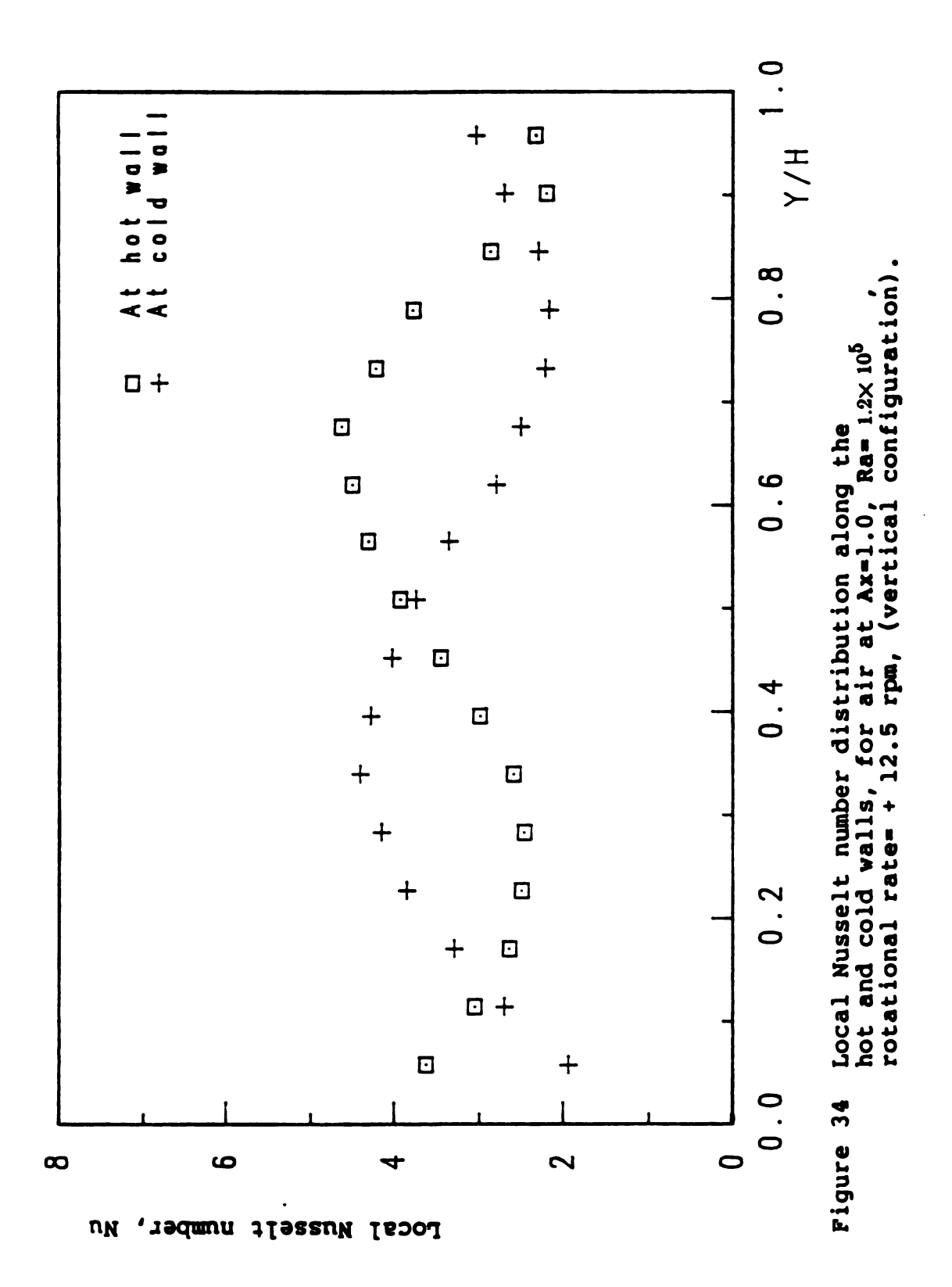


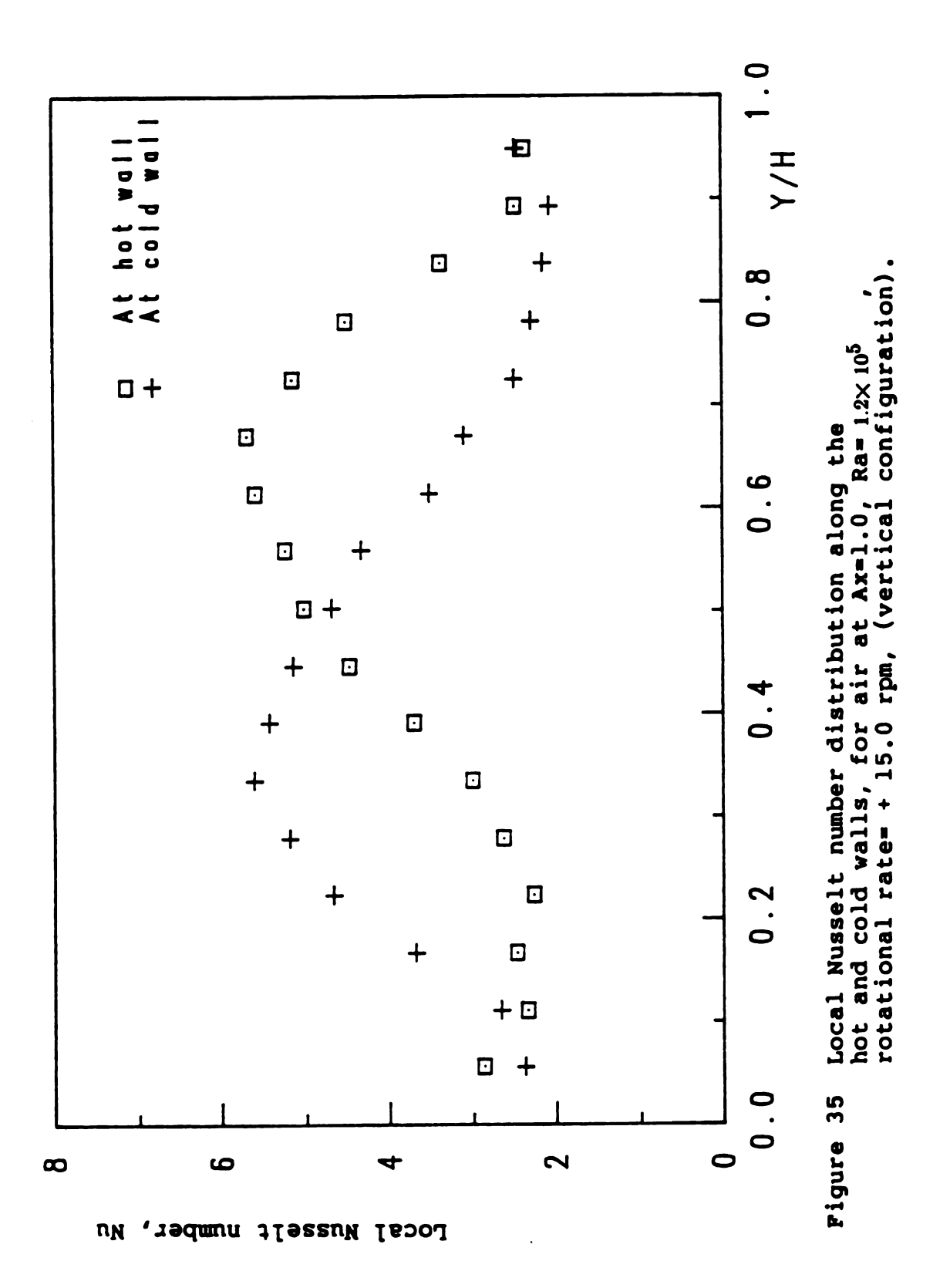
the general character of the local distribution of Nusselt number remains almost the same. This in fact implies an effective increase in the relative strength of the buoyant interaction which tends to improve the local heat transfer.

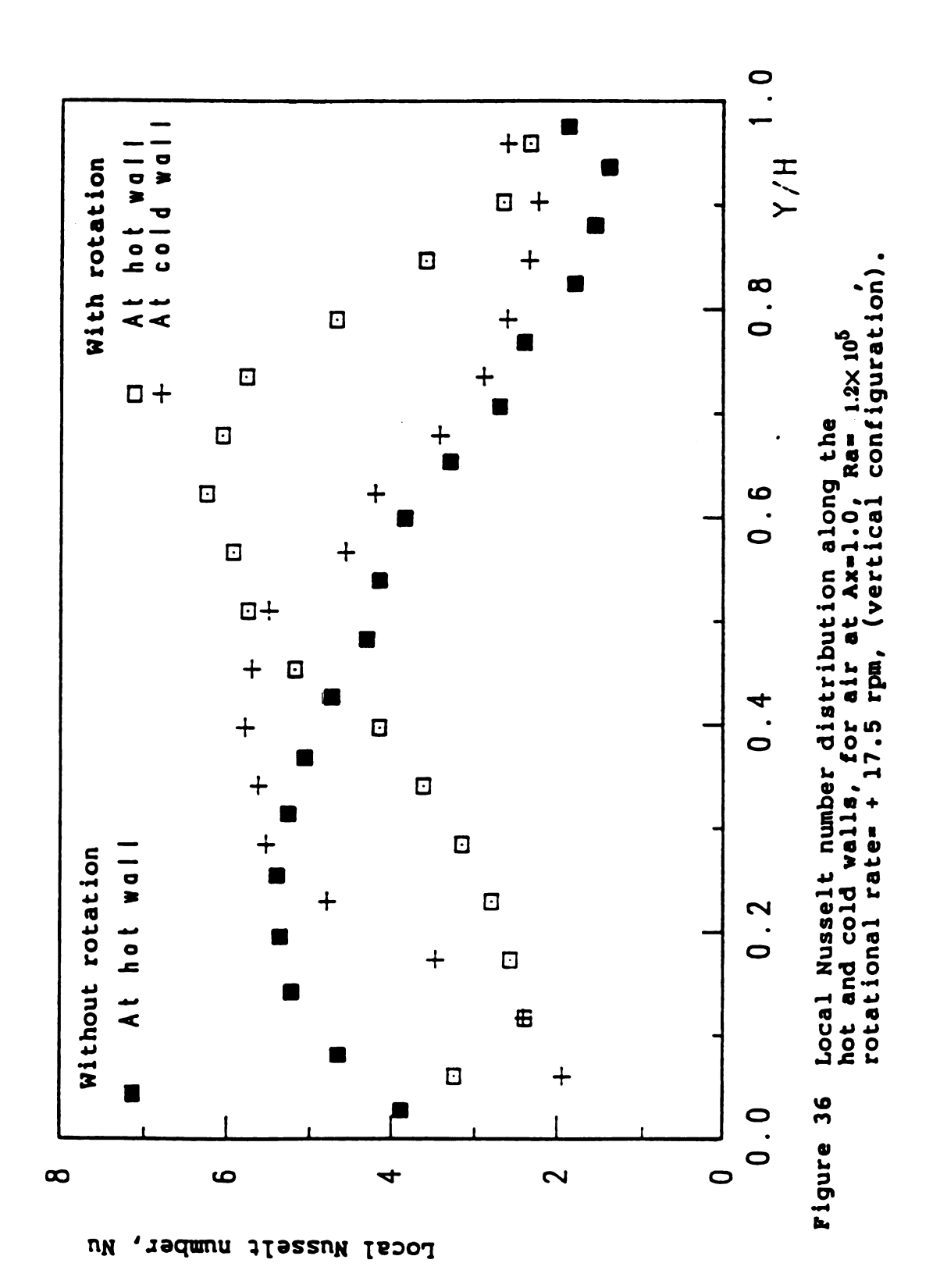
On the basis of the above discussion it may be proposed that at low rotational rates the reduction in local heat transfer is attributed mainly to the Coriolis-induced secondary flow in the xy cross-plane. Increases in the rotational rates will then produce a relatively thin boundary layer near the wall region which tends to improve the heat transfer as compared to the results at low rotational speeds.

So far, the discussion has focussed on the influence of the controlling parameters on the heat transfer results, and the buoyant interaction between centrifugal and gravitational buoyancy at a single gravitational Rayleigh number  $1.2 \times 10^5$ . An assessment of the effect of gravitational buoyancy on the local variations of Nusselt number will reveal more details on the inlfuence of Coriolis acceleration and centrifugal buoyancy. In this respect, Figures 37-40, demonstrate that the general trend of the local heat transfer distribution at gravitational Rayleigh number of  $2.0 \times 10^5$ , at various rotational speeds is similar to the local distributions of Nusselt number at Ra=1.2×10 as presented earlier for various rotational speeds. However, a related improvement in heat transfer is evident in connection with the increase of the operating temperature difference between the walls, which resulted in increasing the buoyant interaction effect on the flow and temperature fields.





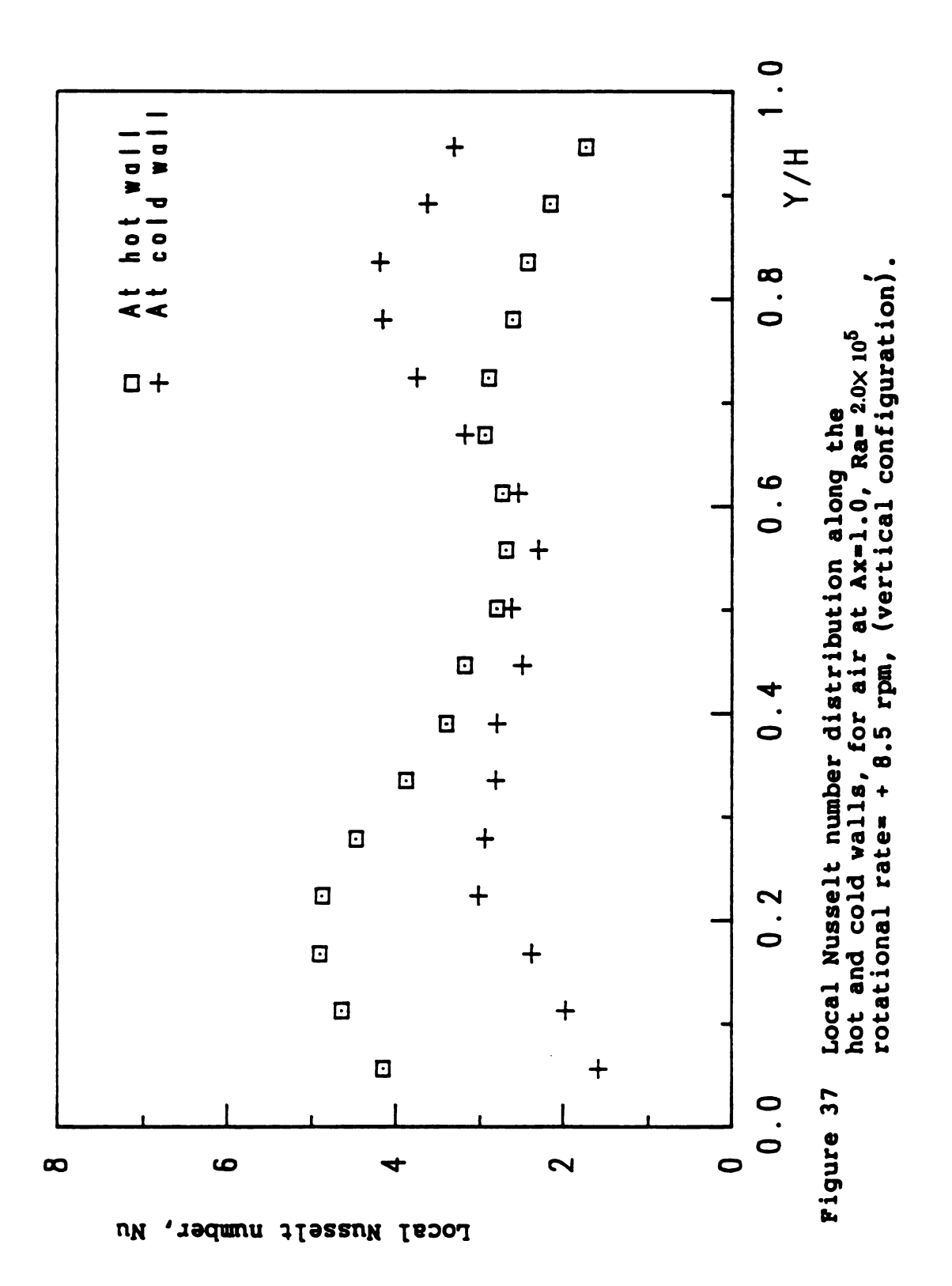


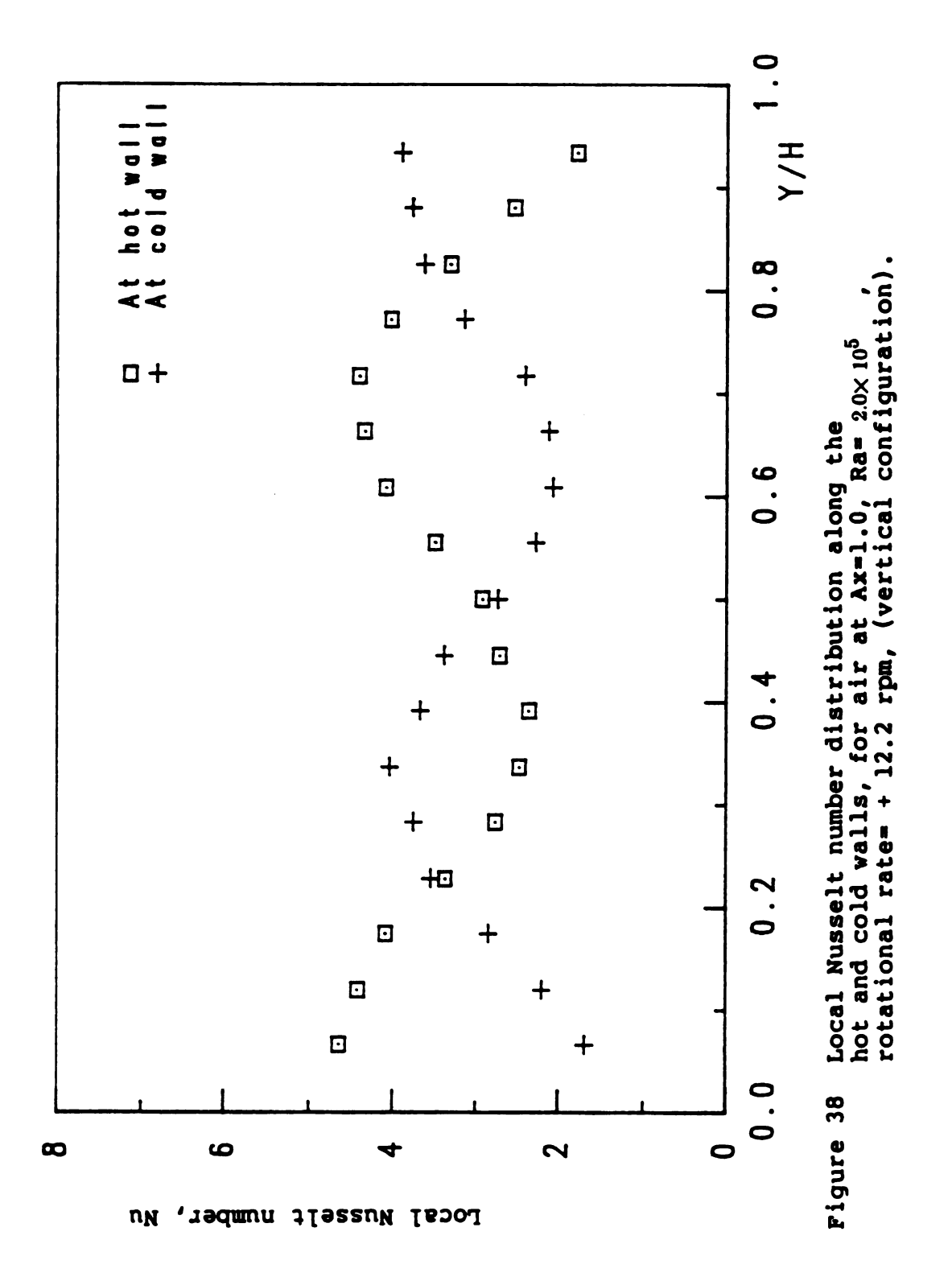


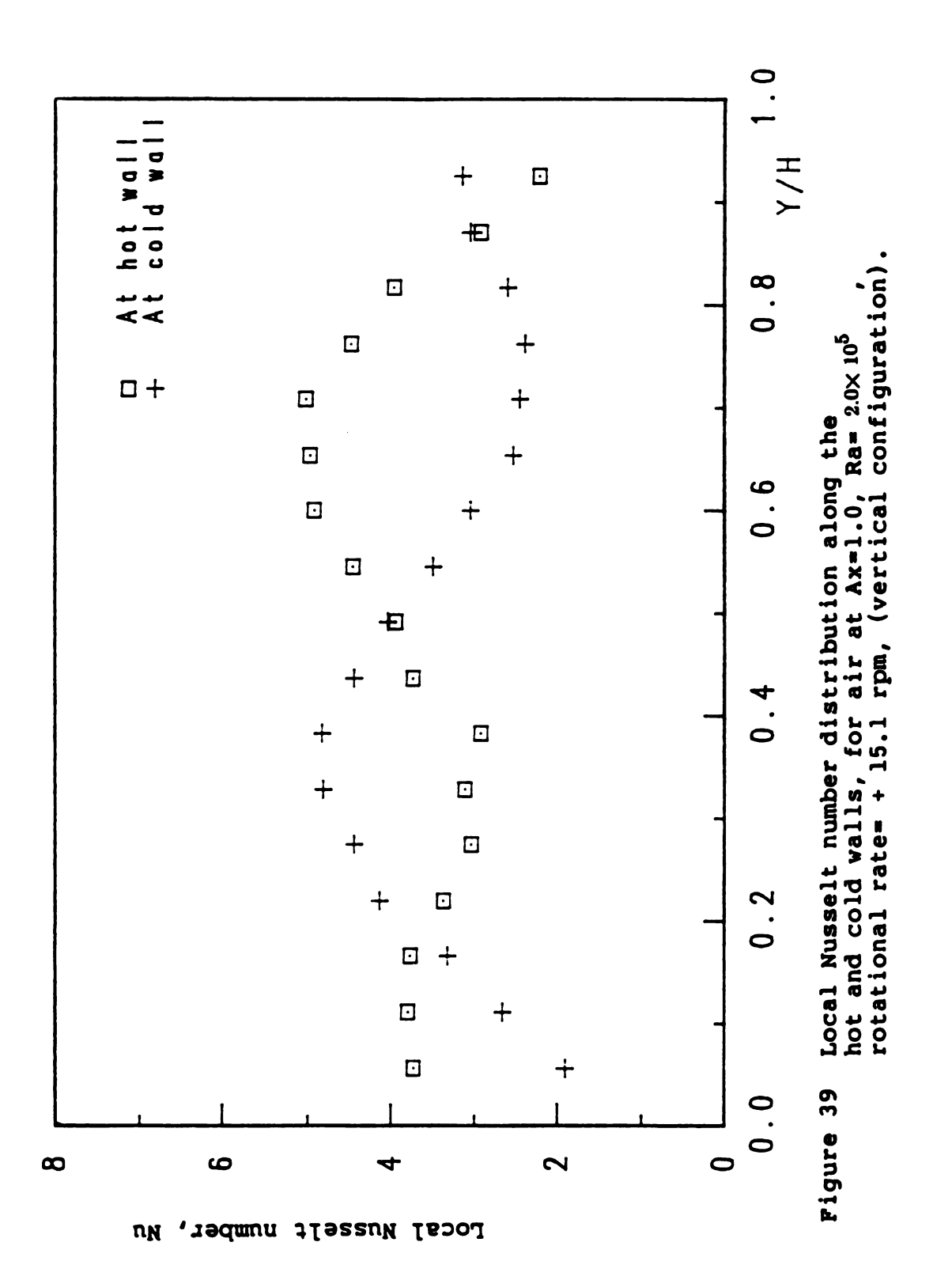
At a higher Rayleigh number, 3.0x10<sup>5</sup>, obtained by increasing the temperature difference between the two walls of the enclosure, Figures 41-45 suggest a relative improvement in the heat transfer with increasing Rayleigh number. However, the general trend of the local distribution of Nusselt number was in a good qualitative agreement with the results of local Nusselt number at Ra=1.2x10<sup>5</sup> for various rotational speeds. In this case the centrifugal buoyancy effect on the local heat flux distribution has occurred at a rotational speed of 12.2 rev/min instead of 8.5 rev/min as described earlier, due to the combined effects of the Coriolis and centrifugal acceleration on the flow. This would imply that in the case of hot air an increase in the tempreature difference between the walls can enhance the Coriolis effect on the flow and decrease the heat transfer.

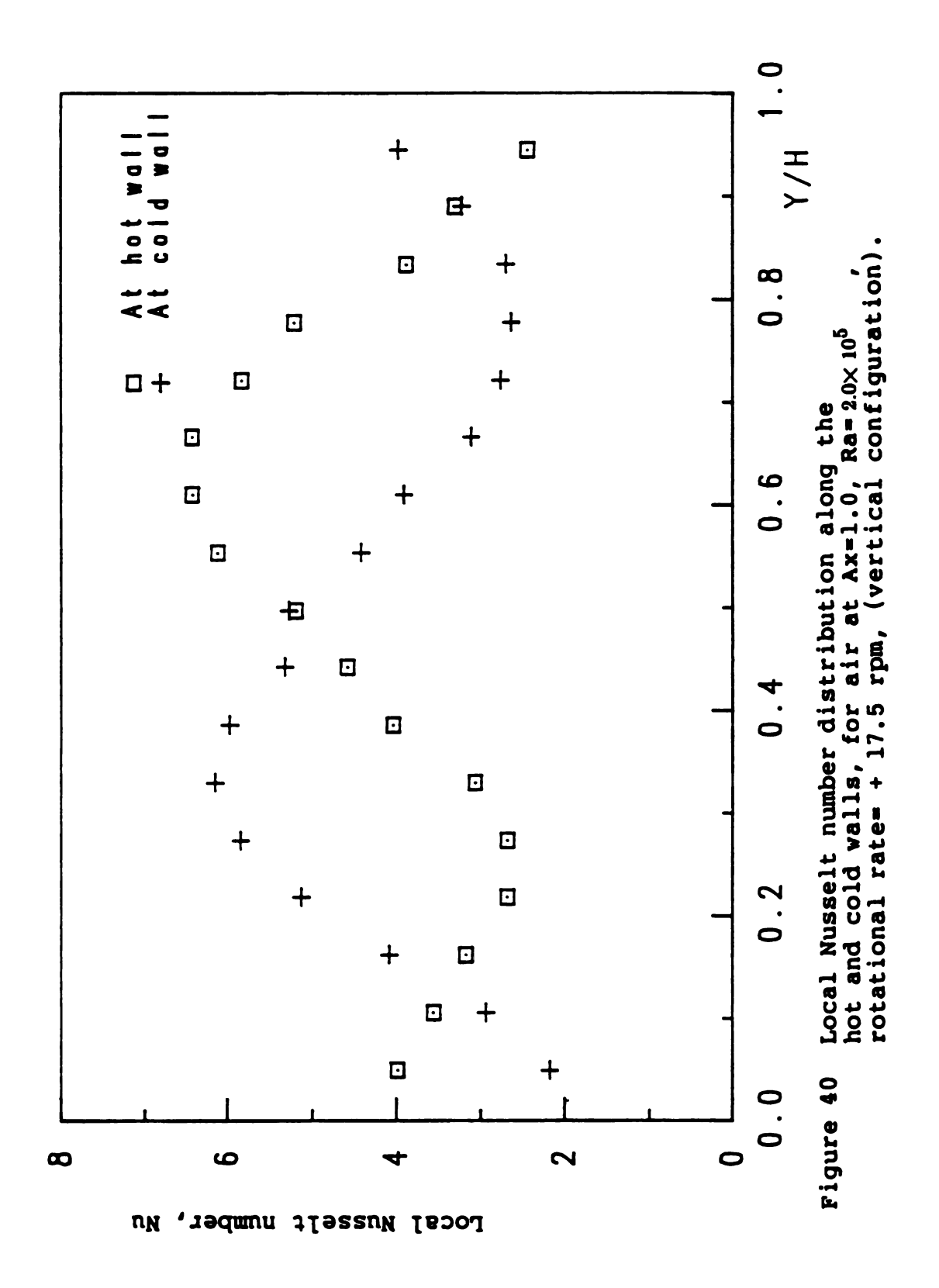
Figures 46-49, illustrate the local distribution of Nusselt number at Rayleigh number 7.4x10<sup>4</sup>. It is interesting to note in these figures that the buoyant interaction commences its influence on the flow and heat transfer at rotational speed 6.1 rev/min, compared with the local Nusselt number results presented in Figures 41-45. Hence, by decreasing the imposed temperature difference between the walls, the Coriolis effect on the local heat transfer variation can be made less significant.

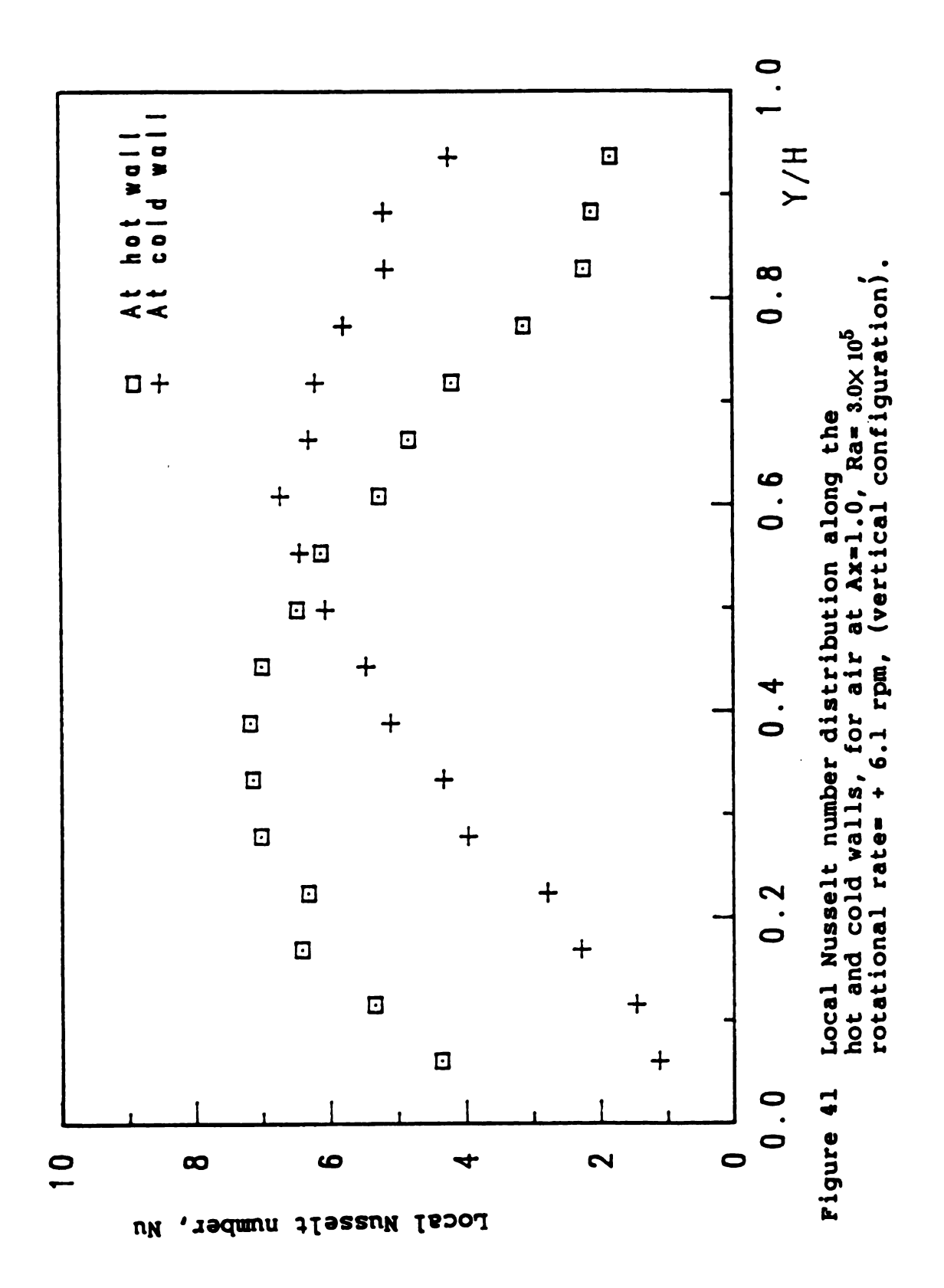
Thus far in this analysis the influence of rotation on the local Nusselt number variation showed a significant response to different values of the temperature difference between the walls. This was largely a consequence of the buoyant interaction. In this accord, the influence of rotation on mean Nusselt number can be explicitly connected to the above analysis. Figure 50, illustrates the results of

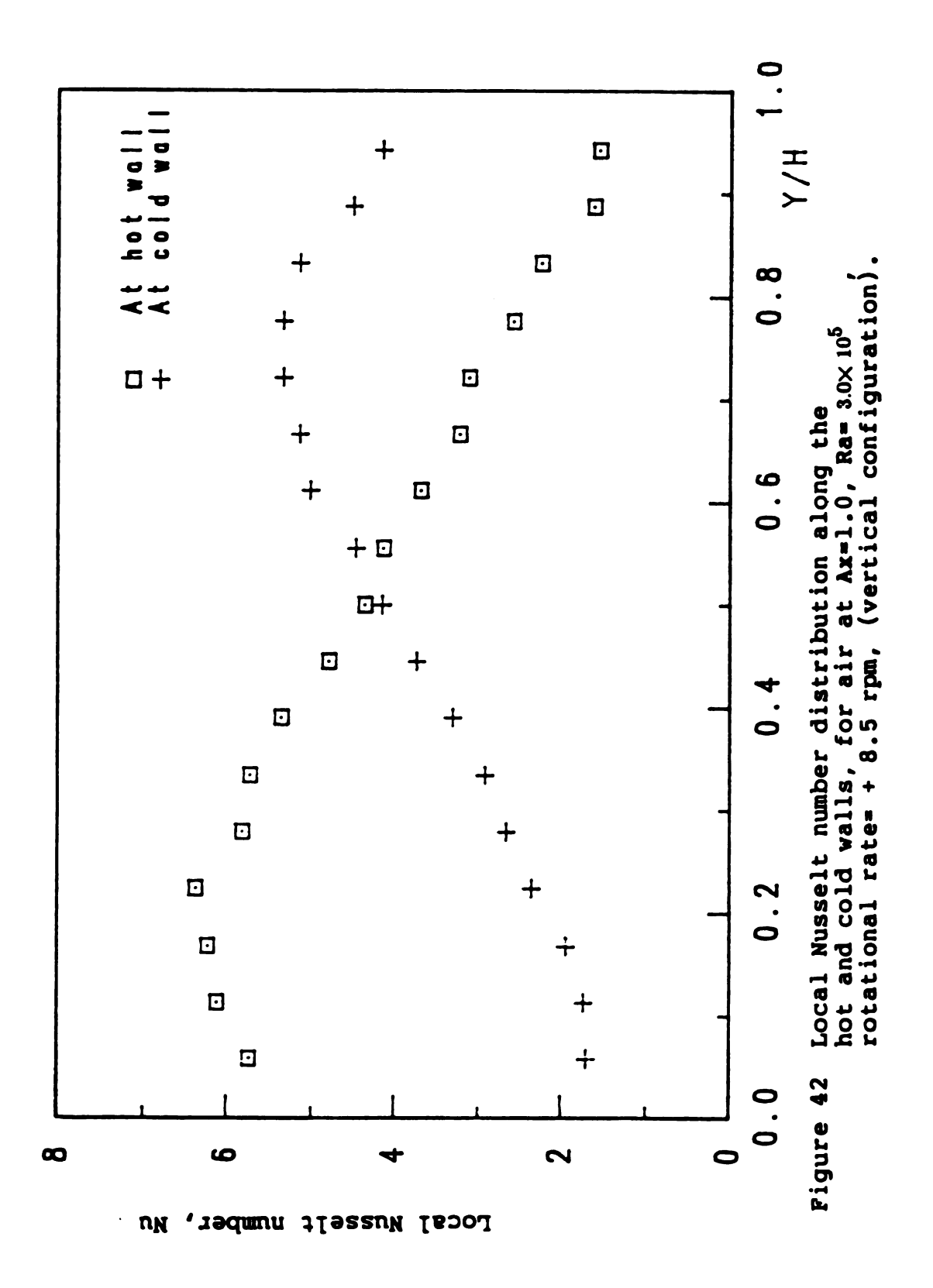


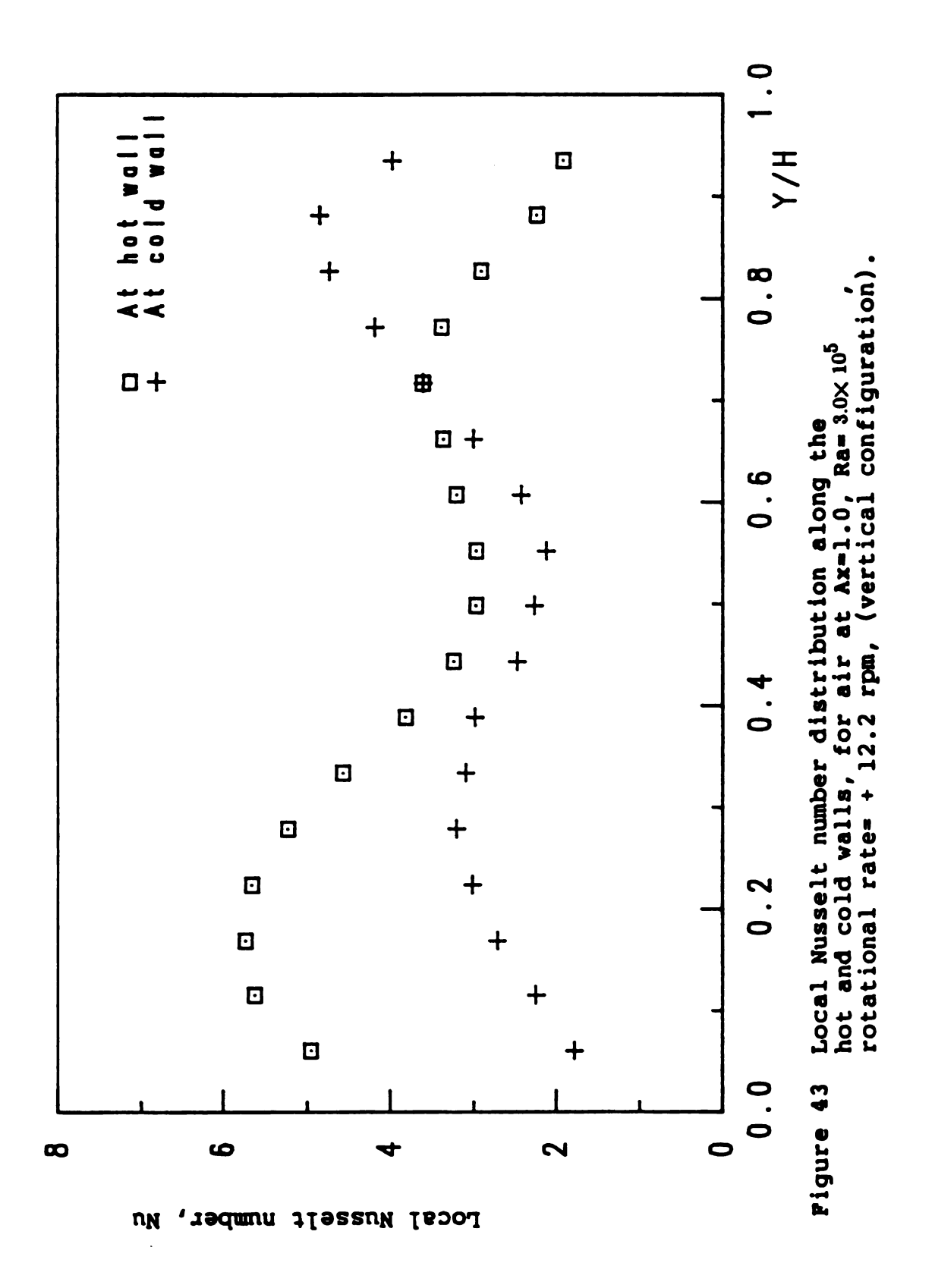


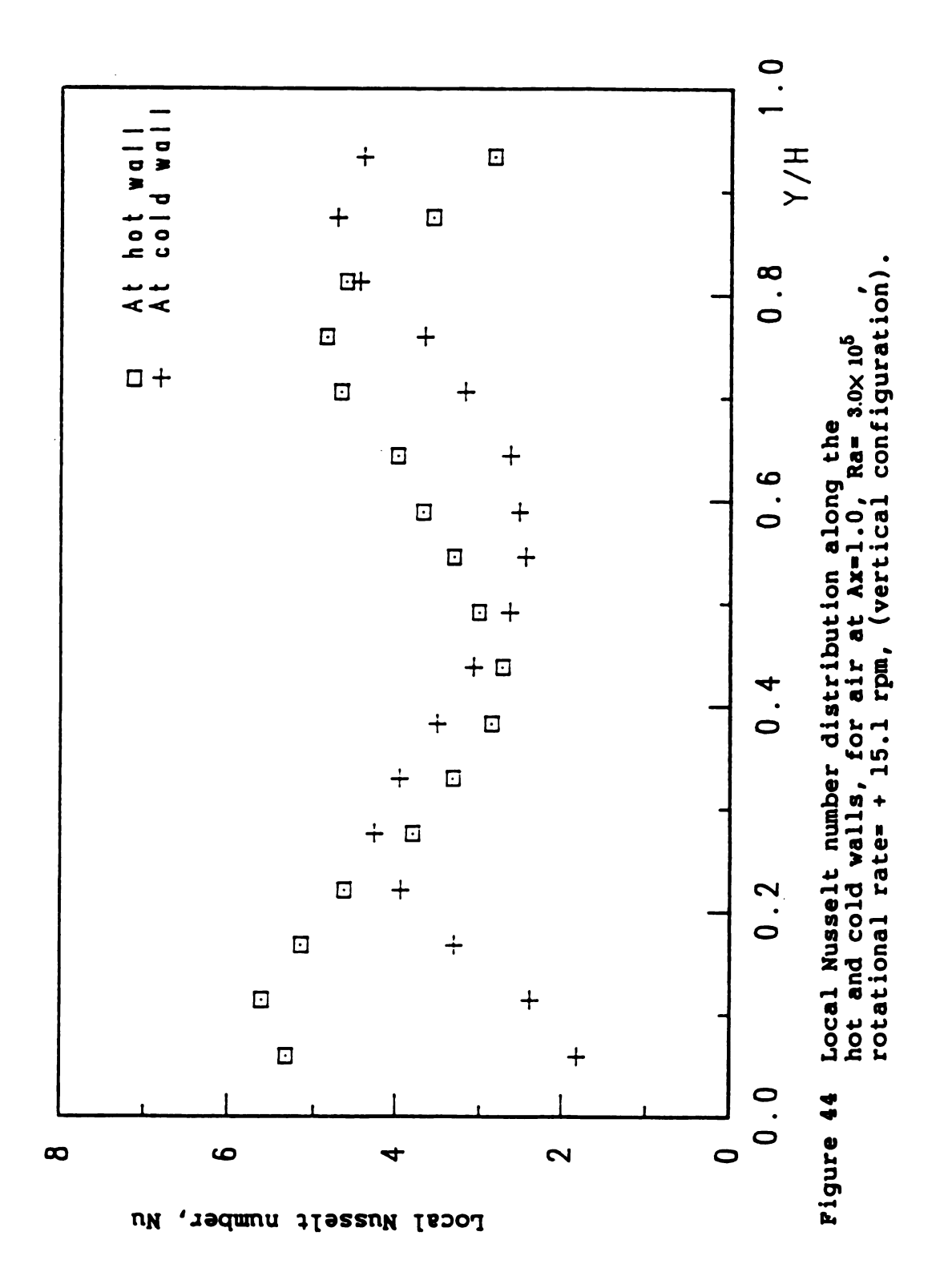


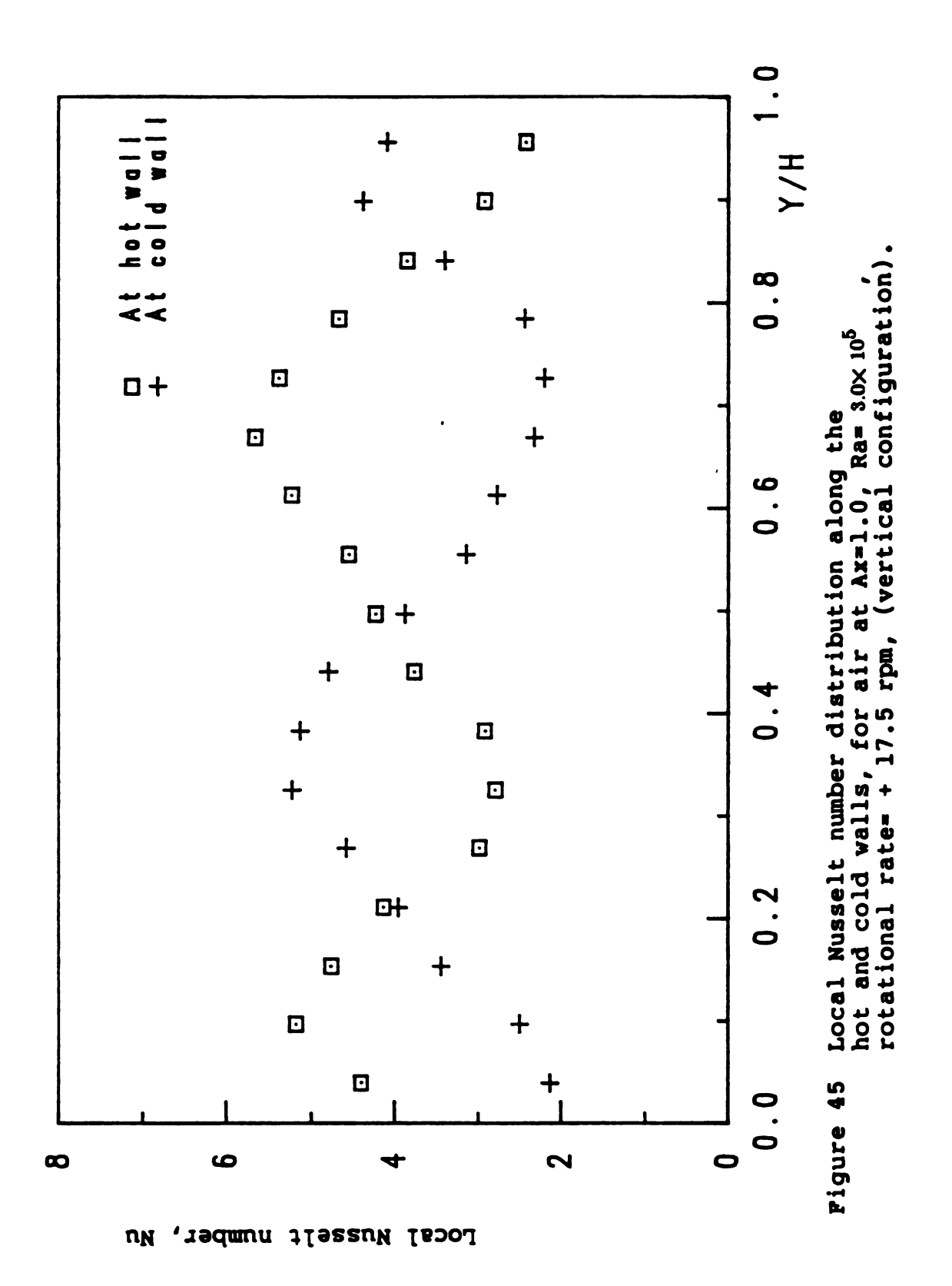










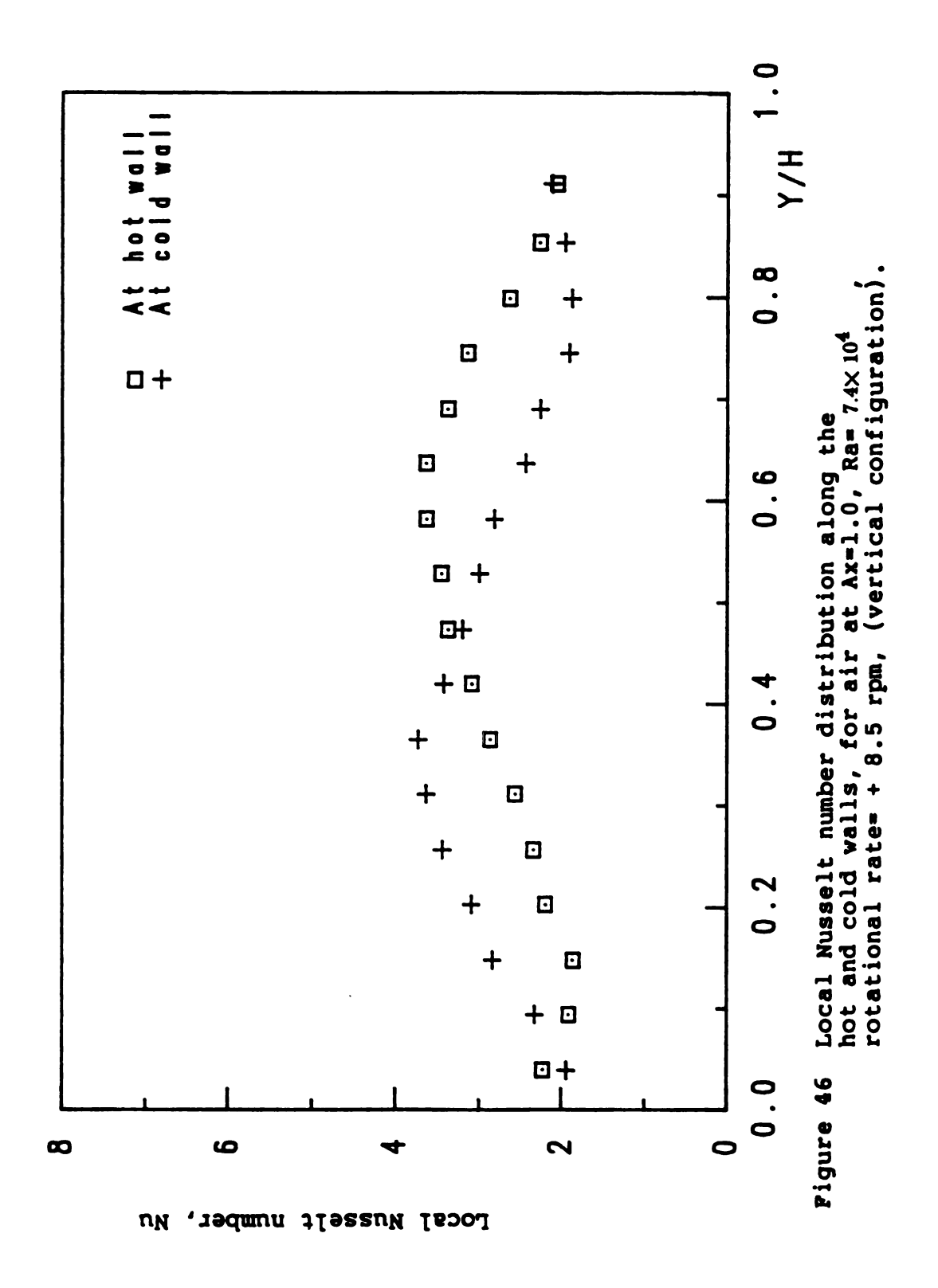


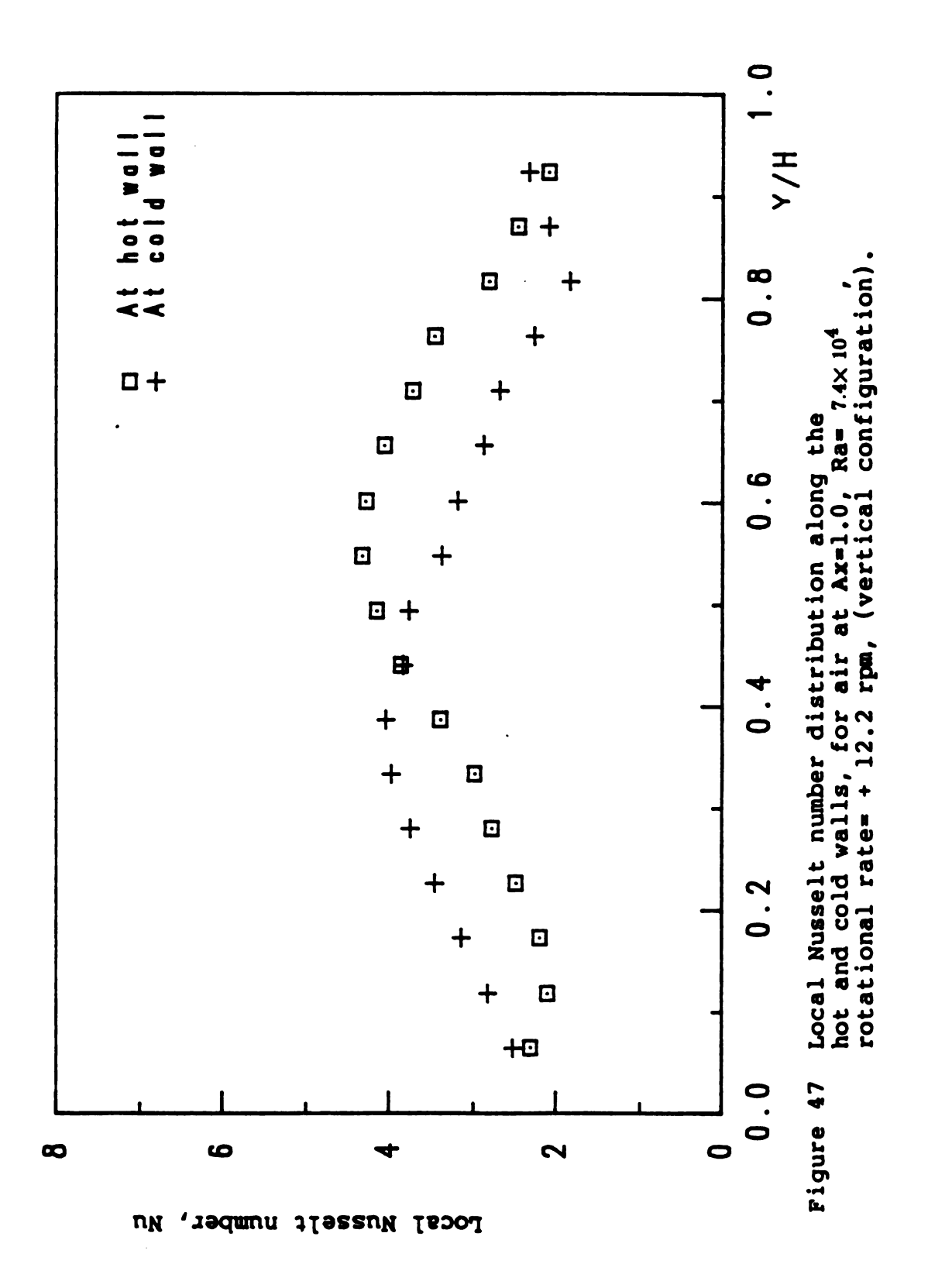
mean Nusselt number obtained with all rotational speeds at various gravitational Rayleigh numbers. This figure suggests that the Coriolis acceleration becomes very important at low values of rotational speed. At Taylor number of  $2.3 \times 10^{8}$  (-8.5 rev/min), it is observed that the mean Nusselt number attains its minimum value which indicates quantitatively the interaction between Coriolis acceleration and buoyant forces. However, with a further increase of the rotational speed the mean Nusselt number gradually increases due to the prevailing effect of the buoyant interaction on the flow and temperature fields.

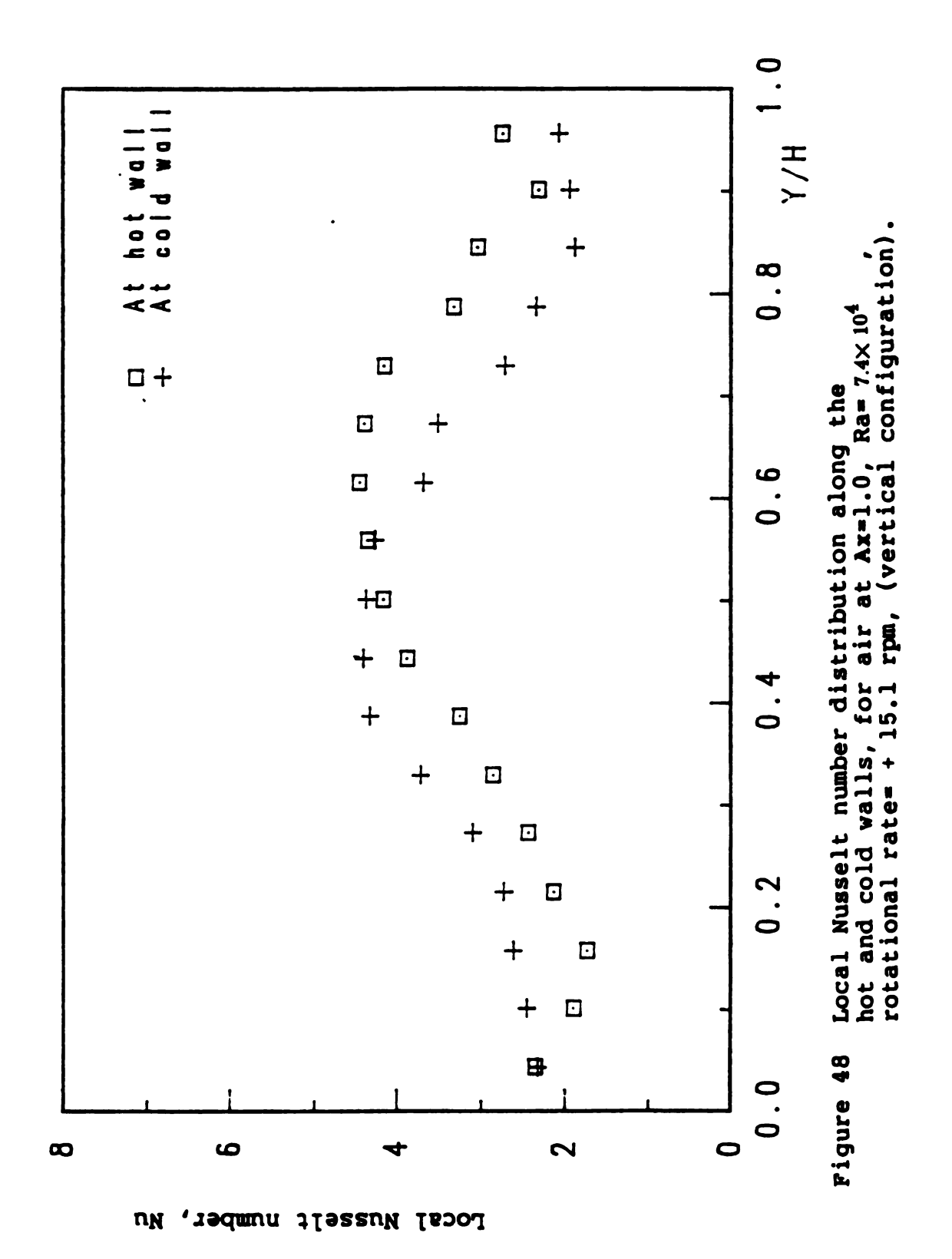
Figure 51a, shows the influence of rotation on mean heat transfer when plotted against the gravitational Rayleigh number. It is evident that a gradual increase of mean Nusselt number occurs due to increases in the rotational speeds. Figure 51b suggests a similar improvement in heat transfer when plotted as a function of the rotational rate, with the gravitational Rayleigh number as a parameter. This is a clear indication that, the buoyant interaction enhances the mean Nusselt number values. Furthermore, The experimental data displayed in Figures 51a and 51b, are correlated by the following equation,

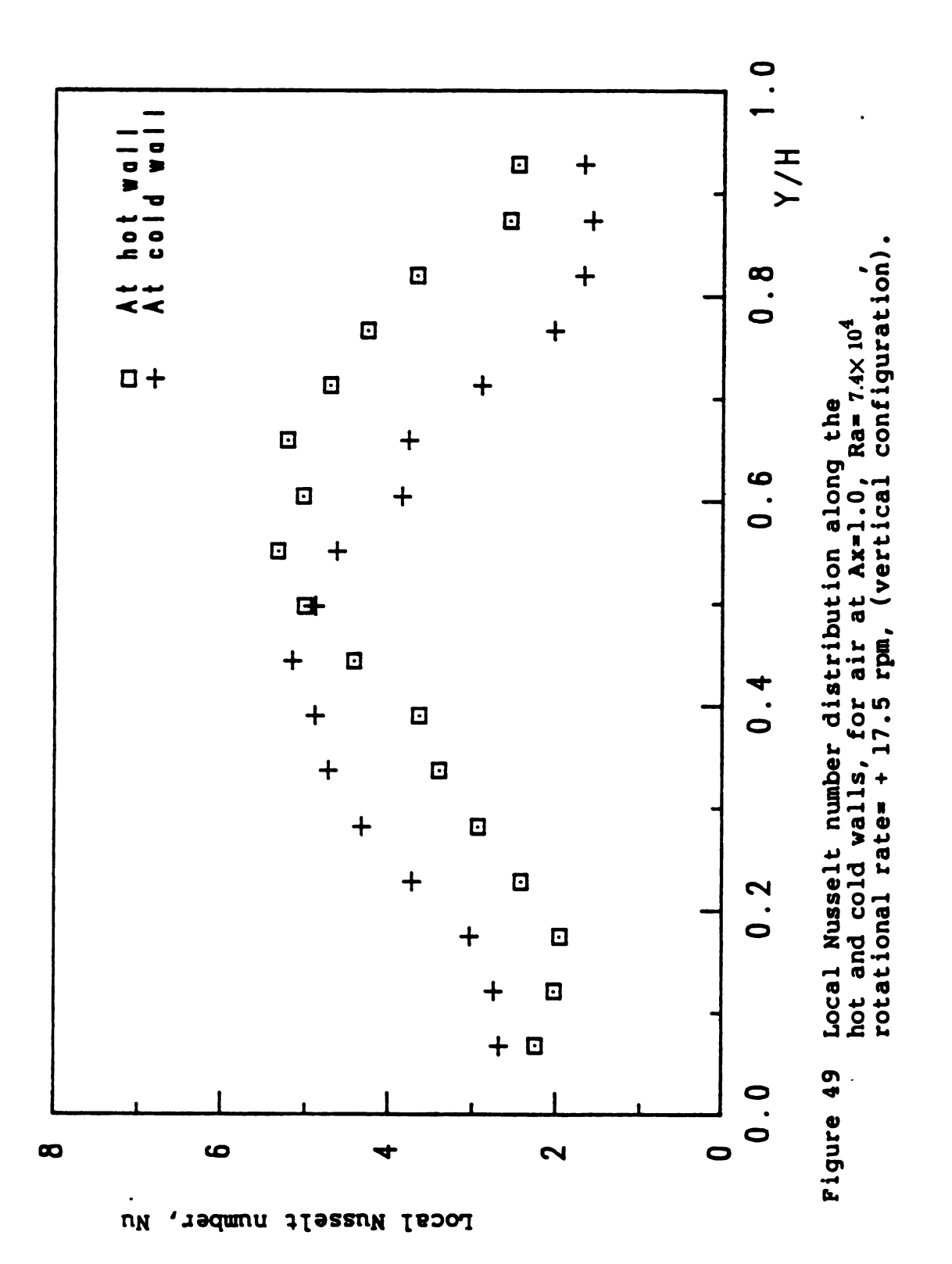
$$\overline{Nu} = 0.068 \text{ Ra}^{0.123} \text{ Ta}^{0.288}$$
 (4.2)

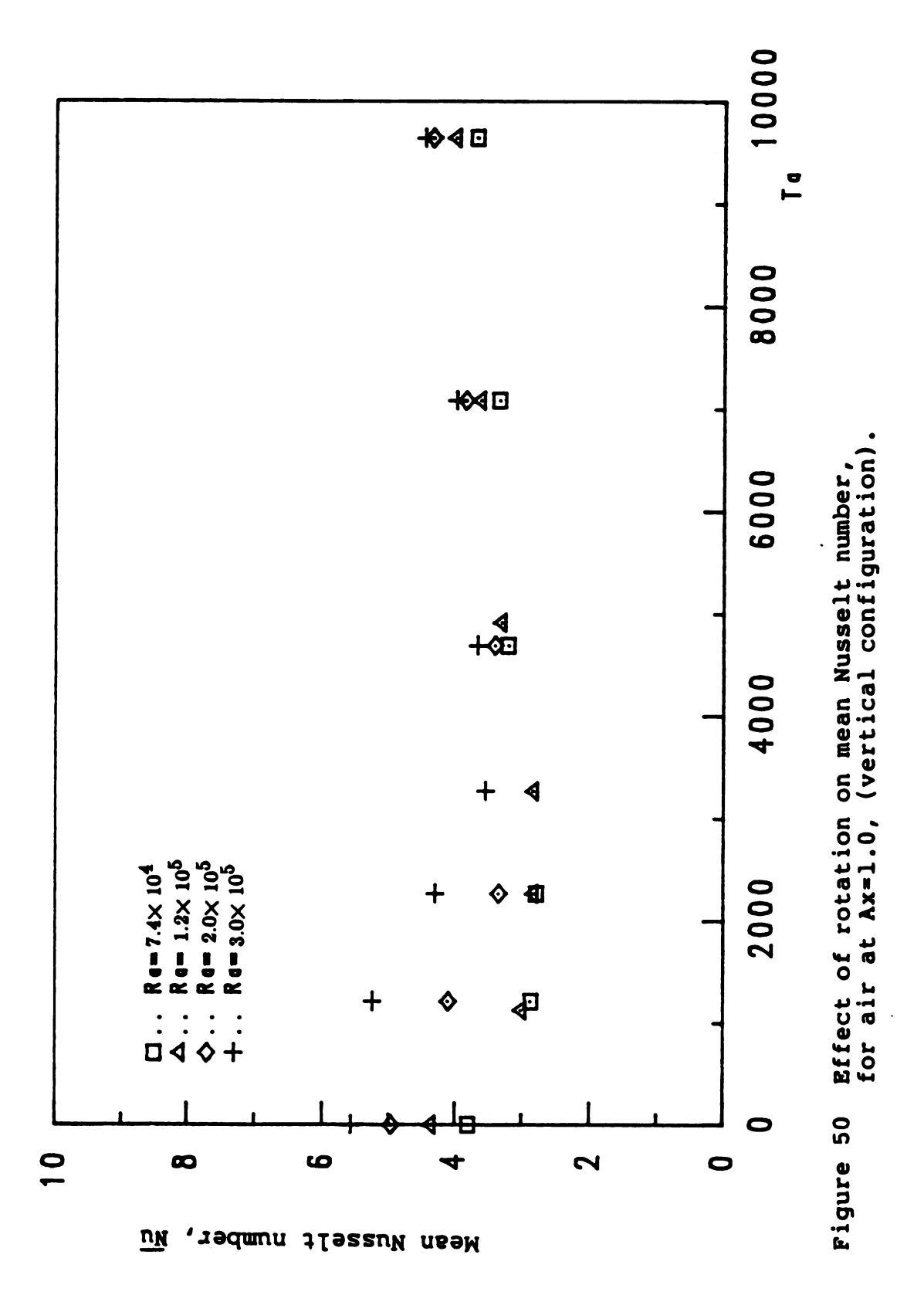
this equation predicts the experimental data within  $\pm$  4 % over a Rayleigh number range of  $10^4$  -  $3x10^5$ , and Taylor numbers between  $10^4$  . Figure 52 shows a comparison between the experimental data and the values from equation (4.2).





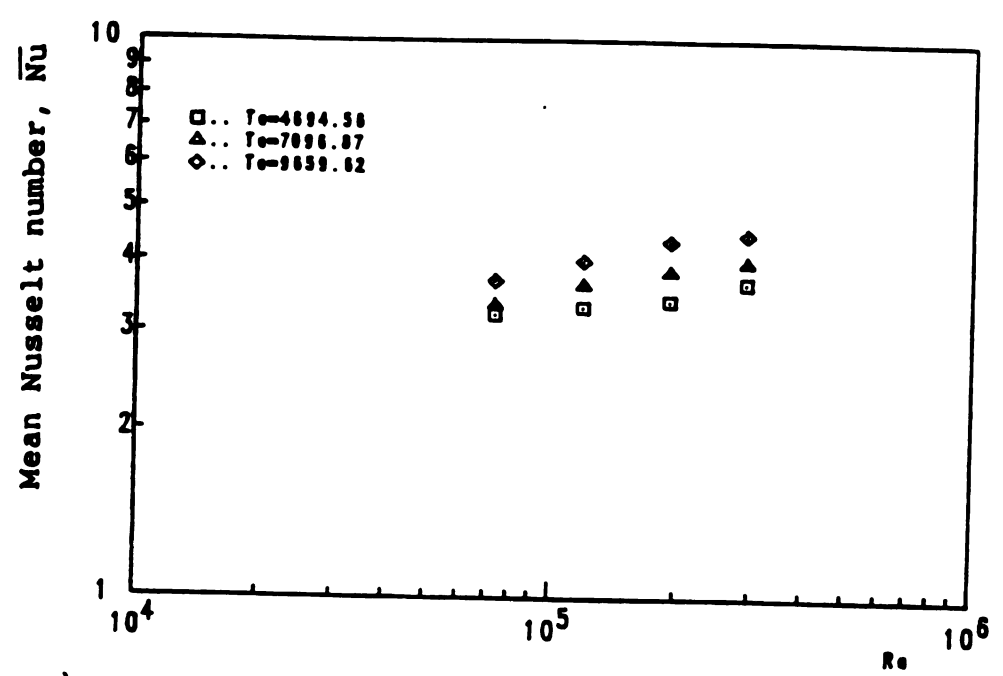




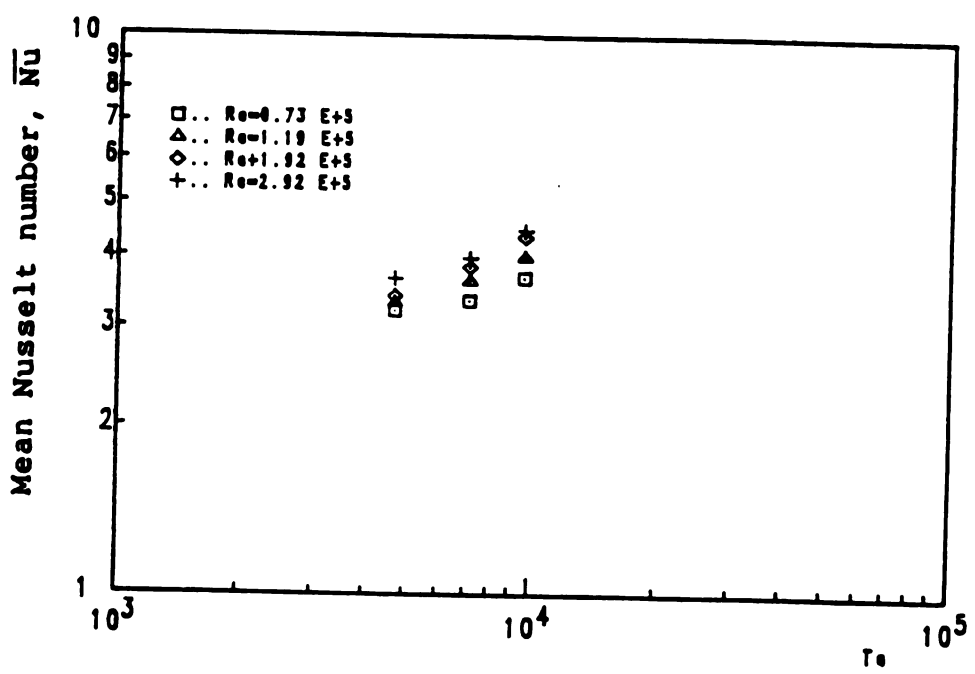


The way in which rotation affects the local and mean Nusselt numbers has been presented for the condition where the enclosure is rotated in the direction of the flow along the hot wall (aiding configuration). In contrast, for an enclosure rotating in the opposite direction to the flow along the hot wall (opposing configuration), it was found that the effect of rotation tends to decrease the heat transfer relative to the stationary condition with increases of the rotational speeds. Figures 53 and 54, clearly illustrate the reduction in the local heat transfer with increasing rotation rate. This may be accounted for by the complex interaction between the Coriolis acceleration and the centrifugal

buoyancy, which apparently tend to reduce the the heat transfer within the rotational speed limit (17.5 rev/min) considered in this study.

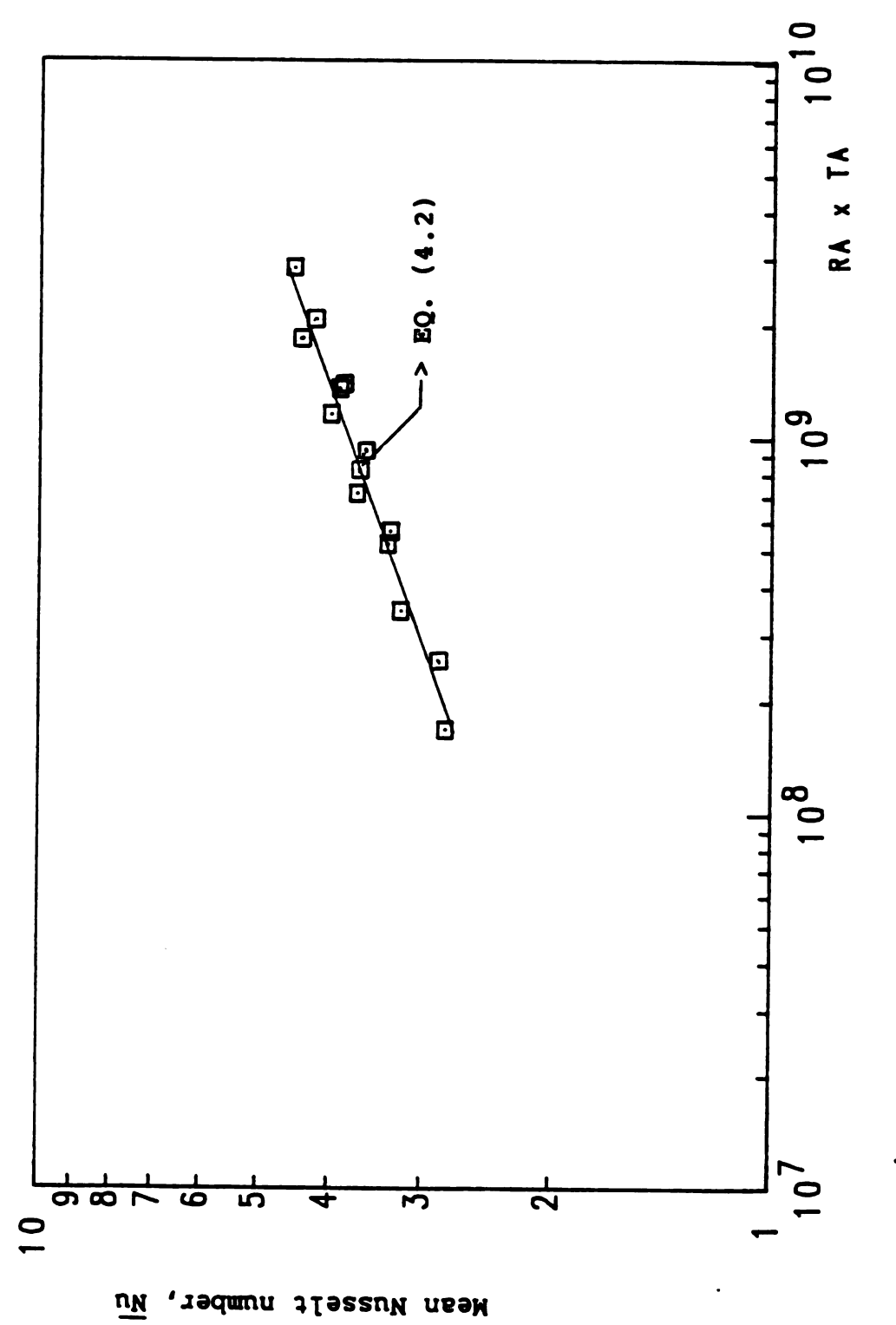


a) Mean Nusselt number versus Rayleigh number

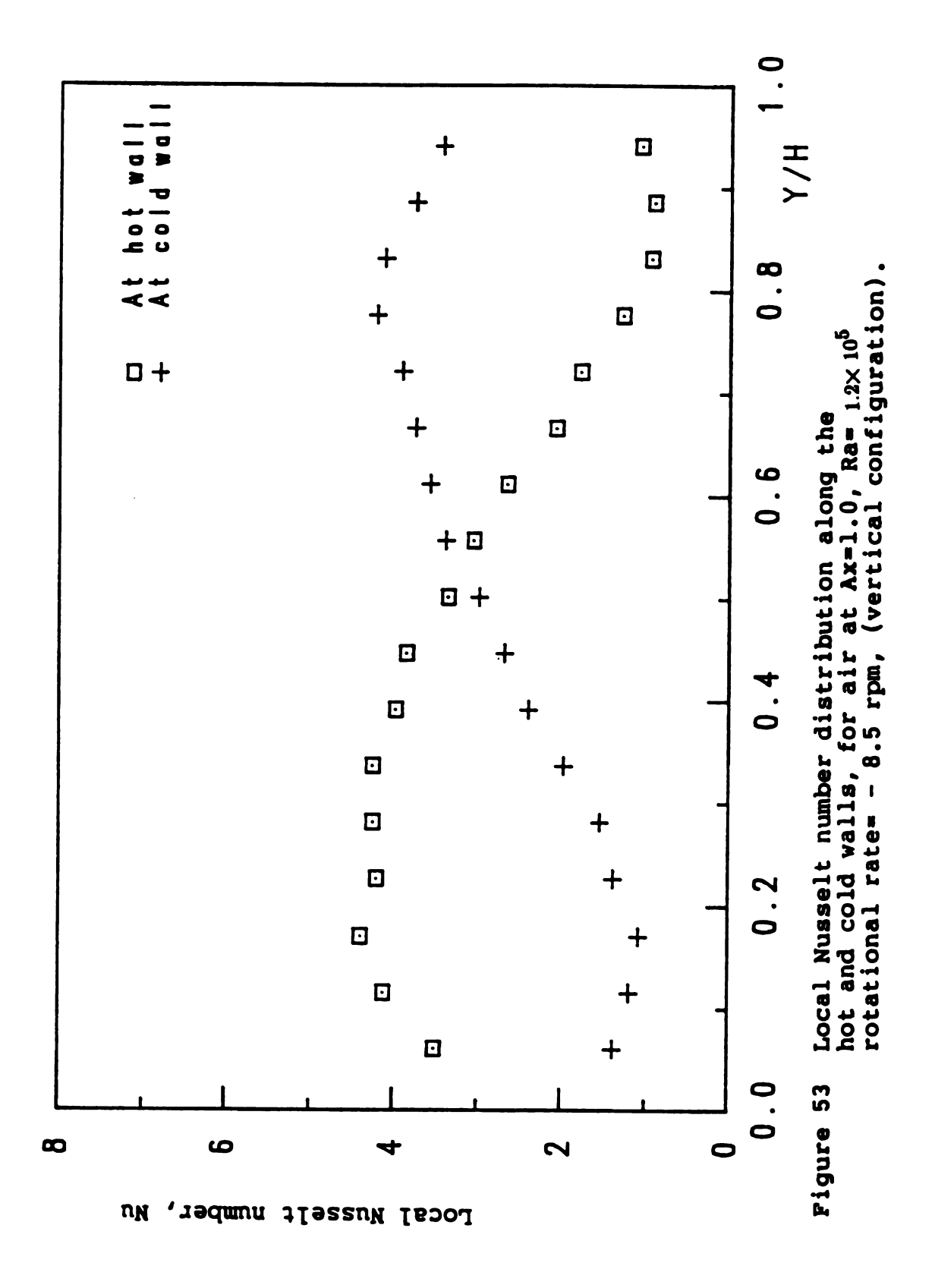


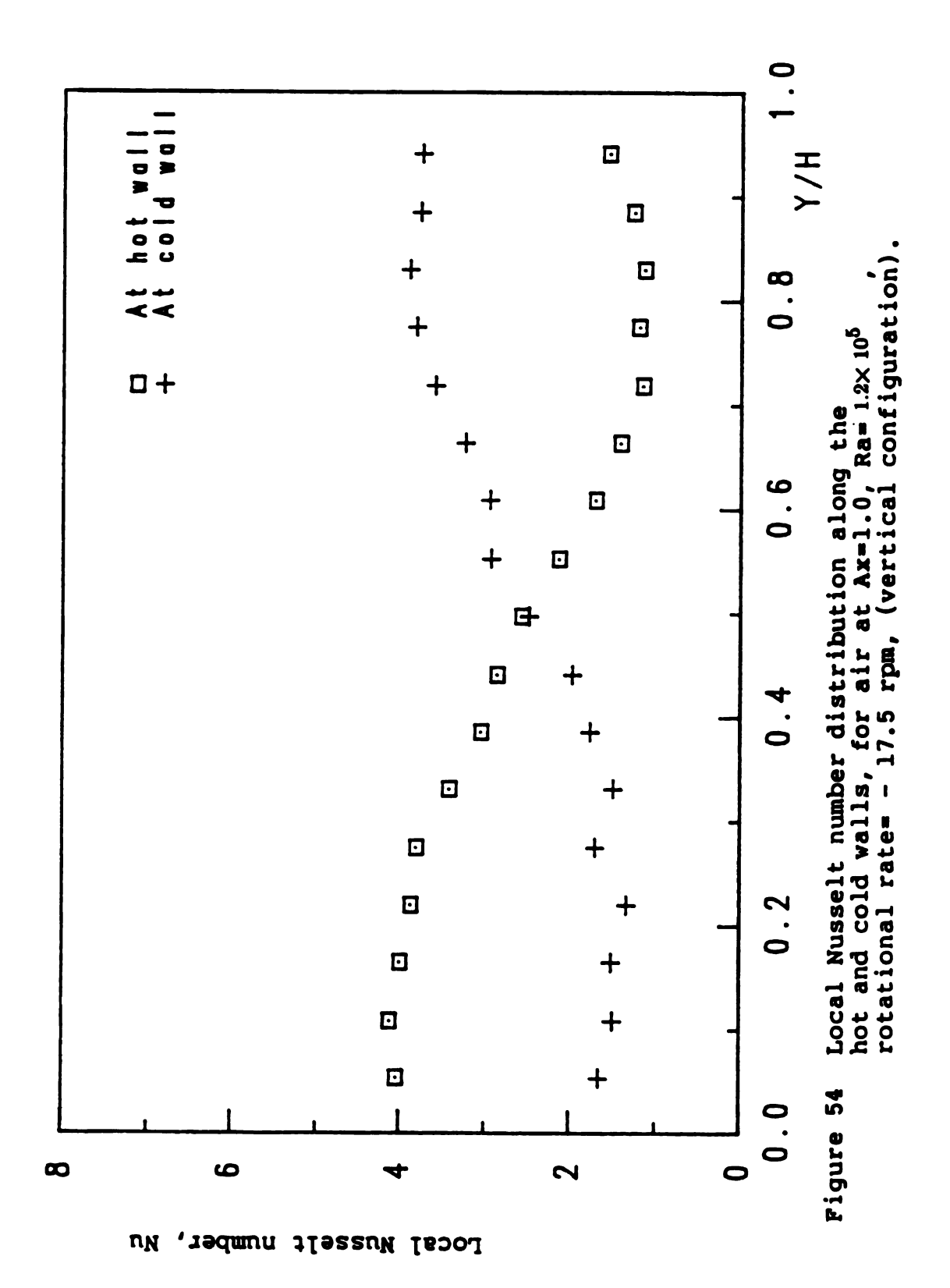
b) Mean Nusselt number versus Taylor number

Figure 51 Effect of rotation on mean Nusselt number, for air at Ax=1.0, (vertical configuration).



Mean Nusselt number as a function of Taylor and Rayleigh numbers. Figure 52





# 4.2.2 Heat Transfer Results in a Heated Rotating Enclosure at Angular Position of 180 Deg. (Heated from Below)

The present sub-section examines the effect of rotation on the onset of cellular motions in a rotating heated from below air-filled enclosure (Benard convection). This should lead to better insight into the hydrodynamic and thermal boundary layer developments under the influence of the controlling parameters, namely, the Taylor, rotational and gravitational Rayleigh numbers.

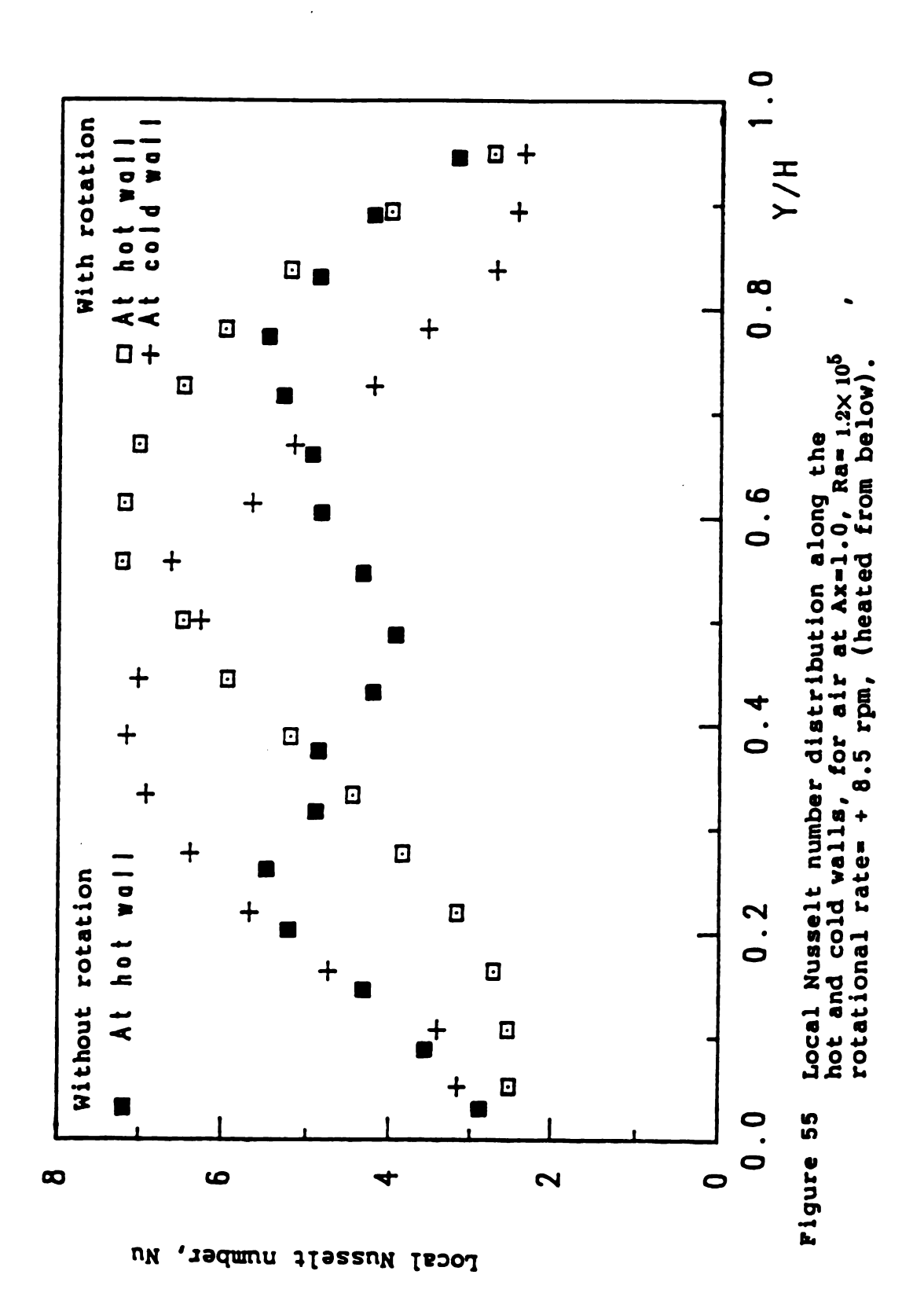
The onset of convection in a non-rotating enclosure was described previously in Figures 28a,b. Unstable temperature stratification in the vertical direction, a flow of a series of roll-cells with their axes oriented normally to the isothermal walls were observed. Accordingly, the inhibiting effect of rotation on the onset of the thermal instability will be analyzed relative to these aspects. The measurements of local Nusselt number will demonstrate the corresponding variations of the thermal boundary layer thickness, and the extent of inhibition on the onset of cellular convection.

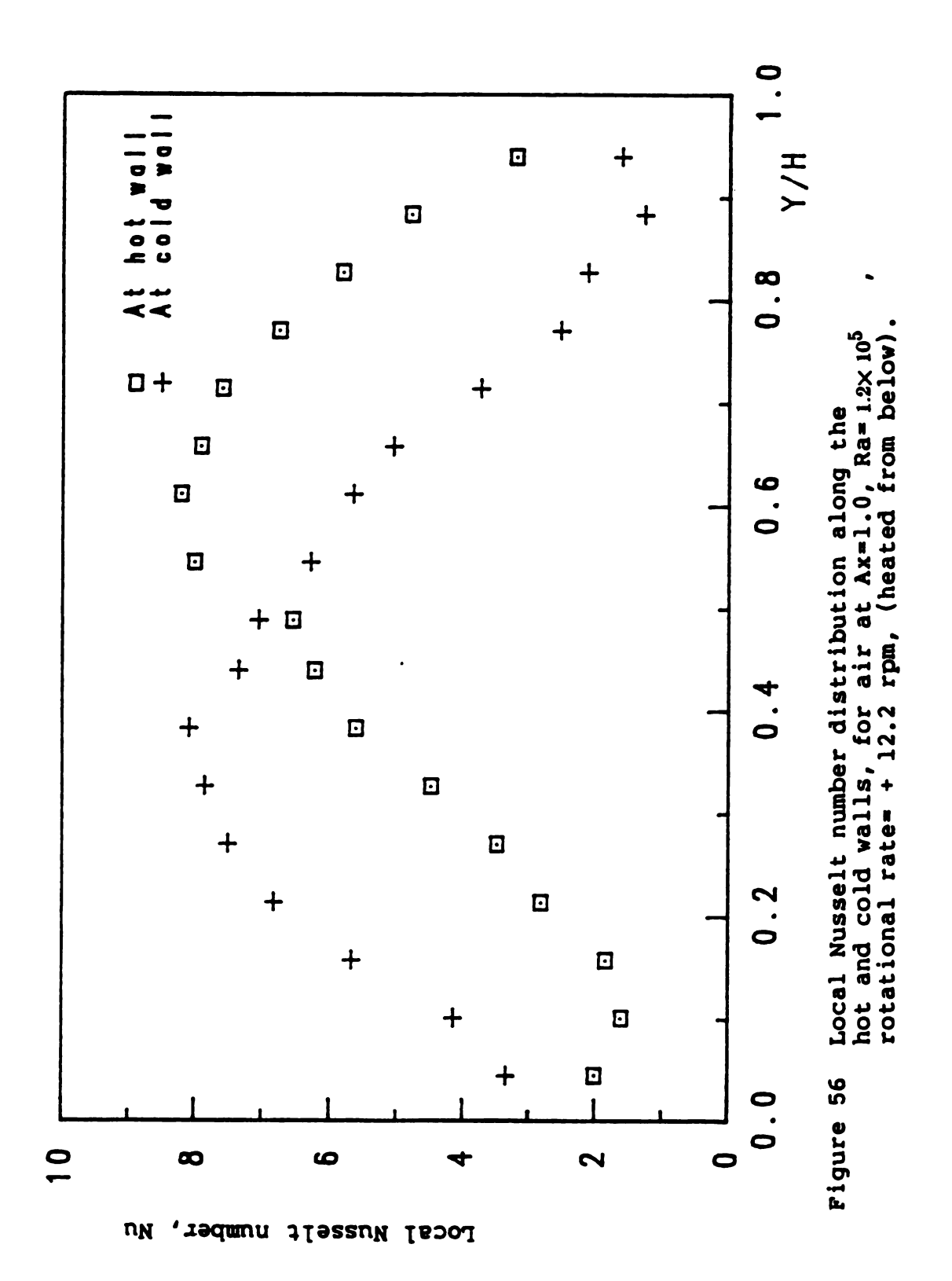
The way in which rotation affects the local distribution of Nusselt number is demonstrated in Figure 55 for Ta= 2.278x10 (-8.5 rev/min), Ra<sub>r</sub>=1.21x10, and Ra=1.2X10. It is evident from this figure that rotation produces a marked effect on the local heat transfer distribution as compared to the stationary experimental data. Two explanations may be argued for the characterization of rotational effect. First, it is reasonable to assume that the combined effect of Coriolis force and buoyant interaction has a strong influence on the cellular motions (unstable condition), which in turn tends to inhibit the thermal instability. Secondly, for the current operating

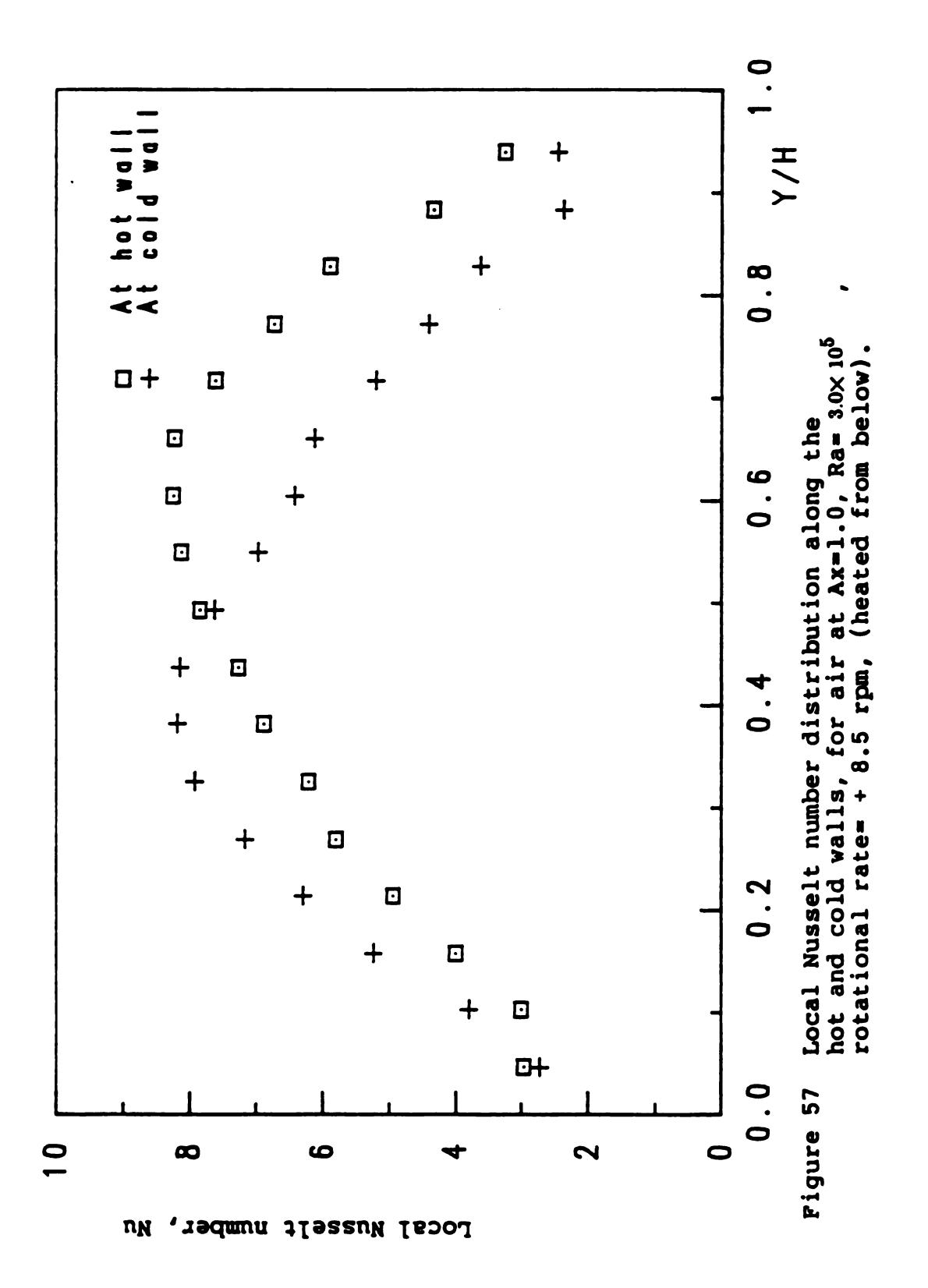
conditions, it is found that transition from a cellular motion to a longitudinal roll-cell has occurred, since in this case buoyant interaction between centrifugal and gravitational buoyancy dominates the flow development and consequently the thermal boundary layer. Moreover, the local distribution of Nusselt number reflects clearly the subsequent thinning in the thermal boundary layer near one end of the isothermal wall and a relative thickening near the other. This is significantly different from the thermal boundary layer encountered in the stationary situation of the unstable fluid. This aspect is mainly a result of the longitudinal flow pattern generated in the vicinity of the wall region, which indicates the significant effect of rotation on the flow, and hence delays the onset of thermal instability to at least a higher operating temperature difference, and slightly improves the heat transfer. Both these concepts offer areas where further development can be extended in the future to the case of higher rotational speeds and various Prandtl numbers.

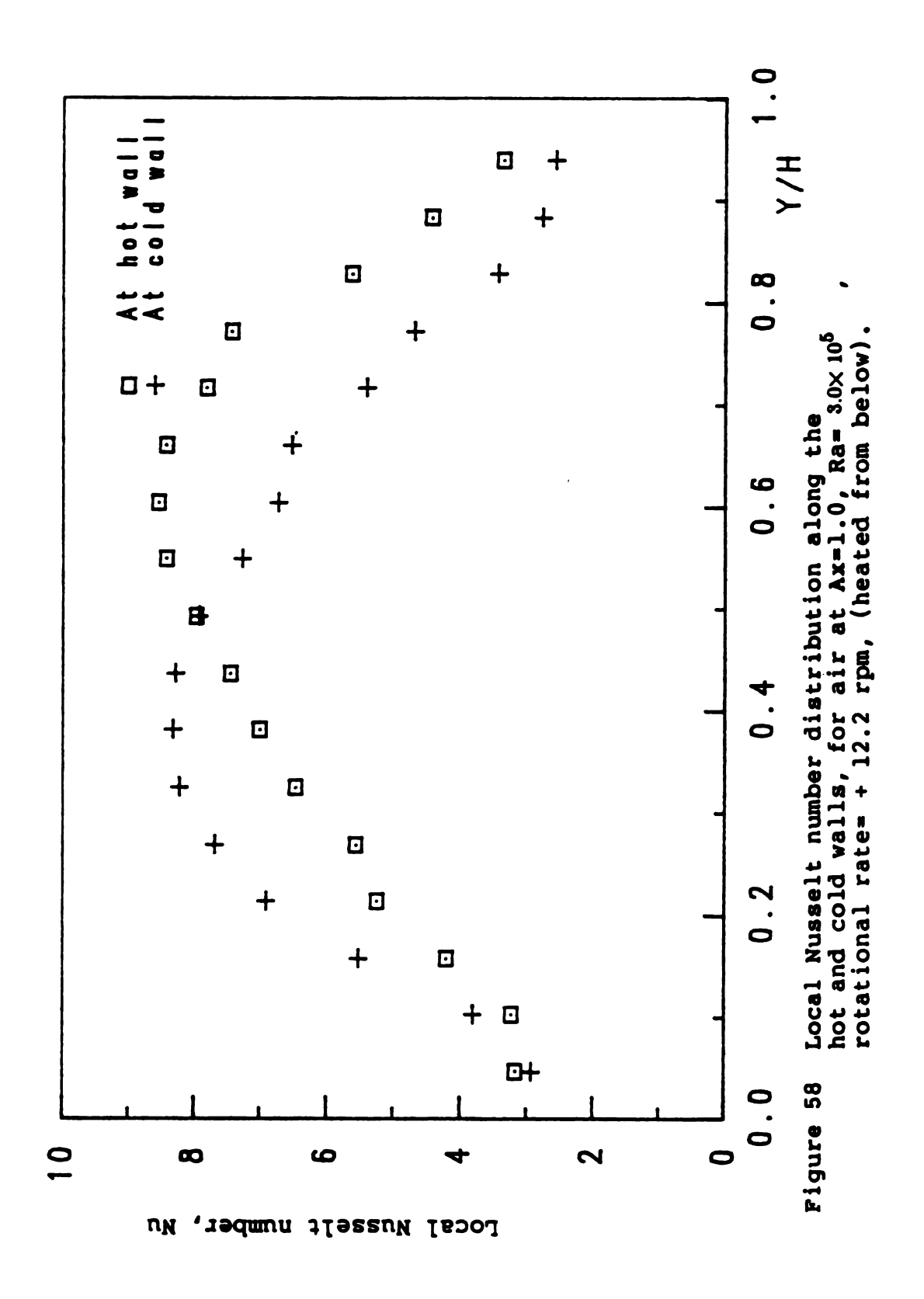
Figure 56 shows the distribution of local heat transfer at a rotational speed 12.2 rev/min. It is interesting to note that the distribution of local Nusselt number is very similar to the results presented in Figure 55. Hence it suggests no significant changes in the hydrodynamic and thermal boundary layers have taken place. A small increase in heat transfer has occurred.

The local Nusselt number distributions for rotational rates of 8.5 and 12.2 rev/min, and for Rayleigh number  $3.0 \times 10^5$  are illustrated in Figures 57 and 58. It is apparent that the distribution of local Nusselt number is almost as before, however the improvement in heat transfer with increases in rotational speed and imposed temperature difference is detectable but not very marked.





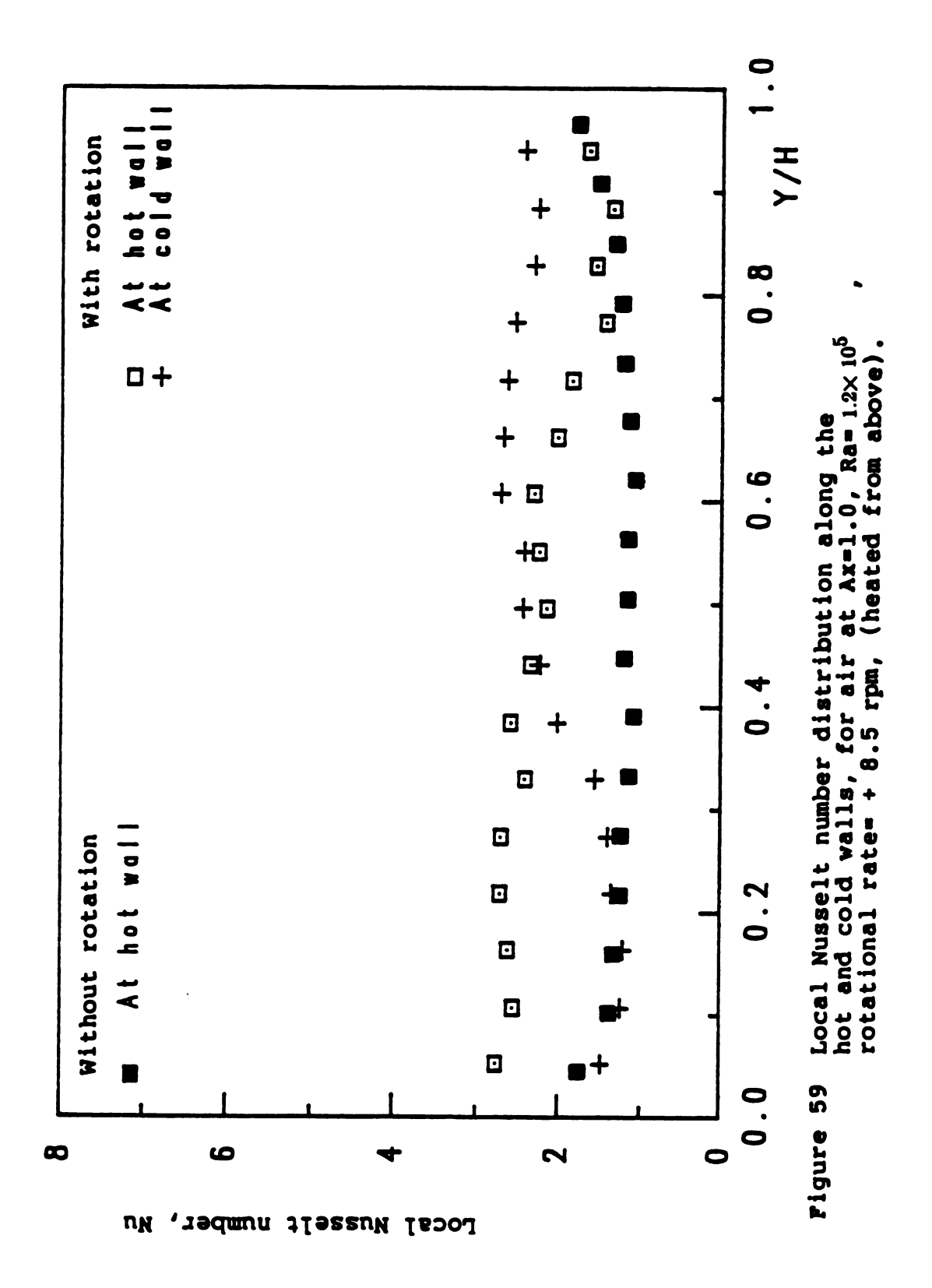


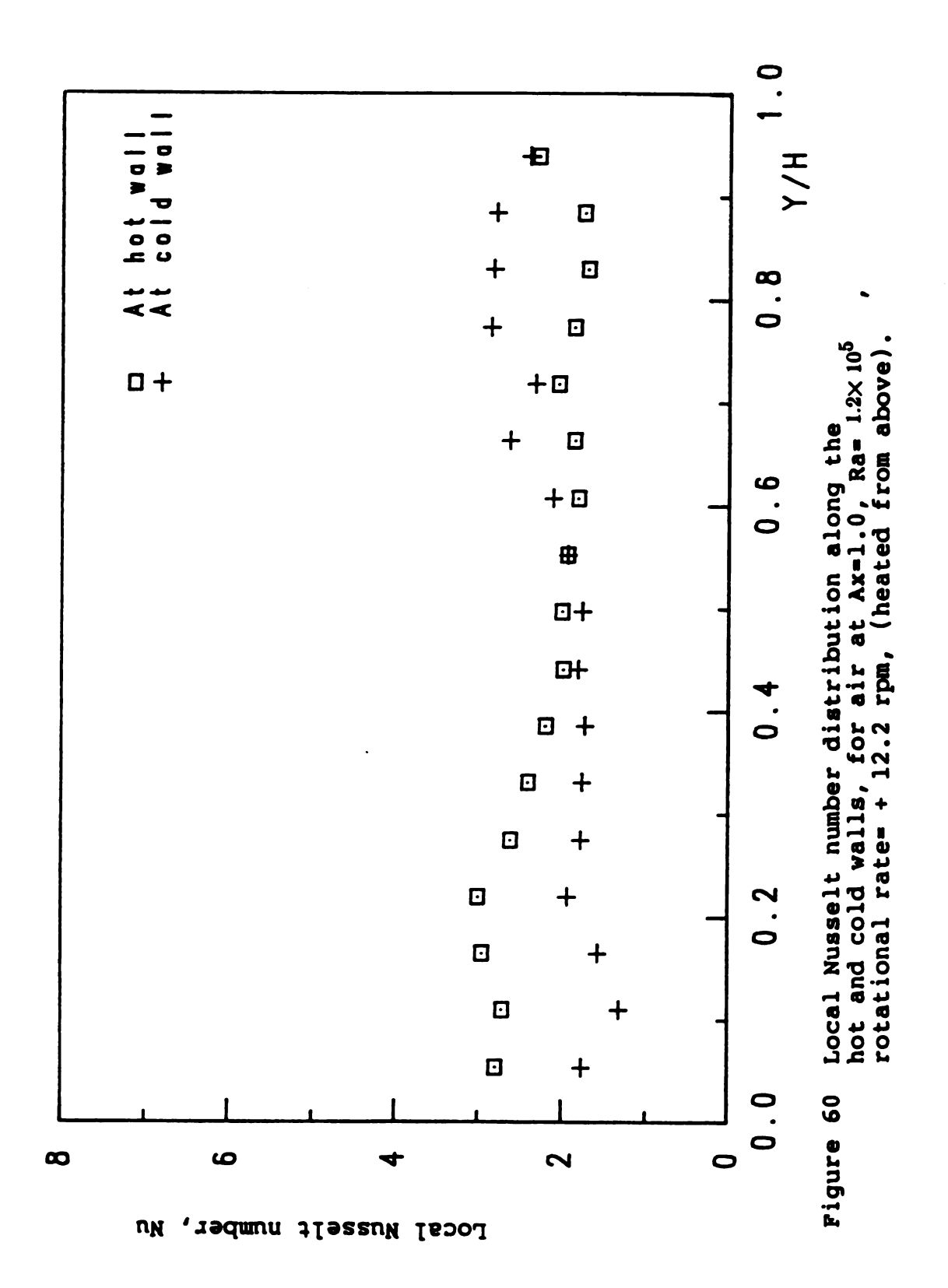


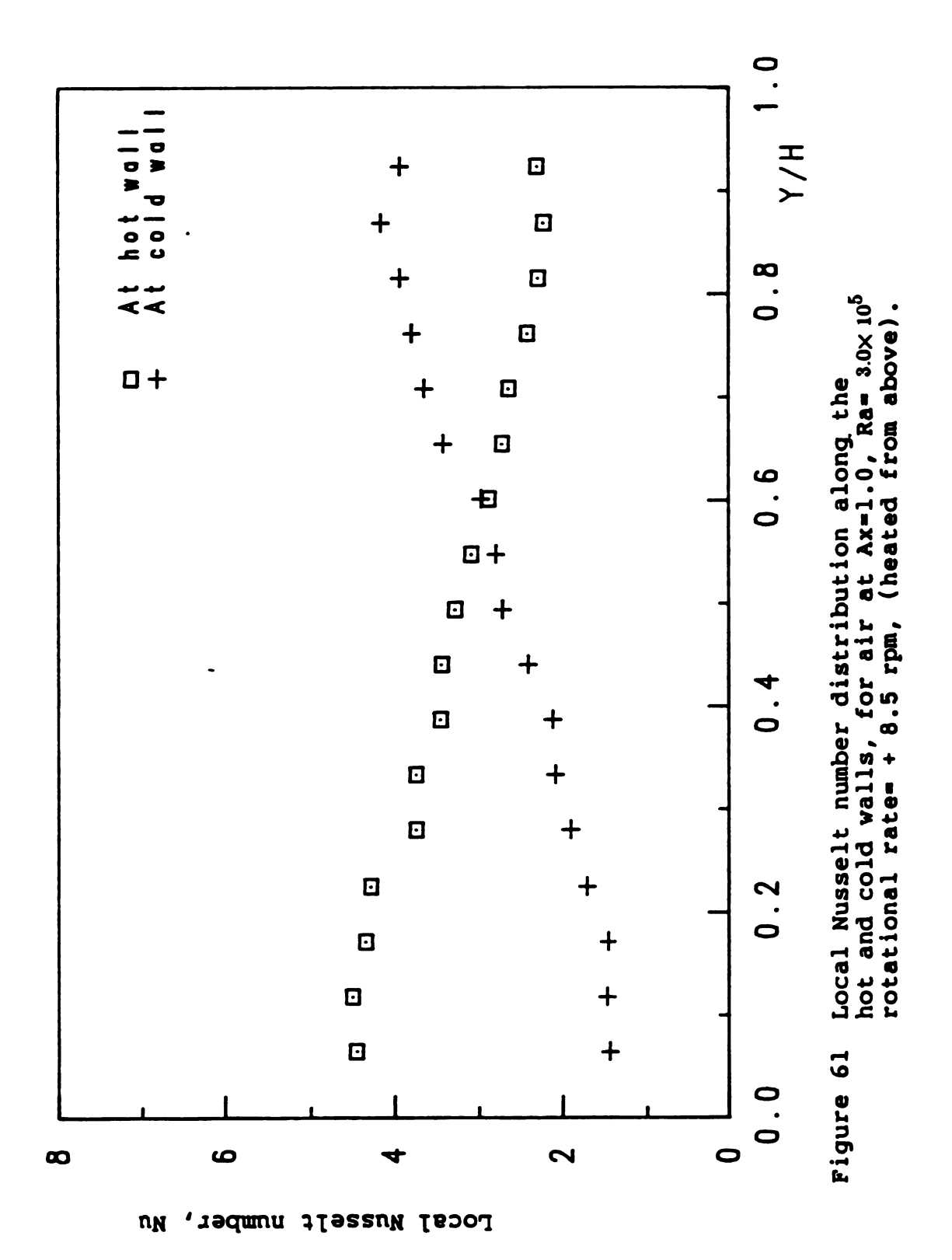
# 4.2.3 Heat Transfer Results in a Heated Rotating Enclosure at Angular Position of O deg. (Heated from Above)

The flow and temperature fields of natural convection in a nonrotating enclosure heated from above are usually characterized by
stable stratification, except near the corners under certain boundary
conditions as mentioned earlier. In addition local and mean Nusselt
values are approximately equal to one for all imposed temperature
differences, as might be expected any disturbance in the flow pattern
may cause an increase in the heat transport. Therefore since rotation
is capable of distorting the flow pattern, in particular at a large
imposed temperature difference as a consequence of the gravitational
and centrifugal buoyant interaction, one should expect to observe
significant effects on heat transfer as a result of rotation.

At a rotational rate of 8.5 rev/min and Rayleigh number of  $1.2 \times 10^5$ , Figures 59 and 60 demonstrate the local variation in heat transfer together with the experimental data in a non-rotating enclosure. Here, the distortion in heat transfer profiles are quite evident. However, the increase in average heat transfer is not significant. In contrast, with increasing the imposed temperature difference between the walls of the test section, the buoyant interactions are clearly in evidence as suggested by a marked enhancement in heat transfer as shown in Figures 61 and 62. Also a transition to a longitudinal roll-cell has occurred near the wall region, which contributes substantially to the thinning of the thermal boundary layer, and produces an increase in the heat transfer of approximately 40 %.







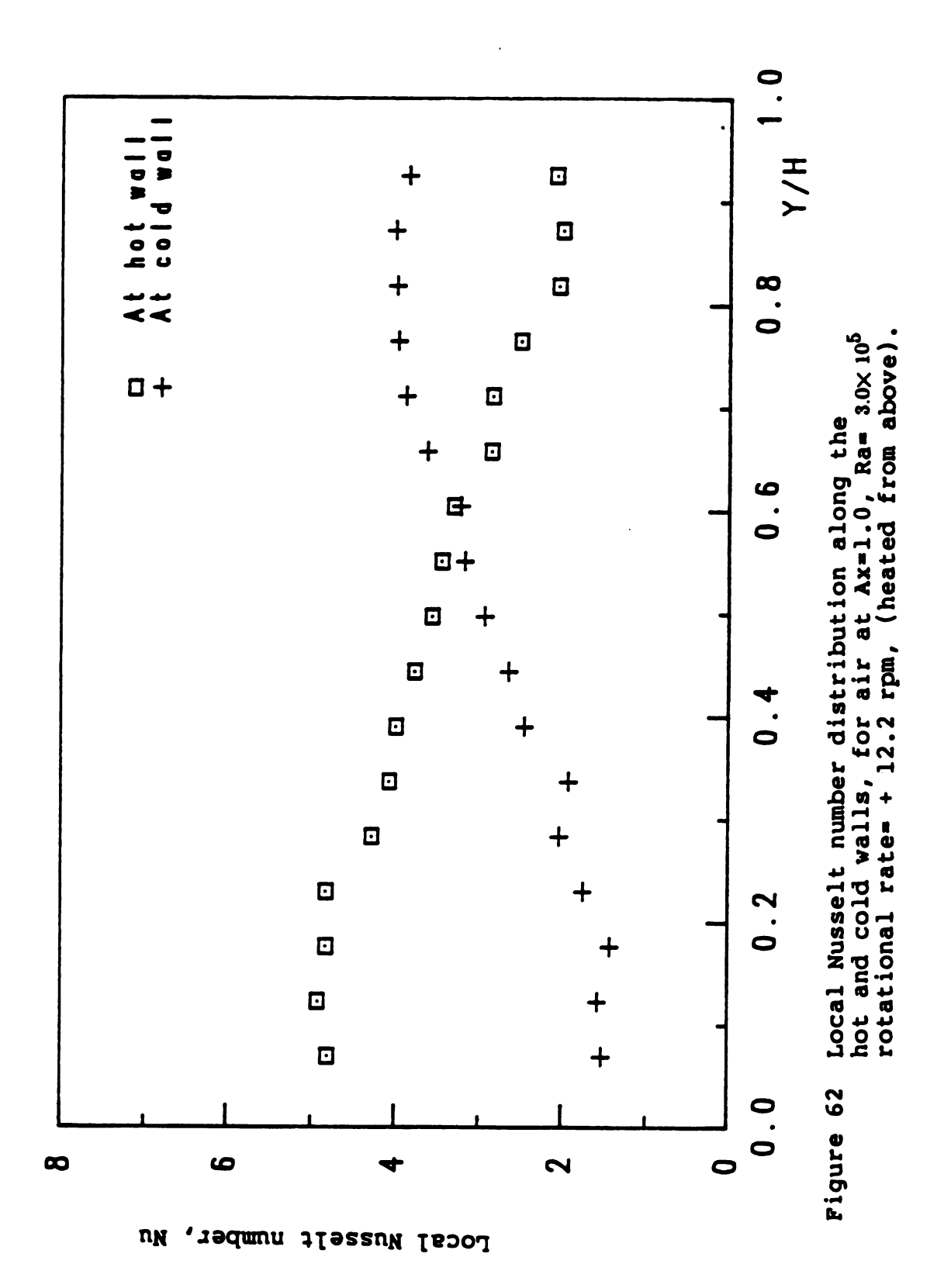


Figure 63 reveals the manner in which rotation influences the mean Nusselt number result at angular positions of 0, 90, and 180 deg. relative to the stationary results. It is noticed that there is a pronounced improvement in heat transfer at 0 deg., a reduction at 90 deg., and a small increase at 180 deg.

Figure 64 shows pictures of the interference fringe patterns which in turn illustrate the thermal boundary layer configuration in the vicinity of the wall region in non-rotating and rotating enclosures at various angular positions. These interferograms provide a comprehensive qualitative description of the general trend of the local heat transfer variation along the differentially heated walls of the test section. For instance, at 0 deg. (heated from above) the developed thermal boundary layer in the rotating enclosure, Figure 64b, gives a clear indication of the convective flow existence which is produced by the combined effect of heating and rotation. At angular position 90 deg. the recirculation of the thermally induced secondary flow from the upper and lower corners of the rotating enclosure toward the core region contributed to thickening the thermal boundary layer as shown in Figure 64d, and a consequent decrease in the heat transfer. At 180 deg. (heated from below) the thinning of thermal boundary layer near one end of the rotating enclosure Figure 64f, is a result of the transition from a cellular motion to a longitudinal flow pattern.

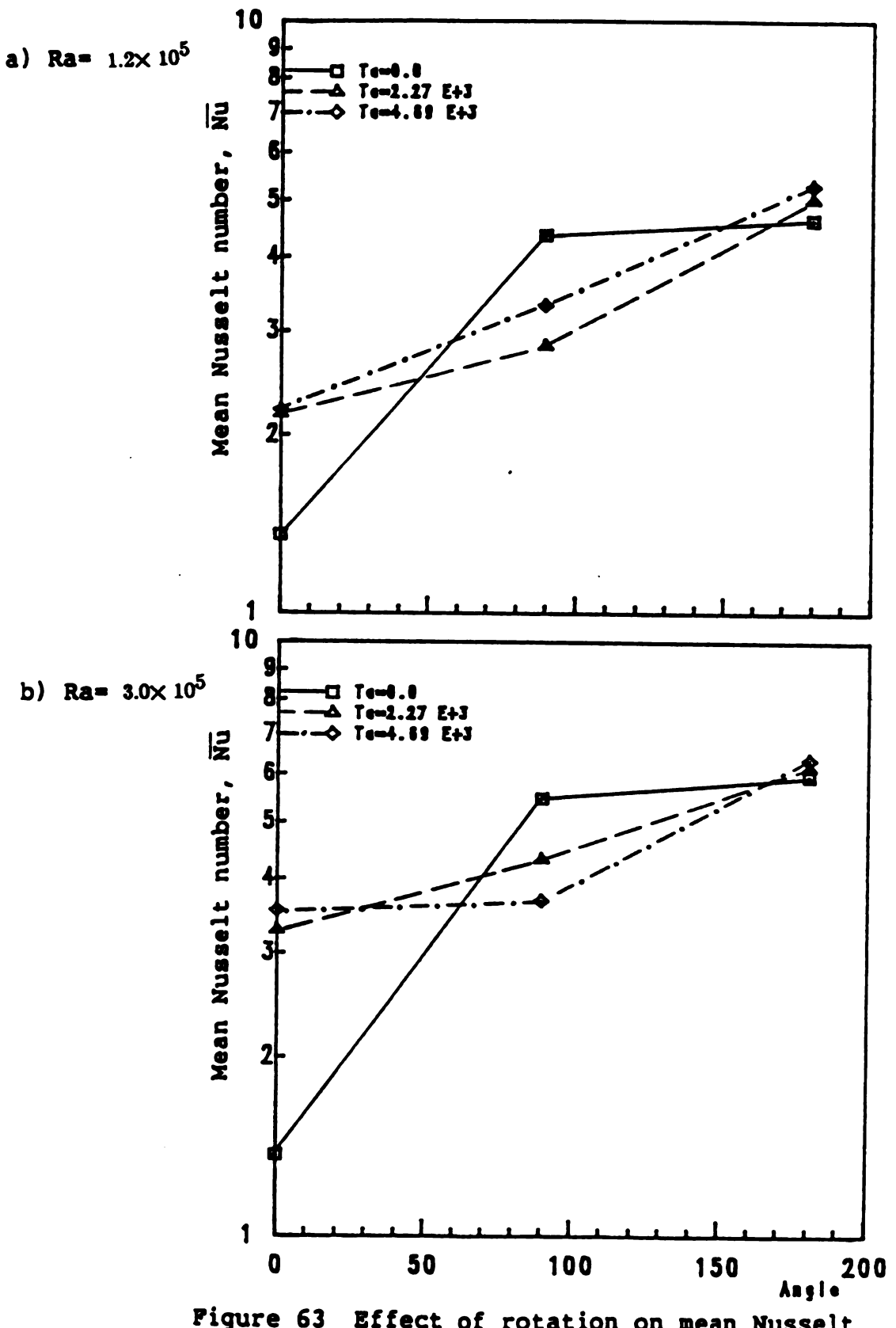


Figure 63 Effect of rotation on mean Nusselt number at various angular positions.

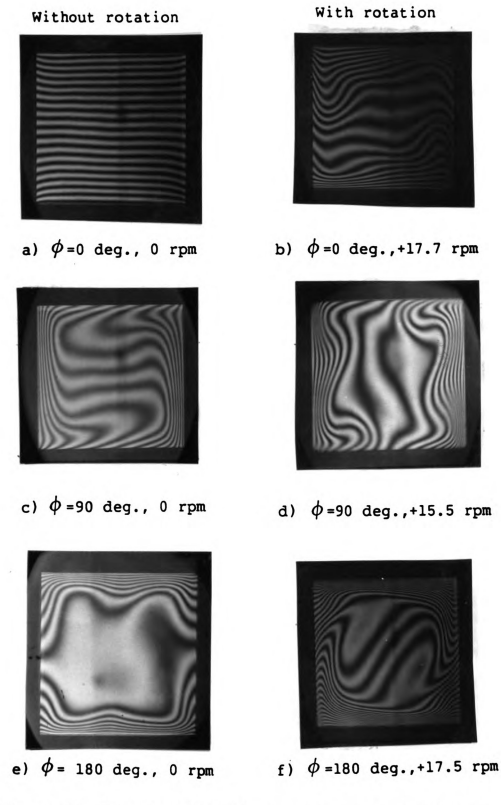


Figure 64 Interference fringe patterns at Ra=  $3.0 \times 10^5$ 

#### CHAPTER 5

## SUMMARY AND CONCLUSIONS

In this experimental study local and mean natural convection heat transfer characteristics have been considered in an air-filled differentially heated enclosure with cross-sectional aspect ratio one. The Mach-Zehnder interferometer was employed to reveal the entire temperature field which enabled the measurement of local and mean Nusselt numbers along the heated surfaces, while a laser sheet-smoke visual study of the flow patterns provided a greater understanding of the hydrodynamic and thermal boundary layers interaction.

The effects of the various physical factors on the heat transfer behaviors are analyzed in inclined and rotating enclosures which are inclined or rotated about their longitudinal horizontal axes.

The first part has shown the importance of including the effect of inclination angle in treating problems of natural convection in an inclined enclosure. The following features are worthy of note for Rayleigh numbers ranging from  $10^4$  to  $10^6$  and inclination angles between 0 and 180 deg.

1. For  $\phi \leq 30$  deg. (heated from above), it was shown that the conduction dominates the heat transfer and that the flow is very slow. However, at 30 deg. the existence of the thermal and hydrodynamic boundary layers were observed which in turn contributed to an improvement in the heat transfer.

- 2. For 30 <  $\phi \leq$  90 deg. buoyancy-driven flow commenced its influence on the flow. At 60 deg. the thermally induced secondary flow in the form of two vortical tubes is generated in the core region near the center of the heated walls at Ra $\approx$ 10 . Skewness in the vortical structure at 90 deg. implied a relatively thin boundary layer near the lower and opposite upper corners of the hot and cold surfaces, which in fact exhibited a substantial increase in the heat transfer.
- 3. For 90 <  $\phi \le 120$ , a transition of the thermally induced secondary flow from the core region at 90 deg. to the upper and opposite lower corners of the enclosure has occurred at 120 deg. This in fact contributed to improving the heat transfer at an angle between 110 -120 deg.
- 4. For  $120 < \phi \le 180$  deg., it was interesting to note that the thermally induced secondary flow occurred near the upper and opposite lower corners of the enclosure. In contrast, the core region was characterized by a longitudinal roll-cell before a transition to three-dimensional flow approximately between 150-160 deg. and then to cellular motions at 180 deg. The local distribution of Nusselt number reflected the manner in which the thermal boundary layer responded to the flow development.
- 5. The influence of inclination on mean Nusselt number was characterized by a local maximum value between 110-120 deg. and a local minimum between 150-160 deg., as a consequence of the disappearance of the secondary flow from the core region and the translation in flow pattern respectively. On the whole, the average Nusselt number results were in excellent agreement with existing numerical and experimental data.

In the second part the influence of combined gravitationally driven and rotationally driven flows on the thermal and hydrodynamic

boundary layers was discussed in accordance with the Taylor, the rotational and the gravitational Rayleigh numbers as the governing parameters. In view of the experimental results, it may concluded that:

- 6. For the angular position of 90 deg. (vertical enclosure), the Coriolis and buoyant interaction effect on the local distribution of Nusselt number illustrated clearly the subsequent development of the thermal boundary layer and showed a minimum in the heat transfer near 8.5 rev/min. This reduction may be argued in connection with the recirculated secondary induced flow radially toward the core region which in turn generated a complex flow pattern. However, a relative improvement in heat transfer was observed at higher rotational speed as a result of the buoyant interaction dominating effect.
- 7. For angular position of 180 deg. (heated from below), it was found that rotation indeed inhibits the onset of the cellular convection, and a longitudinal flow pattern was generated. Also, a small increase in heat transfer was produced.
- 8. For angular position of 0 deg. (heated from above) an increase in heat transfer was shown with increases in the rotational speed. However, it was more markedly influenced by the imposed temperature difference. In this event, the flow pattern was characterized by a longitudinal roll-cell.

Finally, progress has been made in the quantitative description of heat transfer in the inclined and rotating enclosures, but much research remains to be done. For instance, study the effect of rotation on the flow and heat transfer at higher rotational speeds over a wide range of Rayleigh number values, and for different Prandtl numbers remains to be done. Also, investigation of the possible delay of transition to turbulent flow as a result of the stabilizing influence

of rotation on the flow field. In addition, it is very important to consider the direction of rotation in rotating enclosures.

## PHYSICAL PROPERTIES

Interferometry is an optical technique where the index of refraction distribution throughout a transparent medium of fluid can be obtained directly. The density field can then be determined by the Lorentz-Lorenz relation.

$$\frac{\binom{n^2-1}{2}}{\binom{n+2}{2}} \frac{1}{\rho} - C \tag{A.1.1}$$

where C is a characteristic constant of the fluid independent of the temperature. Since n=1.000276 for air, equation (A.1.1) can be rearranged to,

$$G = \frac{(n-1)}{\rho} \tag{A.1.2}$$

values for (n-1) were taken from the American Institute of Physics Handbook [147] as follows:

Air at  $\lambda = 5461 \text{ Å}, (n-1) = 0.2937 \times 10^{-4}$ 

Using the perfect gas relationship, to measure the air-density

$$P = \rho RT \tag{A.1.3}$$

The Gladstone-Dale constant was found to be:

$$G_a = 2.27014 \times 10^{-4} \frac{m}{kg}$$

The physical properties of air,  $\mu$ , k, Pr, were taken from Ref. [148].

## INTERFEROGAM ANALYSIS

## 2.1 Relation between Fringe Shift and Temperature Change

The difference in the optical paths of the two light beams results in a phase shift of one beam with respect to the other. The equation for th fringe shift along the light beam can be expressed as,

$$\epsilon = \frac{1}{\lambda_0} \int_0^L [n(x,y,z) - n_0] dz$$
 (A.2.1)

Where  $(n-n_0)$  is the change of the index of refraction at some point in the test region relative to the reference region,  $\lambda_0$  is the wavelenght of light in the reference beam (5461Å). In interferometric analysis the variation in the index of refraction along the light beam, n(z), is usually very small, thus equation (A.2.1) integrates to,

$$\epsilon = \frac{1}{\lambda_0} [n(x,y) - n_0]$$
 (A.2.2)

Then the Gladstone-Dale equation (A.1.2) and the perfect-gas relationship (A.1.3) can be introduced into equation (A.2.2),

$$\epsilon = \frac{GLP}{\lambda_0 R} \left[ \frac{1}{T_{ref}} - \frac{1}{T} \right]$$
 (A.2.3)

which gives the relationship between fringe shift and temperture change. In the present study the reference temperature is equal to the cold wall temperature which maintained close to the room temperature. Then,

$$\epsilon = \frac{\text{GLP}}{\lambda_0 R} \left[ \frac{1}{T_C} - \frac{1}{T} \right] \tag{A.2.4}$$

In this equation all the terms are known except  $\epsilon$  and T. Since  $\epsilon$  can be measured directly from the interferogram, only T remains to be found, then equation (A.2.4) can be solved for the temperature,

$$T = \frac{T_C GLP}{GLP - T_C \epsilon \lambda_0 R}$$
 (A.2.5)

## 2.2 Evaluation of the Fringe Shift

A traveling microscope made by Gaertner Scientific Corporation of 0.0001 X-Y resolution was used to analyse the interferograms. The interferogram was placed on the micropositioning stage and then aligned such as the hot and cold walls are parallel to the Y-crosshair of the microscope. The sides of the interferogram were measured precisely by using the XY Vernier Micrometers, in order to determine the scaling factor which is equal to the ratio of the enclosure height to the interferogram height. The photo was then taped to the stage and a glass cover palced on it.

The Interfergram height was divided in equisteps of 0.05H, to determine the local heat transfer coefficients along the hot and cold surfaces. For instance at a given height y on the wall with respect to origin (xo,yo), the fringe shift was determined at 30 points between the hot and cold walls. However, the points were more concentrated near the isothermal walls. At least five points were taken in 1.0 mm range to determine the temperature gradient at that location.

Figure 65 of the interferogram demonstrates the procedure to estimate the fringe shift along y starting from the cold wall where the fringe shift is zero. Fractions of a fringe shift are measured by the

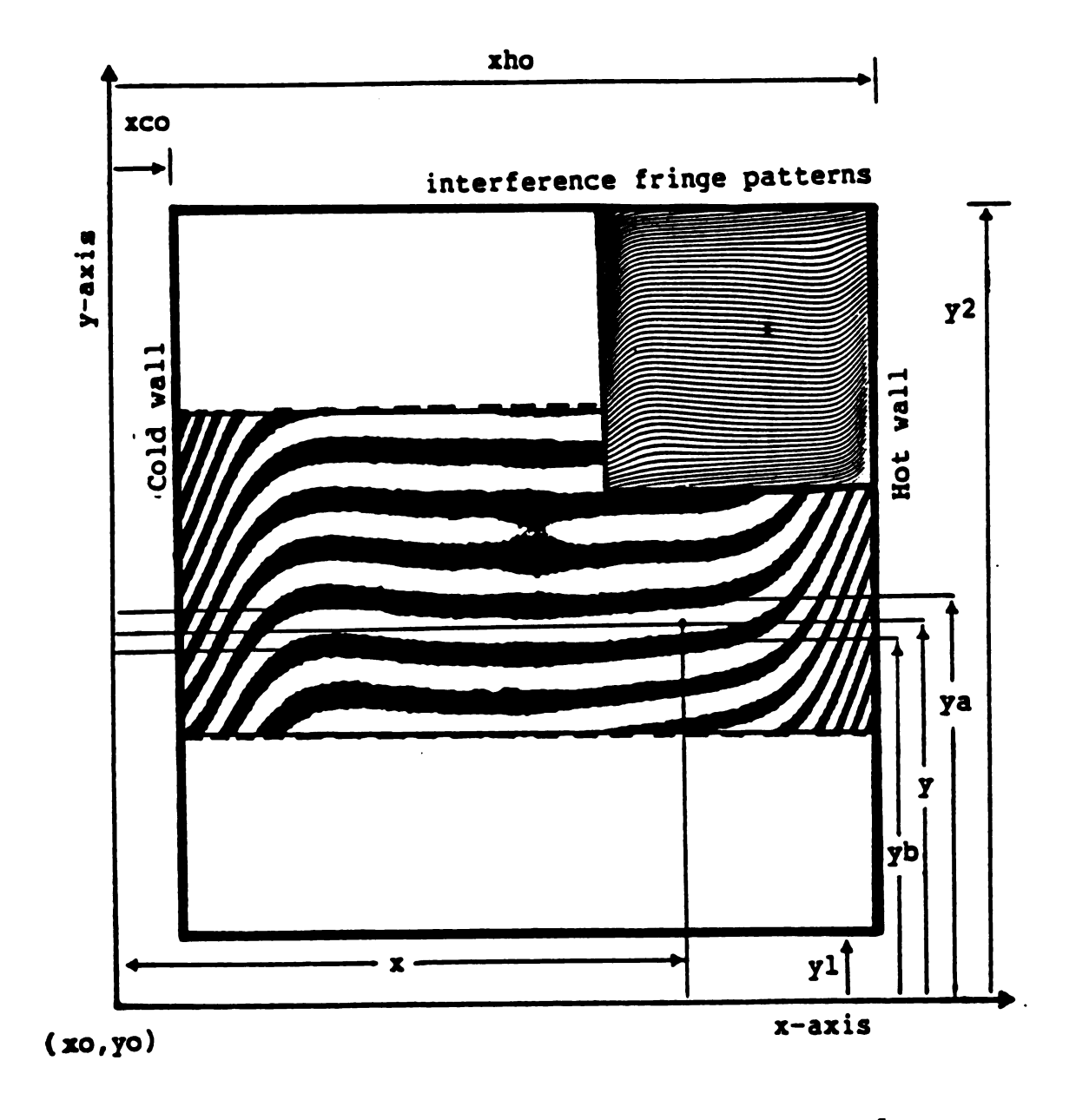


Figure 65 Fringe shift evaluation, at Ra =  $1.1 \times 10^5$   $\phi$  = 90 deg.

relation (ya - y)/(ya - yb) as indicated in the figure. A computer program called FRNG was used to calculate and plot the fringe shift as a function of the non-dimensional distance along the x-axis, (x/H). A second program called TEMP is used to measure and plot the fringe shift correction due the end effects and the non-dimensional temperature versus (x/H). The program was used also to estimate the non-dimensional temperature gradients along the hot and cold surfaces, by using a least square fit to the experimental data. In addition, the standard deviation was estimated on each measurement and local Nusselt numbers were plotted as function of the non-dimensional height of the test section. A listing of the two programs and a sample calculation are given in Appendix 5.

## 2.3 End Effect Correction

The fringe shift at the hot wall can be determined from,

$$\epsilon_{o} = \frac{GLP}{\lambda_{o}R} \left[ \frac{1}{T_{C}} - \frac{1}{T_{H}} \right]$$
 (A.2.6)

However, The existence of the optical flats at the ends of the test section will in turn contribute to an additional fringe shift, because the measuring beam did not reach immediately the ambient temperture. The fringe shift correction due to the end effect is given in [149] as,

$$\Delta \epsilon = \frac{1}{\lambda_0} \int_0^H \Delta T \, n \, \frac{dn}{dT} \, dx$$
 (A.2.7)

Since the thermal conductivity of glass is large compared to air, then a linear horizontal temperature distribution in the glass will be a good assumption. Therfore, a linear fringe shift correction can be applied,

$$\epsilon - \epsilon_{\rm m} - \epsilon_{\rm C} (1 - \frac{\rm x}{\rm H}) [(\epsilon_{\rm H} - \epsilon_{\rm C}) - \epsilon_{\rm o}]$$
 (A.2.8)

where  $\epsilon$  represents the corrected fringe shift,  $\epsilon_{\rm m}$  the measured fringe shift from the interferogram,  $\epsilon_{\rm o}$  is measured from equation (A.1.6), and  $\epsilon_{\rm C}$ ,  $\epsilon_{\rm H}$  are the fringe shifts at the cold and hot walls determined from the plots of  $\epsilon_{\rm m}$  versus (x/H). Detailed analysis of the end effect correction is given in Ref. [40,149].

## HEAT FLUX MEASUREMENTS

The picture in Figure 65 illustrates the interference fringe patterns of the refractive index distribution, which in turn allows a subsequent calculation of the entire temperature field, and hence the local temperature gradient at the wall. The coefficient of heat transferis defined as.

$$h - \frac{q}{\Lambda T} \tag{A.3.1}$$

where q is the heat transferred per unit area and  $\Delta T$  is the imposed temperature difference between the walls. In a thin layer of air in the immediated vicinity of the isothermal walls, heat transfer will take place largely by conduction,

$$q - k_s \left(\frac{\partial T}{\partial x}\right)_s$$
 (A.3.2)

where  $k_g$  is the thermal conductivity of air at the temperature of the heated surface,  $(\partial T/\partial x)_g$  the temperature gradient within the thin layer of air, and x the distance normal to the isothermal surfaces. From equation (A.3.1) and (A.3.2) the non-dimensional local heat transfer coefficient, the local Nusselt number

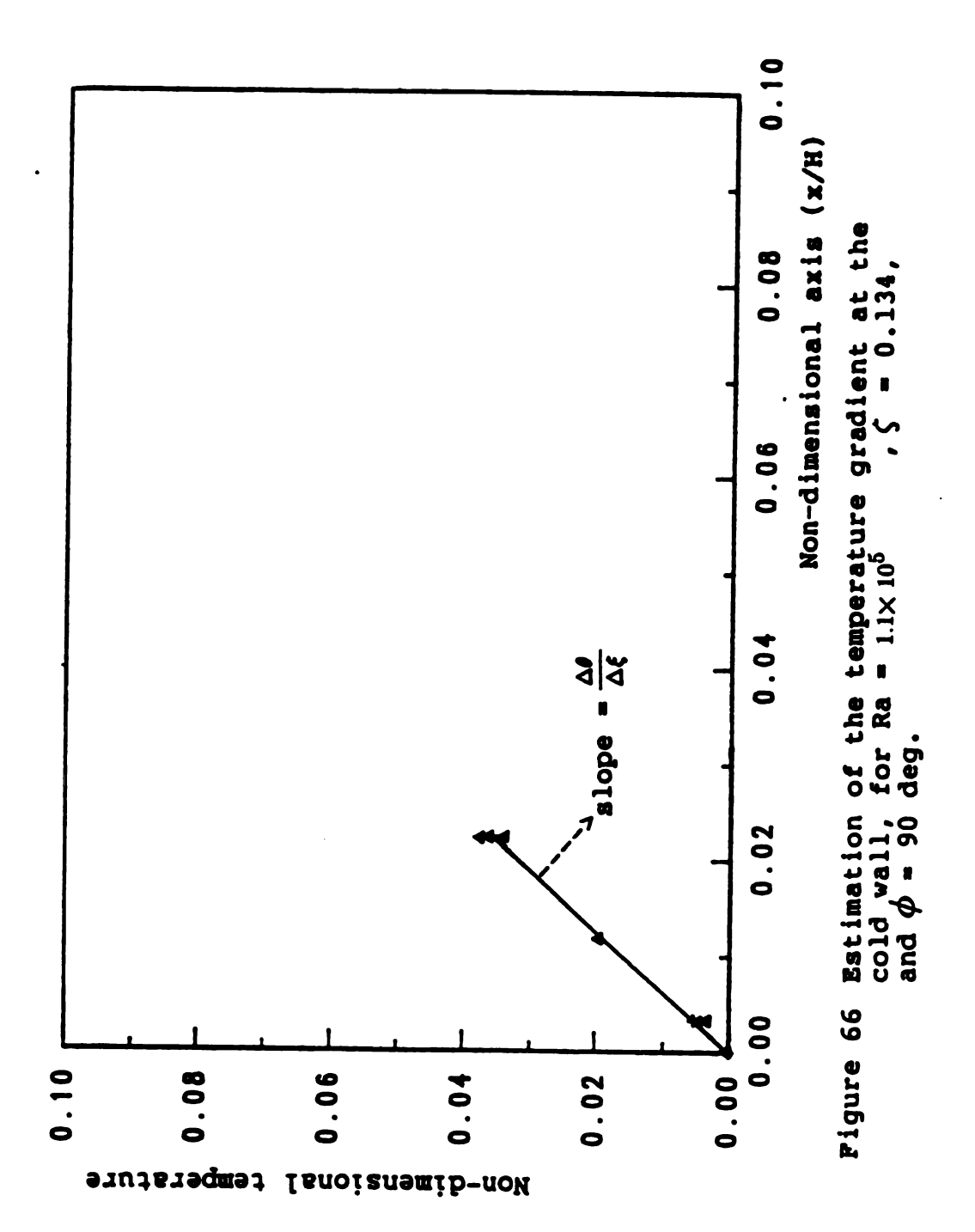
$$Nu = \frac{hH}{k}$$
becomes,
$$Nu(\zeta) = \left[ \frac{k_H}{k_C} \frac{\partial (T-T_C)/(T_H-T_C)}{\partial (x/H)} \right]_s$$
or,
$$Nu(\zeta) = \frac{k_H}{k_C} \left( \frac{\Delta \theta}{\Delta \xi} \right)$$
(A.3.3)

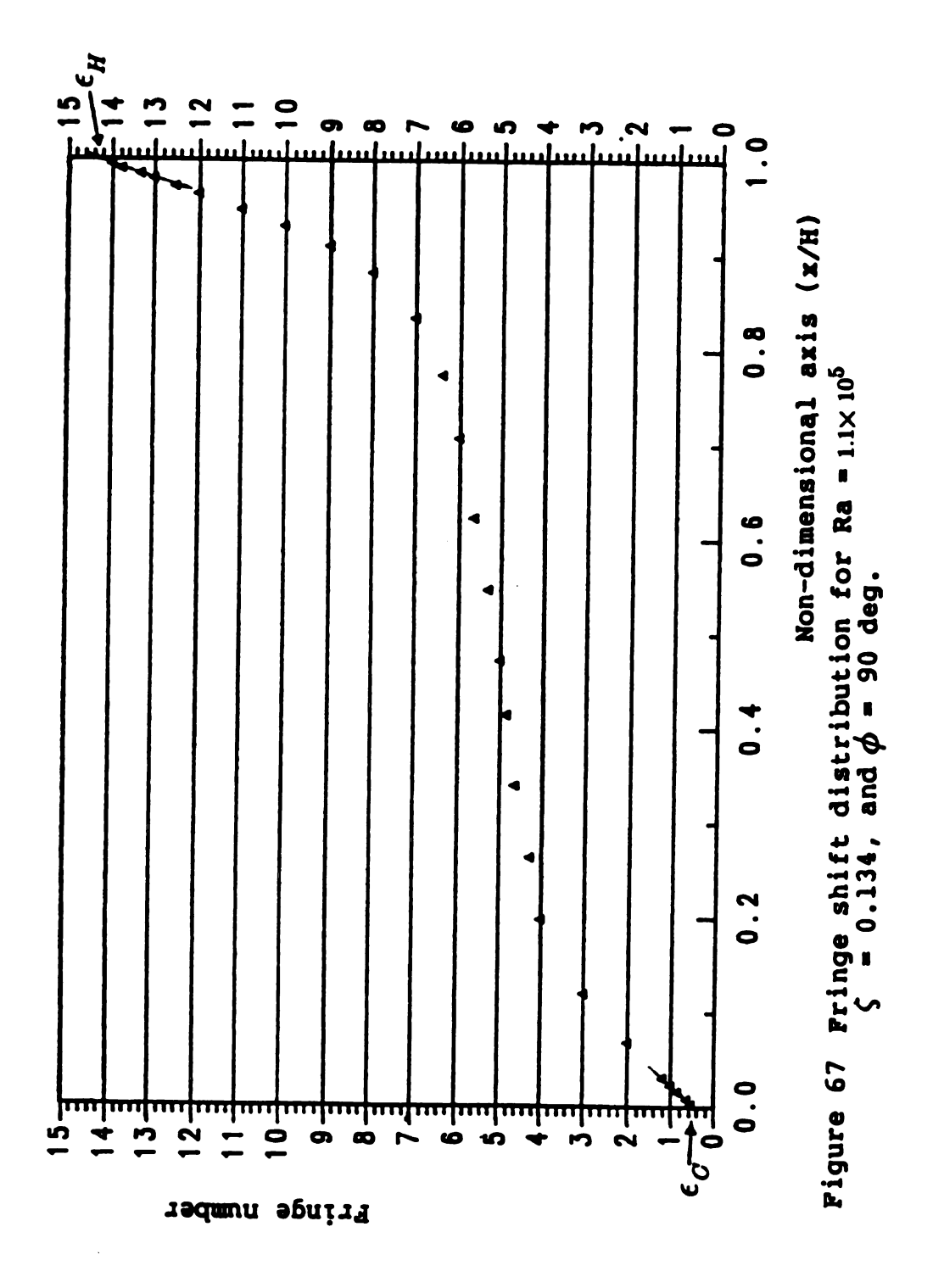
in equation (A.3.3)  $k_H$ ,  $k_C$  are evaluated at the hot and cold walls temperature,  $\theta$  is the non-dimensional temperature and  $\xi$  is the non-dimensional distance normal to the heated wall.  $(\Delta\theta/\Delta\xi)$  can be determined from the temperature profile near the isothermal walls as demonstrated in Figure 66. In addition, Figures 67 and 68 represent the corresponding fringe shift and the temperature profile at  $\xi=0.1340$ . Experimental data is given in Table 1.

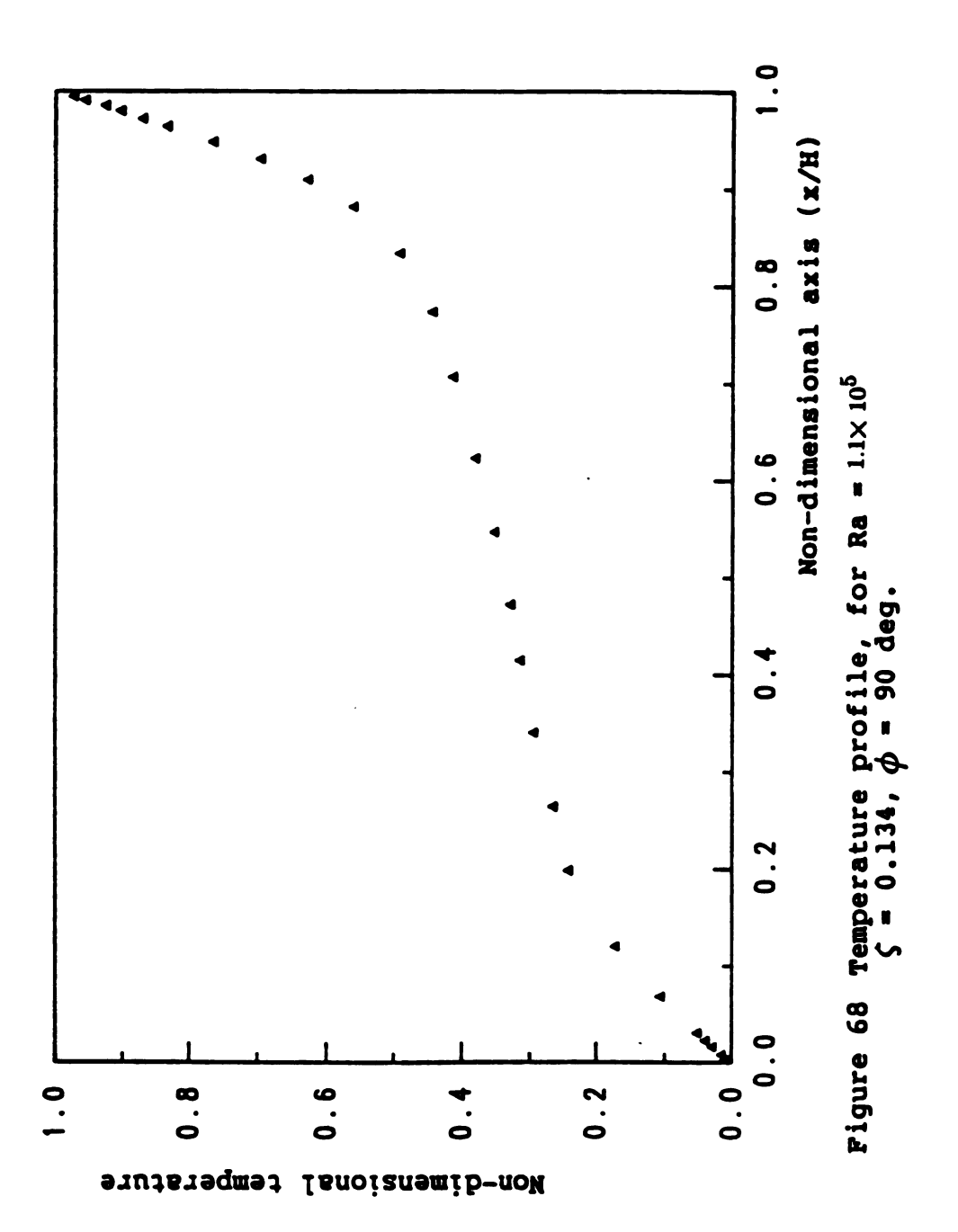
The mean Nusselt number is determined by numerically integating the local values over the entire wall height,

$$\overline{Nu} = \frac{k_{H}}{k_{C}} \int_{0}^{1} Nu(\zeta) d\zeta$$
 (A.3.4)

The Simpson's rule Ref. [150] was used to evaluate the integral.







Sample calculation of the fringe shift and the temperature distribution, at Ra =  $1.1\times10^5$  and  $\zeta$  (=  $\gamma/H$ ) = 0.1340. Table 1

	> 000	4 4 4 4 4 4 4 4 4 4 4 4 4 4 4 4 4 4 4	1 60 1	7.000	×   9.99	8 0	X/H X/H 20000	EPS	S	TK 12.4)		(TH
				7750 7750 7750 7750 7750 7750 7750		6 0000 6 00000 6 0000 6 0000 6 0000 6 0000 6 0000 6 0000 6 0000 6 000	0.9980 0.9980 0.9980 0.9980 0.9980 0.7039 0.7080	,0,00000000000	11.2.2.2.2.2.2.2.2.2.2.2.2.2.2.2.2.2.2.	- 7 8 8 9 9 9 9 9 9 9 9 9 9 9 9 9 9 9 9 9	- <b>a</b> - 4 n a n u u u 4 4 4 4	2000 2000 2000 2000 2000 2000 2000 200
NN4444WW000	00000000000	4 4 10 4 4 4 4 4 4 6 6 6 4 6	44444444	2000 2000 2000 2000 2000 2000 2000 200	0.00 1.444 1.444 0.00 1.464 1.00 1.0	,	4446400000	27.000 64.000 62.000 600 600 600 600 600 600	2	6 - 1 - 1 - 1 - 1 - 1 - 1 - 1 - 1 - 1 -		0.00000000000000000000000000000000000

## ERROR ANALYSIS

To ensure confidence in the experimental results, it is desirable to monitor the accuracy of the experiments by checking that all the measurements are adequately within an acceptable error bound. The types of error involved in this study are optical and measurement errors

## 4.1 Optical Errors

The optical errors are caused by refraction and end effects in the interferometric system. The refraction errors encountered in the measurements are due to the gradient of the refractive index in the direction normal to the beam of light. Consequently, the tempreature distribution or the temperature gradient measured from the interferogram can involve significant errors. Now, assuming the temperature variation in the direction of light is very small compared to the temperature difference between the walls, then the gradient of the index of refraction dn/dx, can be considered as a constant, and the temperature difference between the refracted and unrefracted beams according to Ref. [151] is

$$\Delta T = \frac{GL^{2}P}{8n_{o}RT^{2}} \left(\frac{dT}{dx}\right)^{2}$$
 (A.4.1)

In the present study the maximum temperature difference between the walls was 27.42 K, and  $\Delta\theta/\Delta\xi$ =11.86. This in turn yields a temperature gradient of  $\Delta T/\Delta x$ =5687.32 K/m and the refraction error from equation (A.4.1) is T=0.026 K. However, as described earlier in Appendix 2 the fringe shifts were corrected so that the total fringe shift would agree with the fringe shift related to the wall temperature. This in fact, will account for the refraction error. On the other hand, correction for the end effect was given in Appendix 2.

## 4.2 Measurement Errors

Errors in measurements are mainly encountered in the determination of the center of the fringe from the micrometer readings. This error is estimated to be within the range of  $\pm$  1/20 of a fringe or approximately  $\pm$  0.0012 cm in the micrometer readings. This resulted in a fringe error of less than 0.01 %.

Another important source of error is occurred in estimating the temperature gradient at the isothermal walls. For this reason mainly the estimated standard deviation were measured on the local values of the temperature gradients as will be illustrated in the sample calculation in Appendix 5. On the whole, the error in estimating the temperature gradient along the isothermal walls are within  $\pm$  3 % and the Total possible error is in the order of 6 % .

## APPENDIX 5

## COMPUTER PROGRAMS AND SAMPLE CALCULATION

```
----- PROGRAM FRNG.-----
C
     THIS PROGRAM IS USED TO EVALUATE THE FRINGE SHIFT
C
     FROM THE DATA MEASURED BY THE MICROMETER.
   ----- VARIABLE IDENTIFICATION. -----
C
C
          COEFFICIENT OF CUBICAL EXPANSION.
     В
CC
          GLADSTONE-DALE CONSTANT.
    DW TEST SECTION WIDTH.
č
    EPS FRINGE SHIFT.
CC
     G
          GRAVITATIONAL ACCELERATION.
    GR GRASHOF NUMBER.
č
    PR PRANDTL NUMBER.
CC
   RA GAS CONSTANT.
RAY RAYLEIGH NUMBER.
č
     SF
          SCALING FACTOR.
C
     TAUY DIMENSIONAL LENGTH NORMAL TO THE HOT PLATE.
C
     TAUX DIMENSIONAL LENGTH ALONG THE PLATE.
C
     TC
          COLD WALL TEMPERATURE.
C
     TH HOT WALL TEMPERATURE.
Č
    V
        KINEMATIC VISCOSITY.
C
    X
         COORDINATE IN DIRECTION ALONG THE PLATE.
C
          COORDINATE NORMAL TO THE HOT PLATE.
C
   ----- ENTRY AND STORAGE BLOCK. -----
C
     REAL TAUPT(40), EPSPT(40)
     CHARACTER *80 TITLE
     REAL*8 GRX, GRW, RAY
C
     DATA IN/10/, IO/11/, INI/12/
C
   ----- PROCESS BLOCK. -----
C
     CALL INITT(480)
     CALL OPENTK ('GFNG', IERROR)
     OPEN(10, FILE='RA3F8')
     OPEN(11, FILE='OFILE')
     OPEN(12,FILE='INPUT')
     READ(IN, 16) TITLE
16
     FORMAT(A80)
C
C
     PHYSICAL CONSTANT REQUIRED FOR THE CALCULATION
     OF GRASHOF NUMBER.
```

```
C
      G = 9.8
      RA=286.87081
      C=2.27014E-04
C
C
      PHYSICAL FACTORS DERIVED FROM THE KNOWN TEMP.
C
      OF THE HOT AND COLD WALLS.
      READ(IN,*) JJ,KK
      READ(IN, *)TH, TC
      READ(IN, *)B, V, DW, PR
      WRITE(INI, 180) TH, TC
C
C
      INSERTING THE SCALE FACTOR AND THE LENGTH
C
      OF THE HOT PLATE BY READING THE TWO EDGES.
C
      READ(IN,*) SF,X1,X2
C
C
      CALCULATION OF THE FRINGE SHIFT DEPENDING ON
C
      THE GIVEN DATA.
      DO 50 J=1,JJ
      NPT=0
      WRITE(10,160)
C
C
      INPUT OF THE MICROMETER READINGS CORRESPONDING
C
      TO THE FRINGE PATTERNS, AND THE LOCATIONS
C
      OF THE HOT AND COLD PLATES.
C
      READ(IN,*) XO, YHO, YCO
C
C
      NON-DIMENSIONALIZING THE HEIGHT, AND
C
      CALCULATION OF THE LOCAL GRASHOF NUMBER.
      TAUX=(XO-X1)/(X2-X1)
      X=2.54*SF*(XO-X1)
      XM = 0.01 * X
      GRX=(G*B*(TH-TC)*(XM**3))/(V**2)
      GRW = (G*B*(TH-TC)*(DW**3))/(V**2)
      RAY=GRW*PR
C
      WRITE(IO, *)
      WRITE(IO, *)
      WRITE(IO, *)
      WRITE(IO, 17) TITLE
      WRITE(10,60) TAUX
      WRITE(INI,65) TAUX
      WRITE(IO,70) GRX
```

```
WRITE(INI,75) GRX
      WRITE(IO,85)GRW
      WRITE(INI,95)GRW
      WRITE(IO,96)RAY
      WRITE(INI, 105)RAY
      WRITE(10,80) XO
      WRITE(10.90) X1
      WRITE(IO,100) X2
      WRITE(IO,110) YHO
      WRITE(IO,120) YCO
C
CC
      FRINGE SHIFT CALCULATIONS.
      WRITE(10,125)
      WRITE(10,130)
      WRITE(10,135)
      DO 40 K=1,KK
      READ(IN,*) Y,I,XA,XB
      TAUY = (Y - YCO) / (YHO - YCO)
      DIFF=XO-XA
      IF(ABS(DIFF).LT.2E-04) THEN
      EPS=FLOAT(I)
      ELSE
      EPS=FLOAT(I)+(XO-XA)/(XB-XA)
      END IF
      WRITE(10,170) Y,I,XA,XB,TAUY,EPS
      NPT=NPT+1
      WRITE(INI, 200) TAUY, EPS
      TAUPT (NPT) = TAUY
      EPSPT(NPT)=EPS
40
      CONTINUE
      WRITE(10,195)
      CALL PLOT(TAUPT(1), EPSPT(1), KK, J)
50
      CONTINUE
C ----- FORMAT STATEMENTS. -----
C
17
      FORMAT('1',10X,A80/)
60
      FORMAT(10X,'Y/H=',1X,F7.4,1X,'AT INCLINATION
     + ANGLE=0 DEG.')
65
      FORMAT (F5.4)
70
      FORMAT(10X,'GRY=',E15.8)
75
      FORMAT(E15.8)
80
      FORMAT(10X,'YO=',F7.4)
      FORMAT(10X, 'GRW=', E15.8)
85
      FORMAT(10X, 'RA=', E15.8//)
FORMAT(10X, 'Y1=', F7.4)
96
90
95
      FORMAT(E15.8)
```

```
100
      FORMAT(10X,'Y2=',F7.4)
105
      FORMAT(E15.8)
110
      FORMAT(10X,'XHO=',F7.4)
FORMAT(10X,'XCO=',F7.4)
120
125
      FORMAT(9X,
           '/)
130
      FORMAT(13X,'X',7X,'I',8X,'YA',9X,'YB',
     +10X,'X/W',8X,'EPS'/)
135
     FORMAT(9X,
         '/)
160
      FORMAT(/)
170
      FORMAT(10X,F8.4,2X,I2,4X,F8.4,4X,F8.4,4X,F8.4,4X,
     FORMAT(F10.4,2X,F10.4)
180
     FORMAT(/9X,'
195
         ')
200
      FORMAT(F10.4,2X,F10.4)
      CLOSE(IN)
      CLOSE(IO)
      CLOSE(INI)
      CALL CLOSTK(IERROR)
      PRINT *,'****** JOB DONE ******
C
      CALL EXIT
      END
C ----- SUBROUTINE PROCESS BLOCK. -----
C.1
      SUBROUTINE PLOT(X,Y1,IVALUE,IFIG)
      DIMENSION X(IVALUE), Y1(IVALUE)
      INTEGER IVALUE, IERROR, IFIG
      CHARACTER*2 CFIG
C
      CALL BINITT
      CALL NEWPAG
      CALL NPTS(IVALUE)
      CALL FRAME
      CALL XFRM(3)
      CALL XMFRM(3)
      CALL XLEN(15)
      CALL YLEN(15)
      CALL YTICS(14)
      CALL YMTCS(5)
      CALL XDEN(7)
      CALL DLIMX(0.,1.0)
      CALL DLIMY(0.0,18.0)
      CALL CHECK(X,Y1)
      CALL SYMBL(3)
```

```
CALL SIZES(0.8)
      CALL LINE(-4)
      CALL DSPLAY(X,Y1)
      CALL DINITY
      CALL YLOCRT(0)
      CALL DLIMY(0.0,18.0)
      CALL CHECK(X,Y1)
      CALL SYMBL(0)
      CALL LINE(-1)
      CALL DSPLAY(X,X)
      CALL MOVABS (560,40)
      CALL CHARTK ('DIMENSIONLESS AXIS (X/L)',0.7)
      CALL MOVABS(80,15)
      CALL CHARTK('FIG.(), FRINGE SHIFT ESTIMATION.
          +',1.)
      CALL CHARTK('FIG.(',0.7)
      WRITE(CFIG, '(12)') IFIG
      CALL CHARTK(CFIG, 0.7)
      CALL CHARTK('), FRINGE SHIFT ESTIMATION', 0.7)
      CALL MOVABS (75,760)
      CALL CHARTK ('FRINGE NUMBER EPS.',1.)
      CALL CHARTKV(50,650, 'FRINGE NUMBER', 0.85)
      CALL ANMODE
      RETURN
      END
C.2
      SUBROUTINE CHARTKY (IPOSX, IPOSY, ANAME, SCALE)
C
      CHARACTER ANAME*(*),A*1
      REAL SCALE
      INTEGER IPOSX, IPOSY, N, I
      N = LEN(ANAME)
C
      DO 10 I = 1.N
        IY = IPOSY - (I-1)*24*SCALE
        CALL MOVABS(IPOSX, IY)
        A = ANAME(I:I)
        CALL ANMODE
        WRITE(1,*) A
        CALL RECOVR
        CALL CHARTK(A, SCALE)
10
      CONTINUE
C
      RETURN
      END
```

```
----- PROGRAM TEMP. ------
C
C
      THIS PROGRAM IS USED TO EVALUATE AND PLOT THE
     FRINGE SHIFT CORRECTION AND NON-DIMENSIONAL
Č
     TEMPERATURE TOGETHER WITH THE LOCAL NUSSELT
C
     NUMBER AND THE ESTIMATED STANDARD DEVIATION.
C
C
C
      ----- VARIABLE IDENTIFICATION. -----
C
    C
           GLADSTONE-DALE CONSTANT.
CCCCCC
     EPS
           FRINGE SHIFT.
     EPSCO FRINGE SHIFT GIVEN BY EQ.
           CORRECTED FRINGE SHIFT.
     FSCW COLD WALL FRINGE SHIFT.
     FSHW HOT WALL FRINGE SHIFT.
     G
           GRAVITATIONAL ACCELERATION.
CCCCC
     KC
           THERMAL CONDUCTIVITIES OF FLUID EVALUATED
     KH
           AT THE COLD AND HOT PLATE TEMP.
          LOCAL NUSSELT NUMBER.
     NU
     P
           PRESSURE
     SL
          TEST SECTION LENGTH.
C
     WL
           WAVELENGTH.
C
        ----- ENTRY AND STORAGE BLOCK.----
C
C
      REAL TAUPT(0:40), TEMPT(0:40), YHE(0:40), BNH(30)
      REAL YCE(0:40), BNC(30), ESDH(30), ESDC(30), MESDH
      REAL BNHO(30), BNCO(30), TAUN(30), MESDC
      CHARACTER *80 TITLE
      REAL *8 GRX, GRW, RAY, KH, KC, KR
C
      DATA INI/12/, IO/13/, NU/14/
C
  ----- PROCESS BLOCK.-----
C
      CALL INITT(480)
      CALL OPENTK ('GTEMP', IERROR)
      OPEN(12, FILE='RA3T8')
      OPEN(13, FILE='OUTPUT')
      OPEN(14,FILE='NUSLT')
C
C
      PHYSICAL CONSTANTS REQUIRED FOR THE CALCULATION
C
      OF GRASHOF NUMBER.
      G=9.8
```

```
WL=0.5461E-06
      RA = 286.87081
      C=2.27014E-04
C
      READ(INI, 16) TITLE
16
      FORMAT(A80)
      READ(INI,*) JJ,KK,NH,NC
      READ(INI,*) P
      READ(INI, *) SL
      READ(INI,*) TH, TC, KH, KC, KR
C
      EPSCO=(1.0/TC-1.0/TH)*C*SL*P/(WL*RA)
C
      SNUH=0.0
      SNUC=0.0
      SESDH=0.0
      SESDC=0.0
C
      DO 30 J=1,JJ
      WRITE(IO, *)
      WRITE(IO, *)
      WRITE(IO,*)
      WRITE(IO,*)
      WRITE(IO, *)
      WRITE(IO, 17) TITLE
C
      READ(INI, *) TAUX
      READ(INI,*) GRX
      READ(INI,*) GRW
      READ(INI,*) RAY
      READ(INI,*) FSHW,FSCW
C
      WRITE(10,150)
      WRITE(IO, 160) TAUX
      WRITE(IO, 170) GRX
      WRITE(IO, 175) GRW
      WRITE(IO, 186) RAY
      WRITE(10,210) TH
      WRITE(IO, 220) TC
      WRITE(10,230) P
      WRITE(IO, 240) FSCW
      WRITE(IO, 250) FSHW
      WRITE(IO, 260) EPSCO
      WRITE(10, 265)
      WRITE(10,180)
      WRITE(10,185)
C
      DO 10 K=1,KK
```

```
C
      READ(INI,*) TAUY, EPS
C
      FS=EPS-FSCW-(TAUY) * (FSHW-FSCW-EPSCO)
      DIN=C*SL*P-WL*RA*TC*FS
      TEMP=C*SL*P*TC/DIN
      THETA=(TEMP-TC)/(TH-TC)
C
      WRITE(IO, 200) TAUY, EPS, FS, TEMP, THETA
      TAUPT(K)=TAUY
      TEMPT(K)=THETA
10
      CONTINUE
      WRITE(10,270)
      SUMXH=0.0
      SUMYH=0.0
      SUMXC=0.0
      SUMYC=0.0
      TAUPT(0)=1.0
      TEMPT(0)=1.0
      DO 15 I=1,NH
      SUMXH=TAUPT(I)+SUMXH
      SUMYH=TEMPT(I)+SUMYH
15
      CONTINUE
C
      XHME=SUMXH/NH
      YHME=SUMYH/NH
C
      SUMNH=0.0
      SUMDH=0.0
      DO 35 JL=1,NH
      SUMNH=(TAUPT(JL)-XHME)*(TEMPT(JL)-YHME)+SUMNH
      SUMDH=(TAUPT(JL)-XHME)**2+SUMDH
35
      CONTINUE
      BH1=SUMNH/SUMDH
      BHO=YHME-BH1*XHME
      BH=(KH*BH1)/KR
C
      SMYH=0.0
      DO 40 I=1,NH
      YHE(I)=BHO+BH1*TAUPT(I)
      SMYH = (TEMPT(I) - YHE(I)) **2 + SMYH
40
      CONTINUE
      VYH=(SMYH*KH)/((NH-2)*KR)
      VBH=VYH/SUMDH
      ESDBH=SORT(VBH)
C
```

```
CALL PLOT1(TAUPT(0), TEMPT(0), YHE(0), (NH-1))
C
      TAUPT(KK+1)=0.0
      TEMPT(KK+1)=0.0
C
      DO 18 N=6,NC
      SUMXC=TAUPT(N)+SUMXC
      SUMYC=TEMPT(N)+SUMYC
18
      CONTINUE
      XCME=SUMXC/(NC-5)
      YCME=SUMYC/(NC-5)
      SUMNC=0.0
      SUMDC=0.0
      DO 37 NL=6,NC
      SUMNC=(TAUPT(NL)-XCME)*(TEMPT(NL)-YCME)+SUMNC
      SUMDC = (TAUPT(NL)-XCME) **2+SUMDC
37
      CONTINUE
C
      BC1=SUMNC/SUMDC
      BCO=YCME-BC1*XCME
      BC=(KC*BC1)/KR
C
      SMYC=0.0
      DO 47 N=6,NC
      YCE(N)=BCO+BC1*TAUPT(N)
      SMYC = (TEMPT(N) - YCE(N)) **2 + SMYC
47
      CONTINUE
      VYC = (SMYC)/(NC-7)
      VBC=VYC/SUMDC
      ESDBC=SQRT(VBC)
      TAUN(J) = TAUX
      ESDH(J) = ESDBH
      ESDC(J)=ESDBC
      BNHO(J)=BH
      BNCO(J) = BC
      SESDH=ESDH(J)+SESDH
      SESDC=ESDC(J)+SESDC
C
      CALL PLOT(TAUPT(1), TEMPT(1), KK, J)
      CALL PLOT4 (TAUPT(8), TEMPT(8), YCE(8), 5)
30
      CONTINUE
C
      K1=(JJ-1)/2
      PTS=3*(JJ-1)
      SNUH1=0.0
      SNUC1=0.0
      DO 50 K=1,K1
```

```
SNUH1=4*BNH(2*K)+SNUH1
      SNUC1=4*BNC(2*K)+SNUC1
50
      CONTINUE
      SNUH2=0.0
      SNUC2=0.0
      DO 55 K=2,K1
      SNUH2=2*BNH(2*K-1)+SNUH2
      SNUC2=2*BNC(2*K-1)+SNUC2
55
      CONTINUE
      SNUMH=(1/PTS)*(BNH(1)+BNH(JJ)+SNUH1+SNUH2)
      SNUMC=(1/PTS)*(BNC(1)+BNC(JJ)+SNUC1+SNUC2)
C
      WRITE(IO, 290) SNUMH
      WRITE(IO, 295) SNUMC
C
      CALL PLOT2(TAUN(1), BNH(1), BNC(1), JJ)
      CALL PLOT3(TAUN(1), BNC(1), JJ)
C
      WRITE(IO,*)
      WRITE(IO, *)
      WRITE(IO,*)
      WRITE(IO,*)
      WRITE(IO, 300) RAY
      WRITE(10,310)
      WRITE(10,320)
      WRITE(10,330)
C
      DO 45 K=1,JJ
      WRITE(IO, 340) TAUN(K), BNH(K), BNC(K), ESDH(K)
     +,ESDC(K)
45
      CONTINUE
      WRITE(10,350)
      WRITE(IO, 360) SNUMH
      WRITE(IO, 365) SNUMC
      WRITE(IO, 370) MESDH
      WRITE(IO, 375) MESDC
C
        ----- FORMAT STATEMENTS.-----
C
17
      FORMAT('1',10X,A80/)
150
      FORMAT(/)
160
      FORMAT(11X,'Y/H=',1X,F7.4,1X,', AT ROTATIONAL
     +RATE=8.5 rpm -A')
      FORMAT(11X, 'GRY=', E15.8)
170
175
      FORMAT(11X, 'GRW=', E15.8)
      FORMAT(11X,'RA=',E15.8)
FORMAT(14X,'X/W',6X,'EPS',8X,'FS',8X,'TK',4X,
186
180
```

```
+'(T-Tc)/(Th-Tc)'/)
185
      FORMAT(10X,'
     +'/)
200
      FORMAT(11X, F8.4, F10.4, F10.4, F12.4, F10.4)
210
      FORMAT(11X, 'HOT WALL TEMP.=',F7.3,2X, 'DEG. K')
FORMAT(11X, 'COLD WALL TEMP.=',F7.3,2X,
220
     +'DEG. K'/)
      FORMAT(11X,'PRESSURE=',E15.8,2X,'PA.')
FORMAT(11X,'FSCW=',F7.3)
230
240
      FORMAT(11X, 'FSHW=', F7.3)
250
      FORMAT(11X, 'EPSCO=',F7.4)
260
265
      FORMAT(10X,'
     +'/)
270
      FORMAT(10X,'
     +')
      FORMAT(11X.'** MEAN NUSSELT NUMBER AT HOT WALL
290
     +NU=',F10.3)
      FORMAT(11X,'** MEAN NUSSELT NUMBER AT COLD WALL
295
     +NU=',F10.3)
300
      FORMAT('1', 10X, 'LOCAL NUSSELT NUMBER AS A
     +FUNCTION OF THE'//
     +,10X,'DIMENSIONLESS DISTANCE AT THE HOT
     +AND THE'//
     +,10X,'COLD WALL AT RAYLEIGH NUMBER RA=',
     +E12.7//
     +,10X,'
              AND ROTATIONAL RATE=8.5 rpm -A'//)
      FORMAT (9X, '
310
                                      1/)
      FORMAT(12X, 'Y/H', 7X, 'NUH', 7X, 'NUC', 7X, 'ESDH', 6X,
320
     +'ESDC'/)
330
      FORMAT (9X, '
     + '/)
      FORMAT(10X, F7.4, 2X, F8.3, 2X, F8.3, 2X, F8.3, 2X,
340
     +F8.3/)
350
      FORMAT (9x.'
                                     '/)
      FORMAT(10X, ** MEAN NUSSELT NUMBER AT THE HOT
360
     +WALL NU=',F8.3/)
      FORMAT(10X,'** MEAN NUSSELT NUMBER AT THE COLD
365
     +WALL NU=',F8.3)
      FORMAT(10X,'** MEAN E.S.D. OF NU AT THE HOT WALL
370
     +=',F8.3)
      FORMAT(10X,'** MEAN E.S.D. OF NU AT THE COLD
375
     +WALL=',F8.3)
C
      CLOSE(INI)
      CLOSE(IO)
      CLOSE(NU)
      CALL CLOSTK (IERROR)
      PRINT *,'***** JOB DONE ******
```

```
CALL EXIT
      END
C
C ----- SUBROUTINE PROCESS BLOCK. -----
C.1
      SUBROUTINE PLOT(X,Y1,IVALUE,IFIG)
      DIMENSION X(IVALUE), Y1(IVALUE)
      INTEGER IVALUE, IERROR, IFIG
      CHARACTER*2 CFIG
C
      CALL BINITT
      CALL NEWPAG
      CALL NPTS(IVALUE)
      CALL FRAME
      CALL XFRM(3)
      CALL YFRM(3)
      CALL XMFRM(3)
      CALL YMFRM(3)
      CALL XLEN(15)
      CALL YLEN(15)
      CALL STEPS(1)
      CALL CHECK(X,Y1)
      CALL SYMBL(3)
      CALL SIZES(0.5)
      CALL LINE(-4)
      CALL DSPLAY(X,Y1)
      CALL MOVABS(560,45)
      CALL CHARTK('DIMENSIONLESS AXIS (X/L)',1.0)
      CALL MOVABS(80,15)
      CALL CHARTK('FIG.(',0.7)
      WRITE(CFIG, '(12)') IFIG
      CALL CHARTK(CFIG, 0.7)
      CALL CHARTK(') TEMPERATURE PROFILE', 0.7)
      CALL CHARTKY (50,650, 'DIMENSIONLESS TEMP.'
     +,0.85)
      CALL ANMODE
      RETURN
      END
C. 2
      SUBROUTINE PLOT1(X,Y1,Y2,IVALUE)
      DIMENSION X(IVALUE), Y1(IVALUE), Y2(IVALUE)
      INTEGER IVALUE, IERROR
C
      CALL BINITT
      CALL NEWPAG
      CALL NPTS(IVALUE)
      CALL FRAME
```

```
CALL XFRM(3)
      CALL YFRM(3)
      CALL XMFRM(3)
      CALL YMFRM(3)
      CALL XLEN(15)
      CALL YLEN(15)
      CALL STEPS(1)
      CALL DLIMX(0.92,1.0)
      CALL DLIMY(0.85,1.0)
      CALL CHECK(X,Y1)
      CALL SYMBL(3)
      CALL SIZES(0.5)
      CALL LINE(-4)
      CALL DSPLAY(X,Y1)
      CALL SYMBL(8)
      CALL SIZES(0.5)
      CALL LINE(0)
      CALL DSPLAY(X,Y2)
      CALL MOVABS(560,45)
      CALL CHARTK('NON-DIMENSIONAL AXIS (X/L).'
     +.0.7)
      CALL MOVABS(80,15)
      CALL CHARTK('FIG.( ), NUSSELT NO.MEAS. FROM
     +THE GRADIENT ',0.7)
CALL MOVABS(75,740)
      CALL CHARTK('NON-DIMENSIONAL TEMP. NEAR THE
     +HOT WALL',0.7)
      CALL ANMODE
      RETURN
      END
C.3
      SUBROUTINE PLOT2(X,Y1,Y2,IVALUE)
      DIMENSION X(IVALUE), Y1(IVALUE), Y2(IVALUE)
      INTEGER IVALUE, IERROR
C
      CALL BINITT
      CALL NEWPAG
      CALL NPTS (IVALUE)
      CALL SLIMX(170,880)
      CALL SLIMY(175,675)
      CALL FRAME
      CALL XFRM(3)
      CALL YFRM(3)
      CALL XMFRM(3)
      CALL YMFRM(3)
      CALL XLEN(15)
      CALL YLEN(15)
      CALL STEPS(1)
```

```
CALL DLIMX(0.,1.0)
      CALL DLIMY(0.0,7.0)
      CALL CHECK(X,Y1)
      CALL SYMBL(4)
      CALL SIZES(0.8)
      CALL LINE(-4)
      CALL DSPLAY(X,Y1)
      CALL DLIMX(0.0,1.0)
      CALL DLIMY(0.0,7.0)
      CALL CHECK(X,Y2)
      CALL SYMBL(8)
      CALL SIZES(0.8)
      CALL LINE(-4)
      CALL DSPLAY(X,Y2)
      CALL MOVABS(680,620)
      CALL SYMOUT(4,0.8)
      CALL MOVABS(700,615)
      CALL CHARTK('
                    At hot wall', 0.85)
      CALL MOVABS(680,600)
      CALL SYMOUT(8,0.85)
      CALL MOVABS(700,595)
      CALL CHARTK(' At cold wall', 0.85)
      CALL MOVABS(800,120)
      CALL CHARTK('Y/H',1.0)
      CALL MOVABS(100,100)
      CALL CHARTK('Figure
                              Local Nusselt number
     +at the hot and cold', 0.85)
      CALL MOVABS(157,80)
      CALL CHARTK(' wall for air, at (Ax=1.0,
     +Ra=2.923E+5 ',0.85)
      CALL MOVABS (157,60)
      CALL CHARTK('
                         and rotational rate = 8.5
     +rpm -A.', 0.85)
      CALL MOVABS(80,600)
      CALL CHARTK('Nu',1.0)
      CALL ANMODE
      RETURN
      END
C.4
      SUBROUTINE PLOT3(X,Y1,IVALUE)
      DIMENSION X(IVALUE), Y1(IVALUE)
      INTEGER IVALUE, IERROR
C
      CALL BINITT
      CALL NEWPAG
      CALL NPTS(IVALUE)
      CALL FRAME
      CALL XFRM(3)
```

```
CALL YFRM(3)
      CALL XMFRM(3)
      CALL YMFRM(3)
      CALL XLEN(15)
      CALL YLEN(15)
      CALL STEPS(1)
      CALL DLIMX(0.,1.0)
      CALL DLIMY(0.0,12.0)
      CALL CHECK(X,Y1)
      CALL SYMBL(3)
      CALL SIZES(0.5)
      CALL LINE(-4)
      CALL DSPLAY(X,Y1)
      CALL MOVABS(560,45)
      CALL CHARTK('DIMENSIONLESS AXIS (Y/L)',0.7)
      CALL MOVABS(80,15)
      CALL CHARTK('FIG.('), NU AT THE COLD WALL
     +RA= 8.7191804E+5 ,AND ANGLE=135 DEG.',0.7)
      CALL CHARTKV (50,650, LOCAL NUSSELT NO. '
     +,0.85)
      CALL ANMODE
      RETURN
      END
C.5
      SUBROUTINE PLOT4(X,Y1,Y2,IVALUE)
      DIMENSION X(IVALUE), Y1(IVALUE), Y2(IVALUE)
      INTEGER IVALUE, IERROR
C
      CALL BINITT
      CALL NEWPAG
      CALL NPTS(IVALUE)
      CALL FRAME
      CALL XFRM(3)
      CALL YFRM(3)
      CALL XMFRM(3)
      CALL YMFRM(3)
      CALL XLEN(15)
      CALL YLEN(15)
      CALL STEPS(1)
      CALL DLIMX(0.0,0.1)
      CALL DLIMY(0.0,0.1)
      CALL CHECK(X,Y1)
      CALL SYMBL(3)
      CALL SIZES(0.5)
      CALL LINE(-4)
      CALL DSPLAY(X,Y1)
      CALL SYMBL(8)
      CALL SIZES(0.5)
```

```
CALL LINE(0)
      CALL CPLOT(X,Y2)
      CALL MOVABS(560,45)
      CALL CHARTK ('NON-DIMENSIONAL AXIS (X/L).'
     +,0.7)
      CALL MOVABS(80,15)
      CALL CHARTK('FIG.( ), NUSSELT NO.MEAS. FROM
     +THE GRADIENT ',0.7)
      CALL MOVABS(75,740)
      CALL CHARTK ('NON-DIMENSIONAL TEMP. AT THE
     +COLD WALL',0.7)
      CALL ANMODE
      RETURN
      END
C.6
      SUBROUTINE CHARTKY (IPOSX, IPOSY, ANAME, SCALE)
      CHARACTER ANAME*(*), A*1
C
      REAL SCALE
      INTEGER IPOSX, IPOSY, N, I
      N = LEN(ANAME)
      DO 10 I = 1, N
        IY = IPOSY - (I-1)*24*SCALE
        CALL MOVABS(IPOSX, IY)
        A = ANAME(I:I)
        CALL ANMODE
        WRITE(1,*) A
        CALL RECOVR
        CALL CHARTK(A, SCALE)
10
      CONTINUE
C
      RETURN
      END
```

Sample calculation of the fringe shift and the temperature distribution, from the interference fringe patterns, in Figure 65. Table 2

	гн-тс)	4 4 4 4 4 4 4 4 4 4 4 4 4 4 4 4 4 4 4
	(Т-ТС)/(ТН-ТС	99999972699844888442229999999
* · • • · · · · · · · · · · · · · · · ·		0634 0634 0634 0634 0634 0634 0634 0634
	+ X	2006 2006 3006 3007 3007 2007 2007 2007 2007 2007 2007
=307.08 =307.08 +05.99.59 90.57 17 18 18 18 18 18 18 18 18 18 18 18 18 18	S.	13 . 8052 13 . 1245 13 . 1245 12 . 3648 11 . 8800 11 . 8800 11 . 8800 11 . 8800 12 . 8800 12 . 8800 12 . 8800 12 . 8800 12 . 8800 12 . 8800 13 . 7683 14 . 2511 17 . 8800 17 . 8800 17 . 8800 18 . 8
767 +5 tempere temper 0.9829 100 2792	EPS	13.9259 13.62685 13.24662 12.34662 12.34662 12.0000 10
V/HE 0.0 RB 1.1 Hot wall Cold wall Pressures FSCW 0. FSHW 14.	H/X	0.9970 0.9970 0.9970 0.97082 0.97082 0.9639 0.9245 0.9245 0.7816 0.3027 0.3027 0.0316 0.0316 0.0316
ė	EPS	13.9258 13.60258 12.3456 12.3456 12.3456 10.0000 10.00000 10.00000 10.00000 10.00000 10.00000 10.0000 10.0000 10.0000 10.0000 10.0000 10.0000 10.0000 10.0000
geb 06=90	H/X	0.9970 0.9980 0.99817 0.99857 0.99782 0.99245 0.98245 0.98245 0.98245 0.98245 0.98245 0.98245 0.9827 0.9827 0.9827 0.9827 0.9827 0.9827 0.9827 0.9827 0.9827 0.9827 0.9828 0.9827 0.9828
lination Angl	AB	0.3860 0.3860 0.38845 0.38845 0.38845 0.3866 0.3866 0.3866 0.3867 0.3866 0.3867 0.3866 0.3867 0.3866 0.3867 0.3866 0.3867 0.3867 0.3866
At Incl	٧,	0.4227 0.4288 0.4281
767 8+ 5	1	EEEE6660000000000000000000000000000000
V/H= 0.0 Re= 1.1 E V= 0.4000 V1= 0.299 V2= 1.609 XHO= 1.62 XCO= 0.29	×	1.6220 1.6070 1.5070 1.5070 1.5070 1.5537 1.5257 1.43634 1.43637 1.3360 1.0250 0.8000 0.8000 0.8000 0.9000 0.3500 0.3500 0.3200 0.3200

Table 2 (cont'd.).

	2010	1001	08=4(004 001+401	oep Ogse(o		V/H= 0.0	0195 At	Inc   instion	Angle=90 de	
32.0	:	, <b>"</b>	65	3	<u>.</u>	Hot wall Cold wall	Deratur mperatu 3829000	= 30 = 2 = + 05	deg. K	
# 0 0	098					FSCW= 0.6 FSHW= 15.0 EPSCO=14.2	92. F.	Inge Shif	at the Cold at the Hot (A.2.4)	
×	-	××	8	n/x	EPS	H/X	EPS	FS	TK (;	(T-TC)/(TH-TC)
22	4	.343	318	.997	1.	66			06.751	•
•	7	.336	.309	.991	.42	8	•	•	06.339	9
~ .	4 6	325	325	98.	٠,	•	14.0000	•	05.790 05.404	
1.5850	E	. 333	307	969	. 33	96			04.928	
•:	13	.325	.325	96.	8	8		•	04.802	•
1.5600	12	.337	.315	. 95	w.	. 95	•	•	03.844	•
1.5379	2 :	0.3250	0.3250	0.8337	12.0000	0.8337	12.0000	11.2673		0.7791
	2	325	325	85		85			00.692	
. "	<b>o</b>	.325	.325	.77	0.0				435	, ru
	<b>6</b>	.336	.318	. 73	₩.		•	•	948	ĸ.
	<b>10</b>	325	.325	999	. r	٠ •	•	•	178	٠,٠
٠,	. ~	325	325	53	9	שיי				, ,
	•	.335	317	.47	'n	٦.			399	
ä	9	.325	.325	.39	9		•	•	. 69	ო.
٠.	<b>ب</b> و	. 332	314	.32	٠,٠	<u>ن</u> د	•	•	975	i.
	۲ ۹		 	7.5		•	•	•	25.	i.
	<b>m</b>	325	325	60					056	! -
٣,	~	.336	314	.05	'n				482	-
٠,	8	.325	.325	.03	.000	9	•	•	.873	9
"	-	.341	318	.02	. 758	.024	•	•	590	•
۳.	-	.336	.314	9	ě	.016	1.5300	•	323	۰.
۳.	_	. 331	.309	8	98	0.0080	1.2864	•	038	۰.
۳.	-	. 325	. 325	8	0	.002	1.0000	•	705	۰.

Table 2 (cont'd.).

V/H= 0.13	340	At Inclin	Ination Ang	geb 08=e1g	÷	V/H= 0.13	0 At	Inclination	< €	
V= 0.4750 V1= 0.2995 V2= 1.6090 XHO= 1.626 XCO= 0.298	:		e 83 83				temperat 0.982900 00 F	ure =289.590 000E+05 PA. ringe Shift a ringe Shift a	deg. K t the Cold t the Hot (A.2.4)	W W W W W W W W W W W W W W W W W W W
×	-	*	<b>6</b>	H/X	EPS	H/X	EPS	S.	TX (T	Т-ТС)/(ТН-ТС)
8	4	475	78	9	000	9		3.878	567	9
615	- E	. 495	468	•	3.76	•	3.7	.630	. 247	9
607	e :	483	457	on o	926	<b>a</b> , c	ب د	3.199	.691	9
3 8	2 2	488	462	e a	2.515	, a	E	2.387	640	. 4
579	12	475	75		8	9	. 6	1.869	988	
.557	=	.475	475	æ	1.000	•	•	0.864	714	۲.
. 534	2	.475	21	<u>م</u> و	98	9	91	. 859	450	
. 506	<b>)</b>	475	4 / 5 4 / 5 7 / 5	æ. ⊲	. c	9	. c	400	9 C	. ע
00	۰ د	475	35	9	88	• •	. 0	. 832	707	7
.325	9	.483	460		.378	۲.		197	928	٦.
. 238	9	.475	0.4750	۲.	900	۲.	۰.	. 797	448	e.
. 125	<b>ග</b>	490	65	ص	•	9	<b>.</b>	.387	952	<u>ب</u>
1.0250	ທ	0.4820	0.4562	0.5474	5.273	0.5474	5.2713	5.0242	ი -	0.3386
.850	4	.501	2	•	. 849	. •	. 6	566	964	
. 750	4	.497	5	<u>س</u>	4.6218	ღ.	Ψ.	.316	. 665	ä
. 650	4	. 483	20	. 26	. 252	7	~	.926	199	u.
. 562	◀ (	.475	75	199	000.	٦.	0	. 655	876	~
. 459	m (	. 475	2		000.	- '	9	. 633	665	٦,
388	7 .	.475	Ō٠	. 068	900.	9	9	.619	473	٦,
. 645 0 40 0 40		. 480	4513	. בככ	•	9.9		900	_ (	
920	- c		1 4	220.	200	?	סטט פיני	. 600 888	110	
310	9 0	404	4 6 6	י כ	635		635	238	8.65	90
302	, 0	490	0.4614	.003	539	90		139	9.751	. 0

Table 2 (cont'd.).

		•	•	;		V/H= 0.16	1913 At I	Inclination	Angle=90	. <b>0eb</b>	
V/H= 0.18 V= 0.5500 V1= 0.299 V2= 1.609 XHO= 1.62 XCO= 0.28		see Figure	ation Angl		<u>.</u>	COLD ED POST OF THE PROPERTY O	temperature temperature 0.98290006 600 . Frin 600 . Frin 2792. Frem	#307.088 #289.590 +05 PA. 00 Shift Equation	deg. K deg. K at the Col at the Hot (A.2.4)	I I GM P	
×	-	*	VB	н/х	EPS	ж/н ж/н	EPS	S.F.	¥	(т-тс)/(тн-тс	3
1 8	1	9	0.5283	988	. 235	988	. 236	619	06.614	9.0	1
6	7	'n	S.		4.000	6	90	٦.	.30	8.0	
9	13	က္		.984	444	.984	444	61.	05.588		
<b>0</b> 10	<u>د</u> و	ığ ı	י פּע	. 977	3.000 3.000	778.	900	٠,	9.0		
58	2 2	ט ע	o c	2 6	2 000	2 % 3 d	4 0	- E	304.3430		
55	: =	ຸທ	9	947	8	. 947	88	. ש	4	0	
(7)	2	ະດ	S.	.931	900	.931	.000		20.	0.0	
8	•	'n	8	.912	000	.912	900	₽,	2	9.0	
4:	<b>œ</b> (	ri G	10	.887		.887		9	24	9.0	
4 4	~ «		0.5500	0.6452	6.2885	0.8452	7.0000 8.2885		296.5782	0.3994	
58	ω (	ຸດ	ຸດ	706	000	706	9	. 10	2	0.0	
2	ß	ທ	ĸ	.606	. 765	. 606	. 766		8	0	
8	တ	ທ	'n	. 531	.618	. 531	. 618	-	69	0.9	•
8	<b>ທ</b> ເ	RÜ I	Ö	.457	.538	.457	. 538		90.0	9.0	
. A	o c	ט ע	. ע	200	564		. 566 8.4	ָ כ	5.0	9.0	
52	<b>w</b>	9	9	. 177	90	177		•	82	0.2	
4	4	'n	'n	. 119	.000	119	000	₹.	9	0.5	
.39	က	ø.	ö	.079	000	.079	8	۲.	4	-	
.35	~	S.	ö	.045	900.	.045	900.	٦	. 23	0.0	
.34	_	ö	ö	.038	. 784	.038	. 784	٦.	. 97	0.0	
.33	-	S.	0.5365	.030	.547	.030	.547	σ.	69	0.0	
.32	-	'n	ö	.023	.325	.023	.325	۲.	4.	0.0	
٤.	-	'n	0.5231	.015	٦.	.015	. 106	'n	. 18	0.0	
.30	0	ĸ.	Ö	.009	0.9018	<b>6</b> 00.	0.9018	<u>ب</u>	2	0.0	

Table 2 (cont'd.).

	9			9		V/H= 0.24	2486 At	Inclination	Angle=90 d		
V/H= 0.2	4 80 80	At Inclin <b>e</b>	Instion Angl	00p 08=010	•	Ot #811	temperatur	-307.088	9. K		
V* 0.6250	:	see Figure	90			= "	temperature:	.289.	8		
- c						o o	. 100	Shi	t the Cold	Well	
XHO= 1.6260 XCO= 0.2980	9 0					EPSC0=14.0	::	shif Equati	<b>B</b> t the Hot (A.2.4)	_	
×	1	۸ <b>۸</b>	89	<b>ж/н</b>	EPS	X/H	EPS	F.	TK (T-	-тс)/(тн-тс)	
8	9	000	1	8	W	800	13 5244	2	84	•	
		. 638	•		; c	A			7 7 A B	. a	
		637	•	9		980	475	7	5. 109	. =	
591		625		6	. •	.973	000	. 28	1.498		
1.5718	:=	0.6250	0.6250	0.9592	11.0000	0.9592	1.000	1.2	303.2191		
.551		625		9	9	. 943	900	. 25	1.950	۲.	
. 528	•	. 625	•	6		.926	٠.	. 25	0.690	₩.	
. 501	00	.625	•	8	۰.	906	•	.24	.440	ĸ	
.465	7	.625	•	.87	9	. 879	•	. 23	3.197	٦.	
.406	9	.625	•	.83	۰.	.834	•	.2	3.956	۲.	
.325	ស	.638	•	.77	ĸ.	.773	•	8	3.324	<u>ن</u>	
. 225	ß	.634	•	. 69	е.	. 698	•	.47	3.054	е.	
. 125	ß	.631	•	. 62	~	. 622	•	.36	8.818	<u>ب</u>	
.025	ß	.632	•	.54	4	. 547	•	₹.	8.897	e.	
.925	S	.634	•	47	4	.472	•	.37	5.935	G.	
.825	ហ	.640	•	.39	٩.	. 396	6.4323	<b>9</b>	3.067	ო.	
.725	ഗ	.647	•	.32	Ψ.	. 321	•	99.	3.288	ო.	
.625	ß	. 650	•	. 24	ø.	. 248	•	. 65	3.275	ო.	
.514	S	.625	•	-18	۰.	. 163	9	98.	5.439	ຕຸ	
.448	4	.625	•	Ξ	٥.	. 13	۹.	4	1.219	~	
.402	<b>e</b>	.625	•	.07	9	.078	۰.	. 82	1.015	-	
.363	7	.625	•	9	٥.	.049	۰.	6	1.824	٦.	
.340	_	. 635	•	9	ო.	.031	•	. 23	.023	۰.	
.327	_	.625	•	9	.000	.022	۰.	8	643	0	
.320	0	.647	•	<u>-</u>	. 750	.016	۲.	. 65	.350	0	
.310	0	.638	•	8	4	800.	0.4338	.33	978	0	
.302	0	.631	•	8	.217	. 003	ü	Ξ	.727	•	

Table 2 (cont'd.).

Table 2 (cont'd.).

V/H= 0.3	631	At Incl	inat ion	Angle=90 deg	÷	0.3	31 At	nclinati	Angle=90	d <b>e</b> g.
= 0.7750 1= 0.299 2= 1.609		*** F19U	• •			ot wall old wall ressure SCW# 0.	temperature temperature 0.98290000E+	=307.088 =289.590 +05 PA. ge Shift	deg. K deg. K the C	
	0 0					FSHW= 14.6	::	Shift	#5	-
×	-	<b>A</b>	89	н/х	EPS	н/х	EPS	S.	TK (T	-TC)/(TH-TC)
820	3	"		۱ ۳	4.148			82	. 502	"
?=	· •			. 9	د		•	.36	8	•
1.5980	5	٦.		•	900.	•	•	<b>.</b>	.02	<b>8</b> .0
. 588	12	ς.	•	9	;	•	'n,	. 22	4	<b>9</b> 6
76	12	Γ.	•	<b>.</b>	2.0	•	•	.67	7.4	
. 556	=	Γ.	•	œ, '	- 0	•	<u>-</u> ,	. 675	.47	0.0
'n	2	Γ.	•	œ. '	9	•	•	.673	.21	0
. 506	<b>a</b>	Γ,	•	œ, (		•	•	.672	9	9.0
₹.	<b>©</b> (	ς,	•	. ·	. c	•	•	0.0	26	9 6
2 6	~ •	0.7750	0.7750	0.8422	4205	0.8422	A 4205	6.0803	296, 7910	Ġ
	<b>.</b>	: -		. •	•			. 105	82	7
: -:	9			9.	'n			180	9	7.
•	9	٣.	•	ĸ,	9	•	•	.326	8	0.
₩.	9	۳.	۲.	٦.	₩.	•	•	. 526	. 33	7.0
۲.	7	Γ.		<u>س</u>	-	•	•	.781	40	•
۳.	~	٦,	•	Ġ,	<u>س</u> (	•	•	363	3	5 6
w,	_	Γ.	'.	<b>-</b> '	9,6	•	•	<b>1</b> 0 0		
۲.	10	٦,	•	٦,	9,0	124	•		7	
٩,	Ω.	`.'	•	? (	9,0	80.	•	. פֿכּי	5 6	2 6
	4 (	٦,	`.'		? (	990.	•	000	5	, .
.327		`.	•	•	? '	440	•	200	3	
.34	~	. 786		9		0.0316	•	300	2	
. 330	~	. 775	۲.	•	9	.024	•		5	- 6
.320	-	. 791	۲.	٠.	ω.	9	•	8	8	) )
.310	-	0.7815	۲.	٠.	'n	600.	•	. 812	. 53	0
.302	0	.800	۲.	٠.	0.8877	8	•	0.4880	0.15	0.

Table 2 (cont'd.).

Y/H= 0.4204 Y= 0.8500 . Y1= 0.2995 Y2= 1.6090 XHO= 1.6260 XCO= 0.2980		At Incl	inacton An	00 00 = 00 0 00 00 00 00 00 00 00 00 00	<u>.</u>	COLDER DO A STATE OF A	temperature =307.08( temperature =307.08( temperature =289.5( = 0.9829000E+05 PA .050 . Fringe Shift .800 . Fringe Shift .2792. From Equation	Inclination Lre =307.088 Lure =289.590 Lure = 289.590 Lure = 289.5	Angle=90 deg. K deg. K deg. K st the Col	
×	-	۸×	89 >	H/X	EPS	H/X	EPS	S.	TK C	(T-TC)/(TH-TC)
820	5	•	"	900	6	"	380	3.867	يع ا	9
1.6121	E	0.8500	8	8	, e	. 63	13.0000	7		0.9404
900	12	₽.	₩.	æ	ä	3	.456	٠.	Θ.	œ.
6	12	•	•	σ.	ä	۳.	000	,	۲.	₩.
ĸ,	=	₽.	₩.	•	•	₩.	8	•	۳	۲.
'n	0	₩.	₩.	œ,	ö	œ. ۱	8	ò	٦,	٦.
ĸi.	<b>a</b> (	æ (	æ .	o, c	•	97.0	9,9	•	<u>ت</u> م	
•	<b>20</b> P	0.8500	0.8500	0.8871	. 0000 . 0000	0.8871	8 .0000 2 .0000	7 4089	298.0043	0.0707
re	· •	9	. 8	. 8					. 7	. 4
. ~	•				•		.063	•	_	•
Ξ.	•	۳.	₩.	₩.	•	₽.	. 185	٦.	ď	۲.
•	9	•	9	<b>.</b>	•	'n.	•	٦.	<u>ن</u> ا	٦.
œ, c	•	æ,	æ.	•	6.5223	۲,	6.5223		ם מו	٠,
	0 €	9	9		•			5	•	•
. ເວ	· ~			~	•			8	9	•
₹.	9	₩.	₩.	٦.	•	Ξ.	•	.02	_	۲.
₹.	ĸ	₽.	₽.	9	•	Ξ.	•	.003	4	σ.
ო.	4	•	0.8200	6	4.0000	٩.	•	ä	N	. 28
ღ.	<b>6</b>	•	•		•	۰.	8	. 978	0	199
ო.	7	Φ,	8	9	•	9	42	. 396	ຕ	. 159
e	_	œ (	8	.031	•	9	95	. 788	67	. I 9
<u>ب</u>	_	₩.	∞.	.024	•	024	8	<b>3</b> 8		.088
ო.	_	•	. 850	.017	•	0.7	8	. 959	702	.063
.310	0	0.8645	0.8374	600.		8		8	_	.032
. 302	0	. 855	.827	0.0030	- 8	003	<b>®</b>	140	75	600
									ı	

Table 2 (cont'd.).

Table 2 (cont'd.).

						V/H≈ 0.5	.6349 At 1	Inclination	Ang 1 . * 90	deg.
Y/H= 0.53 V= 1.0000 V1= 0.2998 X2= 1.6096 XHO= 1.626 XCO= 0.298	84.0 80.0 90.0 90.0 90.0 90.0 90.0 90.0 90	At Incl	ination Angle 6 65	0 = 0 0 de	·	COLD TENT	temperature =307.( 1 temperature =289 = 0.98290000E+05 1.700 . Fringe Sh 300 . Fringe Sh 1.2792 . From Equal	=307.088 = 1289.580 E+05 PA. nge Shift nge Shift	deg. K deg. K ti the Cold t the Hot (A.2.4)	W W W W W W W W W W W W W W W W W W W
×	-	<b>*</b>	<b>a</b> >	H/X	EPS	H/X	EPS	FS	TX (T	(T-TC)/(TH-TC)
2	5	8	0000	6	14,0000	99		•	06.693	.977
9	9	1.0210	0.9918	Ø		.98	13.7192		6.326	•
1.6030	5 5	1.0095	9		•	.982	•	i,	05.820	.927
20	13	1.0000	.000	978	е е	.976	•	9	.387	902
20	12	1.0176	•	888	•	9				2 4
S	2 :		0000	8008.0 0.00	11.0000			9.09	8	75
	: 9	0000	• •	916		<u> </u>			528	.682
4		0000		•		. 88	0000.6	•	. 258	. 609
42	•	1.0000	•	8	•	9	•	۳,	.987	537
.30	7	1.0133	•	۲,	•	.75	4 1	c		9
1.2000	١ م	1.0188	0.9865	0.6792	7.5820	0 (	90	7.0404		0.4880
- 6	<b>~</b>	0000	•	מי		2	9	. ש		ຸດ
82	<b>.</b>	1.0063		. ຕ		8	٦.			'n
.72	•	1.0115	.978	ღ.	•	.32	•	۳,		ا <u>ب</u>
.62	<b>6</b> 0	1.0117	σ,	~	<u>س</u> (	2.	8.3762	9,		ກຸພ
90.4	<b>6</b> 0 r	0000	0000							. 4
. 4	- œ	0000	•	. 9						ິ.
39	<b>o</b>	0000	1.0000	9	•			e.		~
38	4	1.0000	000	۰.		۰.	•	е.		~
8	က	1.0000	1.0000	۰.	8	۹.	8	ლ.		٦.
E	7	1.0133	. 985	۰.	•	9	478			- (
32	~	1.0000	1.0000	۰.	2.0000	•	8	e.		•
်.	_	1.0138	. 985	.012	. 491	<u>-</u>	6	<b>o</b>		•
.30	-	1.0000	1.0000	0.0047	0000.	0.0047	1.0000	. 303		•

Table 2 (cont'd.).

1         VA         VB         X/H         EPS         X/H         EPS         TK           6200         13         10861         1.0576         0.9855         13.3865         0.9858         13.3865         13.472         306.643           6008         13         1.0750         1.0750         0.9878         13.0000         13.472         306.643           6008         13         1.0750         1.0750         0.9878         12.2000         13.472         306.643           6008         13         1.0570         0.9878         12.2000         0.9878         12.2000         13.472         306.643           6000         11         1.0750         0.9878         12.2000         0.9878         11.2060         10.486         10.0760         10.486         10.0760         10.486         10.0760         10.486         10.0760         10.486         10.0000         11.4461         303.450         10.0860         10.9878         11.0000         11.4461         303.450         10.0800         10.9878         11.0000         11.4461         300.414         10.0414         10.0000         10.8878         10.0000         10.9878         11.0000         10.9878         10.0000         10.9878         10.000	V/H= 0.56 V= 1.0750 V1= 0.2990 V2= 1.6090 XHO= 1.6290 XCO= 0.290	5922 0 96 260 980	At Inclin	85 85	Angle=90 deg		Hot wall ter Cold wall to Presence 0. FSHWH 13.80C EPSCO#14.276	mperatur emperatur .0829000 Fr	perature =307.088 mperature =289.590 98290000E+05 PA. Fringe Shift Fringe Shift 2 From Equation	deg. K deg. K mat the Co mat the Ho (A.2.4)	
Color   Colo	×	-	<b>*</b>	<b>48</b>	H/X	EPS	н/х	۰ م		*	(T-TC)/(TH-TC)
6986         13         10750         107	820	5	-   ≪	1.0576	988		895		3.866	06.552	0.969
6000         12         10936         10644         0.9804         12.5357         13.1036         305.56862         0.98           58910         12         10833         1.0538         0.9736         12.2814         0.9673         12.0000         12.4603         304.7427         0.88           58910         12         1.0750         1.0750         0.9673         11.5366         0.9678         11.5366         0.9673         12.0000         12.4603         304.7427         0.8           5500         11         1.0750         1.0750         0.9847         11.0000         0.9848         10.0000         11.4361         302.1736         0.9           4438         1         1.0750         1.0750         0.9824         10.0000         10.4356         300.9017         0.9         10.4366         300.9017         0.9         42.06         300.9017         0.9         42.06         300.9017         0.9         42.06         300.9017         0.9         0.9         42.06         300.9017         0.9         42.06         300.9017         0.9         42.06         300.9017         0.9         42.06         300.9017         0.9         42.06         300.9017         0.9         42.06         300.9017	609		20	1.0750	8		.987	•	3.472	.043	0.840
550         10	600		083	1.0644	.980	2.635	980	2.635	3.103	568	0.013
5500         11         1000         11         4461         304.1436         0.9578         11.5366         11.9914         304.1436         0.9578         11.5366         11.9914         304.1436         0.9578         0.9428         11.0000         11.4461         303.4502         0.7550         0.9248         11.0000         11.4461         303.4502         0.7550         0.9248         11.0000         0.9436         300.9017         0.9100         0.9426         300.0001         0.9436         302.1735         0.7550         0.9628         11.0000         0.9426         300.0001         0.9436         200.0001         0.9436         200.0001         0.9436         200.0001         0.9426         0.0000         0.9426         0.0000         0.9426         0.0000         0.9426         0.0000         0.9426         0.0000         0.9426         0.0000         0.9426         0.0000         0.9426         0.0000         0.9426         0.0000         0.9426         0.0000         0.9426         0.0000         0.9426         0.0000         0.9426         0.0000         0.9426         0.0000         0.9426         0.0000         0.9426         0.0000         0.9426         0.0000         0.9426         0.0000         0.9426         0.0000         0.9426	591		083	1.0538	ص o	2.281	2/8/2	2.781	2./45 2.480	747	
5500         11         10750         107	. 582		000	0.070	, a	1.536	.957	;	1.99.1	143	0.831
6261         10         1	550		075	1.0750		8	.942		1.446	450	0.79
4438         9         1.0750         0.8887         9.0000         0.8887         9.0000         9.4209         299.6334         0.5448           4438         1.0750         0.8887         9.0000         0.6628         7.0903         0.7545         7.0903         7.4274         298.6334         0.5639           2000         7         1.0636         0.6792         7.2704         7.6539         298.6334         0.5639           1000         7         1.0636         0.6039         7.2704         7.6639         298.6028         0.6639           1000         7         1.0636         0.6039         7.2704         7.6639         7.7963         298.6028         0.6639           1000         7         1.0693         0.6039         7.6668         0.6039         7.6639         7.7963         298.603         298.603           1000         7         1.0686         0.6039         7.6668         7.7963         298.6143         0.663           1000         7         1.0750         0.2441         8.000         0.2440         8.000         8.0412         298.6455         0.663           4811         7         1.0750         0.1041         8.000         0.144 <td< td=""><td>.52</td><td></td><td>.075</td><td>1.0750</td><td>9</td><td>0.000</td><td>.924</td><td><u>.</u></td><td>0.435</td><td>. 173</td><td>2.0</td></td<>	.52		.075	1.0750	9	0.000	.924	<u>.</u>	0.435	. 173	2.0
3000         7         1.0779         1.0458         0.7545         7.0903         7.4274         298.4352         0.6792           2000         7         1.0739         1.0458         0.6792         7.2704         7.5639         298.6028         0.698           1000         7         1.0930         1.0618         0.6792         7.2704         7.5639         298.6028         0.698           1000         7         1.0930         1.0698         0.6038         7.5455         0.6038         7.8681         8.0628         298.603         298.603           9750         7         1.016         1.0698         0.6038         7.8681         8.0628         299.1413         0.698           8250         7         1.016         1.0560         0.2441         8.0000         0.2440         8.0472         8.0472         8.0472         0.6583         0.6583         0.6583         0.6583         0.6583         0.6583         0.6583         0.6683         0.6683         0.0000         0.0448         3.0000         0.9868         292.69         0.6583         0.0448         3.0000         0.9868         2.9859         0.6583         0.0683         4.0000         0.0448         3.0000         2.9259         <	7:	<b>a</b> a	.075	1.0750			989.	•	300		0.0
2000         7         1.0836         1.0518         0.6792         7.2704         7.5639         298.6026         0.6039           1000         7         1.0930         1.0600         0.6039         7.5455         0.6039         7.75453         298.8074         0.603           1000         7         1.016         1.0686         0.6038         7.8061         0.6038         7.7963         298.8074         0.603           1000         7         1.016         1.0686         0.6038         7.8061         0.6032         0.603	6	۸ ه	7.00	1.0458	"	900	754		. 427	435	0.0
1000         7         10930         1.0800         0.6039         7.5455         0.6039         7.5456         7.5456         7.5456         7.5456         7.5456         7.5456         7.5456         7.5456         7.5456         7.5451         7.5451         7.5451         7.5451         7.5451         7.5451         7.5451         7.5451         7.5451         7.5451         7.5451         7.5451         7.5441         8.0472         8.1334         299.1906         0.559.169         0.5451         9.5441         8.0472         8.1334         299.1906         0.559.1906	202	~	.083	1.0518		.270	.679	•	. 563	. 602	0.0
9750         7         1016         1.0686         0.5098         7.8061         0.5098         7.8061         0.5098         7.8061         0.5098         7.8061         0.5098         7.8061         0.7936         299.1413         0.509           .7250         8         1.0765         1.0447         0.3215         8.0472         8.0472         8.0472         9.99.3042         0.6           .6221         8         1.0750         1.0750         0.1379         7.0000         0.1379         7.0000         0.9144         299.3042         0.6           .4363         6         1.0750         0.1041         6.0000         0.1041         6.0000         6.9769         297.8870         0.4           .4047         6         1.0750         0.1041         6.0000         0.1041         6.0000         9.966.455         0.4           .4047         6         1.0750         0.1048         3.0000         0.0623         4.0000         3.9361         294.2109         0.2           .3575         3         1.0750         0.0448         3.0000         2.9259         291.010         0.1           .3450         2         1.0750         0.0354         2.4181         2.3186         2	2	^	.093	1.0600	₩.	'n	.603	•	. 795	887	0.0
B250         7         1069         10727         0.3968         7.8327         0.3468         7.8327         0.3468         7.8327         0.3468         7.8327         0.3468         7.8327         0.3468         7.8327         0.3468         7.8328         0.0472         0.3468         8.0472         0.346         8.0472         0.346         8.0472         0.346         8.0472         0.346         8.0414         299.3042         0.6           6221         8         1.0750         1.0750         0.1379         7.0000         0.1379         7.0000         0.1379         7.0000         0.1379         7.0000         0.1379         7.0000         0.1379         7.0000         0.1041         297.8870         0.0           4461         5         1.0750         0.1041         6.0000         0.1041         6.0000         4.9465         295.4212         0.3           3807         4         1.0750         0.0623         4.0000         0.0623         4.0000         3.9361         294.2109         0.0           3575         3         1.0750         0.0448         3.0000         2.9259         292.3101         0.0           3560         2         1.0750         0.0288         2.0000	6	7	<u>.</u>	1.0686	w.	8	.509	•	99.	141	0
(221)         8         (244)         (244)         8         (244)	. 62	<b>~</b> 0	106	1.0727	<u>ن</u> د	ai c	32.5	•	133	306	
4811         7         1.0750         1.0750         0.1379         7.0000         0.1379         7.0000         6.9799         297.8870         0.448           4363         6         1.0750         1.0750         0.1041         6.0000         6.0000         6.9799         297.8870         0.04           4047         6         1.0750         0.1041         6.0000         0.0803         5.0000         4.9465         296.4212         0.3           3807         4         1.0750         0.0823         4.0000         3.9361         294.2109         0.2           3575         3         1.0750         0.0448         3.0000         2.9259         293.0110         0.1           3450         2         1.0870         0.0354         2.4181         2.3386         292.3177         0.1           3363         2         1.0750         0.0218         2.0000         0.0288         2.0000         1.9167         291.8218         0.1           3370         1         1.0869         1.0000         0.0148         1.0000         0.9085         290.6435         0.0           3050         0         1.0840         1.0850         0.0063         0.3104         0.2134		D @	0 / C	1.0750	יי פ		244		3	190	
4363         6         1.0750         1.0750         0.1041         6.0000         0.1041         6.0000         6.0000         8.9663         296.6455         0.04           4047         5         1.0750         1.0750         0.0803         5.0000         4.9465         295.4212         0.3           3807         4         1.0750         1.0750         0.0623         4.0000         3.9361         294.2109         0.2           3575         3         1.0750         0.0448         3.0000         2.9259         293.0110         0.1           3450         2         1.0870         0.0354         2.4181         2.3386         293.3177         0.1           3363         2         1.0750         0.0358         2.0000         0.0288         2.0000         1.9167         291.8218         0.1           3370         1         1.0889         1.0608         0.0218         1.0847         0.0148         1.0000         0.9085         290.6435         0.0           3176         1         1.0840         1.0650         0.0063         0.3103         0.3104         0.2134         289.8365         0.0	4	, ~	.075	1.0750	-	•	137		.979	887	0
4047         5         1.0750         1.0750         0.0803         5.0000         4.9465         295.4212         0.3           .3807         4         1.0750         1.0750         0.0623         4.0000         3.9361         294.2109         0.2           .3575         3         1.0750         1.0750         0.0448         3.0000         2.9259         293.0110         0.1           .3450         2         1.0870         1.0583         0.0354         2.4181         2.3366         292.3177         0.1           .3363         2         1.0750         0.0288         2.0000         0.0288         2.0000         1.9167         291.8218         0.1           .3370         1         1.0688         1.0608         0.0218         1.4947         0.0148         1.0000         0.9085         290.6435         0.0           .3176         1         1.0840         1.0550         0.0053         0.3103         0.3104         0.2134         289.8365         0.0	.436	9	.075	1.0750	Ξ.	•	<u>.</u>	•	960	645	0.
3807         4         1.0750         1.0750         0.0623         4.0000         0.0623         4.0000         3.9361         284.2109         0.2357           .3575         3         1.0750         1.0750         0.0448         3.0000         0.048         3.0000         2.8259         293.0110         0.1           .3450         2         1.0750         0.0354         2.4181         2.3386         292.3177         0.1           .3363         2         1.0750         0.0218         2.0000         0.0288         2.0000         1.9167         291.8218         0.1           .3270         1         1.0689         0.0218         1.4847         0.0148         1.0847         1.4947         1.4947         1.4947         0.9065         291.2253         0.0           .3176         1         1.0750         0.0148         1.0000         0.9065         290.6435         0.0           .3050         0         1.0840         1.0650         0.0063         0.3103         0.3104         0.2134         289.8365         0.0	404	w	075	1.0750	۰.	•	. 080	۹.	. 946	421	0.3
.3575         3         1.0750         1.0750         0.0448         3.0000         0.0448         3.0000         2.8259         293.0110         0.1           .3450         2         1.0670         1.0583         0.0354         2.4181         2.3481         2.3386         292.3177         0.1           .3363         2         1.0750         1.0750         0.0288         2.0000         0.0288         2.9000         0.9187         1.4917         291.2253         0.0           .3270         1         1.0608         0.018         1.04947         0.0218         1.04947         0.9985         291.2253         0.0           .3176         1         1.0750         1.0750         0.0148         1.0000         0.9188         1.0000         0.9085         290.6435         0.0           .3050         0         1.0840         1.0850         0.0063         0.3103         0.3104         0.2134         289.8365         0.0	.380	4	.075	1.0750	۰.	000.	.062	9	. 936	210	0.
.3450 2 1.0870 1.0583 0.0354 2.4181 0.0354 2.4181 2.3386 292.3177 0.1 3363 2 1.0870 1.0583 0.0288 2.0000 1.9167 291.8218 0.1 3270 1.0750 1.0750 0.0288 2.0000 1.9167 291.8218 0.1 3270 1 1.0889 1.0608 0.0218 1.4847 1.4073 291.8253 0.0 3177 1 1.0750 1.0750 0.0148 1.0000 0.0148 1.0000 0.9068 290.6435 0.0 3176 1 1.0850 1.0750 0.0148 1.0000 0.0153 0.3104 0.2134 289.8365 0.0	.357	ო	075	1.0750	9	000	.044	•	. 925	5	0
.3363 2 1.0750 1.0750 0.0288 2.0000 0.0288 2.0000 1.9167 291.8218 0.1 3270 1 1.0889 1.0608 0.0218 1.4947 0.0218 1.4947 1.4073 291.2253 0.0 3176 1 1.0750 1.0750 0.0148 1.0000 0.0148 1.0000 0.9085 290.6435 0.0 3176 1 1.0750 1.0850 0.0148 1.0000 0.0148 1.0000 0.9085 290.6435 0.0 3176 1 1.0840 1.0850 0.0053 0.3103 0.3104 0.2134 289.8365 0.0	.345	~	.087	1.0583	ဗ	418	038	7	. 338	92.317	- -
.3270 1 1.0889 1.0608 0.0218 1.4847 0.0218 1.4847 1.4073 291.2253 0.0 .3176 1 1.0750 1.0750 0.0148 1.0000 0.0148 1.0000 0.9085 290.6435 0.0 .3050 0 1.0840 1.0550 0.0053 0.3103 0.0053 0.3104 0.2134 289.8365 0.0	.336	7	.075	1.0750	.02	000	028	8	916	91.821	- 0
.3176 1 1.0750 1.0750 0.0148 1.0000 0.0148 1.0000 0.9085 290.6435 0.0 .3050 0 1.0840 1.0550 0.0053 0.3103 0.0053 0.3104 0.2134 289.8365 0.0	.327	-	088	090	.021	484	.021	49	.407	91.225	0.0
.3050 0 1.0840 1.0550 0.0053 0.3103 0.0053 0.3104 0.2134 289.8365 0.0	.317	-	75	1.0750	.01	900.	9	8	908	643	0.0
	.305	0	8	9	.005	E	.005	<u>.</u>	. 213	9.836	0.0

Table 2 (cont'd.).

						Y/H= 0.6	.6495 At	Inclination	Angle=90 d	.00
/H= 0.6	495	<b>~</b>	Instion Angl	010=90 deg		ot wall		=307.088	deb X	
1. 150 0.29	:	see Figure	65			Cold wall	mpera 38290	=289. +05 P	₩.	
2= 1 6= 1.	~ ö							2 S	• •	Well
C	0					EPSC0=14.	:	om Equation		
×	-	<b>4</b> >	٧B	н/х	EPS	H/X	EPS	FS	TK (T	-тс)/(тн-тс)
1 8		1 9		8		8				8
9	2 :	200		200	13.7087		. / CB	13.8648	0./00 8./73	20/8.0
- 6	2 5	ש פ	1281	- 40		- 400	3.00.6 2.00.6	י	7.7.0	
) G	2 =		1500	979	! 0	979	000	ָר פּי	770	924
S)	12	_	1.1421	.972			2.74	2	5.431	
S	12	_	1.1324	.965	٦.	.965	2.40	2.6	4.991	. 880
6	12	~	1.1500	.956	•	.956	٠.	2.2	4.462	.848
	=	٦.	1.1500	. 932	-	.932	1.00	.2	3.163	.775
r.	2	٦.	1.1500	. 905	9	. 905	000.	Ξ.	1.872	.701
7	<b>a</b> (	7	1.1500	.87	٩	.87	8	٦,	0.584	. 628
i, c	<b>~</b> a		1.1450	. 754 870		754	486	œ	80.038	623
1.0750	<b>9 6</b>	1.1603	1, 1271	0.5851	B. 3102	0.5851	<b>8</b> .3102	8.2247	289.4169	0.5616
	•	-	1.1328	509	₹.	509	.465	· C.	9.527	.567
₩.	<b>©</b>	٦.	1.1378	.396	₩.	.396	.625	e.	<b>9</b> .602	.572
۲.	•	-	1.1335	.321	₩.	.321	. 665	ო.	9.569	.570
	∞ •	_	1.1362	. 246	ro .	. 248	550	-∵	9.345	. 557
'n.	<b>©</b> 1	-	1.1500	. 162	9,6	. 162	800	rio (	. 576	.513
٠, ۱	٠,	- '	000	<u>.</u>		֓֓֓֓֓֓֓֓֓֓֓֓֓֓֓֓֓֓֓֓֓֓֓֓֓֓֡֓֓֡֓֓֡֓֓֡֓֓֡		٠ !	400	440
	<b>D</b> (	- 1	000	96		800		•	֓֓֓֓֓֓֓֓֓֓֓֓֓֓֓֓֓֓֓֓֓֓֓֓֓֡֓֓֓֡֓֡֓֓֓֡֓֓	200
	n •			֓֡֓֜֝֓֓֓֓֓֓֓֓֓֓֓֓֓֓֓֓֡֓֓֓֡֓֓֡֓֡֓֡֓֡֓֓֡֓֡֓֡֓֡֡֡֡		֡֜֜֜֝֓֓֓֓֓֓֓֓֓֓֓֓֓֓֓֓֓֓֓֓֡֓֓֡֓֓֡֓֡֓֓֓֡֓֜֓֡֓֡֓֡֓֡֓֡֓֡֓֡֡֡֡֓֡֡֡֓֡֡֡֡֓֡֡֡֡֡֡		ŗ	9 4	
3.6	•	7350	1850	מפרים מרים	ם כ	200	900	ŗЧ	2 5	16.5
. "	. ~		1.1295	027	. ~	027	275	_	567	
	· –	-	1.1423	.020		020	738	156	931	076
<u>ب</u>	_		1.1274	•	~	0	209	.621	308	0
G.	0	٦.	1.1402	.005	9	.005	.657	.062	89.661	.004

Table 2 (cont'd.).

V/H= 0.7068 V= 1.2250 . V1= 0.2995 V2= 1.6090 XHO= 1.6260 XCO= 0.2980		At Incl	10at 10a	Angle=90 deg	<u>.</u>	TOOT TOOL TOOL TOOL TOOL TOOL TOOL TOOL	temperature # 1 temperature # 0.98290000E+.800 . Fring. 2702 Fring.	ure #307.088 ture #307.088 ture #289.590 0000E+05 PA. Fringe Shift Fringe Shift	Angles00 dep. K dep. K at the Col	deo. G Wall
×	-	<b>4</b> >	<b>6</b>	H/X	EPS	X/H	EPS	FS	1 X	(Т-ТС)/(ТН-ТС)
1.6200	7	25	1.2250	%		6	4	4		9.0
615	13	. 25	1.2224	•	.9	8	6	9.6		0
80	13	. 243	1.2142	9	•	8	د	ه. ص	63.6	0.0
	<u> </u>	1.2331	1.2028	0.9744	13.2673	1786.0	13.26/3		305.4996	0.9092
;2	2 2	244	1.2135			8		2.6	. •	0
.560	12	. 236	205	9	•	95	~	2.4	w	0
.547	12	225	1.2250	σ.	•	9	ä	•	_	0.6
. 509	=	. 226	1.2250	σ,	•	ē.		0.		0
. 460	2 9	225	225	æ, r	•	.87	ە ە	OD, W	ם נא	0 0
1.2500	<b>o c</b>	250	1.2136	7	•			່າເ	, –	
080	æ	. 225	225	. 10	• •	28			0	0
.972	<b>o</b>	231	199	ĸ.	•	.50	. 189	₩.	_	0.
. 825	<b>o</b>	. 233	1.2015	ო.	•	.38	.270	8	Ξ.	0.
.725	<b>a</b>	32	1.2020	ص	•	.32	. 245	۲.	0	0
.601	<b>o</b> n o	225	1.2250	7	•	. 22		٠,		9.0
437	۰ ۵	226	1.2250		•	? =		? ?	, 0	. 0
408	•	225	1.2250	. 0		80	000	~	•	0
.381	ស	25	1.2250	•	•	90.	90.	~	(C)	0.7
.361	4	. 225	1.2250	.047	•	9	.000	~	ന	0.7
.341	က	25	1.2250	.032	•	.03	.000	~	_	-
. 332	7	38	1.2095	.025	•	.02	۲.	ø	S	<u>.</u>
.322	7	25	1.2250	9	•	<u>.</u>	000.	~	0	0.0
.315	_	1.2391	ద్	012	1.5444	ē	•	۲.	4	0.
. 305	_	25	25	.005	1.0000	8	8	~	8	0.

Table 2 (cont'd.).

	(T-TC)/(TH-TC)	0.9556 0.9556 0.9556 0.8980 0.8980 0.8880 0.7266 0.7266 0.6145 0.
Anglesto dep deg. K deg. K st the Cold W et the Hot We (A.2.4)	TK (T-1	306.5961 306.3120 306.0395 306.0395 306.0395 304.9966 304.1103 303.4319 300.3868 300.3868 300.3868 300.3618 300.3618 300.3511 300.519 297.8779 297.8779 298.692 299.0092 291.8214 291.622
1001000 307.088 289.590 05 PA. 6 Shift Equation	FS	133 - 6898 133 - 6898 122 - 16898 123 - 16898 124 - 68988 127 - 16898 127 - 16898 127 - 16898 127 - 16898 128 - 16898 128 - 16898 128 - 16898 128 - 16898 128 - 16898 128 - 16898 129 - 1
wall temperature =   wall temperature =   wall temperature   wall temp	EPS	13.2023 13.2023 12.24412 12.24412 12.24412 11.0000 11.0000 11.0000 12.0000 12.0000 11.3900 11.3900 11.3900 12.253
TOTAL	н/x	0.09865 0.09865 0.098630 0.098630 0.098630 0.088630 0.088630 0.098630 0.02820 0.02820 0.02820 0.02820 0.02820 0.02820 0.02820
·	EPS	13.24232 12.24232 12.2006 12.2006 12.2008 11.2000 11.5234 11.5234 11.5234 11.5234 12.0000 12.0000 12.0000 12.0000 13.0000 1.3902 1.0000
Angle=90 deg	ж/н	0.09888 0.09888 0.09820 0.09528 0.09353 0.05280 0.05280 0.05280 0.05280 0.05280 0.05280 0.05331 0.05331 0.05331
1næt 1on	<b>∀B</b>	1.2831 1.2771 1.2913 1.2821 1.2821 1.3000 1.3000 1.2815 1.2816 1.2816 1.3000 1.3000 1.3000 1.3000 1.3000 1.3000 1.3000
At Inclinat	<b>*</b>	1.30000 1.30000 1.30000 1.30000 1.30000 1.30000 1.30000 1.30000 1.30000 1.30000 1.30000
.7640 00 995 090 6260 2980	-	~~~~~~~~~~~~~~~~~~~~~~~~~~~~~~~~~~~~~~
V/H= p.76 V= 1.3000 V1= 0.2996 V2= 1.6096 XHO= 1.626 XCO= 0.296	×	1.5900 1.603 1.603 1.603 1.603 1.6000 1.

Table 2 (cont'd.).

	-TC)	
. 35	-тс)/(тн-тс	0.0959 0.0959 0.09543 0.09111 0.09111 0.09111 0.0916 0.0501 0.0501 0.0501 0.0501 0.0501 0.0501 0.0501 0.0501 0.0501 0.0501
Angle=90 de deg. K deg. K it the Cold it the Hot W (A.2.4)	TK (T-	306.4820 306.2880 306.2880 305.7948 305.7948 304.8326 304.5708 300.9220 300.6220
1 0 0 0 0 0 0 0 0 0 0 0 0 0 0 0 0 0 0 0	ş	8 1 6 5 6 6 1 7 6 8 1 6 5 6 1 7 6 3 6 6 1 7 6 3 6 6 1 7 6 3 6 6 6 1 7 6 8 6 6 1 7 6 6 8 6 7 8 6 6 7 1 8 6 7 1 8 1 8 7 1 8 6 7 1 8 7
At Inclination of the control of	<b>L</b>	74 15 13 13 13 13 13 13 13 13 13 13 13 13 13
tem tem 1 tem 1.200 1.200 1.278	EPS	
TOOTO	H/X	0.9955 0.99819 0.98819 0.98739 0.98739 0.98717 0.98717 0.78742 0.78742 0.78742 0.78742 0.78742 0.78742 0.78742 0.78742 0.78742 0.78742 0.02873 0.02873 0.02873 0.02873
	EPS	13. 7416 13. 4622 13. 4622 13. 2000 12. 4673 12. 2648 11. 6278 11.
Angle=90 deg	H/X	0.09888 0.98880 0.98290 0.98239 0.98233 0.98217 0.98217 0.7420 0.7274 0.0253 0.0253
c •	4B	1.3550 1.3550 1.3550 1.3550 1.3550 1.3550 1.2550 1.3550 1.3550 1.3550 1.3550 1.3550 1.3550 1.3550 1.3550 1.3550 1.3550 1.3550
. At Incl	<b>\$</b>	13 1.3968 1.3674 0.9968 133 1.3924 1.3627 0.9880 133 1.3924 1.35627 0.9880 133 1.3627 1.3562 0.9819 133 1.3750 0.9633 133 132 1.3926 1.3579 0.9428 122 1.3926 1.3579 0.9428 122 1.3926 1.3750 0.9227 122 1.3926 1.3750 0.7904 100 1.3750 1.3616 0.9051 111 1.3750 1.3616 0.9051 111 1.3750 1.2618 0.7904 100 1.3938 1.2613 0.5663 99 1.3894 1.2593 0.4157 99 1.3750 1.3750 0.02274 88 1.3750 1.3750 0.0253 1.3750 1.3750 1.3750 0.0253 1.3750
6213	-	
Y/H= 0.8; Y= 1.3750 Y1= 0.296; Y2= 1.609( XHO= 1.62; XCO= 0.29	×	1.6200 1.6100 1.55000 1.55000 1.55000 1.55000 1.55000 1.55000 1.55000 1.55000 1.55000 1.55000 1.55000 1.55000 1.55000 1.55000 0.9500 0.9500 0.3200 0.3200 0.3200

Table 2 (cont'd.).

;		•	•	1		V/H= 0.93	359 At 1	Inclination	Ang 1 90	. <b>de</b> p
. 0896 0896	n 1004	At Inc.	666		<u>.</u>	- " .	2900	#307.088 #289.590 +05 PA. 50 Shift	deg. K	1
0.29	00					PSC0=14.		Equat ton	(A.2.	
×		<b>*</b>	48	H/X	EPS	H/X	EPS	S	) XI	(T-TC)/(TH-TC)
90	-	9	با ا	, °	"	9	384	180	06.805	"
15	7	. 533	ĸ.	σ,	<u>ن</u>	œ	.313	.988	06.7	<u>.</u>
05	4	. 528	ri i	<del>ص</del> (	٦,	<u>ص</u> (	. 138	018	98.	<u>.</u>
282	<b>4</b> 6	. 520 848	1.5250	, G	. e	39 O		.667		
570	<u> </u>	540	מי נ	. 9			688	328	שיי	
545	6	. 533		σ.	്.		340	066	7	
511		. 525	w.	œ.	٠,	•	.000	.638	•	0.
.475	12	. 539	w ·	₩,	Θ,	•	. 604	. 228	٦,	
. 397		. 525	w;	æ, 1	٠.	₽.	8	1.596	Ψ.	9.
.325	= :	. 535	ייא	٠.'	4. (	٠,	.455	.026	<u>س</u> ،	
. 245	= 9	. 525	1.5250	٠. ٩	9	٠. ٩	•	. 541	<u>س</u> ۾	
1.0586	2 2	1.5250	1.5250	0.5727	10.0000	0.6416	10.0000	9.4745	300.9689	ja
.950	•	534		٩.	٦.	•	•	.892		0
.857	<b>o</b>	. 525	1.6250	4.	٠.	۲.	•	<b>6</b>	•	<b>8</b> .
.672	œ r	72	1.5250	٠.	9,0	٠.	•	.335	<u>ن</u> د	•
. 56.	- 0	070.	1.0250				•	787.		<b>.</b>
104	<b>9</b> (c	525	1.5250	. 9	5.0000	- 0	•		· .	200
379	4	. 525	1.5250	0	0	9		229	. 62	0
.350	ო	. 525	1.5250	9	•	0	•	.219	Ξ.	<u>.</u>
.325	_	47	1.5219	•	₩.	٥.	. 880	8	•	0.0
.320	-	. 542	1.5171	•	9	•	•	. 895	Φ.	0.0
.315	-	. 535	_	•	4	.012	က	Φ.	<u>س</u>	0.0
.310	_	. 530	9	٥.	C)	8	1.2105	•	0.0	0.0
. 305	-	25	1.5250	۰.	0000.	.005	0	~	₽.	0.0

Table 2 (cont'd.).

V/H= 0.97 V= 1.5750 V1= 0.2995 V2= 1.6090 XHO= 1.626 XCO= 0.298	9740	. At Incl	instion Angl	geb 00==12	<u>.</u>	HOT TO T	.9740 . At Inc! temperature #3   tempera	1inetion 307.088 8289.590 05 PA: 6 Shift 6 Shift	Angle=90 d deg. K deg. K deg. K at the Cold at the Hot (A.2.4)	
×	-	<b>4</b> >	× 8	H/X	EPS	H/X	EPS	FS	TK (T	-TC)/(TH-TC)
		1	1 '							
1.6200	7	2	ശ	. 995	. 398	. 995	4.398	•	.823	188
1.6100	<u> </u>	8	•	8	. 237	8	4.237	•	9.0	.972
1.5995	4	75	1.5750	.980	000.	. 980	000	•	. 298	. 954
1.5920	13	9	1.5721	. 974	3.872	.97	3.872	•	129	.945
S	13	591	S	0.9691	.747	969	747	•	.965	.935
1.5750	13	98	9	0.9616	.540	96	3.540	•	.694	.920
1.5650	13	83	ທ	0.9541	.38	. 954		•	.486	80
S	13	575	1.5750	0.9321	•		3.0	•	.981	۳.
4	12	8	ĸ.	0.9014	•	σ,	2.5	•	.352	₩.
₹	12	575	ĸ	0.8581	•	.858	2.0	•	629	₩.
۳.	=	75	1.6750	0.7594	•	75	9	•	.335	۲.
7	<u>0</u>	8	w.	0.6980	•	89.	9.	•	638	۳.
٦.	<b>o</b>	8	ທ	0.6039	•	8	۲.	•	. 650	•
1.0200	<b>.</b>	1.5810	•	0.5437	9.3191	ω	9.3191	8.7797	300.1042	0.6009
æ	•	2	'n	0.4880	•	8	٠.	•	.682	G)
•	•	83	1.5657	0.4345	•	€4.	٦.	•	. 991	w,
	•	575		0.3657	•	.36	•	•	.371	w.
Θ.	_	575	1.5750	0.2457	•	.24	•	•	.079	٩.
'n	<b>©</b>	575	1.5750	. 158	•	. 5	80.	•	. 817	
4	S.	. 575	'n	104	•	104	80.	•	. 586	~
ო.	4	75	S.	•	•	.069	•	•	376	ď
ო.	ო	75	w.	.042	۰.	.042	000	•	178	٦.
ო.	~	575	ĸ.	.021	000.	.021	000.	•	994	•
ო.	7	75	ທ	.02	000.	.021	80.	•	994	.080
ຕ.	_	9	ĸ.	.012	.626	.012	.626	.832	. 554	.055
ო.	_	8	ທ	600.	•	8	₹.	9	290.2962	•
ღ.	_	75	'n	8	1.0000	.004	000	0.2021	823	.013

Table 3 Sample calculation of local the Nusselt number from the temperature gradients, in Table 2.

Local Nusselt number as a function of the dimensionless distance along the hot and the cold wall for Rayleigh number RA=  $1.1\times10^5$  and inclination angle=90 deg.

Y/H	NU Hot Wall	NU Cold Wall	E.S.D. Hot Wall	E.S.D. Cold Wall
0.0195	3.888	2.093	0.085	0.091
0.0767	4.647	1.396	0.024	0.027
0.1340	5.144	1.572	0.087	0.060
0.1913	5.448	2.057	0.075	0.027
0.2486	5.422	2.630	0.052	0.055
0.3058	5.313	3.108	0.078	0.024
0.3631	5.111	3.442	0.079	0.040
0.4204	4.731	3.806	0.050	0.040
0.4777	4.617	4.164	0.135	0.067
0.5349	4.304	4.309	0.065	0.033
0.5922	3.892	4.727	0.049	0.051
0.6495	3.389	5.135	0.036	0.136
0.7068	2.860	4.896	0.066	0.046
0.7640	2.557	5.133	0.044	0.058
0.8213	1.836	4.858	0.057	0.069
0.8786	1.630	4.791	0.050	0.096
0.9359	1.507	4.041	0.052	0.086
0.9740	2.000	3.304	0.060	0.147

<sup>•</sup> Mean Nusselt number at the hot wall NU = 3.759

<sup>\*</sup> Mean Nusselt number at the cold wall NU = 3.479

## REFERENCES

- Ostrach, S., "Natural Convection in Enclosures," Advances in Heat Transfer, Vol. 8, pp. 161-227, 1972.
- Catton, I., "Natural Convection in Enclosures," Proceedings of the Sixth International Heat Transfer Conference, Vol. 6, pp.13-31, 1978.
- Batchelor, G.K., "Heat Transfer by Free Convection Across a Closed Cavity between Vertical Boundaries at Different Temperatures," Quarterly Journal of Applied Mathematics, Vol. 12, pp. 209-233, 1954.
- Poots, G., "Heat Transfer by Laminar Free Convection in Enclosed Plane Gas Layers," Quarterly Journal of Mechanics and Applied Mathematics, Vol. 11, pp.257-267, 1958.
- 5 Carlson, W.O., "Interferometric Studies of Convective Flow Phenomena in Vertical, Plane Enclosed Air Layers," Ph.D. Thesis, Univ. of Minnesota, Minneapolis, Minn., 1956.
- Eckert, E.R.G., and Carlson, W.O., "Natural Convection in an Air Layer Enclosed between Two Vertical Plates with Different Temperatures," Int. J. Heat Mass Transfer, Vol. 2, pp. 106-120, 1961.
- Ostrach, S., "Natural Convection Heat Transfer in Cavities and Cells," Proceedings of the Seventh International Heat Transfer Conference, Vol. 1, pp. 365-379, 1982.
- 8 Gill, A.E., "The Boundary-Layer Regime for Convection in a Rectangular Cavity," J. Fluid Mech., Vol. 26, pp. 515-536, 1966.
- Elder, J.W., "Laminar Free Convection in a Vertical Slot," J. Fluid Mech., Vol. 23, pp. 77-98, 1965.
- 10 Elder, J.W., "Turbulent Free Convection in a Vertical Slot," J. Fluid Mech., Vol.24, pp. 99-111, 1965.
- Mynett, J. A., and Duxbury, D., "Temperature Distributions within Enclosed Plane Air Cells Associated with Heat Transfer by Natural Convection," Proc. of the Fifth International Heat Transfer Conference, Vol. 3. pp. 13-31, 1974.
- Raithby, G.D., Hollands, K.G.T., and Unny, T.E., "Analysis of Heat Transfer by Natural Convection Across Vertical Fluid Layers," J. Heat Transfer, Vol. 99, pp. 287-293, 1977.
- 13 Yin, S.H., Wung, T.Y., and Chen, K., "Natural Convection in an Air Layer Enclosed within Rectangular Cavities." Int. J. Heat Mass Transfer, Vol. 21, pp. 307-315, 1978.

- Bejan, A., "A Synthesis of Analytical Results for Natural Convection Heat Transfer Across Rectangular Enclosures," Int. J. Heat Mass Transfer, Vol. 23, pp. 723-726, 1980.
- Boyak, B. E., and Kearney, D.W., "Heat Transfer by Laminar Natural Convection in Low-Aspect Ratio Cavities," ASME pap. 72-HT-52, 1972.
- Sernas, V., and Lee, E.I., "Heat Transfer in Air Enclosures of Aspect Ratio Less than One," ASME paper 78-WA/HT-7, 1978.
- 17 Lee, E.I., and Sernas, V., "Numerical Study of Heat Transfer in Rectangular Air Enclosures of Aspect Ratio Less Than One," ASME pap. 80-WA/HT-43, 1980.
- 18 Sernas, V., Fletcher, L.S., and Rago, C., "An Interferometric Study of Natural Convection in Rectangular Enclosure of Aspect Ratio Less Than One," ASME pap. 75-HT-63, 1975.
- Bauman, F., Gadgil, A., Kammerud, R., and Greif, R., "Buoyancy-Driven Convection in Rectangular Enclosures: Experimental Results and Numerical Calculations," ASME publication 80-HT-66, 1980.
- Wilkes, J.O., and Churchill, S.W., "The Finite Difference Computation of Natural Convection in a Rectangular Enclosure," A.I.Ch.E. Jl, Vol. 12, No. 1, pp. 161-166, 1966.
- De Vahl Davis, G., "Laminar Natural Convection in an Enclosed Rectangular Cavity," Int. J. Heat Mass Transfer, Vol. 1, pp. 1675-1693, 1968.
- 22 Rubel, A., and Landis, E., "Numerical Study of Natural Convection in a Vertical Rectangular Enclosure," International Symposium on High Speed Computer in Fluid Mechanics, American Institute of Physics, New York, pp. 208-213, 1969.
- Rubel, A., and Landis, E., "Laminar Natural Convection in a Rectangular Enclosure with Moderate Large Temperature Differences," Proceedings of the Fourth International Heat Transfer Conference, Vol. 4, paper NC 2.10, 1970.
- Quon, C., "High Rayleigh Number Convection in an Enclosure: A Numerical Study," Physics of Fluids, Vol. 15, pp. 12-19, 1972.
- Thomas, R.W., and De Vahl Davis, G., "Natural Convection in Annular and Rectangular Cavities, A Numerical Study," Proceedings of the Fourth International Heat Transfer Conference, Vol. 4, NC 2.4, 1970.
- Spradley, L.W., and Churchill, S.W., "Pressure-and-Buoyancy-Driven Thermal Convection in a Rectangular Enclosure," J. Fluid. Mech., Vol. 70, part 4, pp. 705-720, 1975.
- Berkovsky, B.M., and Polevikov, V.H., "Heat Transfer at High Rate Free Convection," Proceedings of the Fifth International Heat Transfer Conference, Vol. 3, NC 3.1, pp. 85-89, 1974.

- Catton, I., Ayyaswamy, P.S., and Clever, R.M., "Natural Convections Flow in a Finite Rectangular Slot Arbitrarity Oriented with Respect to the Gravity Vector," Int. J. Heat Mass Transfer, Vol. 17, pp. 173-184, 1974.
- 29 Hutchinson, R.W., and Schiesser, W.E., "Trancation Error Correction Applied to Nonlinear Partial Differential Equations," Proceedings of the 1971 Summer Computer Simulation Conference, Publication Board of Simulation Conferences, Denver, Colo., pp. 112-117, 1971.
- Churchill, S.W., Chao, P., and Ozoe, H., "Extrapolation of Finite Difference Calculations of Laminar Natural Convection in Enclosures to Zero Grid Size," Numerical Heat Transfer, Vol. 4, pp. 39-51, 1981.
- Quon, C., "Free Convection in an Enclosure Revisited," J. Heat Transfer, Vol. 99, pp. 340-342, 1977.
- Quon, C., "Effects of Grid Distribution on the Computation of High Rayleigh Number Convection in a Differentially Heated Cavity," Numerical Properties And Methodologies In Heat Transfer, eds. T.M. Shih, Hemisphere Publishing Corporation, New York, pp. 261-282, 1983.
- Kublbeck, K., Merker, G.P., and Straub, J., "Advanced Numerical Calculation of Two-Dimensional Time-Dependent Free Convection in Cavities," Int. J. Heat Mass Transfer, Vol. 23, pp. 203-217, 1980.
- De Vahl Davis, G., and Jones, I.P., "Natural Convection in a Square Cavity: A Comparison Exercise," Report/FMT/3, ISSN 0157-5104, School of Mechanical and Industrial Engineering, The University of New South Wales, 42 pp, 1982.
- Graham, E., "Numerical Simulation of Two Dimensional Compressible Convection," J. Fluid Mech., Vol. 70, pp. 689-708, 1975.
- 36 Leonardi, E., and Reizes, J.A., "Convective Flows in Closed Cavities with Variable Fluid Properties," Numerical Methods in Heat transfer, eds. K. Morgan and A.C. Zinkiewicz, John Wiley & Sons, New York, pp. 387-412, 1981.
- Zhong, Z.Y., Yang K.T., and Lloyd, J.R., "Variable Property Effects in Laminar Natural Convection in a Square Enclosure," J. Heat Transfer, Vol. 107, pp. 133-138, 1985.
- Zhong, Z.Y., "Variable-Property Natural Convection and Its Interaction with Thermal Radiation in Tilted Square Enclosures." Ph.D. Thesis, University of Notre Dame, 1983.
- 39 Bajorek, S.M., and Lloyd, J.R., "Experimental Investigation of Natural Convection in Partitioned Enclosures," J. Heat Transfer, Vol. 104, pp. 527-532, 1982.

- 40 Bajorek, S.M, "Experimental Investigation of Natural Convection in Partitioned Enclosures," M.S. Thesis, University of Notre Dame, 1981.
- Chang, L.C., Lloyd J.R., and Yang, K.T., "A Finite Difference Study of Natural Convection in Complex Enclosures," Proceedings of The Seventh International Heat Transfer Conference, Vol. 2, pp. 183-188, 1982.
- Bilski, S.M., Lloyd, J.R., and Yang, K.T., "An Experimental Investigation of the Laminar Natural Convection Velocity Field in Square and Partitioned Enclosures," Proceedings of the 8th International Heat Transfer Conference San Francisco, Ca., Vol. 4, pp. 1513-1518, 1986.
- Holster, J., Hale, L.A., and Kettleborough, C.F., "Finite Element Analysis of Transient Natual Convection in Enclosed Spaces," ASME, pap. 79-HT,49, 1979.
- Pepper, D.W., "Calculation of Natural Convection within a Heated Enclosure Using the Method of Second Moments," ASME pap. 83-WA/HT-33, 1983.
- Grareth, P. W., "Numerical Integration of the Three-Dimensional Navier-Stokes Equations for Incompressible Flow," J. Fluid Mech., Vol. 37, part 4, pp. 727-750, 1969.
- Chorin, A.J., "Numerical Solution of the Navier-Stokes Equations," Mathematics of Computation, Vol. 22, pp. 745-762, 1968.
- Leonard, B.P., "A Survey of Finite Differences of Opinion on Numerical Modeling of the Incomprehensible Defective Confusion Equation," City University of New York, College of Staten Island New York.
- Pao, H.S., "A Numerical Computation of a Confined Rotating Flow," J. Appl. Mech., Vol. 37, pp. 480-487, 1970.
- Brian, P.L.T., "A Finite Difference Method of High-Order Accuracy for the Solution of Three-Dimensional Transient Heat Conduction," A.I.Ch.E. JL. Vol. 7, pp. 367-370, 1961.
- Mallinson, G.D., and De Vahl Davis, G., "The Method of the False Transient for Solution of Coupled Elliptic Equation," J. Comp. Phys., Vol. 12, pp. 435-561, 1973.
- Briley, W.R., and McDonald, H., "Solution of the Multidimensional Compressible Navier-Stokes Equations by a Genralized Implicit Method," J. Comp. Physics, Vol. 24, pp. 372-397, 1977.
- Polezhaev, V. I., "Numerical Solution of a System of Two-Dimensional Unsteady Navier-Stokes Equations for a Compressible Gas in a Closed region," Fluid Dynamics, Vol. 2, pp. 70-74, 1967.

- Mallinson, G.D., and De Vahl Davis, "Three-Dimensional Natural Convection in a Box," J. Fluid Mech., Vol. 83, Part 1, pp. 1-31, 1977.
- Reddy, J. N., "Finite-Element Simulation of Natural Convection in Three-Dimensional Enclosures," ASME, pap. 82-HT-71.
- 55 Aziz, K., and Hellums J.D., "Numerical Solution of the Three-Dimensionnal Equations of Motion for Laminar Natural Convection," The Physics of Fluids, Vol. 10, No.2, pp. 314-324, 1967.
- Ozoe, H., Yamamoto, K., Churchill, S.W., and Sayama, H., "Three-Dimensional Numerical Analysis of Laminar Natural Convection in a Confined Fluid Heated from Below," J. Heat Transfer, Vol. 98C, pp. 202-207, 1976.
- 57 Lipps, F.B., "Numerical Simulation of Three-Dimensional Benard Convection in Air," J. Fluid Mech., Vol. 75, part 1, pp. 113-148, 1976.
- Pepper, D.W., and Harris, S.D., "Numerical Solution of Three-Dimensional Natural Convection by the Strongly Implicit Procedure," ASME pap. July 31, 1978.
- 59 Schinkel, W.M.M., Linthorst, S.J.M., and Hoogendooen, C.J., "The Stratification in Natural Convection in Vertical Enclosures," J. Heat Transfer, Vol. 105, pp. 267-272, 1983.
- De Vahl Davis, G., "Laminar Natural Convection in an Enclosed Rectangular Cavity," Int. J. Heat Mass Transfer, Vol. 11, pp. 1675-1693, 1968.
- De Graaf, J.G.A., and Von Der Held, E.F.M., "The Relation Between the Heat Transfer and the Convection Phenomena in Enclosed Plane Layers," App. Sci. Res., section A, Vol. 3, pp. 393-409, 1953.
- Dropkin, D., and Somerscales, E., "Heat Transfer by Natural Convection in Liquids confined by Two Parallel Plates Which are Inclined at Various Angles With Respect to the Horizontal," J. Heat Transfer, Vol. 87, pp. 77D-84, 1965.
- 63 Landis, F., "see (3.19) J. Heat Transfer, Vol. 87, pp. 82-83, 1965.
- 64 Kurzweg, U.H., "Stability of Natural Convection Within an Inclined Channel," J. Heat Transfer, Vol. 92, pp. 190-191, 1970.
- 65 Hart, J. E., "Stability of the Flow in a Differentially Heated Inclined Box," J. Fluid Mech., Vol. 47, pp. 547-576, 1971.
- 66 Hollands, K.G.T., and Konicek, L., "Expermimental Study of the Stability of Differentially Heated Inclined Air Layers," Int. J. Heat Mass Transfer, Vol. 16, pp.1467-1476, 1973.

- 67 Hollands, K.G.T., "Natural Convection in Horizontal Thin-Walled Honeycomb Panels," J. Heat Transfer, Vol. 95, pp. 439-444, 1973.
- 68 Unny, T.E., "Thermal Instability in Differentially Heated Inclined Fluid Layers," J. of Appl. Mech., Vol. 39, pp. 41-46, 1972.
- 69 Clever, R.M., "Finite Amplitude Longitudinal Convection Rolls in an Inclined Layers," J. Heat Transfer, Vol. 95, pp. 407-408, 1973.
- 70 Ayyaswamy, P.S., and Catton I., "The Boundary-Layer Regime for Natural Convection in a Differentially Heated, Tilted Rectangular Cavity," J. Heat Transfer, Vol. 95, pp. 543-545, 1973.
- Ozoe, H. Sayama, H., and Churchill, S.W., "Natural Convection in an Inclined Rectangular Channel at Various Aspect Ratios and Angles-Experimental Measurements," Int. J. Heat Mass Transfer, Vol. 18, pp. 1425-1431, 1975.
- Ozoe, H., Sayama, H., and Churchill, S.W., "Natural Convection in an Inclined Square Channel." Int. J. Heat Mass Transfer, Vol. 17, pp. 401-406, 1974.
- Ozoe, H., Yamamoto, K., Sayama, H., and Churchill, S.W. "Natural Circulation in an Inclined Rectangular Channel Heated on One Side and Cooled on the Opposing Side," Int. J. Heat Mass Transfer, Vol. 17, pp. 1209-1217, 1974.
- Ozoe, H., Fujii, K., Lior, N., and Churchill, S.W., "Long Rolls Generated by Natural Convection in in Inclined Rectangular Enclosure," Int. J. Heat Mass Transfer, Vol. 26, pp. 1427-1438, 1983.
- 75 Ozoe, H., Yamamoto, K., and Sayama, H., and Churchill, S.W., "Natural Convection Patterns in a Long Inclined Rectangular Box Heated from Below," Int. J. Heat Mass Transfer, Vol. 20, pp. 131-139, part 2, 1977.
- 76 Ozoe, H., Yamamoto, Sayama, H., and Churchill, S.W., "Natural Convection Patterns in a Long Inclined Rectangular Box Heated from Below," Int. J. Heat Mass Transfer, Vol. 20, pp. 123-129, part 1, 1977.
- Ozoe, H., Churchill, S.W., Okamoto, T., and Sayama, H., "Natural Convection in Doubly Inclined Rectangular Boxes," Proceedings of the Sixth International Heat Transfer Conference, Vol. 2, paper NC-19, pp. 293-298, 1978.
- 78 Ozoe, H., Chao, P.K., Churchill, S.W., and Lior, N., "Laminar Natural Convection in an Inclined REctangular Box with the Lower Surface Half Heated and Half Insulated," ASME, pap. 82-HT-72.
- 79 Arnold, J.N., Catton, I., and Edwards, D.K., "Experimental Investigation of Natural Convection in Inclined Rectangular

- Regions of Differing Aspect Ratios, "J. Heat Transfer, Vol. 98, pp. 67-71, 1976.
- Buchberg, H., Catton, I., and Edwards, D.K., "Natural Convection in Enclosed Spaces- A Review of Application to Solar Energy Collection," J. Heat Transfer, Vol. 98, No.2, pp. 182-188, 1976.
- 81 Hollands, K.G.T., Unny, T.E., Raithby, G.D., and Konicek, L., "Free Convective Heat Transfer Across Inclined Air Layers," J. Heat Transfer, Vol. 98, pp. 189-193, 1976.
- Schinkel, W.M.M., and Hoogendoorn, C.J., "An Interferometric Study of the Local Heat Transfer by Natural Convection in Inclined Air-Filled Enclosures," Proceedings of the Sixth International Heat Transfer Conference, Vol. 2, paper NC-18, pp.287-292, 1978.
- Linthorst, S.J.M., Shinkel, W.M.M., and Hoogendoorn, C.J., "Flow Structure with Natural Convection in Inclined Air-Filled Enclosures," J. Heat Transfer, Vol. 103, pp. 535-539, 1981.
- Linthorst, S.J.M., and Hoogendoorn, C.J., "Natural Convection Heat Transfer in Three-Dimensional Inclined Small Aspect Ratio Enclosure," Proceedings of the 8th International Heat Conference San Francisco, Ca., Vol. 4, pp. 1501-1505, 1986.
- Jannot, M., and Mazeas, C., "Experimental Study of Natural Convection in a Rectangular Vertical Enclosure," Int. J. Heat Mass Transfer, Vol. 16, pp. 81-100, 1973.
- Randall, K.R., Mitchell, J.W., and El-Wakil, M.M., "natural Convection Heat Transfer Characteristics of Flat Plate Enclosures," Trans. of ASME, J. Heat Transfer, Vol. 101, pp. 120-125, 1979.
- 87 Meyer, B.A., Mitchell, J.W., and El-Wakil, M.M., "Natural Convection Heat Transfer in Moderate Aspect Ratio Enclosures," Trans. of ASME, J. Heat Transfer, Vol. 101, pp. 655-659, 1979.
- Zhong, Z.Y., Yang, K.T., and Lloyd, J.R., "Variable Property Natural Convection in Tilted Cavities with Thermal Radiation," Numerical Methods in Heat Transfer, ed. R.W. Lewis, and Morgan, Vol. 3, pp. 195-214, John Wiley, Chichester, 1985.
- Yang, H.Q., Yang, K.T., and Lloyd, J.R., "Flow Transition in Laminar Buoyant Flow in a Three-Dimensional Tilted Rectangular Enclosure," Proceedings of the 8th International Heat Transfer Conference San Francisco, Ca., Vol. 4, pp. 1495-1500, 1986.
- 90 Elsherbiny, S.M., Raithby, G.D., and Hollands, K.T.G., "Heat Transfer by Natural Convection Across Vertical and Inclined Air Layers," ASME pap. 80-HT-67, 1980.
- 91 Acharya, S., "Natural Convection in an Inclined Enclosure Containing Internal Energy Sources and Cooled from Below," The Int. J. Heat and Fluid Flow, Vol. 6, no.2, pp. 113-120, 1985.

- 92 Chen, C.J., and Talaie, V., "Finite Analytic Numerical Solutions of Laminar Natural Convection in Two-Dimensional Inclined Rectangular Enclosures," ASME, pap.85-HT-10., 1985.
- 93 Reddy, C.S., "Numerical Simulation of Laminar Natural Convection in Shallow Inclined Enclosures," Proceedings of the Seventh Interntional Heat Transfer Conference, Vol.2, pp. 263-268, NC24, 1982.
- 94 Symons, J.G., Peck, M.K., "Natural Convection Heat Transfer Through Inclined Longitudinal Slots," J. Heat Transfer, Vol. 106, pp. 824-829, 1984.
- 95 Elsherbiny, S.M., Hollands, K.G.T., and Raithby, G.D., "Effect of Thermal Boundary Conditions on Natural Convection in Vertical and Inclined Air Layers," J. Heat Transfer, Vol. 104, pp. 515-520, 1982.
- 96 Wirtz, R.A., Righi, J., and Zirilli, F., "Measurements of Natural Convection Across Tilted Rectangular Enclosures of Aspect Ratio 0.1 and 0.2," J. Heat Transfer, Vol. 104, pp. 521-526, 1982.
- 97 Seki, N., Fukusako, S., and Yamaguchi, A., "An Experimental Study of Free Convective Heat Transfer in a Parallelogrammic Enclosure," J. Heat Transfer, Vol. 105, pp. 433-439, 1983.
- Greenspan, H.P., "The Theory of Rotating Fluids," University Press, Cambridge, 1968.
- 99 Greenspan, H.P., and Howard, L.N., "On a Time-Dependent Motion of a Rotating Fluid," J. Fluid Mech., Vol. 17, pp. 385-404, 1963.
- 100 Greenspan, H.P., "On the General Theory of Contained Rotating Fluid Motions," J. Fluid Mech., Vol. 22, part 3, pp. 449-462, 1965.
- 101 Morris, W. D., "Heat Transfer and Fluid Flow in Rotating Coolent Channels," Research Studies Press, A Division of John Wiley, New York, 1981.
- 102 Shmidt, E. H., "Heat Transmission By Natural Convection at High Centrifugal Acceleration in Water-Cooled Gas-Turbine Blades," General Discussion in Heat Transfer, Inst. Engr., London, 361, 1951.
- 103 Mori, Y., and Nakayama, W., "Convective Heat Transfer in Rotating Radial Circular Pipes," 1st Report, Int. J. Heat Mass Transfer, Vol. 11, pp. 1027-1040, 1968.
- 104 Mori, Y., Fukada, T., and Nakayama, W., "Convective Heat Transfer in a Rotating Radial Circular Pipe," 2nd Report, Int. J. Heat Mass Transfer, Vol. 14, pp. 1807-1824, 1971.
- 105 Cannon, J.N., and Kays, W.M., "Heat Transfer to a Fluid Inside a Pipe Rotating About its Longitudinal Axis," J. Heat Transfer, Vol. 91, pp. 135-139, 1969.

- 106 Morris, W.D., "Laminar Convection in a Heated Vertical Tube Rotating About a Parallel Axis," J. Fluid Mech., Vol. 21, part 3, pp. 453-464, 1965.
- 107 Davis, T.H., and Morris, W.D., "Heat Transfer Characteristics of a Closed Loop Rotating Thermosyphon," Third International Heat Transfer Conference, Chicago, paper 59, Vol. 2, pp. 172-181, 1966.
- 108 Mori Y., and Nakayama, W., "Forced Convective Heat Transfer in a Straight Pipe Rotating Around a Parallel Axis," 1st. Report, Int. J. Heat Mass Transfer, Vol. 10, pp. 1179-1194, 1967.
- 109 Humphrey, J. F., Morris, W.D., and Barrow, H., "Convective Heat Transfer in the Entry Region of a Tube which Revolves About an Axis Parallel to Itself," Int. J. Heat Mass Transfer, Vol. 10, pp. 333-347, 1967.
- 110 Sakamoto, M., and Fukui, S., "Convective Bent Transfer in a Rotating Tube Revolving About an Axis Parallel To Itself," Fourth International Heat Transfer Conference, Paris-Versailles, Vol.3, FC 7.2, 1970.
- 111 Neti, S., Warnock, A. S., Levy, E. K., and Kannan, K. S., "Computation of Laminar Heat Transfer in Rotating Rectangular Ducts," J. Heat Transfer, Vol. 107, pp. 575-582, 1985.
- 112 Levy, E., Neti, S., Brown, G., and Bayat, F., "Laminar Heat Transfer and Pressure Drop in a Rectangular Duct Rotating About a Parallel Axis," J. Heat Transfer, Vol. 108, pp. 350-356, 1986.
- 113 Luk, K.H., Millsaps, K., and Pohlhausen, K., "An Exact Solution for the Combined Free and Forced Convection in Flows Due to Rotating Disks," Fourth International Heat Transfer Conference, Paris-Versailles, Vol. 4, NC 4.2, 1970.
- 114 Riley, N., "Thermally Induced Boundary-Layer Flows in a Rotating Environment," J. Fluid Mech., Vol. 29, part 2, pp. 241-257, 1967.
- Edwards, D. K., "Rotating-Induced Free Convection Heat Transfer in a Zero-Gravity Field," AIAA J., Vol. 5, No. 2, pp. 333-342, 1967.
- 116 Kreith, F., Doughman, E., and Kozlowski, H., "Mass and Heat Transfer from an Enclosed Rotating Disk with and without Source Flow," J. Heat Transfer, Vol. 85, pp. 153-164, 1963.
- 117 Duncan, I. B., "Axisymmetric Convection between Two Rotating Disks," J. Fluid Mech., Vol. 24, part 3, pp. 417-449, 1966.
- 118 Homsy, G.M., and Hudson, J.L., "Centrifugally Driven Thermal Convection in a Rotating Cylinder," J. Fluid Mech., Vol. 35, part 1, pp. 33-52, 1969.
- 119 Homsy, G.M, and Hudson, J.L., "Heat Transfer in a Rotating Cylinder of Fluid Heated from Above," Int. J. Heat Mass Transfer, Vol. 14, pp. 1149-1159, 1971.

- 120 Abell, S., and Hudson, J.L., "An Experimental Study of Centrifugally Driven Free Convection in a Rectangular Cavity," Int. J. Heat Mass Transfer, Vol. 18, pp. 1415-1423, 1975.
- 121 Chandrasekhar, S., "The Intstability of a Layer of Fluid Heated Below and Subject to Coriols Forces," Proceedings of the Royal Society, Series A, Vol. 217, May 7, 1953.
- 122 Veronis, G., "Motions at Subcritical Values of the Rayleigh Number in a Rotating Fluid," J. Fluid Mech., Vol. 24, part 3, pp. 545-554, 1966.
- 123 Veronis, G., "Large-Amplitude Bernard Convection in a Rotating Fluid," J. Fluid Mech., Vol. 31, part 1, pp. 113-139, 1968.
- Rossby, H. T., "A study of Bernard Convection with and without Rotation," J. Fluid Mech., Vol. 36, part 2, pp. 309-335, 1969.
- 125 Catton, I., "The Influence of Rotation on Natural Convection in Horizontal Liquid Layers," Fourth International Heat Transfer Conference, Paris-Versailles, Vol. IV, NC 4.1, 1970.
- Homsy, G.M, and Hudson, J.L., "Centrifugal Convection and its Effect on the Asymptotic Stability of a Bounded Rotating Fluid Heated from Below," J. Fluid Mech., Vol. 48, pp. 605-624, 1971.
- Hunter, C., and Riahi, N., "Nonlinear Convection in a Rotating Fluid," J. Fluid Mech., Vol. 72, part 3, pp. 433-454, 1975.
- 128 Clever, R. M., and Busse, F. H., "Nonlinear Properties of Convection Rolls in a Horizontal Layer Rotating about a Vertical Axis," J. Fluid Mech., Vol. 94, part 4, pp. 609-627, 1979.
- 129 Buhler, K., and Oertel, H., "Thermal Cellular Convection in Rotating Rectangular Boxes," J. Fluid Mech., Vol. 114, pp. 261-282, 1982.
- 130 Gray, D.D, and Giorgini, A., "The Validity of the Boussinesq Approximation for Liquids and Gases," Int. J. Heat Mass Transfer, Vol. 19, pp. 545-551, 1976.
- 131 Goldstein, R. J., "Interferometer for Aerodynamic and Heat Transfer Measurements," The Review of Scientific Instruments, Vol. 36, No. 10, pp. 1408-1410, 1965.
- 132 Gebhart, B., and Knowles, C. P., "Design and Adjustment of a 20 cm Mach-Zehnder Interferometer,' The Review of Scientific Instruments, Vol. 37, No. 1, pp. 12-15, 1966.
- Bennett, F.D., "Optimum Source Size for the Mach-Zehnder Interferometer," J. App. Phys., Vol. 22, pp. 184-190, 1951.
- Bennett, F.D., and Kahl, G.D., "A Generalized Vector Theory of the Mach-Zehnder Interferometer," J. Opt. Soc. Amer., Vol. 43, pp. 71-78, 1953.

- 135 Kahl, G.D., and Bennett, F.D., "Experimental Verification of Source Size Theory for the Mach-Zehnder Interferometer," J. App. Phys. Vol. 23, No. 7, pp. 763-767, 1952.
- 136 Johnstone, R.K.M, and Smith, W., "A Design for a 6 in. Field Mach-Zehnder Interferometer," J. Sci. Instrum., Vol. 42, pp. 231-235, 1965.
- 137 Brooks, R.G, Probert, S.D., and Maxwell, J., "Field Mach-Zehnder Interferometer for Heat Transfer Studies," Measurement and Control, Vol. 1, pp. 9-16, 1968.
- 138 Wilkie, D., and Fisher, S.D., "Measurement of Temperature by Mach-Zehnder," Proc. Instn. Mech. Engrs., Vol. 178, pt 1, No. 17, pp. 461-472, (1963-64).
- Oertel, H., and Buhler, K., "A Special Interferometer Used for Heat Convection Investigations," Int. J. Heat Mass Transfer, Vol. 21, pp. 1111-1115, 1978.
- 140 Hauf W., and Grigull U., "Optical Methods in Heat Transfer," Advances in Heat Transfer, Vol. 6, pp. 133-366, 1970.
- 141 Mayinger, F., and Panknin, W., "Holography in Heat and Mass Transfer," Proceedings of the 5th Int. Heat Transfer Conference, Japan, Vol. 6, pp. 28-43, Sept. 3- Sept. 7, 1974.
- 142 McKeon, W. J., and Tarasuk, J. D., "Accurate Method for Locating Fringes on Interferogram," Rev. Sci Instrum., Vol. 52, pp. 1223-1225, 1981.
- 143 Mehta, J. M., and Black, W. Z., "Errors Associated with Interferometric Measurement of Convective Heat Transfer Coefficients," Appl. Opt., Vol. 16, pp. 1720-1726, 1977.
- 144 Flack, R. D., "Mach-Zehnder Interferometer Errors Resulting from Test Section Misalignment," Appl. Opt., Vol. 17, pp. 985-987, 1978.
- 145 Flack, R. D., "Shearing Interferometer Inaccuracies Due to a Misaligned Test Section," Appl. Opt., Vol. 17, pp. 2873-2875, 1978.
- 146 Boxman, R. L., and Shlien, D. J., "Interferometric Measurement Technique for the Temperature Field of Axisymmetric Buoyant Phenomena," Appl. Opt., Vol. 17, pp. 2788-2793, 1978.
- 147 Gary, D.E, "American Institute of Physics Handbook," McGraw-Hill Book Co., P. 110, 1963.
- 148 Incropera, F.P., and Dewitt, D.P., "Fundamentals of Heat Transfer," John Wiley & Sons, Inc., p. 775, 1981.
- 149 Bratis, J.C., "Interaction of Gaseous Radiation and Natural Convection Heat Transfer in an Enclosed Layer Between Two Vertical Parallel Plates," Ph.D., Dissertation, Univ., of Notre Dame, 1972.

- 150 Pearson, C.E., " Handbook of Applied Mathematics," Van Nostrand Reinhold Company, N.Y., p. 105, 1983.
- 151 Eckert, E.R.G., and Soehngen, E., "Distribution of Heat Transfer Coefficients Around Circular Cylinders in Cross Flow at Reynolds Numbers from 20 10 200," Trans. of ASME, 74, 343, 1952.

